EXPERIMENTAL AND MODELING STUDY OF PITCH PYROLYSIS KINETICS

by

CHENGQING YUE

B.Eng. China University of Mining and Technology, 1984

M.Sc. Beijing Coal Chemistry Research Institute, 1987

A THESIS SUBMITTED IN PARTIAL FULFILLMENT OF

THE REQUIREMENTS FOR THE DEGREE OF

DOCTOR OF PHILOSOPHY

in

THE FACULTY OF GRADUATE STUDIES

Department of Chemical Engineering

We accept this thesis as conforming

to the required standard

THE UNIVERSITY OF BRITISH COLUMBIA

November 1995

In presenting this thesis in partial fulfilment of the requirements for an advanced degree at the University of British Columbia, I agree that the Library shall make it freely available for reference and study. I further agree that permission for extensive copying of this thesis for scholarly purposes may be granted by the head of my department or by his or her representatives. It is understood that copying or publication of this thesis for financial gain shall not be allowed without my written permission.

Department of CHEMICAL ENGINEERING

The University of British Columbia
Vancouver, Canada

Date April 25, 1996

ABSTRACT

Kinetics of thermal pyrolysis of both CANMET and Syncrude pitches from heavy oil upgrading have been studied with Thermogravimetric Analysis (TGA), and with Pyroprobe-Gas Chromatography (Pyroprobe-GC). In the latter technique samples are pyrolyzed at high heating rates and products analyzed with in-line gas chromatography.

Experiments with TGA were carried out at atmospheric pressure and at temperatures between 700 and 950 °C. The heating rates were 25, 50 100 and 150 °C/min. The sample weight was varied between 3 and 17.2 mg. The effects of sample weight, heating rate and final temperature on the weight loss as a function of time were examined.

Experiments with Pyroprobe-GC were carried out at atmospheric pressure and at temperatures between 500 and 1000 °C. The heating rates were 600, 3000, 30000, 300000 °C/min, using a sample weight of about 5 mg. The accumulated pyrolysis products were analyzed and lumped into major groups for yield estimation based on number of carbon atoms. The final weight of residue was also determined. The effects of the final temperatures on the yield of each major group were examined.

At temperatures below 150 °C, there is little pyrolysis of either pitch. At higher temperatures, the pyrolysis takes place in two following stages, with a first stage of low activation energy barrier and low pre-exponential factor, and the second stage of higher activation energy and pre-exponential factor. Higher conversion to volatiles was achieved with Syncrude pitch than with CANMET pitch. Heating rates had a minor effect on the weight loss. The total weight loss decreased slightly with the increase of sample weight, and final temperatures.

The most abundant components of the pyrolysis products were species lighter than C_7, which are primarily gases. The C_{10} group yield was strongly influenced by heating rates. Higher molecular weight components C_{11}, C_{12}, C_{13}, and C_{14} were also detected. The pyrolysis products

from Syncrude pitch consisted of higher yields of lighter components (C_7) than those from CANMET pitch.

A general first order equation for the kinetics of volatile release under temperature programmed conditions is widely used in the pyrolysis literature. Interpretation of results via the single stage integral method and methods due to Coats-Redfern, Chen-Nuttall and Friedman were tested with the TGA data and found inadequate. The single stage first order model of Anthony and Howard, which incorporates a Gaussian distribution of activation energies also failed. An adequate description of the pitch pyrolysis kinetics was achieved using a 2-stage first order model with the integral analysis method. The 2-stage model reflects changes in the chemical constitution or structure as conversion proceeds using two sets of kinetic parameters. This feature is essential to describe the dependence of devolatilization rates on remaining volatile content. The transition between these two stages is a sharp one, occurring at about 450 °C for both CANMET and Syncrude pitches. The magnitude of the activation energies suggested that both stages are kinetically controlled. The analysis methods of Coats-Redfern, Chen-Nuttall, and Friedman were also tested as two stage methods and found to be inadequate to describe the pitch pyrolysis kinetics in the temperature range studied.

The pre-exponential factors and activation energies from the different kinetic methods exhibited the compensation effect, in which the values of the derived pre-exponential factors and activation energies are related. This mutual dependence prompted an the examination of the accuracy of these kinetic parameters, and a search for a single set of parameters for each stage of the pitch pyrolysis. It was found that the accuracy of these kinetic parameters derived by different analysis procedures are not identical, and a single set of kinetic parameters for each stage can be obtained with adequate fitting of the experimental data.

Indexing terms: Pitch, Residuum, TGA, Pyroprobe-GC, Pyrolysis, Kinetics, Modeling, Kinetic Compensation Effect.

TABLE OF CONTENTS

LIST OF TABLES

LIST OF FIGURES

Chapter 3

Chapter 4

Chapter 6

NOMENCLATURE

a	kinetic compensation constant in Chapter 2 fitting parameter in Chapter 5
B	maximum possible devolatilization rate, S^{-1}
b	kinetic compensation constant in Chapter 2 fitting parameter in Chapter 5, b=-E/R
C	heating rate, °C/min
E, E_o	activation energy, J/mol
E_i	activation energy of ith stage of reaction, J/mol
f(E)	distribution function of activation energy
H_{PT}	rate of heat supply for volatile evaporation per unit mass, kJ/s.kg coal
h_{LV}	total heat of volatile evaporation per unit mass of coal, kJ/kg coal
k, k_1, k_2, k_3	rate constant represented by an Arrhenius expression, min^{-1}
k_o, k_{o1}, k_{o2}	pre-exponential constant of Arrhenius equation, min^{-1}
k_{oi}	pre-exponential factor of ith stage reaction, min^{-1}
$\bar{k}$	nominal rates $\bar{k} = (dV / dt) / (V^* - V)$, min^{-1}
$m_C(0)$	initial mass of coal, kg
m_C	mass of coal at any time t, kg
m_C(final)	mass of coal at the end of pyrolysis reaction, kg
m_I	mass of the reactive intermediate, kg
m_T	mass of tar, kg
n	no. of reaction stages which are first order reaction
R	gas constant, 8.314 J/mol.K
R^2	linear regression constant
s	standard deviation of activation energy, J/mol

s.e.e.	standard deviation error
T	temperature, °C (or K)
T_i	critical temperature, at which reaction behavior is undergoing visible change in terms of the ratio dV/dT or rate dV/dt due to the change of reacting residue, K
To	initial temperature for TGA, 50 °C
T_P	coal particle temperature, °C (K)
T_V	volatile evaporation temperature, °C (or K)
V	volatile released at time t, % (or kg)
$V_{t=0}$	volatile yield at t=0 minutes, %
$V_{t=10}$	volatile yield at t=10 minutes, %
V*	total volatile yield, % (or kg)
X	reciprocal of temperature 1/T, K^{-1}
X_V	fraction of volatile material to be released
Y	LHS of each of the single overall first order reaction methods
α, α_1, α_2	kinetic compensation constant
α_1, α_2	mass stoichiometric factors representing the extents of devolatilization via reaction 1 and 2 respectively in Chapter 2
α_i	constant used to characterize the gradual change of the chemical structure of reacting residue. α_i =1 when $T_{i-1} \leq T < T_i$, otherwise α_i =0
β	shape parameter of Weibull distribution
β, β_1, β_2	kinetic compensation constant
η	scale parameter of Weibull distribution
γ	threshold or location parameter of Weibull distribution

ACKNOWLEDGMENTS

I am grateful to my supervisor, Professor A. P. Watkinson, for his guidance and interest in this research. I am also indebted to many others who helped during the course of this work:

To the University of British Columbia which contributed financial support in the form of University Graduate Fellowships.

To the Natural Science and Engineering Research Council of Canada which provided financial support in the form of research grants.

To the Combustion Group of the Department of Chemical Engineering, UBC, which provided the CANMET pitch sample.

To Syncrude Canada Ltd. which provided the Syncrude pitch sample.

Special thanks are due to my mother, sisters and younger brother for their encouragement, understanding and patience.

CHAPTER 1 INTRODUCTION

Pyrolysis of high molecular mass carbon and hydrogen containing materials is viewed as depolymerization in parallel with thermal decomposition of functional groups. The primary products compete for the donatable hydrogen for stabilization [1]. Pyrolysis is the first step in some conversion processes for hydrocarbon containing materials such as coal, heavy petroleum, and oil shale. It is the step which is most dependent on the properties of the hydrocarbons [2]. In combustion and gasification, pyrolysis precedes reaction by oxygen, steam, hydrogen or carbon dioxide [3]. In coking processes, pyrolysis of petroleum, semi-solids (mainly residua) and solids (mainly coals) results in the formation of a complete range of products from solids to gas. In addition to its importance in the hydrocarbon conversion process, analysis of pyrolysis products can supply important clues to the structure of the parent hydrocarbon.

The last several decades have seen an improvement in the understanding of coal and biomass pyrolysis in processes such as gasification, combustion, and liquefaction [1-4]. More rigorous information has also been developed for the light hydrocarbons. For complex feedstocks such as above, the approach taken to pyrolysis has been mainly semi-empirical. The literature contains relatively fewer attempts to deal with moderately heavy hydrocarbon feedstocks and the related mechanism involved, especially the secondary reactions which are often ignored in coal pyrolysis. Secondary reaction refers to the cyclization and condensation of the pyrolysis volatiles before leaving the reacting hydrocarbon matrix. For coal, secondary reactions are complex, being influenced by coal type, heating rate, residence time, temperature, intra- and extra-particle heat and mass transfer, and physical structure of the reacting coal. Further, these reactions can be heterogeneous (vapor-solid, vapor-liquid, or liquid-solid) or homogeneous (vapor phase or liquid phase) [5].

The pyrolysis of coal and biomass has been widely investigated since the late 1970's to maximize the liquid product yield in order to find a substitute for petroleum or for generation of chemicals. This has resulted in the development of several coal conversion processes [6, 7] in which the knowledge of pyrolysis is used to predict the product yields and distribution quite reasonably and successfully. For biomass, the complexity of the liquid products generally defies prediction.

The knowledge of pitch pyrolysis is also quite limited and has been borrowed from that for coal. Most known technology for processing of bitumen, coal, petroleum, and oil sands produces pitch. Pitch is commonly used to describe the liquid or semi-liquid fraction of a reaction product that boils above 524 °C and which arises as a by-product from processing of crude oil or bitumen. Its relatively high H/C atomic ratio (about 1.0 compared to about 0.5 for coke and 0.3 to 0.9 for coal) [8, 9] suggests that it should be possible to produce liquids by additional processing. Furthermore an appreciation of pitch pyrolysis might lead to new methods of pitch utilization. Thus, there is a clear need for further study in this field, to clarify the behavior of pitch in pyrolysis, which will improve the understanding of the processes and mechanisms involved, and hopefully lead to a proper way to process pitch, and generate economic and environmental profit.

As Canada, and other countries rely increasingly on heavy oils, residues from upgrading will become more of a disposal problem. Hydrogen or fuel gas production via gasification is a possible route to utilization. When pitches are heated prior to gasification their large volatile content is released, leaving a char. To understand kinetics, information on volatile yields and composition as function of temperature, atmosphere and pitch type is essential [10, 11]. Syncrude and CANMET processes represent two major bitumen processes which subsequently produce pitch as by-product. CANMET pitch is the residue of Cold Lake bitumen from CANMET hydrocracking process, where an additive is used to inhibit coke formation. This process was

demonstrated at 5000 bpd in Petro-Canada's Montreal refinery and about 10% of the feed ends up as pitch during the upgrading process [12-14]. This demonstration was successful and the technology is ready for commercialization. Syncrude pitch is the residue of Athabasca bitumen from Syncrude LC-Fining process. LC-Fining is a hydroprocessing process where H_2 and catalysts are added in to upgrade bitumen at temperature 375-530 °C and pressure 1100-1600 psi, and currently operating at 715 m^3/D of bitumen. About 4% of the feed ends up as pitch [15].

The objectives of this study were to investigate the pyrolysis reaction mechanism and product distribution for different pitch types, and to formulate a model for the mechanism under conditions of different heating rates, final temperatures and reaction times. The study is concerned with pitch pyrolysis over a range of heating rates and for final temperatures from 700 to 1000 °C, and under normal pressure in an inert atmosphere, so that the first step in atmospheric pressure gasification, pyrolysis and combustion processes can be simulated.

Pitch pyrolysis at low heating rates is studied using a TGA, and at rapid heating rates with a Pyroprobe-equipped gas chromatograph. With TGA, the weight loss rate is investigated quantitatively at different final temperatures and heating rates less than 150 °C/min. Diffusional effects inside the pitch samples are studied by changing the initial pitch sample weight (or pitch sample thickness inside the TGA sample holder). Thus pyrolysis kinetics and relative parameters can be derived from the data. With the Pyroprobe-equipped chromatograph, weight loss is also obtained at different final temperatures and heating rates up to 300,000 °C/min. The Pyroprobe equipped chromatograph permits *in situ* GC analysis, in which the volatile composition is investigated as a function of reaction conditions. With the two procedures, pyrolysis kinetics and reaction parameters can be investigated under a wide range of conditions.

Chapter 2 Literature Review

2.1 Chemical Structure of Pitch

The pyrolysis of relatively simple hydrocarbon compounds is complex and only partly understood. Therefore, it comes as little surprise that the knowledge of chemical mechanisms for pyrolysis of relatively undefined materials such as pitch or coal is lacking.

The characterization of pyrolysis products of coal and/or pitch is a sizable task, as these are usually present as gases, liquids and solids. The number of distinct chemical species is very large, and to facilitate data analysis one must usually resort to judiciously grouping the products into a few key classes of compounds.

With pitch, the characterization of the reactant is as difficult, if not more difficult than, the characterization of the products of the process. Because pitch is a somewhat heterogeneous and only partially soluble in most solvents, many of the traditional chemical and spectroscopic techniques for organic structure determination can not be applied easily or unambiguously. Therefore there is still a fair amount of debate over what constitutes a representative structure for a pitch "molecule". The chemical structures of the pitches studied have not been determined directly in this work. Rather, the structural characteristics must be inferred from a knowledge of the more traditional classification parameters for pitch.

The literature on the structure determination of petroleum derived pitch also contains information on "coal extracts" and other solvated coal and pitch fractions. However, the fraction that is soluble in a given solvent does not represent the total pitch or coal, since solubilization is unlikely to preserve its basic structure. The information is therefore difficult to apply.

2.1.1 The Carbon-Hydrogen Structure

It is generally accepted that an important characteristic of pitch or coal structure is its aromaticity, defined as the fraction of carbon in the pitch or coal which is aromatic in nature. A large number of approaches have been employed to determine the aromaticity and the average number of rings in the condensed polycyclic aromatic "clusters", as a function of carbon content. Various physical techniques [16] have been employed in studying the structure of coal/pitch structure.

From empirical studies on many hydrocarbons Van Krevelen [17] and several coworkers developed several ingenious correlations between measurable physical properties and some much more difficult to measure structural parameters.

Great advances have been achieved during the last decade in the application of NMR in pitch characterization. For measurements on pitch solutions, the main problem is the fact that pitches are not completely soluble in solvents suitable for NMR. Solid state NMR has the disadvantage of insufficient spectral results. As has been shown by Komatsu [18], these disadvantages can be overcome by measuring the spectrum at a temperature above the softening point of the pitch. The method has been applied to various types of pitches using ^{13}C NMR. Well-resolved spectra characterized by a high signal to noise ratio were obtained. Moreover, the measuring time could be markedly shorted compared with the measuring time necessary in organic solutions. ^{13}C NMR not only provides the important aromaticity figure but also detailed information on the aliphatic functional groups present in pitches.

Of course aromaticity alone does not completely characterize the carbon skeletal structure. Information on the distribution of aromatic and nonaromatic carbon is also necessary. It should also certainly be noted that using the total carbon content for the coals or pitch masks

potentially significant differences among the maceral fractions in coals, or the difference among fractions of different solubility in pitches.

Unfortunately data on total hydrogen distribution is not plentiful and its reliability is frequently questioned. Chemical techniques have provided some of the necessary data (such as that for hydroaromatic hydrogen and phenolic hydrogen), while spectroscopic techniques, such as ^{1}H NMR and IR, have provided others.

2.1.2 Solvent Fractionation of Pitches

Solvent fractionation is the most widely used method in pitch characterization. Solvent fractionation uses organic solvents of increasing polarity such as *n*-pentane, benzene and tetrahydrofuran (THF) to give fractions of increasing molar mass and heteroatom content. Three typical fractions are: *n*-pentane solubles, benzene insolubles and asphaltenes (benzene soluble, *n*-pentane insoluble). The fractions can be separated further by chromatographic methods and characterized by a variety of spectroscopic and chemical methods to provide details of individual components and average structures.

Chromatography is widely used in the separation, fractionation and characterization of complex mixtures of organic molecules. Size exclusion chromatography provides a separation mainly on the basis of molecular size which corresponds to separation on the basis of molar mass. It has been extensively used for coal and petroleum derivatives. However, separation occurs partially on the basis of functionality when THF is used as solvent, as well as on molecular size. This makes determination of molar mass distributions unreliable with high concentrations of pitch or tar present.

SARA (saturates, aromatics, resins and asphaltenes) separation is a traditional characterization method for hydrocarbon residuum, based on solubility/polarity of compounds. A

discussion of the chemical structures found in the SARA fractions can be found [19]. In general, the components are alkyl-substituted polycyclic structures related to steranes and hopanes derived from squalene precursors, or to terpenoid skeletons. Following the progression from saturates to aromatics to resins to asphaltenes, these fractions show increased aromaticity, average molecular weight, and heteroatomic content. There is also some overlap of structures and properties between neighboring fractions. Furthermore, variations in the relative amounts of the SARA fractions are accompanied by variations in the physical properties of bitumen. The chemical structures in the different fractions are believed to be related through various diagenetic processes such biodegradation and thermal maturation. However, each SARA fraction is fundamentally different to the extent that it can exhibit some specific chemical attributes.

The studies of SARA fractions have led to insights into the processing of petroleum residuum (pitch etc.). However, attempts to correlate SARA fractions with the processibility of residua have generally also been unsuccessful [20]. The determination of average molecular structures held some promise of providing insight into residuum conversion chemistry.

A promising approach to gain some understanding of the complex chemistry of residuum upgrading [21] by coking, hydrocracking and hydrotreating appears to be to use a combination of yield data obtained over a wide range of conversions, together with average molecular structural data and the extensive knowledge of molecular structures in residua.

2.2 Chemistry of Pyrolysis and Secondary Reaction

2.2.1 Chemical Thermodynamics of the Pyrolytic Reactions

To understand the chemistry of the pyrolysis reaction and the criteria for its chemical control, it is necessary to compare the thermodynamic stability of the various carbon compounds. The comparative stability of the various hydrocarbon groups may serve as a basis for discussing

the probable sequence of a decomposition reaction. Among the three major groups of hydrocarbons, i.e., paraffins, olefins and aromatics, the low molecular weight paraffins are the most stable hydrocarbons up to about 500 °C and among these, methane exhibits the greatest stability. Above 800 °C, the aromatics become the most stable hydrocarbons. In this temperature range (500-800 °C), the thermodynamic stability of the olefins lies between that of the paraffins and aromatics. The stability of paraffins decreases with increasing chain length. In the higher temperature region (>800 °C), the same holds true for the olefins. The alkylated aromatics compounds are less stable than the pure aromatics. With increasing length of the side chain, the stability decreases. Contrary to this, the stability of aromatics increases with increasing number of rings, i.e. with increasing molecular size.

The mean bond energies of organic compounds are obtained by referring the energies of formation to the gaseous elements involved, i.e. carbon and hydrogen, and by then dividing by the number of bonds. Table 2.1 gives bonds energies obtained from thermodynamic data, as compared with those derived from quantum mechanical calculations based on bond length and force constants. Both methods give approximately the same values for the individual bond types.

Table 2.1 Bond Energies Obtained from Thermodynamic Data and from Quantum Mechanical Calculations [22]

From thermodynamic data			From quantum mech. calculations		
Bond	Compound	Mean bond energy kJ/mol	Mean bond energy kJ/mol	Distance between nuclei, Å	Force constant dynes $cm^{-1}x10^{-5}$
C—C	C_2H_6	325.10	--	--	--
C=C	C_2H_4	585.76	597.89	1.337	9.8
C≡C	C_2H_2	808.77	811.70	1.205	15.6
C—C	C_6H_6	517.98	--	--	--
C—H	CH_4	410.87	412.96	1.094	4.88
O—H	HO-H	457.73	462.75	0.98	7.6
C=O	CH_2O	683.25	694.54	1.21	12.1

A comparative consideration shows that the C-H bond is more stable than the C-C bond. Also shown is the higher bond energy of the C-C double bond and the C-C triple bond, which explains the dehydrogenation tendency towards olefins and the stability of acetylene at high temperature.

The high stability of ring compounds and especially of aromatics is due to the resonance energy. The resonance energy increases with increasing molecular size of the ring system, thus explaining the driving force for the chemical condensation of low molecular weight aromatics to polycyclic aromatic systems with the accompanying release of hydrogen. Examples are given in the following Table 2.2.

Table 2.2 Resonance Energies of Cyclic Compounds [22]

Compound	Energy kJ/mol	Compound	Energy kJ/mol
Benzene	150.62	Quinoline	288.70
Naphthalene	255.22	Biphenyl	299.16
Anthracene	351.46	Aniline	167.36
Phenanthrene	384.93	Furan	92.05
Toluene	146.44	Pyrrole	102.51
Styrene	158.99	Indole	205.02
Phenol	150.62	Thiophene	117.15
Pyridine	179.91	Cyclooctatraene	25.10

This qualitative thermodynamic consideration suggests the following trends for the course of pyrolysis of hydrocarbons with the increase of temperature [22]:

1. Cracking of all nonaromatic hydrocarbons to smaller molecules (cracking and dehydrogenation reactions).
2. Cyclization of all hydrocarbon chains to form aromatics. The first and the second reaction trends apply in the same way to aromatics with side chains which can undergo cracking or cyclization.
3. Condensation reactions of aromatics to form polycyclic aromatic systems.

These three principal types of reactions occur in all known technical processes dealing with the formation of carbon via pyrolysis reactions.

2.2.2 Pyrolysis of Unsubstituted Aromatics

Unsubstituted aromatics primarily exhibit direct ring condensation, i.e., the formation of diarenes and triarenes. Whenever sterically possible, chemical condensation can proceed to polycyclic products. Unsubstituted aromatics having the anthracene configuration are more reactive with respect to chemical condensation.

In summary [22], the pyrolysis of hydrocarbons takes place via aromatic intermediates. Results on the pyrolysis of well-defined, pure aromatics have shown the following effects:

1. Unsubstituted aromatics react by chemical condensation to form polynuclear aromatics, the aromatics having an anthracene configuration being the most reactive.
2. Alkyl-substituted aromatics are more reactive than unsubstituted ones, the effect being more pronounced the greater the number and the length of the alkyl groups.
3. The alkyl groups are the positions where the formation of the new aromatic systems takes place.
4. The highest reactivity is exhibited by aromatics containing five-numbered ring systems.

The existing investigations, pertaining to gas phase pyrolysis in a flow system, show that in the early stages the order of reaction is approximately unity for benzene, naphthalene and biphenyl. The apparent first order rate constants for these three aromatics are found to be of the same order of magnitude. The apparent activation energies amount to approximately 292.88 kJ/mol to 334.72 kJ/mol.

2.2.3 Pyrolysis of Mixture of Hydrocarbons

The great complexity of chemical reactions occurring during the pyrolysis of hydrocarbons can be recognized not only from thermodynamic considerations but also from technological experiences gained in different processes. In view of the various mixtures of hydrocarbons used as raw materials and because of the insufficient analytical control of a technical pyrolysis, these processes do not reveal the chemistry in detail. Nevertheless, they provide a fair picture as to process parameters such as temperature, residence time and yield upon pyrolysis. Free radical reactions control the pyrolysis of most organic substances.

2.2.3.1 Pyrolysis of Crude Oil Fractions to Volatile Products

It has been found that the tendency to pyrolysis increases from the paraffins to the olefins and further to the naphthalene and the alkylated aromatics, up to the nonsubstituted aromatics. In case of purely thermal pyrolysis, mild conditions around 400 °C lead primarily to a fracture of the C-C bond, preferentially in the middle of the molecule chain. With increasing temperatures, the position of the fracture shifts towards the chain end, thus producing long chain olefins and increased portions of highly volatile fragments.

Paraffins undergo pyrolysis leading to the formation of saturated and nonsaturated fragments between 400 °C and 600 °C. Depending on the length of the main chain, isoparaffins primarily lose their branches and then behave like straight chain paraffins. Ring paraffins lose parts of their side chains, thus leading to unsaturated fragments. At temperatures above 600 °C, naphthalene rings can be broken to form straight chain olefins. Cycloparaffins containing three carbon atoms are broken most easily, whereas cyclopentane is most stable. Cycloparaffins containing six carbon atoms in the ring become stabilized by aromatization. In the case of

alkylated aromatics, the rupture of the side chains is promoted with increasing length of these chains.

With rising temperature, the rupture of the C-H bond is more strongly enhanced than rupture of the C-C bond. Thus the formation of very small fragments down to hydrogen is favored and diolefins and triolefins with good thermal stability are formed. Above 550 °C, long chain olefins disintegrate, leading to shorter molecules and partial aromatization.

The first step of the hydrocarbon pyrolysis, namely, the decomposition to nonaromatic hydrocarbons takes place in the low temperature region between 400 and 700 °C, whereas the aromatization occurs between 700 and 900 °C. These results are however valid only for short contact times at the described temperature.

Similar experiences pertain to the coal coking processes. The volatile hydrocarbons released at pyrolysis temperatures between 400 and 500 °C consist mainly of noncyclic compounds. In the high temperature range, however, the volatile products found in the coal tar are extremely aromatic.

2.2.3.2 Pyrolysis of SARA Fractions

Evidence from GC, HPLC, and FTIR analysis [23-29] suggests that SARA fractions (saturates, aromatics, resins, and asphaltenes) from heavy hydrocarbon undergo dealkalyation and aromatization when pyrolyzed at temperatures 362 °C to 418 °C. Aromatization and dealkylation of the polycyclic, saturated structures in the saturate fraction lead directly to the production of aromatic compounds. Further aromatization and dealkylation of the aromatic fraction result in resin production. Resins and asphaltenes have chemical and structural similarities. The thermal pyrolysis of the resins and asphaltenes results in further condensation of the polycyclic structure and fragmentation and finally leads to the formation of coke. This process was proven to involve

bond scission and radical reactions. The pyrolysis of each of the SARA fractions appeared first order. The observed apparent activation energy of pyrolysis for aromatics, resins and asphaltenes is 108, 135, 150 kJ/mol respectively [23]. These values fall in the wide range of values 29.1 kJ/mol and 286 kJ/mol [29] for bitumen pyrolysis. Observed values of apparent activation energies depend upon many factors, including the structure and complexity of the kinetic model. The method used to prepare a particular fraction will influence both its chemical composition and behavior, and consequently the values for any kinetic parameters that characterize it. The more chemically-varied the species contained in a particular fraction, the greater will be the number of reactions within the fraction and consequently, the lower will be the observed globe kinetic parameters [13, 30].

2.3 Pyrolysis Models and Comparison

One aim of modeling is to predict the pyrolysis behavior a priori in a conversion system as a function of parameters (temperature, heating rate, pressure, particle size etc.) thus facilitating the design of conversion reactors. Systematic research to this end during recent decades has advanced our knowledge to a stage where reasonable predictions are possible through modeling [31, 32]. These studies have provided valuable insight into the kinetics and the mechanism of the pyrolysis process. The modeling of pyrolysis is relatively straightforward when the chemical reaction is the only process occurring within the reactor and the feed species is simple. There are, of course, different levels of complexity of kinetic models. For simple hydrocarbons, pyrolysis models are based on the free radical mechanism. For propane pyrolysis, for example, the scheme of Trimm and Turner [33] includes one initiation reaction, thirty one propagation reactions, and nine termination reactions. These involved no species of greater molecular weight than C_4H_{10}, and no coke formation. At a less complex level, Sundaram and Froment [34] describe propane

cracking by ten reactions using molecular species rather than free radicals. This reaction scheme yields information on product distributions, but does not represent the mechanism as such. For higher molecular weight hydrocarbon feeds, or complex mixtures such as pitch, it is not feasible to write a kinetic model which reflects all steps in the actual mechanism. For example, the Kumar and Kunzru [35] scheme for naphtha pyrolysis incorporates twenty two reactions which are written in terms of molecular species. Each reaction requires a specified pre-exponential factor and activation energy. However, pyrolysis can involve extra transport steps which introduce complexity.

The review by Jamaludin et al. [36] considers the present understanding of kinetic models, and the review by Suuberg [37] considers the present understanding of general pyrolysis models including the mass transfer limitations of coal pyrolysis. Analogous models are applied to biomass pyrolysis.

At the time of writing, no accurate model has been developed to completely describe pitch pyrolysis. The following work which primarily involves coal pyrolysis is reviewed as that which bears most relevance to the system under investigation. Rather than dealing with individual species, this approach deals with the volatile matter as one or two components. The application of the models to pitch involves some changes, and certain steps which are valid for coal, would not apply to pitch. The two competing reaction model of pyrolysis is shown to be a simple, but effective method for predicting the weight loss due to devolatilization at high temperature and high heating rates for coal pyrolysis.

2.3.1 Constant Evaporation Rate Model

The constant evaporation model is probably the simplest existing pyrolysis model. Proposed by Baum and Street [38], it assumes that pyrolysis does not begin until the particle

temperature exceeds a vaporization temperature T_V, taken as 327 °C. Above T_V, the rate of pyrolysis is controlled by the total heat of evaporation of the volatile, up to an empirically determined maximum value.

The rate of pyrolysis in terms of the fraction of volatile material X_V to be released, can be expressed as

$$\frac{dX_V}{dt} = 0; \qquad T_P<T_V \text{ or } X_V=1.0 \qquad (2.2a)$$

$$\frac{dX_V}{dt} = -H_{PT}/h_{lV}; \qquad T_P \geq T_V \text{ and } X_V<1.0,\ H_{PT}<Bh_{lV} \qquad (2.2b)$$

$$\frac{dX_V}{dt} = -B; \qquad T_P \geq T_V \text{ and } X_V<1.0,\ H_{PT}\geq Bh_{lV} \qquad (2.2c)$$

Where h_{LV} is total heat of volatile evaporation per unit mass of coal, kJ/kg coal, H_{PT} is rate of heat supply for volatile evaporation per unit mass, kJ/s.kg coal. B is the maximum possible devolatilization rate. T_P is the coal particle temperature and T_V the volatile evaporation temperature. Lochwood et al. [39] observed that good predictions are obtained only for coal when $B<H_{PT}/h_{lV}$, while Jamaludin found that using considerably higher values of B compared to the recommended value of 10 s^{-1} did not appreciably change the predicted temperature [36].

By defining $m_C(0)$ as the initial mass of coal (kg), m_C as the mass of coal at any time t (kg), m_C(final) as the mass of coal at the end of pyrolysis reaction (kg), then the volatile released at time t is

$$V = \frac{m_C(0) - m_C}{m_C(0)} \qquad (2.2d)$$

and the total volatile yield is

$$V^* = \frac{m_C(0) - m_C(final)}{m_C(0)} \qquad (2.2e)$$

and the fraction of volatile material X_V to be released is

$$X_V = \frac{m_C - m_C(final)}{m_C(0) - m_C(final)} \tag{2.2f}$$

2.3.2 Single Overall Reaction Model

This model, proposed first by Badzioch and Hawksley [40] for coal pyrolysis, has been widely used due to its simplicity and effectiveness. It is based on the following simplified reaction scheme

$$C \xrightarrow{k} V + R$$

coal C pyrolyzes to produce volatiles V and solid residue R. The reaction is assumed first order, the pyrolysis rate being proportional to the volatile matter yet to be released (V*-V)

$$\frac{dV}{dt} = k(V^* - V) \tag{2.3a}$$

Where V* is the total volatile fraction, and the rate constant k is represented by an Arrhenius expression:

$$k = k_o \exp[-E/RT_P] \tag{2.3b}$$

The fractional devolatilization at any time is obtained by integrating the above equation, then

$$\frac{V}{V^*} = 1 - \exp\left[-\int_0^t k\,dt\right] \tag{2.3c}$$

2.3.3 Two Competing Reaction Model

This model, proposed by Kobayashi et al. [41], and Ubhahayakar et al. [42], represents the overall coal pyrolysis process by two mutually competing first order reactions as:

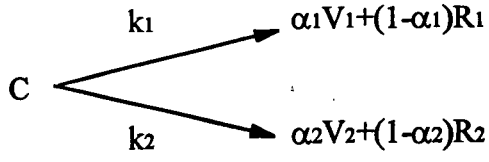

The rate of weight loss of the coal (maf basis) is given by

$$\frac{dm_C}{dt} = -(k_1 + k_2)\, m_C \qquad (2.4a)$$

so that at any time t the mass of material yet to be pyrolyzed is

$$m_C = m_C(0) \exp\left[-\int_0^t (k_1 + k_2)\, dt' \right] \qquad (2.4b)$$

Where the rate of devolatilization at any time is

$$\frac{dV}{dt} = (\alpha_1 k_1 + \alpha_2 k_2)\, m_C \qquad (2.4c)$$

Where α_1 and α_2 are mass stoichiometric factors representing the extents of devolatilization via reaction 1 and 2 respectively. The extent of devolatilization at time t is obtained as

$$V(t) = m_C(0) \int_0^t (\alpha_1 k_1 + \alpha_2 k_2) \exp\left[-\int_0^{t'} (k_1 + k_2)\, dt'' \right] dt' \qquad (2.4d)$$

The rate constants k_1 and k_2 have Arrhenius form, and are such that reaction 1 has a lower activation energy than reaction 2, with the effect that secondary reaction becomes operational only at higher temperature to effect volatile yields in excess of α_1.

2.3.4 Three Reaction Models

The three reaction models, first proposed by Wen and Dutta [43], considers of three parts representing devolatilization, cracking and deposition. The pyrolysis products are gases, tar and solid residual. Tars are defined as species heavier than C_6, and gases those lighter than C_6. The proposed reaction scheme is:

$$C \xrightarrow{k_1} (1 - \alpha_1)\, R_1 + \alpha_1 T \begin{cases} \xrightarrow{k_2} V \\ \xrightarrow{k_3} R \end{cases}$$

The rate of weight loss of the coal particle is given by

$$\frac{dm_C}{dt} = -k_1 m_C \tag{2.5a}$$

By integration, then

$$m_C(t) = m_C(0)\exp\left[-\int_0^t k_1 dt'\right] \tag{2.5b}$$

The net rate of production of tar is

$$\frac{dm_T}{dt} = \alpha_1 k_1 m_C - (k_2 + k_3) m_T \tag{2.5c}$$

Where m_T is the mass of tar, then the yield of tar at any time is given by integration of the above equation.

$$m_T(t) = \alpha_1 m_C(0)\exp\left[-\int_0^t (k_2 + k_3)\, dt'\right]\int_0^t k_1 \exp\left[\int_0^{t'}(k_2 + k_3 - k_1)dt''\right]dt' \tag{2.5d}$$

The corresponding rate of production of volatile is

$$\frac{dV}{dt} = k_2 m_T \tag{2.5e}$$

By integration the above equation, with m_T given by the previous equation, gives the volatile yield at any time t. For isothermal conditions, the expression for the volatile yield simplifies to

$$V(t) = \frac{\alpha_1 k_2 m_C(0)}{k_2 + k_3 - k_1}\left\{\left[1 - \exp(-k_1 t)\right] - \frac{k_1}{k_2 + k_3}\left[1 - \exp\left(-(k_2 + k_3)t\right)\right]\right\} \tag{2.5f}$$

which further simplifies to (by assuming k_1 much smaller than k_2, k_3)

$$V(t) = \frac{\alpha_1 m_C(0)}{1 + (k_3/k_2)}\left[1 - \exp(-k_1 t)\right] \tag{2.5g}$$

A reaction scheme similar to the above was proposed by Niksa et al. [44], using a nonisothermal kinetic analysis, similar to that of Jüntgen and Van Heek [45, 46], to show that faster devolatilization rates were obtained at higher heating rates and they adopted the following competitive scheme to account for the enhanced yield at high heating rates as:

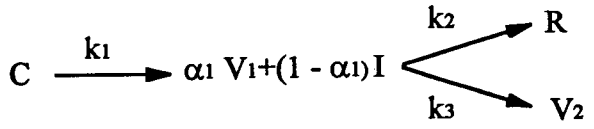

The rate of decomposition of the coal particle is given by the equation

$$\frac{dm_C}{dt} = -k_1 m_C \tag{2.6a}$$

the rate of production of the volatile and the intermediate is then given as

$$\frac{dV_1}{dt} = \alpha_1 k_1 m_C \tag{2.6b}$$

$$\frac{dm_I}{dt} = (1-\alpha_1)k_1 m_C - (k_2 + k_3)m_I \tag{2.6c}$$

$$\frac{dV_2}{dt} = k_3 m_I \tag{2.6d}$$

Where m_I is the mass of the reactive intermediate.

Nsakala et al. [47] proposed the following parallel consecutive reactions scheme based on pyrolysis of lignite at 800 °C as:

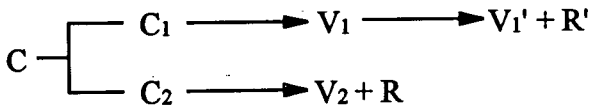

Coal particle C is assumed to consist of two distinct components, C_1 and C_2, of different ease of pyrolysis. In their analysis, Nsakala et al. [48] ignored the secondary cracking of V_1. If, therefore, components C_1 and C_2 decompose isothermally by independent first order reactions

$$C_1 = C_{01} \exp(-k_1 t) \tag{2.7a}$$

$$C_2 = C_{02} \exp(-k_2 t) \tag{2.7b}$$

Where C_{01} and C_{02} are the initial mass of C_1 and C_2. The total weight loss is obtained from

$$V = V_1 + V_2 \tag{2.7c}$$

where V_1 and V_2 are volatile product from C_1 and C_2 components respectively and

$$V_1 = C_{01} - C_1 \tag{2.7d}$$

$$V_2 = C_{02} - C_2 - R \tag{2.7e}$$

$$V = C_{01}\left[1-\exp\left(-k_1 t\right)\right] + \frac{C_{02}}{1+R/V_2}\left[1-\exp\left(-k_2 t\right)\right] \tag{2.7f}$$

At infinite time

$$V^* = C_{01} + \frac{C_{02}}{1+R/V_2} \tag{2.7g}$$

or

$$1-\frac{V}{V^*} = \left(\frac{C_{01}}{V^*}\right)\exp\left(-k_1 t\right) + \left(1-C_{01}/V^*\right)\exp\left(-k_2 t\right) \tag{2.7h}$$

2.3.5 Multiple Parallel Reaction Model

The powerful multiple parallel reaction model, originally proposed by Pitt [48], was later adopted by Anthony and Howard [49, 50] to fit their data. The merit of this model is that it only needs one more adjustable parameter than the single reaction model. The reactions envisaged were

$$Coal \rightarrow \sum_{i=1}^{n} C_i \xrightarrow{k_i} \sum_{i=1}^{n} \left(V_i + R_i\right)$$

The reactions are assumed to have the same pre-exponential factor but different activation energies. The weight loss due to devolatilization at any time is

$$\frac{V}{V^*} = 1 - \int_0^{\infty} \exp\left[-\int_0^t k(E)\,dt\right] f(E)\,dE \tag{2.8a}$$

f(E), denoting the distribution function of activation energy, is assumed to be Gaussian and given by

$$f(E) = \left(\frac{1}{s\sqrt{2\pi}}\right)\exp\left[-\left(E-E_0\right)^2/\left(2s^2\right)\right] \tag{2.8b}$$

Where E_o is the mean activation energy and s the standard deviation.

Instead of using a Gaussian distribution, Laskshmannan [51] used the Weibull distribution to model the kinetics of petroleum generation over a geological time scale. The probability density function f(E) (as applied to describe the distribution of activation energies) for this distribution is given by:

$$f(E)=\left(\frac{\beta}{\eta}\right)\left(\frac{E-\gamma}{\eta}\right)^{\beta-1}\exp\left[-\left(\frac{E-\gamma}{\eta}\right)^{\beta}\right] \text{ for } E \geq \gamma,\ \eta > 0 \text{ and } \beta > 0$$

$$=0 \text{ for all other values of } E,\ \eta \text{ and } \beta \qquad (2.8c)$$

where E is the activation energy expressed in kcal/mol. There are three parameters, namely, η, the scale parameter; β, the shape parameter; and γ, the threshold or location parameter characterizing the distribution. A number of different distributions can be generated by a suitable choice of these parameters. For $\beta=1$, the Weibull distribution coincides with the exponential distribution. For $\beta>1$, the distribution becomes 'bell shaped", but becomes positively skewed. As β increases, the Weibull distribution approaches the Gaussian distribution more and more closely. In fact, for $\beta=4$, the Weibull and Gaussian distributions become almost indistinguishable. This model may be useful for process chemical engineering applications, such as combustion and pyrolysis of coal, oil shale, bitumen and pitch. Unlike the Gaussian distribution, the Weibull distribution is well suited to represent many empirical distributions.

Noting the limitation of these distributions, Miura [52] proposed a mathematical procedure to estimate f(E) from experimental data without assuming any form of distribution. This procedure requires only three sets of experimental data. The procedure to estimate f(E) and k_o is summarized as follows:

1. Measure V/V* vs T relationships at three different heating rates at least.

2. Calculate nominal rates $\overline{k} = (dV / dt) / (V^* - V)$ at several but same V/V* values at different heating rates, then make Arrhenius plots of $\overline{k}$ at the same V/V* values.
3. Determine activation energies from the Arrhenius plots at different levels of V/V* and then plot V/V* against the activation energy E.
4. Differentiate V/V* by E to obtain f(E).
5. Calculate k_o corresponding to each E value at all the heating rates using equation $0.5447\,\alpha\, E/k_o RT^2 = e^{-E/RT}$, then employ the averaged k_o value as a true k_o value.

2.3.6 Complex Models

In order to model more accurately the gross fundamental mechanism involved, Reidelbelbach and Summerfield [53, 54] formulated a model which included six competitive /consecutive reactions. This was later modified by Antal et al. [55] to correct the abnormally high activation energy for the activation step. The reaction scheme is expressed as follows:

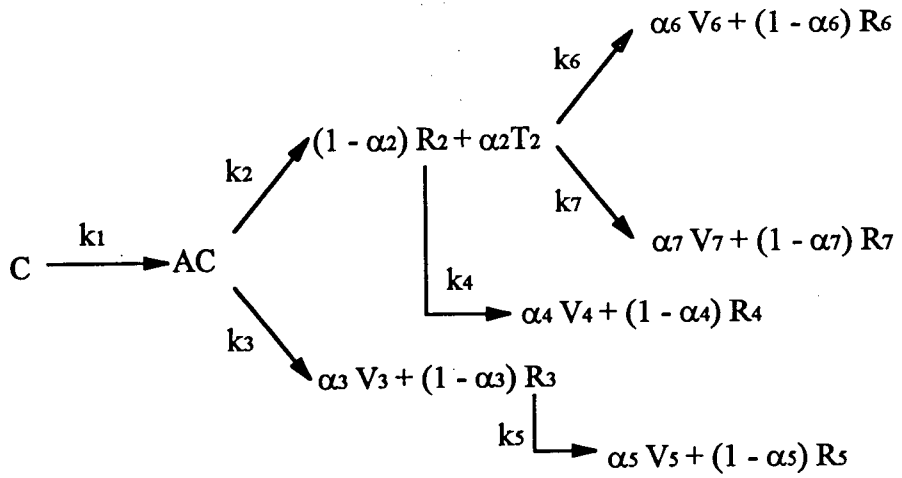

Several consideration went into the model, e.g. reaction 1 was proposed to limit decomposition of coal at low temperature. Further decomposition can then proceed by two routines depending on the heating rate and the temperature. The tar production step (reaction 2) was assigned a low activation energy as tar evolves at comparatively low temperatures. Similarly,

the experimental observation for increased gas/tar ratios and increased yield at high temperature, etc., were also accommodated. Reidelbach and Summerfield achieved good agreement with the experiment data of Badzioch and Hawsley [40] using a simplified version of the model.

2.3.7 Detailed Models

Detailed models of coal pyrolysis attempt to describe the evolution of individual volatile species. One such model is that formulated by Suuberg et al. [56-58] assuming nine volatile products to be formed via fifteen different reactions. The activation energies of the individual reactions when synthesized into a composite distribution function, were found to agree well with the corresponding Gaussian distribution obtained by Anthony et al. [49] solely from the total weight loss data. Tar was assumed to be either converted to coke and light hydrocarbons by secondary reactions, or evolve from the coal particles, as in the two competitive reactions below:

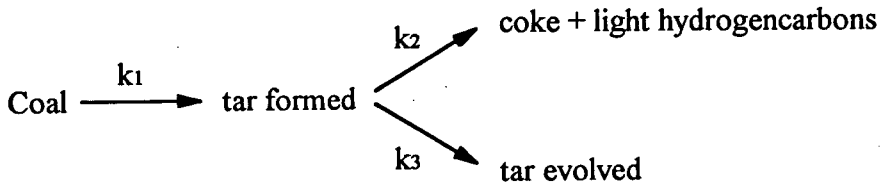

Soloman and coworkers [1-3] have been working towards providing a fundamental basis for pyrolysis reactions though the concept of 'functional groups'. The overall reaction is:

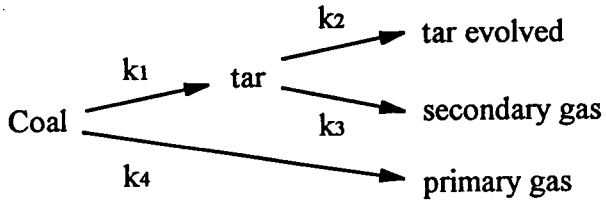

Thus a representative sample of the functional groups evolves without decomposition leaving coal molecule to form tar, while light primary gases are formed by decomposition of some functional groups. These two processes are assumed to be competitive. A single rate is used for tar evolution, and a separate rate for each gaseous species. Distributed (Gaussian) rate kinetics

are used for the gaseous species evolution, and secondary reaction of tar and tar evolution are represented by a separate set of competing reactions. The evolution of ten species (excluding tar) are represented by 15 reactions. Time and temperature dependent devolatilization of coal was predicted by the model using a coal independent set of kinetic parameters and the structural composition.

2.3.8 The Application of Models in Pyrolysis Kinetics

The global pyrolysis kinetics applied to pitch or any other hydrocarbon is generally intended to predict the overall rate and yield of volatile release (i.e. mass loss) from the sample. For a first order process this is given as Equation 2.3: $dV/dt=k(V^*-V)$, where for temperature programmed experiments, $T=f(t)$. For linear rise in temperature $T-T_o=Ct$ where C is heating rate. It has been reported that different volatile products are released depending on the temperature ranges [59] or the temperature histories [60]. This fact has not diminished the interest in the global kinetics for various reasons. One reason is that under certain conditions, tar is a dominant product of pyrolysis for a significant part of the process [59], so that prediction of total mass loss would allow prediction of tar release rate. A second reason is that global kinetics are looked to as offering a clue to the key mechanistic steps in the overall pyrolysis process [61].

Carrasco [62] conducted an extensive review of the different computing methods (used to analyze Equation 2.3) in the literature leading to the determination of the kinetic parameters of thermal decomposition reactions and compared the results obtained by using those methods for coal. Those methods do not reproduce the values of activation energy and reaction order when the same data are taken for computation. Due to the above mentioned shortcomings of these methods listed in Appendix A, these methods are of little use for pitch or bitumen pyrolysis studies, except for the integral method. Table 2.3 summarizes some of the methods used for

analyzing data via Equation 2.3 and the Anthony-Howard model (Equation 2.8). However, there is no comparison of the kinetic parameters derived from the methods listed in Table 2.3 reported yet for pitch. A detailed description of these methods is found in Chapter 5.

Table 2.3 Summary of the Analysis Methods Used in Constant Heating Rate Pyrolysis

Integral Method	$-\ln\left(\frac{V^*-V}{V^*}\right)=\frac{k_o}{C}\left[T e^{-E/RT}+\frac{E}{R}E_i\left(-\frac{E}{RT}\right)\right]$	(2.9)
Friedman Method	$\ln\left(\frac{C}{V^*}\frac{dV}{dT}\right)-\ln\left(1-\frac{V}{V^*}\right)=\ln k_o-\frac{E}{RT}$ The values of dV/dT is calculated by using two adjacent pairs of the volatile and temperature data: $\frac{dV}{dT}=\frac{V_{i+1}-V_i}{T_{i+1}-T_i}$	(2.10) (2.10a)
Coats-Redfern Method	$\ln\left(\frac{-C\ln\left(1-\frac{V}{V^*}\right)}{RT^2}\right)=\ln\frac{k_o}{E}\left(1-\frac{2RT}{E}\right)-\frac{E}{RT}$	(2.11)
Chen-Nuttall Method	$\ln\left(\frac{-C(E+2RT)}{RT^2}\ln\left(1-\frac{V}{V^*}\right)\right)=\ln k_o-\frac{E}{RT}$	(2.12)
Anthony-Howard Model (1976)	$\frac{V}{V*}=1-\int_0^\infty \exp\left[-\int_0^t k(E)\,dt\right]f(E)\,dE$ $f(E)=\left(\frac{1}{s\sqrt{2\pi}}\right)\exp\left[-(E-E_0)^2/(2s^2)\right]$	(2.8a) (2.8b)

where the heating rate C=dT/dt in the above table.

2.4 Compensation Effect of Kinetic Parameters

On determining the kinetic parameters from the thermoanalytical curves with the single overall reaction model (Equation 2.3), variations in the kinetic parameters are encountered due to the variation in physico-chemical properties (such as sample size), measuring conditions and the mathematical methods employed to derive the kinetic parameters. Thus high values of activation energy would be compensated by high values of the pre-exponential factors to give the same rate

constant k value. Further analysis of the variation of the kinetic parameters for a series of reactions leads to a general result of a mutual dependence of the kinetic parameters, termed as the kinetic compensation effect expressed by:

$$\ln k_o = \alpha E + \beta \qquad (2.13)$$

The above equation indicates the linear dependence between the values of the logarithmic pre-exponential factor $\ln k_o$ and the activation energy E with the constants α and β. The simple relationship of the above equation is reproduced on the Arrhenius coordinates, lnk vs. 1/T, with an intersection point called the isokinetic points ($1/T_{iso}$, $\ln k_{iso}$) [63]. Using the isokinetic relationship, the above equation is rewritten as:

$$\ln k = a + b\frac{1}{T} \qquad (2.14)$$

The kinetic compensation effect was first identified by Constable [64] from studies of dehydrogenation of ethanol on copper. Subsequently, a large number of further examples of comparable patterns of kinetic behavior have been described for many diverse surface heterogeneous catalytic reactions. Occurrence of such a compensation behavior between $\ln k_o$ and E has been widely investigated in recent years. In particular, the existence of the compensation effect in thermal dehydration and decomposition reactions of solid inorganic and organic materials has been reported [65]. Numerous papers have dealt with the variation of the apparent kinetic parameters using Equations 2.13 and 2.14. In addition, comparable relationships were found during these analyses of reported kinetic data. Additional trends could be also recognized if the survey was extended further or experimental measurements obtained for additional systems [66]. However, despite these many and various examples of compensation behavior, there remain important difficulties in establishing the range of meaningful application and the usefulness of Equations 2.13 and 2.14 in the understanding of the significance of kinetic observation. Although

the present state of understanding of the kinetic compensation effect can be found in many historical surveys [66-71], no single theoretical explanation of compensation behavior has been recognized as having general application. The factors to which references are made most frequently are surface heterogeneity in catalytic reactions and the occurrence of two or more concurrent and/or consecutive reactions in thermal decomposition processes. The causes of the kinetic compensation effect in thermal decomposition reactions may be classified into the three categories discussed below: sample physico-chemical properties, measuring conditions, and the mathematical methods used to derive the kinetic parameters. At present time, however, doubt remains concerning the general theoretical implications of the compensation relation despite the very many reported instances of obedience of Equation 2.13. Accordingly, this short review emphasizes the interrelation between kinetic characteristics and the chemistry of thermal decomposition processes.

2.4.1 Effect of Sample Physico-Chemical Properties on the Kinetic Compensation Effect

A typical example of the physico-chemical interpretation of the kinetic compensation effect is seen for the thermal decomposition of $CaCO_3$, under various partial pressures of CO_2. In 1935, Zawadski and Bretzsnajder [72] originally pointed out the variation in E with CO_2 partial pressure. Another example is seen for the thermal decomposition of $CaC_2O_4 \bullet H_2O$, with various sample sizes. The activation energy was found to decrease with the increase of sample size [73]. A theoretical interpretation for this effect was attempted by Pavlyuchenko and Prodan [74]. The kinetic behavior was reinvestigated experimentally by Wist [75] and analyzed by Roginski and Chatji [76] from a viewpoint of chemical statistics. Attempts have been made to explain the empirical kinetic compensation effect by using the physico-chemical variables, such as partial pressure of a gas [77], bond energy due to the different metals and ligands [78-80], defect

concentration [81], chemical composition [82], impurities [83] etc., other than reaction rate and temperature. Guarini et al. [84] pointed out that nonlinearity of the Arrhenius plot increases with the sample size, and recommended extrapolation to zero mass to avoid the kinetic compensation effect. Sample size dependent variations in the Arrhenius parameters have been explained by the effect of gradients in temperature and gaseous pressure [73]. In thermal analysis, however, the physico-chemical properties are difficult to identify quantitatively, because of the macroscopic character of the kinetic data derived from TGA curves. Without quantitative identification of the physico-chemical properties, estimation of the linear interdependence of Equation 2.13 does not provide meaningful kinetic interpretation, but only shows an empirical observation of the mutual dependence of the kinetic parameters.

2.4.2 Effect of Experimental Conditions on the Kinetic Compensation Effect

One of the examples is also seen for the thermal decomposition of $CaC_2O_4 \bullet H_2O$, under various heating rates [73, 85, 86]. It was found that the activation energy E decreased with the increase of heating rate. It is generally accepted that the experimentally resolved shape of a TGA curve changes with the measuring conditions applied, such as heating rates, atmosphere, etc. [85]. In many cases, the kinetic parameters obtained from such a TGA curve are also dependent on the measuring conditions applied, showing empirically the kinetic compensation effect. The kinetic compensation effect caused by the effect of heating rate is rather common for the thermal decomposition of solids with gaseous products [87,88]. On discussing the kinetic compensation effect obtained from different measuring conditions, both effects of heating rate on the sample physico-chemical properties and the changes in the sample caused by reaction itself should be taken into consideration. The latter is closely connected with the reliability of the experimentally resolved shape of the TGA curve as a source of kinetic data [89, 90], because such changes in the

sample is not controlled, in a strict sense, in conventional TGA measurements. A typical example can be seen for hydrocarbon pyrolysis in which the chemical structure and makeup is undergoing constant change.

2.4.3 Analysis of One TGA Experiment with Different Models or Methods

Discussion of the mutual dependence of the kinetic parameters has also been attempted from the mathematical and statistical points of view. Because the kinetic parameters have meaning only in relation to the mathematical functions of the kinetic model, these are distorted by an inappropriate kinetic model function. Criado and Gonzalez [91] reported that sets of kinetic parameters calculated using inappropriate kinetic model functions show mutual dependence. The degree of the distortion was further discussed on the basis of an empirical analysis [92, 93] and a mathematical approximation [94]. Reexamination of the kinetic compensation effect of this type was performed by Somasekharan and Kalpagam [95], who suggested the correspondence between the isokinetic temperature and the maximum TGA peak.

However, application of the Arrhenius equation to complicated solid-state processes has been questioned [96]. Hulett [97] made a search for the nonlinearity of the Arrhenius plot, determining that any derivations from a straight line in the plot of lnk(T) vs. 1/T are to be considered as almost certain evidence that the observed process is complex. Drawing the theoretical TGA curves, correlation of the kinetic parameters and its effect on the TGA curves were noticed by Sesták [98] and further analyzed by Zsakó [99]. Exner [100] first suggested that it is not correct to determine the kinetic compensation effect by a linear regression of E vs. $\ln k_o$, because these quantities are mutually dependent. Agrawal [101] proposed dividing the kinetic compensation effect into two groups by the existence of an isokinetic point: one arising from physico-chemical factors and the other from computational and experimental artifacts. Because

k(T) and T can be determined independently, the plot of lnk(T) vs. 1/T is statistically correct. However, Agrawal's procedure of distinguishing a false kinetic compensation effect from a true one was criticized by Sesták [102] and was shown by Zsakó and Somasekharan [103] to be incorrect. Garn's view is that the kinetic compensation effect is simply a consequence of trying to describe a complex process by computing one of the kinetic parameters in Equation 2.3 and dumping the results of computed variations into the remaining 'constant', accepting changes of many orders of magnitude without question or test [104].

2.4.4 Interaction of the Causes

According to the procedure of TGA kinetics of thermal decomposition reactions, the sample physico-chemical properties, experimental conditions and the resulting mutual dependence of the kinetic parameters seem to be interpreted separately [105]. However, the causes seem to be interrelated and inseparable. The TGA curve is a response of a certain averaged behavior of the respective reaction steps involved for the case of the thermal decomposition. The mutual relationship of the consecutive and/or concurrent steps may change with the experimental conditions applied (such as heating rates) and the changes in the sample, influencing the overall characteristics of the reaction. The variation in the overall behavior for a reaction is only detected as changes in the position and shapes of the experimentally resolved TGA curves. The kinetic parameters calculated from these macroscopic data are projected on the Arrhenius coordinates through a particular projection system, i.e., the general kinetic equation. The variation in the respective kinetic parameters apparently results from changes in the experimental and physico-chemical factors. However, the resulting mutual dependence of the kinetic parameters, usually stated as the kinetic compensation effect, seems to be connected with the properties of the mathematical methods used to analyzed the general kinetic equation (Equation 2.3). In such a

case, not knowing the properties of the general kinetic equation concerning the kinetic compensation effect, interpretation of the mutually dependent variation of the Arrhenius parameters connected with the physico-chemical properties of the kinetic process is likely to lead to a speculative conclusion. However, recognition of the kinetic compensation effect would give some insights to the relationship between the logarithm of pre-exponential factor, $\ln k_o$, and activation energy E, and further give guidelines of application and explanation of the kinetic parameters. The magnitude of the rate constant is therefore of more importance than that of each of the kinetic parameters k_o and E.

Chapter 3 Experimental Procedures and Apparatus

3.1 Introduction

In this chapter, the experimental procedures which outline each operational step employed in the present work are discussed. The first part of this chapter deals with the materials, sample preparation and characterization. This is followed by the description of the experimental apparatus. Finally, the experimental techniques are presented.

3.2 Sample Preparation and Characterization

The CANMET pitch was obtained from Combustion Group of Department of Chemical Engineering at UBC, which obtained the pitch sample from CANMET in barrels for combustion study. The Syncrude pitch was obtained from the sample bank of Syncrude Canada Ltd. in 10kg containers. Representative samples were then taken from CANMET pitch barrels and Syncrude pitch containers and stored in a refrigerator for the subsequent characterization analysis, TGA study and Pyroprobe-GC study.

Each of the two pitch samples was used as received. Representative samples of CANMET and Syncrude pitches were sent to MicroAnalytical of Delta, Vancouver for ultimate analysis. Results are given in Table 3.1, along with the proximate analysis determined by TGA and solvent fractionation with pentane and benzene. The latter were determined by dissolving 5 mg of pitch sample into 200 ml pentane and benzene respectively in an ultrasonic bath (~ 25 °C for 30 min). The pentane or benzene soluble fractions were clarified over filter paper and the insolubles washed and dried at room temperature for 12 hours. The weight of the insolubles was recorded. The atomic ratios were also calculated and given in the same table. It is evident that the chemical structure and makeup of Syncrude pitch are different from those of CANMET pitch. Syncrude pitch has higher H/C, S/C atomic ratios and lower N/C, O/C atomic ratios. This observation is in

good agreement with the low pentane and benzene insolubles. It is expected that the pyrolysis behavior of these two pitches might be different due to those chemical differences. Both pitches contain limited amounts of ash and oxygen. Syncrude pitch contains more sulfur than the CANMET pitch.

Table 3.1 Pitch Characterization Analysis -- Ultimate Analysis

As received	CANMET Pitch		Syncrude	Suncor	Maya[106]
	This Work	Lim [10]	Pitch	Pitch [8]	Residuum
Carbon %	85.32	86.2	82.72	82.8	83.6
Hydrogen %	9.33	7.1	10.35	7.9	9.3
Nitrogen %	0.82	1.1	0.52	1.0	0.5
Sulfur %	2.39	2.8	4.73	5.8	5.8
Oxygen %	1.12	1.0	0.97	--	0.5
Others %	1.02	1.8	0.71	--	--
	100.00	100.00	100.00	97.5	99.7
H/C	1.31	0.99	1.50	1.145	1.335
N/C	0.0082	0.011	0.0054	0.0104	0.0051
O/C	0.0098	0.0087	0.0088	--	0.0045
S/C	0.011	0.0012	0.021	0.0263	0.026
Proximate Analysis %					
Volatile	81.17	--	90.11	--	--
Fixed Carbon	18.65	--	8.65	--	--
Ash	0.18	--	1.24	1.6	--
Solvent Fractionation %					
Pentane insolubles	45.15	--	33.58	39.5	--
Asphaltene	35.65	--	25.77	--	--
Benzene insolubles	9.50	--	7.81	--	--

The ultimate analysis results of CANMET and Syncrude pitch samples in this research are similar to those reported by previous workers [8, 10, 106].

3.3 Experimental Apparatus

The CANMET pitch and Syncrude pitch were pyrolyzed with TGA at low heating rates using U.H.P. Nitrogen as purge gas, and with Pyroprobe-GC at high heating rates using U.H.P. Helium as carrier gas. The volatile yield (or the weight loss) was recorded with TGA dynamically as a function of temperature via a computer. The weight of the pitch sample and the residue of

Pyroprobe-GC pyrolysis was recorded before and after each run at the selected operating conditions. The weight loss in the Pyroprobe pyrolysis can then be calculated by subtracting the residue weight from the initial sample weight. The volatiles were swept into the on-line GC for analysis of the chemical composition.

3.3.1 Thermogravimetric Analysis (TGA) Setup and Operation

The pyrolysis of CANMET and Syncrude pitches was performed on a Perkin-Elmer TGS-2 TGA. The model TGS-2 (referred to as the TGA in the following text) is designed for accurately recording the weight loss (or volatile content) of a sample as it is subject to a precisely controlled temperature environment. It is capable of controlled heating rates of 0.31 to 320 °C/min. It is a completely modular system consisting of the following units: the thermo-balance analyzer; the electronic balance control unit; the heater control unit; the temperature program control unit, data acquisition computer, plotter and purge gas system.

The balance system consists of a Perkin-Elmer AR-2 recording balance (including an analyzer and balance control unit) which can be used together with a recorder as a recording balance independently of the other components. The temperature program control is the unit which provides the control over the starting temperature, heating rate, stopping temperature and holding time. The heater control unit is a power supply source which provides the controls for calibrating the furnace so that the sample temperature is that temperature indicated on the programmer readout. It provides thermocouple circuitry for monitoring the temperature of the sample environment.

In order to record the weight loss versus temperature information, the temperature was calibrated each two weeks and when the furnace was changed. An inert purge gas was also used to avoid oxidation of samples and volatiles during each run.

The TGA temperature is controlled through a closed-loop, heater-sensor resistance thermometer circuit, using the furnace winding as both sensor and heater. Reproducible, linear temperature programs are thus achieved. A calibration must be performed, however, to make sure that the temperature at any given moment is that specified during experimental runs.

The calibration is first performed at the factory, where adjustments are made to assure the temperature of the sample agrees with the program temperature. After operating the instrument for a period of time, calibration is also necessary to assure best temperature control accuracy.

The calibration can be accomplished by changing the heater control unit range and zero settings to force agreement between the program temperatures and the thermocouple temperatures (or a magnetic transition standard, a Curie point calibration standard). However, a more convenient method was used, employing a calibration routine built in the heater control unit. This routine automatically checks and corrects the thermocouple temperature at three program temperature points.

The calibration routine forces correspondence between the program and sensor temperature at T MIN (50 °C), T MAX (1000 °C) and the temperature midway between T MIN and T MAX. The calibration sequence is begun by pressing the CALIBRATE and RESET keys on the control unit keypad. The control unit then programs to T MIN, waits for thermal equilibrium, and measures the difference between the sample temperatures and program temperatures. It then corrects the furnace set-point, allows equilibrium, and again checks for agreement. This procedure is repeated until the discrepancy is less than 0.5 °C. The above procedure is repeated for the intermediate temperature and T MAX and the TGA is then considered calibrated.

The control unit forces the sample temperature and the program temperature to agree exactly at 3 points, and approximates a correction for the rest of the scale. The control unit

interpolates correction between T MIN and T MAX, so that the TGA is calibrated for the whole temperature range. When the calibration is completed, the program temperature and actual temperature agrees within 2 °C or better [8, 62].

The positions of the furnace and the sample pan are very important for correct temperature control. The position of the furnace itself can be changed horizontally or vertically by using the adjustments under the furnace support assembly. The ideal position of the furnace is in the center of the furnace assembly as shown in Figure 3.1. A more detailed sketch of the TGA furnace is also shown in the same figure. The top of the furnace should be 10 mm below the anti-convection shield and the top of the stirrup should be recessed by about 1 to 2 mm into the furnace. The bottom of the sample pan should be 2 mm above the tip of the thermocouple. If it is not, another hangdown wire should be prepared, having the appropriate length in order to obtain the best performance.

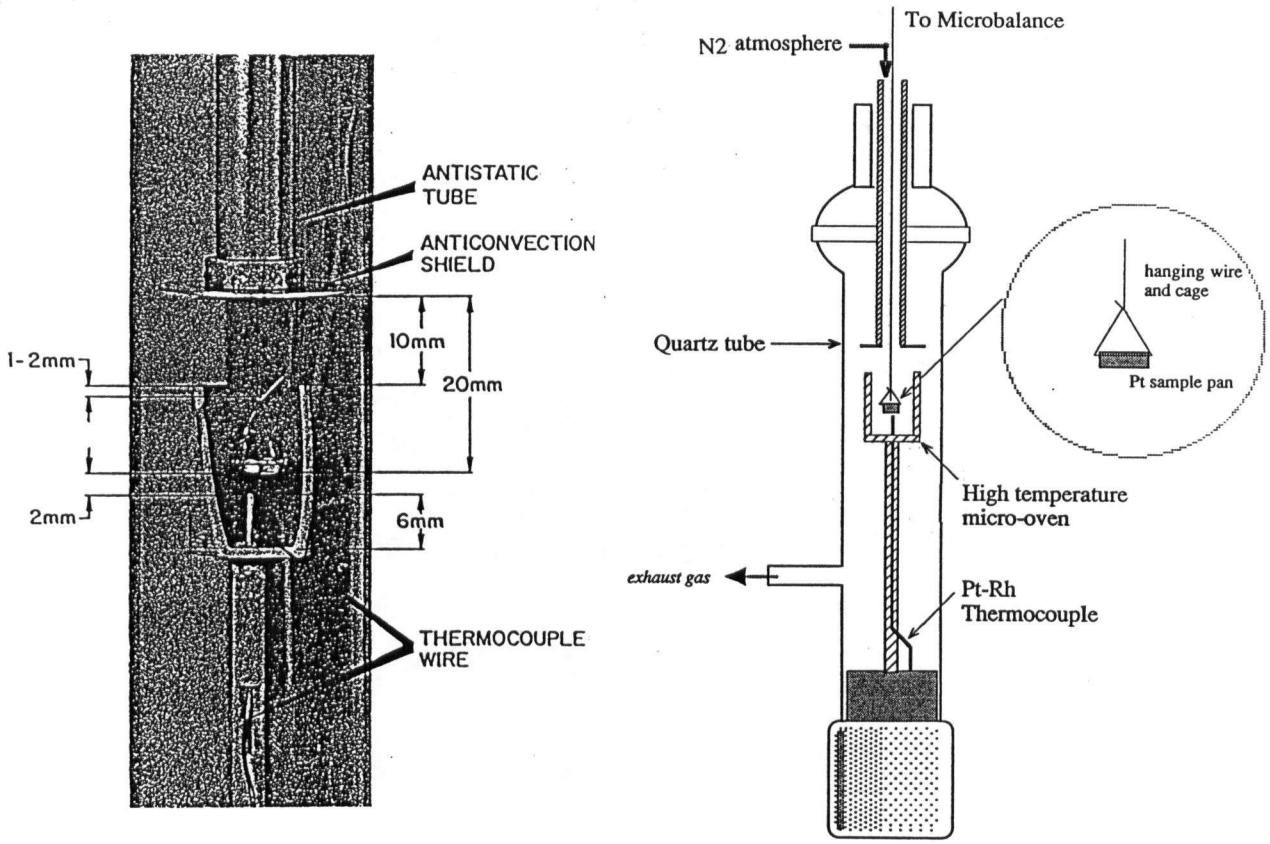

Figure 3.1 The relative position of the furnace and sample pan on the left and the TGA furnace sketch on the right

The thermal balance was continuously purged with inert U.H.P. Nitrogen gas when samples were being pyrolyzed in order to prevent decomposition products from flowing up and contaminating the balance mechanism and oxidation. A 20 minute purge was also applied before each run. The U.H.P. Nitrogen flowrate was set 100 mL/min and checked before each run.

The TGA had been calibrated at the factory so that when the instrument is set up using the proper configuration of furnace height, hangdown wire length, the temperature accuracy should be within one percent over the temperature range of the instrument. Temperature calibration was always made using a U.H.P. Nitrogen gas to achieve the same conductivity as an experimental run.

The pitch sample was applied to the sample pan carefully into a thin layer to achieve a better temperature uniformity and therefore temperature readings.

Once the temperature calibration was achieved, the temperature control unit was used to control the pyrolysis temperature. Different heating rates and final temperatures were used to study their effects on the pyrolysis of CANMET and Syncrude pitches. The heating rates employed in this study are 25, 50, 100, and 150 °C/min, the final temperatures 700, 750, 800, 850, 900, 950 °C. The following temperature program was used to achieve this conditions:

- Purge the TGA system for 20 minutes at room temperature before starting the run and then increase the furnace temperature to 50 °C.
- Hold at 50 °C for 5 minutes and then ramp to the final temperature at each selected heating rate.
- Hold at that final temperature for 10 minutes, then terminate the run and decrease the temperature to room temperature.

The sample temperature and weight (of sample as well as residue after certain pyrolysis) at any time was recorded using a computer data logger. The weight of sample was also recorded

at the beginning of each run. At any time, the remaining sample weight was recorded as the percentages of the original sample weight. The information of weight and temperature was then recorded into the computer, printed out as hardcopies, and converted into data files. The data files were used in the subsequent analysis and modeling.

3.3.2 Pyroprobe-GC

The pyroprobe-GC is a relatively new type of equipment constructed for dynamic analysis of pyrolysis products from the probe by using in-line Gas Chromatography. The main advantages of this piece of equipment are the temperature programmable probe, high temperature ramping rates and small quantity of samples required in the GC analysis. The Pyroprobe-GC consists of the following modular units: Pyroprobe 1000 controller, Pyroprobe interface, Varian GC 3600, Computer Workstation, and gas system, as shown in Figure 3.2.

The CDS Instruments Pyroprobe 1000 is a resistively heated platinum filament pyrolyzer which prepares samples for analysis by gas chromatography. The Pyroprobe 1000 controller calculates the resistance of the filament and supplies the proper voltage needed to achieve the setpoint temperature. Heating rates are selectable in increments of 0.01 °C per millisecond to 20 °C per millisecond. Final temperature ranges in 1 °C increments to a maximum of 1400 °C. Final holding time may be selected from 0.01 seconds to 99.99 seconds. All parameters are entered by simple key strokes on the front panel of the controller module.

Samples may be pyrolyzed using a variety of filament designs. The standard model Pyroprobe 1000 includes a coil element and a ribbon element. The coil element, which heats samples held in a quartz tube, was used to pyrolyze the pitch samples in order to record the weight of the sample and the residue to calculate the volatile yield.

The gas chromatograph interface for the Pyroprobe is a heated chamber which houses the probe during pyrolysis. This chamber attaches to the injection port of the gas chromatograph by means of a welded needle nut assembly which replaces the septum retainer. Carrier gas is brought into the interface, sweeps through the heated chamber containing the probe and exits through the needle nut assembly into the injection port of the gas chromatograph.

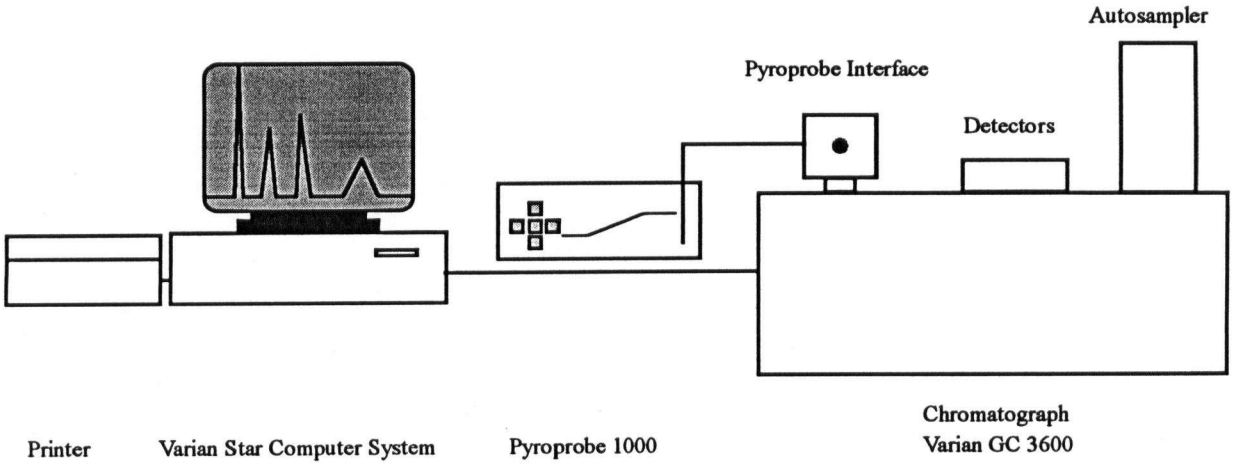

Figure 3.2 The Pyroprobe-GC setup

All flow entering the injection port comes from the interface. It is important to remember that the Pyroprobe interface is plumbed upstream from the column, and opening the chamber for probe placement permits air to enter the chromatographic system. Therefore, probe placement and removal should be performed when the column is cool to prevent oxidation of the column liquid phase.

The Pyroprobe interface was installed (Figure 3.3) by inserting it between the gas chromatograph carrier gas flow controller and the injection port. The standard interface has three gas fittings and one electrical connection. The electrical connector attaches to the rear of the Pyroprobe controller to supply current to heat the interface and permits temperature monitoring. The three gas fittings are: 1) a large opening in the front for the interface to accept the probe; 2) a

1/8" Swagelok fitting which attaches the interface to the welded needle nut assembly of the injection port of the gas chromatograph; and 3) a length of stainless steel tubing with a 1/16" Swagelok fitting to connect to GC carrier flow. The large opening for the probe may be sealed with an interface retainer to permit syringe injections directly into the interface. A more detailed sketch of the pyroprobe head is shown in Figure 3.3a.

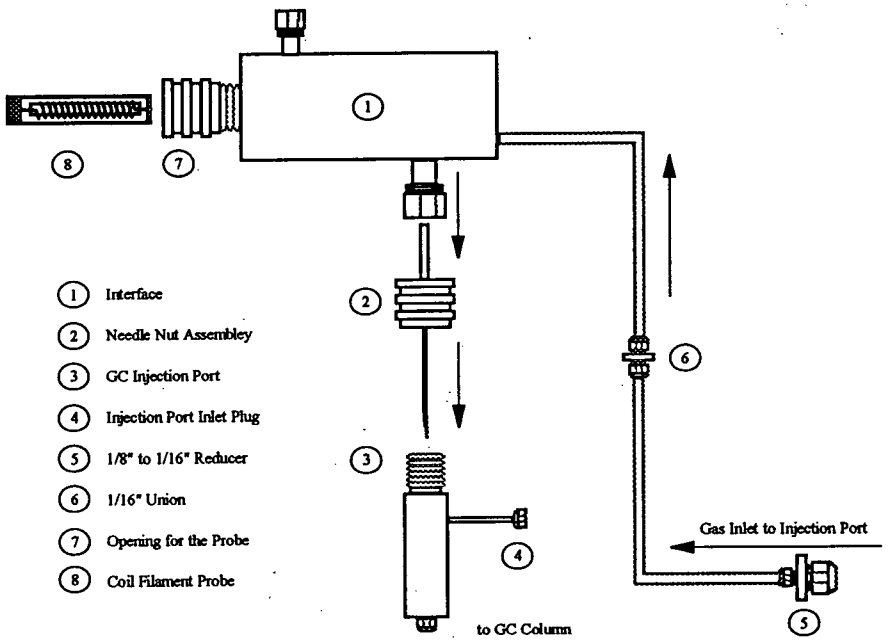

Figure 3.3 The installation of Pyroprobe interface into the GC injection port.

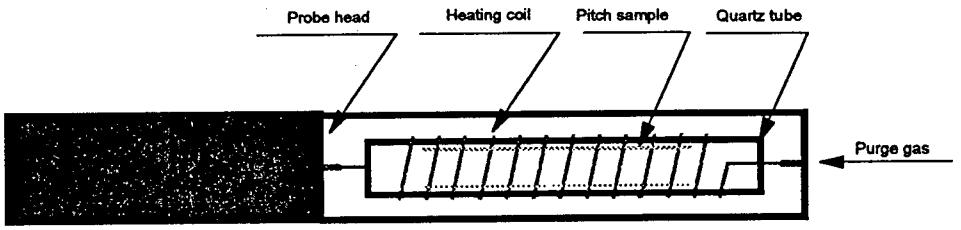

Figure 3.3a The sketch of Pyroprobe with pitch sample applied on the inner surface of quartz tube

The 1/16" stainless steel tubing must be connected to the carrier gas for the GC column. Flow is disconnected from the injection port and the inlet there capped while the flow is connected to the Swagelok fitting on the end of the 1/16" tubing. This will bring GC flow into the

interface, where it proceeds through the probe chamber and then into the injection port through the needle nut assembly. For pyrolysis, the probe seal in the collar of the probe makes a gas tight connection while the probe is in the interface. This seal was checked and replaced regularly to insure sealing.

A sample of around 5 mg was applied uniformly onto the middle section of the inner-surface of the quartz tube which then was inserted into the Pyroprobe heating coil. The quartz tube is 1" long and 1/8" in diameter. The heating coil is interfaced with the GC station as shown in Figure 3.3. The pyrolysis product is purged into the GC injection port by Helium carrier gas.

Proper sample handling plays a very important role in achieving reproducible pyrolysis. Best results are obtained by using as small a sample as possible to prevent thermal gradient effects and to insure that the sample is completely pyrolyzed. It is important to remember that the Pyroprobe is being used as a sample introduction device for the gas chromatograph and the sample size should be consistent with what is generally injected onto the column. The best reproducibility was obtained using samples of about 5 mg.

The Pyroprobe 1000 was used to control the heating rates and final temperature. The temperature was calibrated according to the calibration number of the heating coil supplied by the manufacturer. Heating rates employed in this study are 600, 3000, 30 000 and 300 000 °C/min, and final temperatures are 500, 600, 700, 800, 900, 1000 °C. Pyrolysis times used are 0, 5, 10 seconds. The following temperature program was used:

- Purge the Interface for 20 minutes at room temperature with U.H.P. Helium.
- Ramp to the final temperature at the selected heating rate.
- Hold at that final temperature for the selected pyrolysis time, then terminate the run and decrease the temperature to room temperature.
- Through the experiments, the interface temperature was kept at 50 °C.

In the GC, a J&W DB-5HT fused silica capillary column was used. It is comprised of three major parts. Polymide is used to coat the exterior of the fused silica tubing to protect the fused silica tubing from breaking. The stationary phase is a polymer that is evenly coated onto the inner wall of the tubing. The predominant stationary phases are silicon based polymers (polysiloxanes), polyethlene glycols (PEG, Carbowax^{TM}) and solid adsorbents. The liquid phase in this column is DB-5HT. The column is 30 meters long with a diameter of 0.255 mm, and a film thickness of 0.10 μm. The column can be operated from -60 °C to 400 °C. In this setup the column was installed to FID and PID detectors. U.H.P. Helium is selected as the carrier gas for this capillary column. The carrier gas flow rate was then optimized during test runs as 1 mL/min.

The operation of the GC is controlled using the computer workstation. The GC and the Pyroprobe were started at the same time for each run. The GC analysis results were also gathered through this computer. The results can be printed out as hardcopies (including chromatograph and analysis results).

Due to the fact that this piece of equipment had not been widely used in the pyrolysis kinetic studies, a great deal of effort was required to configure the equipment and optimize the experimental conditions. This step consumed some four months of experimental time. The optimal conditions for pitch pyrolysis were found to be:

- Purging the interface chamber for 20 min. before starting a run.
- GC column temperature program: 40 °C for 10 min., ramping to 120 °C at the rate of 2 °C/min. and holding the final temperature for 10 min.
- GC column carrier gas flow rate 1 mL/min U.H.P. Helium.
- The Hydrogen flow rate is 20 mL/min, and the air flow rate is 375 mL/min.

A summary of the Pyroprobe-GC parameters used by the computer program is listed in Appendix B.

The weights of the sample and residue were recorded before and after each run. The volatile yield was then calculated by subtracting the residue weight from original sample weight at each condition. The FID analysis results of the released volatiles were logged with the computer workstation and used for subsequent recalculation and analysis for both pitches.

A typical Chromatogram is shown in Figure 3.4. The insert is the enlargement of the chromatogram for the period 8 to 45 min. The peaks indicate the major products. As can be seen, most of the pyrolysis products elutes within 5 min. Other products were also identified between retention time 8 and 45 min as shown in Figure 3.4. Syncrude pitch pyrolysis volatile analysis showed a similar chromatogram.

It is clear that it is difficult to identify each of the large number of peaks in Figure 3.4. A grouping scheme was therefore employed to simplify the identification and quantification processes. Similar lumping schemes have been successfully used in coal pyrolysis to estimate the yields of tar and gases [1, 17, 50]. Inseparable peaks were therefore grouped into six single peaks. The retention time of those groups are listed in Table 3.2 for the volatile of both pitches. The identification of species and quantification of yields are discussed in the following section.

Table 3.2 Important Peak Lumps on the Pyrolysis-GC Chromatograms

Lump No.	Retention Time min.	Mid-point min.
1	0.01- 4.73	2.370
2	8.84 - 15.86	12.350
3	19.17 - 23.97	21.570
4	24.24 - 31.72	27.980
5	32.11 - 36.01	34.060
6	37.49 - 42.66	40.070

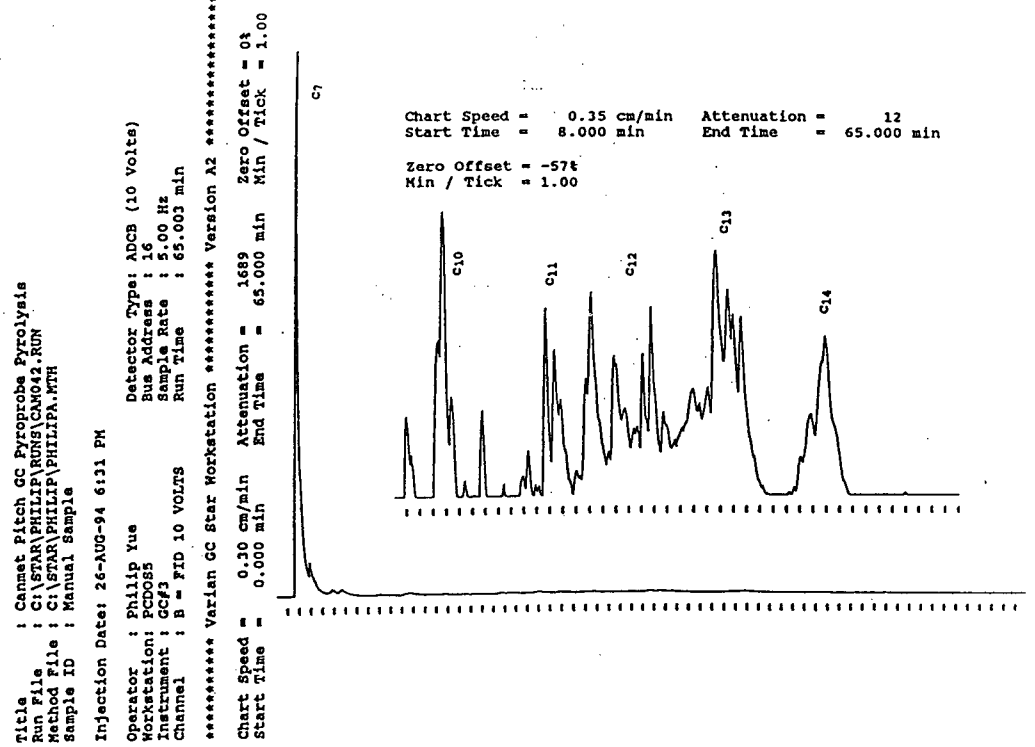

Figure 3.4 Chromatogram of CANMET pitch volatiles

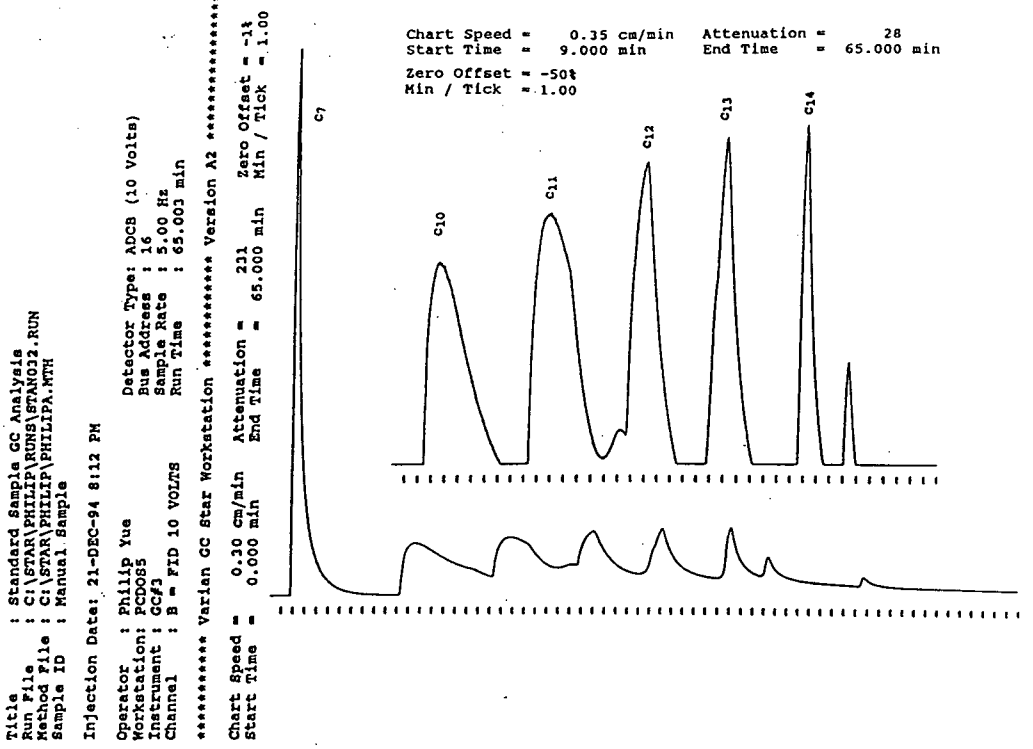

Figure 3.5 Chromatogram of standard sample

3.3.3 Peak Identification and Quantification

In order to identify species from the chromatograms, standard samples of paraffin C_6-C_{16} and aromatics C_6-C_{14} were obtained and analyzed individually for retention time. The retention times of the peaks of interest for both CANMET and Syncrude pitch volatiles match those of paraffin: n-Heptane, n-Decane, n-Undecane, n-Dodecane, n-Tridecane, and n-Tetradecane. A standard sample was then designed according to the individual retention time of each standard sample and the characteristics of the chromatogram obtained for CANMET pitch and Syncrude pitch pyrolysis products. The standard sample consists of equal amount of n-Heptane, n-Decane, n-Undecane, n-Dodecane, n-Tridecane, and n-Tetradecane (C_7, C_{10}, C_{11}, C_{12}, C_{13}, C_{14}). The standard sample analysis chromatogram is shown in Figure 3.5. The insert is the enlargement of the chromatogram from 9 to 45 min. The retention times of aromatics were detected separately and listed in Table 3.3 for comparison. As can be seen, the retention times fall into those of the volatile lumps and close to that of each paraffin component with the same carbon number. The retention time of each component in this standard sample is listed in Table 3.3.

Table 3.3 Retention Time of Each Component

Paraffins	Retention Time min	Aromatics	Retention Time min
Hexane C_6	1.489	Benzene C_6	1.780
Heptane C_7	1.933	Toluene C_7	
Octane C_8	2.959	Xylene C_8	4.684 (p)
Nonane C_9	6.208	Cumene C_9	6.473
Decane C_{10}	12.025	Butylbenzene C_{10}	13.500
Undecane C_{11}	20.882		
Dodecane C_{12}	27.894		
Tridecane C_{13}	34.051		
Tetradecane C_{14}	40.030	Octylbenzene C_{14}	43.212

The peak identification was based on two criteria:

- the time at which the peak elutes (retention time) and
- the size of the peak (response)

Both these criteria were used to identify not only peaks of interest, but also to eliminate from consideration those peaks that are not analytically significant (because of retention time or relative size). The quantification was then performed according to an external standard.

External standard calculation allows one to determine the absolute amount of the compounds of interest, without regard to the total area or height, or the area or height of any other peaks in the chromatogram. The peaks of interest must be identified in a peak table, and the detector response is calibrated to these peaks by injecting a known amount of each compound in a run to determine the Calibration Factor.

Peak lump to 4.73 minutes may contain lighter gases up to C_9. However, it was impossible to separate this lump into detailed peaks in a practical time scale with the column being used since the wide spectrum of the components in the volatile. It was therefore lumped as one peak and estimated using the response factor of C_7. The yield therefore obtained is a rough estimation. The heavier components were lumped in the same fashion. The yield of each is also an estimation.

Following identification of the peaks in the chromatogram, the yields were calculated according to the parameters specified through the computer station. The results can be calculated to meet the analytical requirements. The yields of each component were then calculated using an external standard as outlined in the Varian Star Computer System User Handbook.

In the external standard calculations, peaks were reported in amounts. The calculation in this study gave results in weight (mg). External standard calculation was also done in two stages. First, Calibration Factors developed during a Calibration run are stored in the computer program, then, during an Analysis run, these factors are used to produce the final calculated results.

Calibration Factors for External Standard calculation are absolute factors that are not relative to any component and are based upon an absolute amount injected. The following equation is the formula used to develop Calibration Factors for External Standard calculations:

$$FACTOR_i = \frac{AMOUNT_i \times AMT\ STD}{AREA_i} \times 10000$$

$AMOUNT_i$: Peak$_i$ AMOUNT in Peak Table.

AMT STD: Amount Standard 1.000, constant

$AREA_i$: the Peak$_i$ area.

10000: constant used to calculate the scale factor.

The following equation shows the formula used for External Standard calculations during an analysis run.

$$RESULTS_i = \frac{AREA_i \times FACTOR_i}{DIVISOR \times 10000} \times MLTPLR$$

$AREA_i$: Peak$_i$ area.

DIVISOR: Divisor 1.000, constant

$FACTOR_i$: Peak$_i$ FACTOR in Peak Table is used for identified Peaks

MLTPLR: Multiplier 1.000, constant

10000: constant used to compensate for scaled factor.

$RESULT_i$: Final External Standard calculation results, mg.

The operation parameters used with TGA, Pyroprobe and GC are summarized in Table 3.4.

Table 3.4 The Summary of Operation Parameters Used by TGA, Pyroprobe and GC

	TGA	Pyroprobe	GC
Purge Time min	20	20	20
Purge Gas/Flow Rate mL/min	100	1	1
Initial Temperature	50 (5 min)	50	40 (10 min)
Heating Rate °C/min	25, 50, 100, 150	600, 3000, 30000, 300000	2
Final Temperature °C	700, 750, 800, 850, 900, 950	500, 600, 700, 800, 900, 1000	120
Holding Time	10 min	0, 5, 10 s	10 min

Chapter 4 Experimental Results

4.1 TGA Experimental Results

4.1.1 TGA Pyrolysis of CANMET Pitch

The TGA pyrolysis of CANMET pitch was performed under different experimental conditions to study the effects of sample weight, heating rate, and final pyrolysis temperature. The sample weight was varied between 4.4 and 17.2 mg. The heating rates employed were 25, 50, 100 and 150 °C/min and final temperatures of 700 to 950 °C in 50 °C increments. Each run was performed with a 10 minute holding time at final temperature.

4.1.1.1 Effect of Sample Weight

The sample weight effect on CANMET pitch pyrolysis was investigated under heating rates of 50 °C/min and 100 °C/min and final temperature 900 °C for different sample weights ranging from 4.4 to 17.2 mg. The operating conditions and experimental results are provided in Tables 4.1.1 and 4.1.2. $V_{t=0}$ and $V_{t=10}$ refer to the total volatile yield (or weight loss) in percentage of the original sample weight at 0 minute and 10 minutes pyrolysis reaction time at the final temperature. For this pitch, some 80% is converted into volatiles, and about 20% is left as solid residue under these conditions. The shapes of the chromatograms will be discussed in Section 4.1.3. Here just the final residue numbers are discussed.

Figures 4.1.1 and 4.1.2 show that the weight loss decreased (the solid residue increased) with increases in sample weight. This may indicate an internal mass transfer effect. With larger sample sizes, the volatile release from the residue matrix may be hindered, resulting in more char. It appears that the decrease is not linear and the weight loss exhibited a shallow minimum at a sample weight of about 14 mg for runs at 100 °C/min and 15 mg at 50 °C/min, at both zero and ten minute holding times. Since the slight increase appears at both heating rates, a polynomial

rather than a straight line fit was done to illustrate the general trend of data. The weight loss reduced from 82.89% at sample weight 4.406 mg to 79.85% at sample weight 15.78 mg for t=0 minute, while the weight loss reduced from 83.64% at sample weight 4.406 mg to 80.03% at sample weight 15.78 mg for t=10 minutes for runs at 100 °C/min heating rate. For runs at 50 °C/min heating rate, the weight loss reduced from 84.38% at sample weight 4.979 mg to 80.07% at sample weight 17.17 mg for t=0 minute, while the weight loss reduced from 82.89% at sample weight 4.979 mg to 79.9% at sample weight 17.17 mg for t=10 minutes. It is also clearly shown that the effect of holding time at any sample weight on the total weight loss is not significant for CANMET pitch, i.e. essentially all the reaction occurs during heating to the final temperature for each heating rate. A longer holding time may result in more residual H_2 release from solid char, but the amount is very small. This is in good agreement with the analysis of Nguyen [107], where only 1.56% of H_2 content was observed in the delayed coke. It is generally believed that the weight loss at this stage is caused by the H_2 release from the remaining char [9, 17, 30]. At lower heating rate, the results appear more scattered (Figure 4.1.2), and it may be caused by the longer pyrolysis time. It is expected that at sample weights below 14 mg, the pyrolysis process may be dominated by chemical reaction processes while at higher sample weights diffusional effect may occur. For reference, a single spherical particle of pitch of 14 mg would have a diameter of 1.5 mm. The statistical analysis of the sample size is shown no mass transfer effect in the range of 7.774~12.034 mg at 100 °C/min and 8.011~13.157 mg at 50 °C/min (Appendix I). The difference of weight loss as shown in Figures 4.1.1 and 4.1.2 (and figures in the following sections) is believed not the consequences of experimental errors. For the remaining work, the size of about 9 mg is used. It is believed that the results reflect the intrinsic kinetics and are not significantly affected by mass transfer. As will be subsequently shown, the calculated activation energy is greater than the range 8~24 kJ/mol typical of diffusion processes.

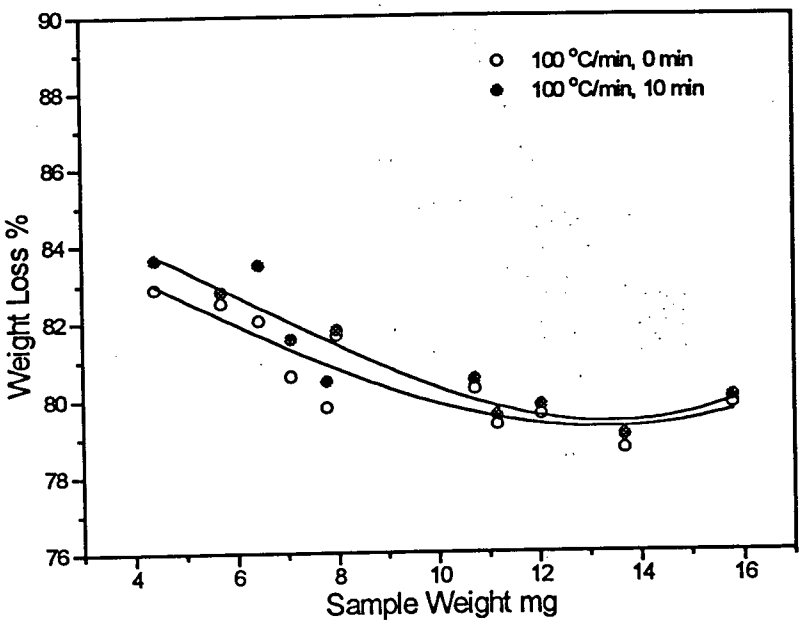

Figure 4.1.1 Sample weight effect on CANMET pitch pyrolysis with TGA at 900 °C and 100 °C/min

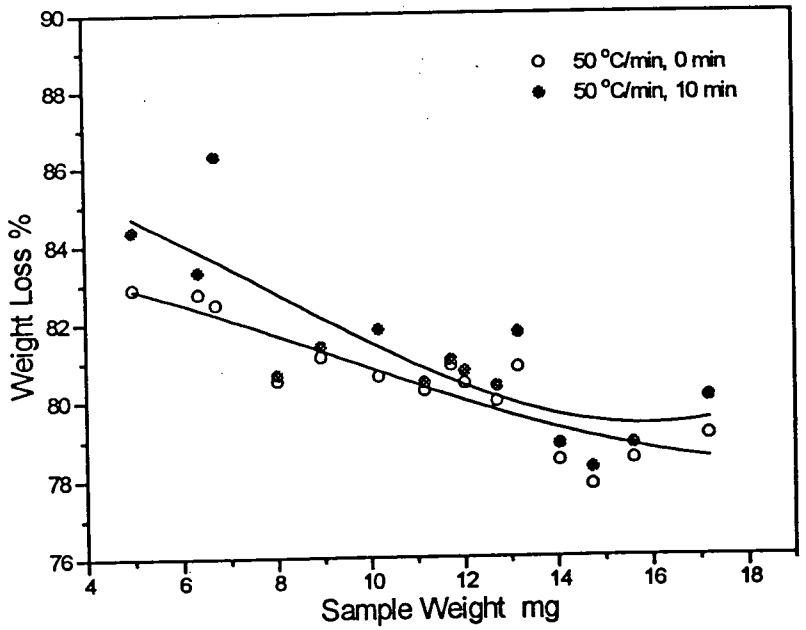

Figure 4.1.2 Sample weight effect on CANMET pitch pyrolysis with TGA at 900 °C and 50 °C/min

4.1.1.2 Effect of Heating Rate

To study the heating rate effect on the pyrolysis total weight loss with TGA, the heating rates were set at 25, 50, 100 and 150 °C/min with final temperatures of 700 °C and 800 °C. The sample weight was held constant around 8.216 to 9.668 mg in order to minimize the sample size effect. The operating conditions for the experiments are provided in Table 4.1.3. The volatile yield is the weight loss which occurred when the final temperature was reached, i.e. the holding time was zero.

Figure 4.1.3 shows the heating rate results with different final set temperatures. From this plot, it is observed that the total weight loss decreases weakly as heating rate is increased at both temperatures. At the same heating rate, the weight loss (volatile yield) is essentially the same for both temperatures, especially at heating rates smaller than 100 °C/min. The total weight loss reached 80.84% and 77.92% at 25 °C/min and 150 °C/min for 800 °C respectively. A decrease of 3% is observed due to the increase of the heating rate by a factor of six. The weight loss at 700 °C decreased to 79.93% at 150 °C/min from 81.59% at 25 °C/min. However, the decrease in total weight loss caused by either the temperature and heating rates is marginal. This indicates that the pyrolysis process is nearly complete at the temperature of 700 °C and further increase of the temperature does not significantly increase the total weight loss. In the range of low heating rates studied with TGA, the volatile "precursors" apparently have enough time to decompose and evolve from the sample, therefore no significant difference of weight loss is observed.

The effect of heating rate was also studied at much higher level with the Pyroprobe using heating rates of 600, 3000, 30,000 and 300,000 °C/min and final temperatures of 700 °C and 800 °C. The sample weight was held around 5.02 to 5.58 mg. The operating conditions are provided in Table 4.1.4. The volatile yield is the weight loss occurred when the final temperature is reached.

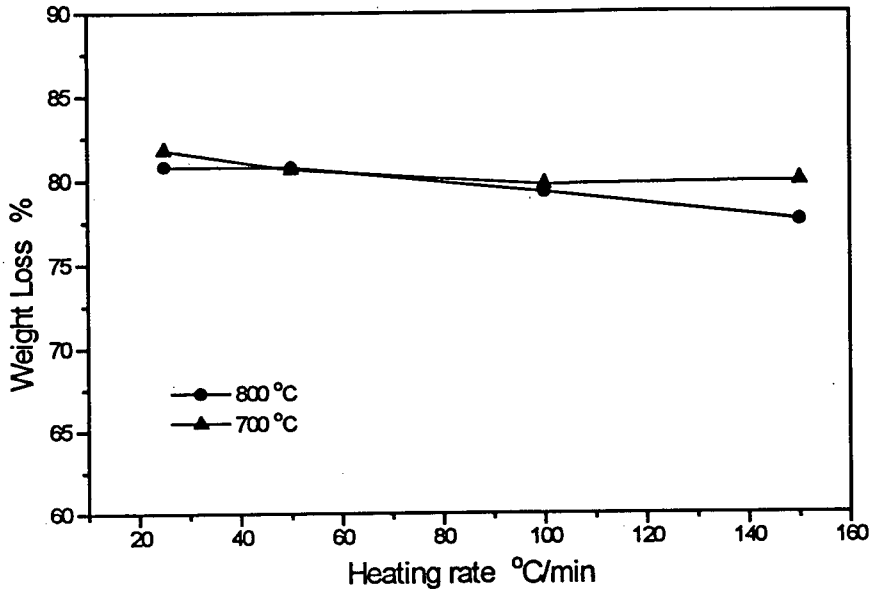

Figure 4.1.3 Heating rate effect on CANMET pitch pyrolysis with TGA

Figure 4.1.4 shows that with the Pyroprobe, the weight loss decreases nonlinearly with the increase of heating rate. The weight loss decreased from 49.06% for heating rate 600 °C/min to 2% for 300,000 °C/min at 800 °C, while the weight loss decreased from 12% for heating rate 600 °C/min to 1.89% for 300,000 °C/min at 700 °C. At very high heating rates, the weight loss is essentially the same for the two final temperatures. This suggests that the reaction time is an important factor. At high heating rates (>10,000 °C/min), the reaction time is extremely short, and the difference of weight loss is small. At low heating rates, the reaction time is long, the difference of weight loss is therefore greater. At very low heating rates, the components have enough time to undergo chemical changes, then the same weight loss would be observed. This is shown in TGA results at ≤ 100 °C/min.

Figure 4.1.5 compares the results using the TGA and the Pyroprobe. Results using the two procedures appear consistent. The weight loss decreased with increased heating rates over the full range studied, i.e., 25 °C/min to 300,000 °C/min. The weight loss decreased from 81.79% for

heating rate 25 °C/min to 1.8% for 300,000 °C/min at 700 °C and decreased from 80.84% for heating rate 25 °C/min to 2% for 300,000 °C/min at 800 °C. It is also observed that the temperature is a significant parameter between heating rate 100 °C/min to 30,000 °C/min, which indicates the pyrolysis is reaction controlled. At heating rates higher than 30,000 °C/min, the weight loss is much less than that at heating rate lower than 150 °C/min. The effect of heating rate may be due to pyrolysis reaction times. At heating rates above 30,000 °C/min, it takes less than 1.6 seconds to reach the final temperature of 800 °C, while it takes 320 seconds to reach the same temperature at 150 °C/min.

The rapid drop-off in Figures 4.1.5 and 4.1.9 which occurs for CANMET pitch heated to 700 °C and for Syncrude pitch may be caused by some combination of time and temperature effect. However, the reasons that it did not occur for CANMET pitch heated to 800 °C are not obvious.

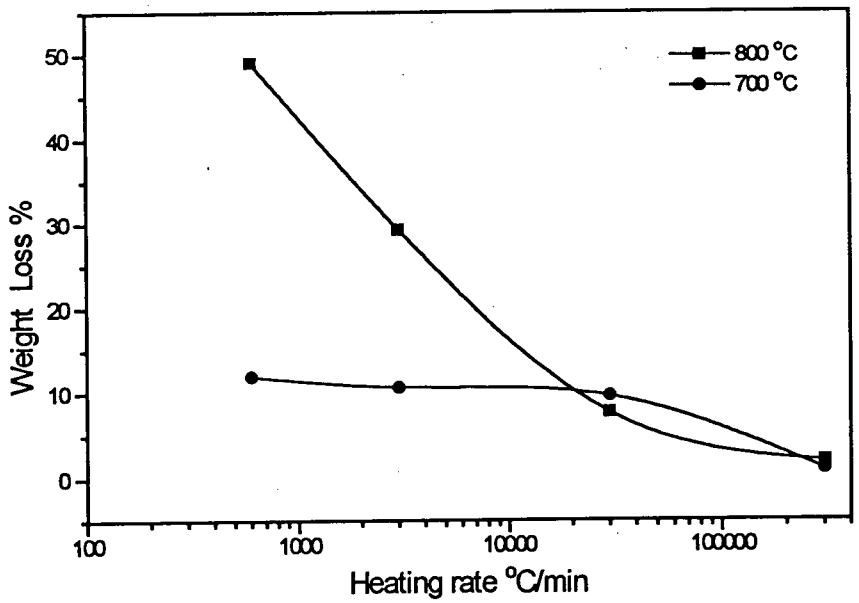

Figure 4.1.4 Heating rate effect on CANMET pitch pyrolysis with Pyroprobe-GC

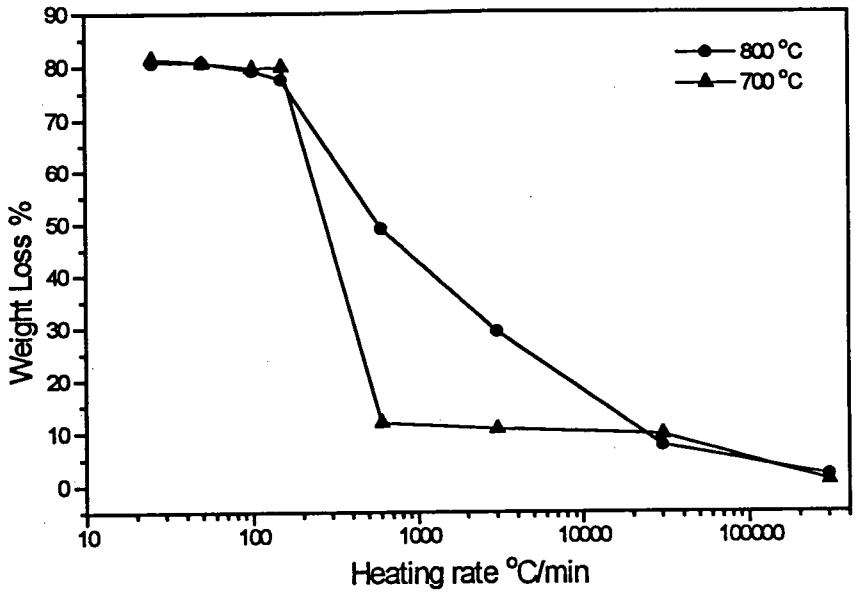

Figure 4.1.5 Heating rate effect on CANMET pitch pyrolysis with TGA and Pyroprobe-GC

4.1.1.3 Effect of Final Temperature

The effect of final temperature was studied at the heating rate 100 °C/min and final temperatures of 700, 750, 800, 850, 900 and 950 °C with 10 minute holding time. The sample weight was held roughly constant (8.13~11.31 mg) for all the runs. The operating conditions are provided in Table 4.1.5. Volatile yields are reported for both zero and ten minute holding time.

Figure 4.1.6 is the weight loss at zero and ten minute holding times vs. final temperature plot. It is observed that the weight loss decreased slightly, reached a minimum and then increased with the increase of temperature. At 0 min holding time, the weight loss decreased from 79.74% at 700 °C to minimal weight loss 79.01% at 850 °C and then increased to 81.58% at 950 °C. While it decreased from 80.20% at 750 °C to minimal weight loss 79.39% at 850 °C and then increased to 81.58% at 950 °C for 10 minute holding time. An increase of weight loss of less than 0.5% was observed over the 10 minute holding time. The residue is already solid char at the temperature 700 °C. That may indicate that pyrolysis of the pitch samples is nearly complete and

that further weight loss may be caused by the release of residue hydrogen in the char matrix at high temperature. The minimal weight loss at 850 °C reflects the complexity of the pitch pyrolysis chemistry. Similar phenomena was also observed by van Krevelen [17]. However, it is yet to be investigated.

4.1.2 TGA Pyrolysis of Syncrude Pitch

The TGA pyrolysis of Syncrude pitch was performed under different experimental conditions to study the effects of heating rate, pyrolysis temperature and sample weight. The sample weight was controlled between 3 and 16 mg. The heating rates employed are 25, 50, 100 and 150 °C/min and predefined final temperatures of 700, 750, 800, 850, 900 and 950 °C. Each run was also performed with a 10 minute holding time.

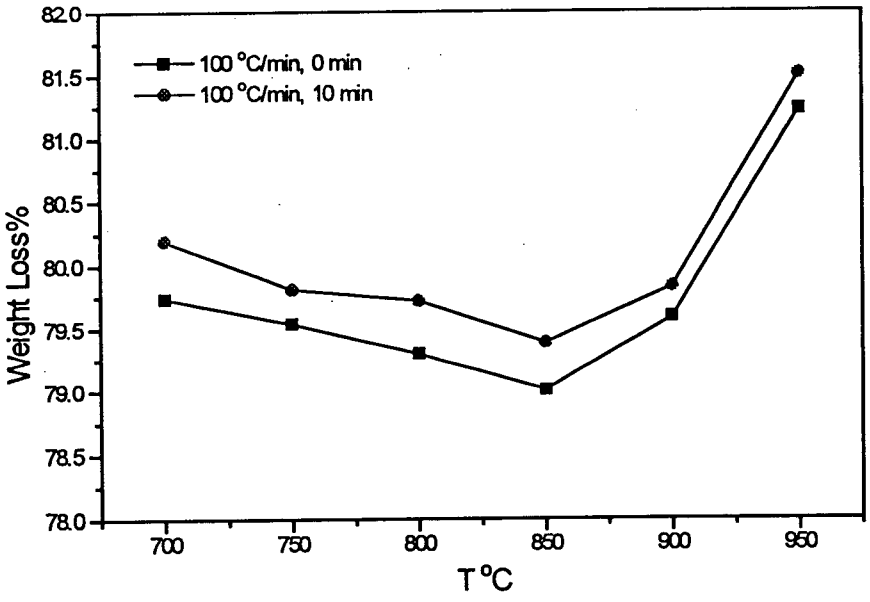

Figure 4.1.6 Final temperature effect on CANMET pitch pyrolysis with TGA at 100 °C/min

4.1.2.1 Effect of Sample Weight

The sample weight effect on Syncrude pitch pyrolysis was investigated under the final temperatures of 700, 800 °C and heating rate 100 °C/min for different sample weight from 3 mg to 16 mg. The operating conditions are provided in Table 4.1.6. Volatile yields are about 90%, leaving 10% of the pitch as non-volatile residue under these conditions.

Figures 4.1.7 and 4.1.8 show that the weight loss decreased as the increase of sample weight for Syncrude pitch, as also observed for CANMET pitch. It is also observed that only slightly higher weight loss is obtained at 10 minute holding time over 0 minute (Table 4.1.6), i.e., almost all reactions occur during the heatup period. These results are in good agreement with those of CANMET pitch. With sample weight increasing from 3 to 14 mg, the weight loss decreased from 92.73% to 89.89% for 0 minute holding time while it decreased from 93.51% to 90.4% for 10 minute holding time for runs at 700 °C. For runs at 800 °C, the weight loss decreased from 91.63% to 90.29% for 0 minute holding time, while it decreased from 91.89% to 91.36% for 10 minutes. The decrease of weight loss happened mostly with sample weights from 3 to 8 mg. Only a very slight decrease of volatile yield was observed with further increases of sample weight.

A comparison of the above results in Figures 4.1.7 and 4.1.8 show that higher weight loss is obtained under higher final pyrolysis temperature for the sample weight higher than 6 mg, while lower weight loss is observed under higher final pyrolysis temperature for a sample size less than 6 mg. This indicated a very complex reaction mechanism and the temperature plays a very important role.

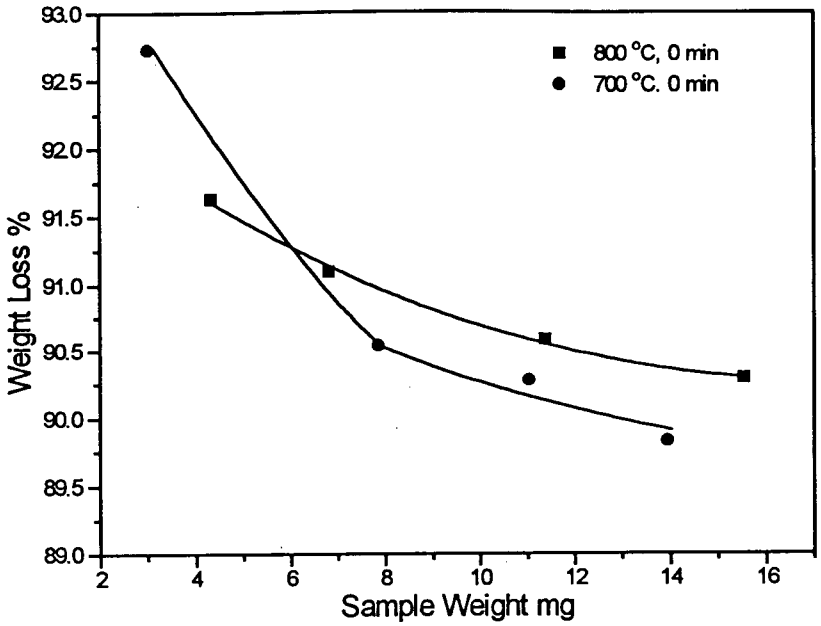

Figure 4.1.7 Sample weight effect on Syncrude pitch pyrolysis with TGA at 100 °C/min and 0 min

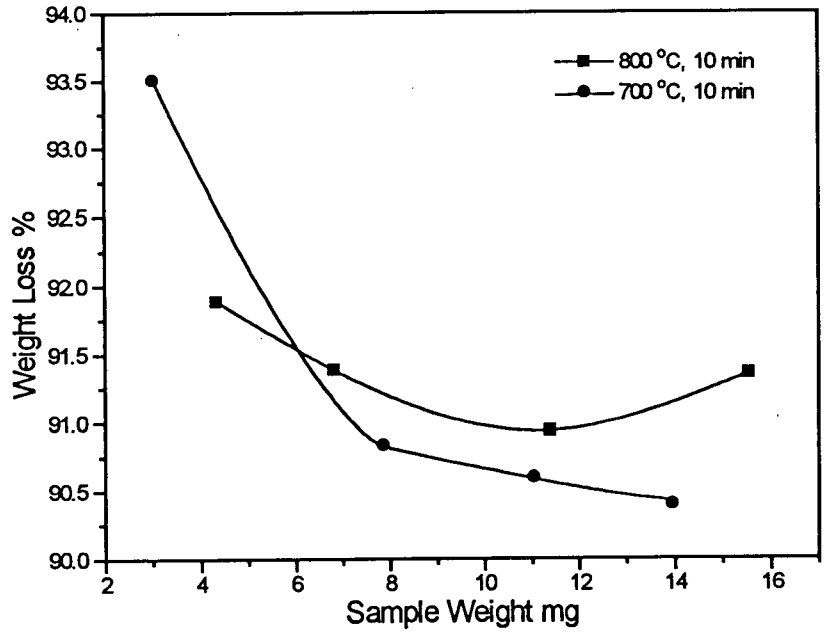

Figure 4.1.8 Sample weight effect on Syncrude pitch pyrolysis with TGA at 100 °C/min at 10 min

4.1.2.2 Effect of Heating Rate

The heating rate was varied from 25 to 300,000 °C/min while that final temperature was held constant at 800 °C (Table 4.1.7). The volatile yield is the weight loss which had occurred when the final temperature was reached.

Figure 4.1.9 is the comparison of the weight loss results of TGA and Pyroprobe. It is observed that the weight loss decreased with the heating rates over the range studied. The weight loss decreased from 90.6% for heating rates less than 150 °C/min to below 9% above 600 °C/min at a final temperature of 800 °C. The trend of results observed is in rough agreement with those of CANMET pitch pyrolysis shown in Figure 4.1.5. At heating rates higher than 3000 °C/min, the weight loss is much less than that at heating rates lower than 150 °C/min due to the different pyrolysis reaction times. The slower the heating rate, the longer the reaction time, and the more weight loss occurs.

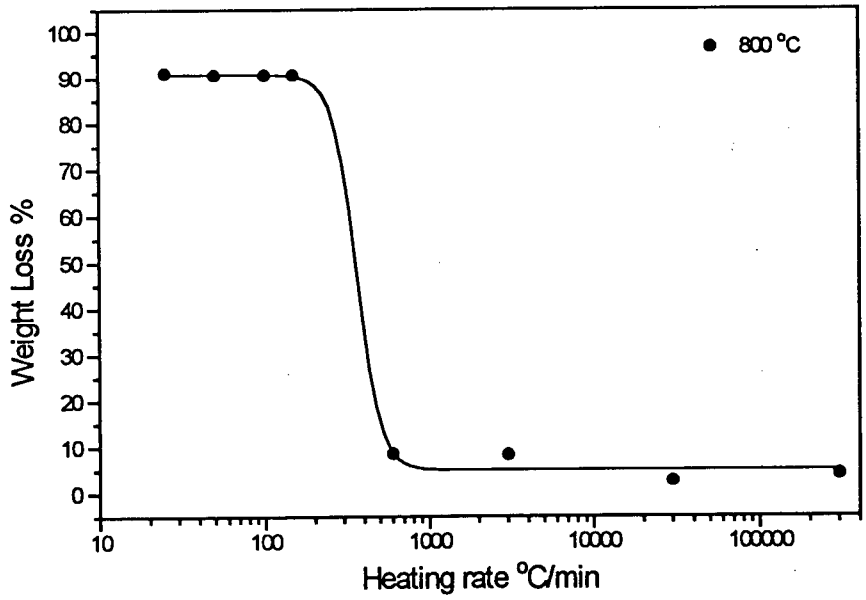

Figure 4.1.9 Heating rate effect on Syncrude pitch pyrolysis with TGA and Pyroprobe-GC (0 minute after reaching 800 °C)

4.1.2.3 Effect of Final Temperature

The effect of final temperature on weight loss was studied at the heating rates of 50 and 150 °C/min and final temperatures of 750, 850 and 950 °C for holding time 0 and 10 minutes. The sample weight was held in a range of 6.9 to 7.5 mg for runs under those conditions (Table 4.1.8).

Figures 4.1.10 and 4.1.11 are the weight loss vs. final temperature plots for runs at different heating rates and holding times. At zero holding time, the weight loss increased slightly with the increase of temperature at the higher heating rate. The weight loss increased from 90.18% at 750 °C to 92.66% at 950 °C for the heating rate 150 °C/min, while the weight loss remained essentially constant at 91 % from 750 °C to 950 °C for the heating rate 50 °C/min. More total weight loss is observed at 150 °C/min than 50 °C/min at temperature higher than 800 °C. At 50 °C/min and 850 °C, the weight loss was lowest, but the sample size was larger, and from Figure 4.1.2 with CANMET pitch, one should expect a lower weight loss. For 10 minute holding time (Figure 4.1.11), the results are essentially similar to those of at zero holding time.

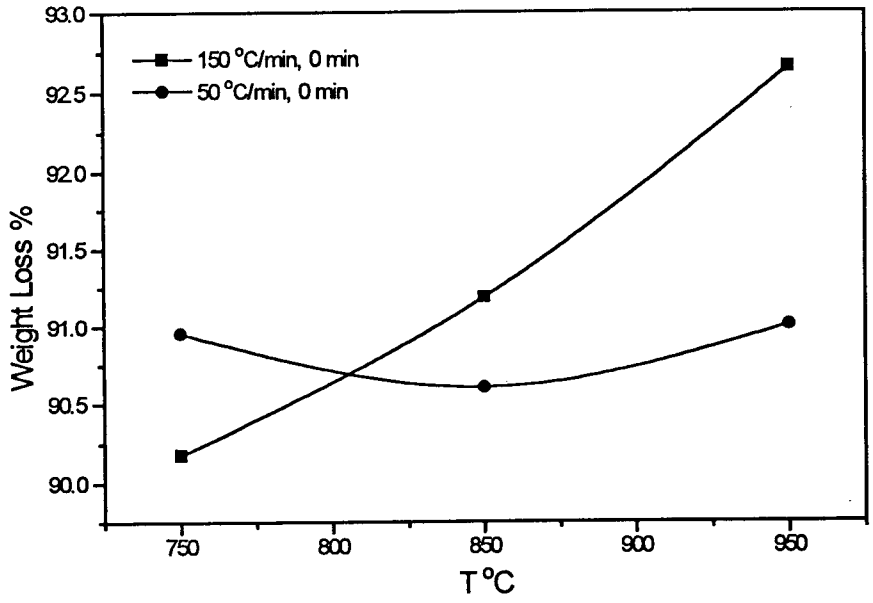

Figure 4.1.10 Final temperature effect on Syncrude pitch pyrolysis with TGA at 0 min

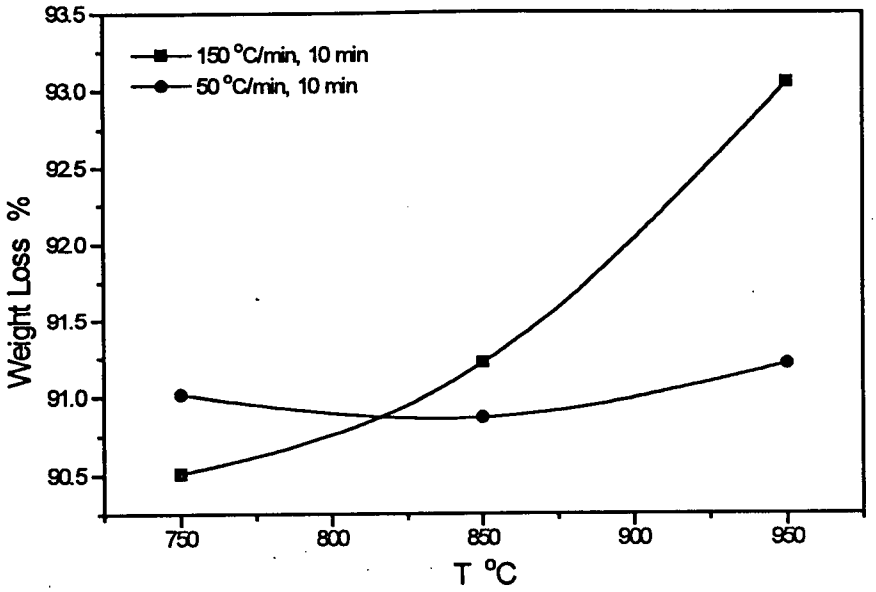

Figure 4.1.11 Final temperature effect on Syncrude pitch pyrolysis with TGA at 10 min

From Table 4.1.8, slightly higher weight loss was observed at 10 minute holding time. The effect of final temperature, as well as holding time, is in accordance with those of CANMET pitch.

4.1.3 TGA Pyrolysis Characteristics

In experiments presented in this section, the pyrolysis heating rate was varied while other parameters such as the final temperature and the sample weight were held constant. The sample weight for CANMET pitch is 8.129 to 10.12 mg and the sample weight for Syncrude pitch is 9.904 to 11.90 mg to permit a direct comparison (Table 4.1.9). The total weight loss (V*) is also listed in the table for each run. The volatile yield (V*) is obtained when the final temperature is reached. The dynamic weight change during the time of heating is discussed.

CANMET and Syncrude pitches both showed similar patterns in the TGA pyrolysis plots. This pattern differs from results found with oil shale or coals. Figures 4.1.12 to 4.1.18 show the nonisothermal devolatilization TGA curves of CANMET pitch and Syncrude pitch at 800 °C final

temperature and heating rates of 25, 50, 100 and 150 °C/min. The nonisothermal devolatilization weight loss vs. temperature behavior is shown in Figures 4.1.12 and 4.1.16 for each pitch respectively. It is observed that a slightly higher weight loss is obtained at a lower heating rate at a given temperature, or a higher temperature is required to reach the same amount of weigh loss for a higher heating rate. However, the effect of the heating rates is not systematic, nor significant. For CANMET pitch, weight loss at 25 and 50 °C/min is noticeably higher than those at 100, and 150 °C/min, while the weight loss is roughly the same for heating rates 25 and 50 °C/min at the same temperature as shown in Figure 4.1.12. For Syncrude pitch (Figure 4.1.16), the weight loss is almost the same at heating rates 25 and 50 °C/min. Also the weight loss is roughly the same at 100 and 150 °C/min. However the weight loss at 25 and 50 °C/min is generally higher that that at 100 and 150 °C/min at the same temperature. Similar behavior was also observed by Milosavljevic [61], but heating rate as such was not considered to be the main reason for the difference. He claimed that the chemical reaction itself caused the change and difference. This seems reasonable in the present case as well. Heating rates do affect the temperature history, however, it is the chemical reaction at the specific temperature which causes formation of volatiles and the weight loss. This is also observed in Figures 4.1.13 and 4.1.17, which show the weight loss results vs. time. As can be seen, the heating rate changed the reaction time, but it did not change the volatile evolution pattern with temperature of either CANMET pitch or Syncrude pitch.

Figures 4.1.15 and 4.1.19 showed the weight loss per degree of temperature rise dW/dT vs. temperature for each pitch. This derivative was calculated with the following formula:

$$\left(\frac{dW}{dT}\right)_i = \frac{W_{i+1} - W_i}{T_{i+1} - T_i}$$

The above equation indicates that dW/dT is the average value of weight loss in a very small temperature interval and represents the weight loss rate divided by the heating rate. dW/dT is also negative because the pyrolysis is a weight loss process with temperature. It is clearly shown that the dW/dT changes with the temperature in a nonlinear manner, passing through three major stages for each type of pitch. At temperatures lower than 150 °C, dW/dT is roughly equal to 0 as observed in Figures 4.1.15 and 4.1.19 for CANMET and Syncrude pitches respectively. This indicates that there is no chemical or physical reaction taking place below this temperature, and that the content of water and low molecular components is negligible. At temperatures between 150 °C to about 400 °C, the weight loss dW/dT slowly decreased to a steady value, which is more evident for the Syncrude pitch results, then dW/dT decreased rather dramatically to its minimum, which occurs at temperatures between 500 °C and 600 °C. The ratio dW/dT then went through the last stage of changing, increasing from its minimum to a very small absolute value at approximately 600 °C. At this condition pyrolysis is nearly complete and further increases of the temperature did not affect the total weight loss significantly. This indicated that the temperature is an important parameter and the change of temperature affects the behavior of the pitch pyrolysis process. It is clearly shown that the pyrolysis process takes place as a two stage process and therefore there are two weight loss peaks as observed in these two plots. However these two stages of pyrolysis overlap and this feature can be easily missed in Figure 4.1.15 for CANMET pitch as they are not clearly separated. This two-peak weight loss feature, i.e. two-stage reaction characteristics is more clearly shown in Figure 4.1.19 for Syncrude pitch. The peak weight loss temperature is also very close to a fixed value for all the heating rates studied for each pitch as shown in Figures 4.1.15 and 4.1.19. This further suggests the chemical nature of the pyrolysis. The first peak temperature is not clearly identifiable for CANMET pitch, but lies in the range of 400 °C and 450 °C for Syncrude pitch. The second maximum weight loss rate temperature is

clearly identifiable for both CANMET pitch and Syncrude pitch. The second peak temperature for CANMET pitch is between 500 °C to 600 °C. It is even better defined for Syncrude pitch in the temperature range of 500 °C and 550 °C. The weight loss for CANMET pitch at 400 °C is between 5% and 25% depending on the heating rate, while the weight loss for Syncrude pitch is between 20% and 40% at the same temperature. The total weight loss for CANMET pitch and Syncrude pitch is 80% and 90% at 800 °C respectively. The most weight loss therefore occurred at temperatures between 400 °C and 600 °C. The weight loss in this temperature range is 65% to 75% for CANMET pitch and 50% to 70% for Syncrude pitch respectively. Figures 4.1.13 and 4.1.17 showed the weight loss vs. time for each pitch at different heating rates. Figures 4.1.14 and 4.1.18 showed the weight loss rate dW/dt vs. time for each pitch at different heating rate. It is also observed that the pyrolysis occurs in stages at different time scales with changes in heating rate. The two peak weight loss character is also identified in these two plots, attesting the results in Figures 4.1.15 and 4.1.19.

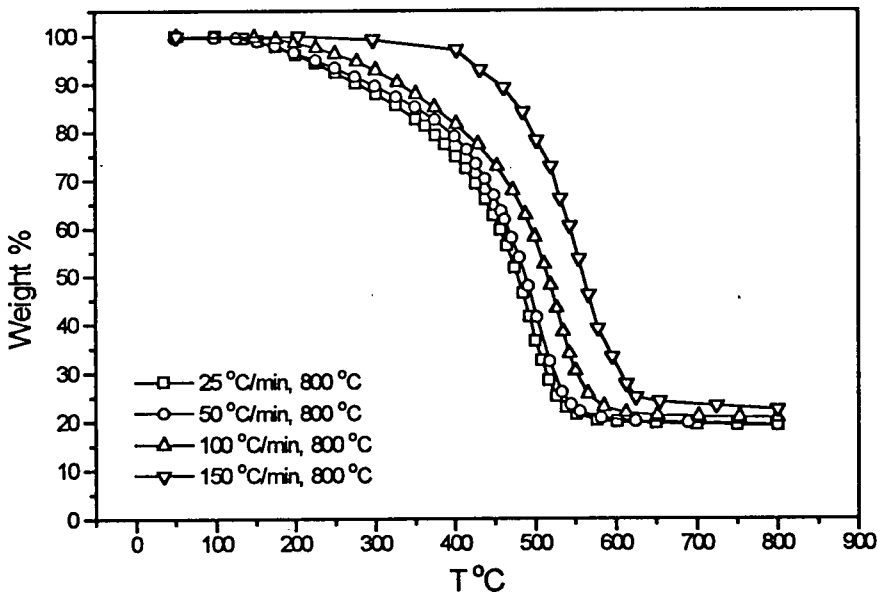

Figure 4.1.12 CANMET pitch weight loss vs. temperature at different heating rates and final temperature 800 °C measured via TGA

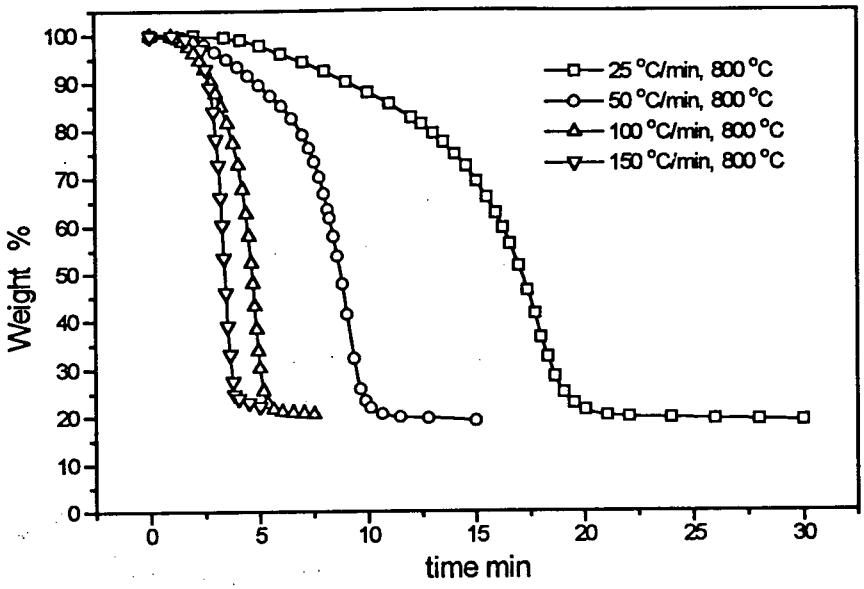

Figure 4.1.13 CANMET pitch weight loss vs. time at different heating rates and final temperature 800 °C measured via TGA

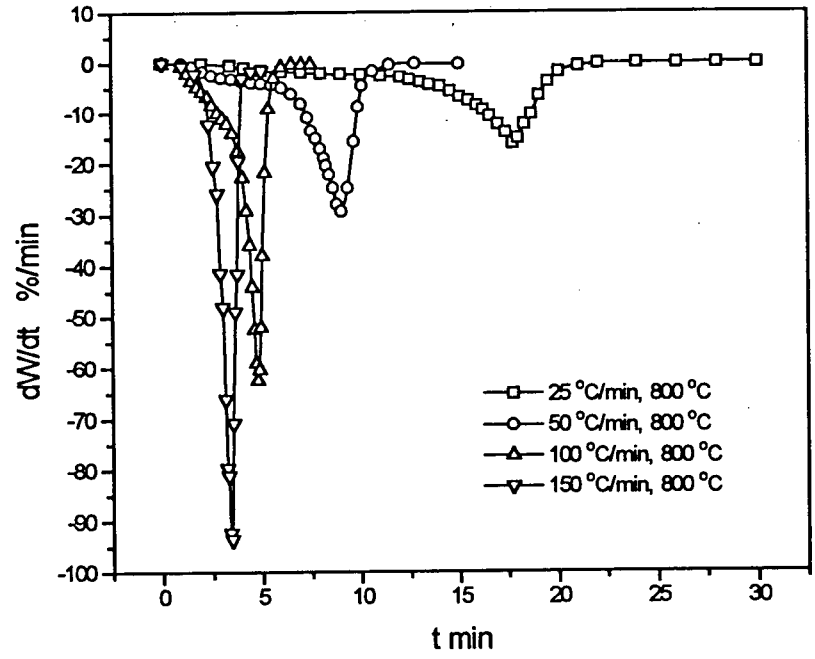

Figure 4.1.14 CANMET pitch weight loss rate vs. time at different heating rates and final temperature 800 °C measured via TGA

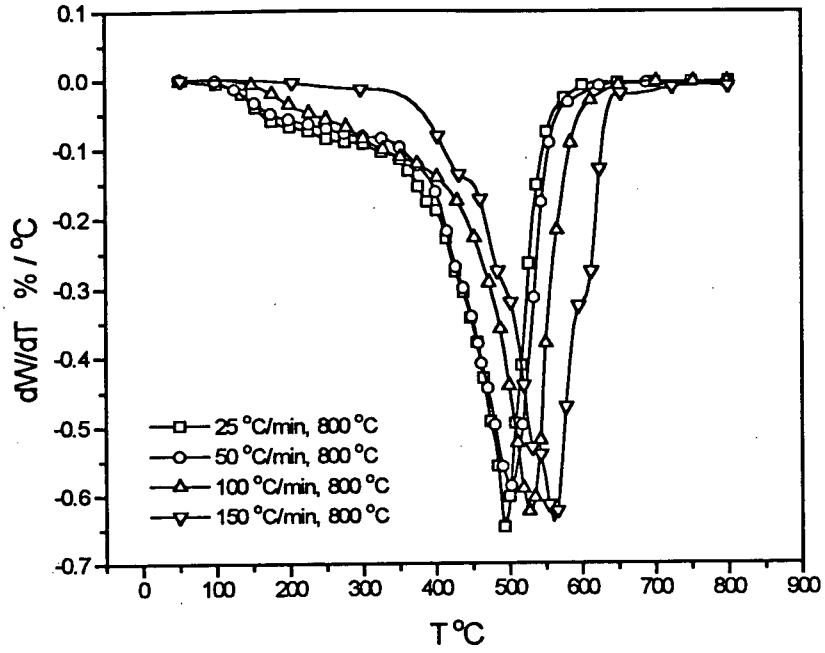

Figure 4.1.15 CANMET pitch weight loss dW/dT vs. temperature at different heating rates and final temperature 800 °C measured via TGA

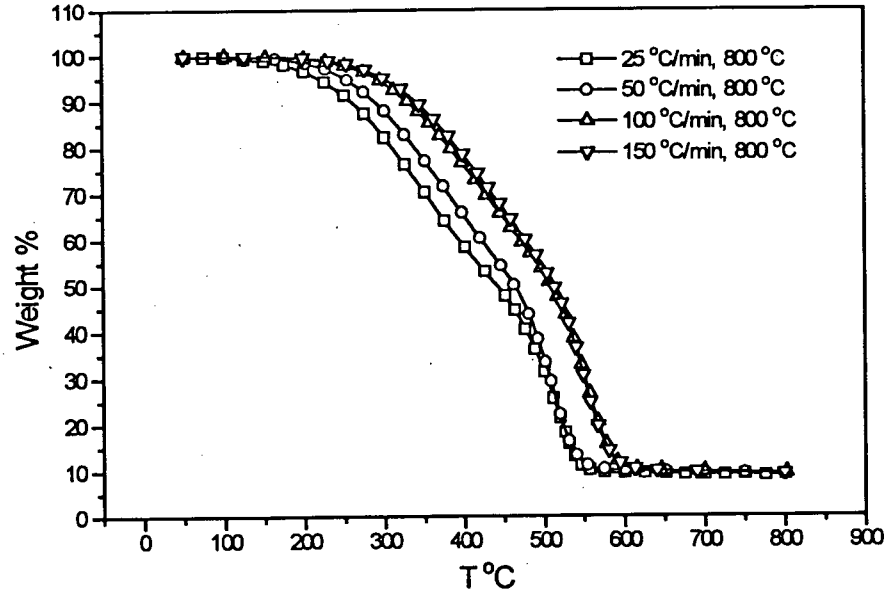

Figure 4.1.16 Syncrude pitch weight loss vs. temperature at different heating rates and final temperature 800 °C measured via TGA

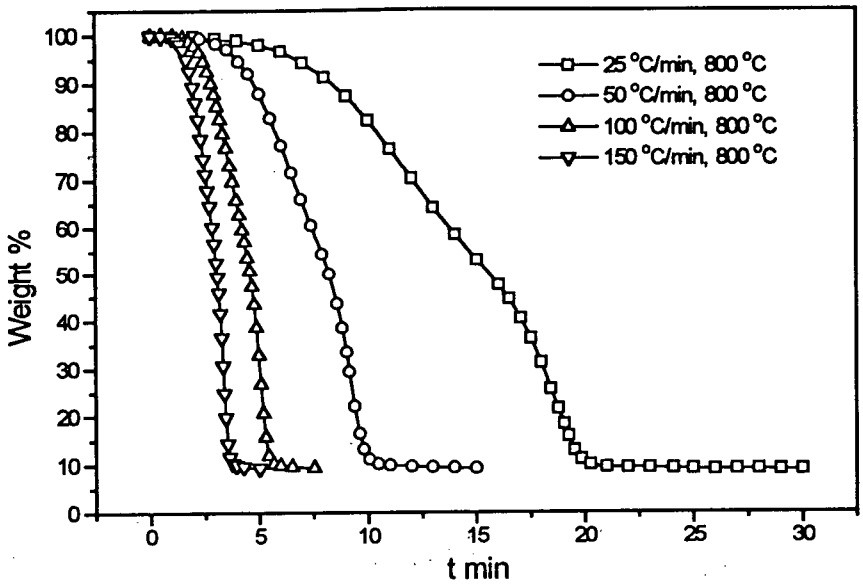

Figure 4.1.17 Syncrude pitch weight loss vs. time at different heating rates and final temperature 800 °C measured via TGA

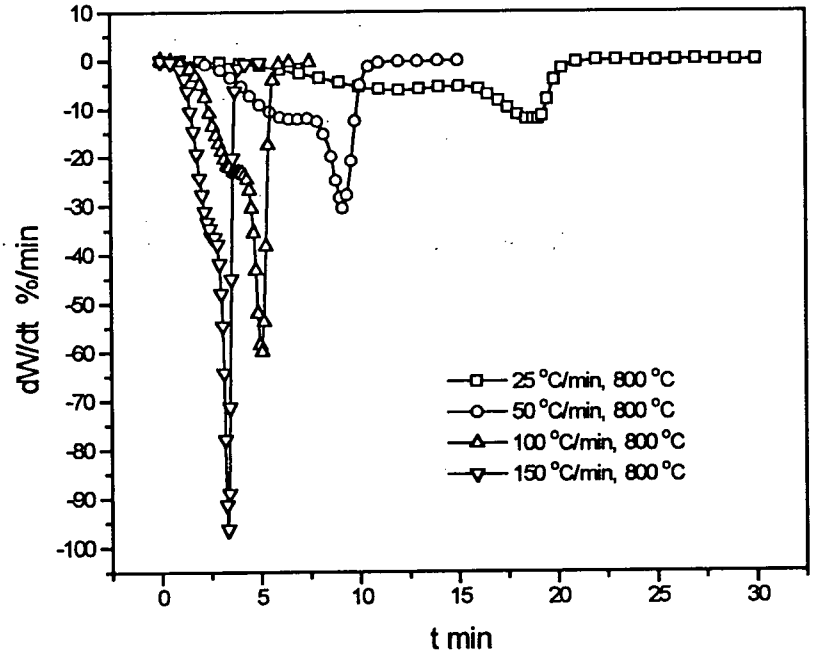

Figure 4.1.18 Syncrude pitch weight loss rate vs. time at different heating rates and final temperature 800 °C measured via TGA

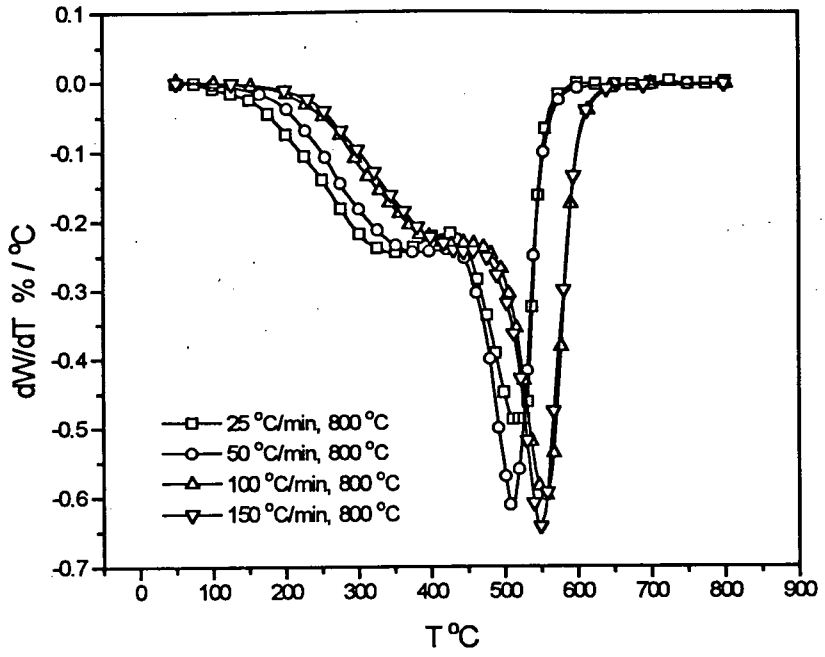

Figure 4.1.19 Syncrude pitch weight loss dW/dT vs. temperature at different heating rates and final temperature 800 °C measured via TGA

4.1.4 Discussion and Conclusion

It is shown that the heating rates slightly affect the weight loss, however, it is believed that the temperature history, not the heating rate as such causes the difference. Temperature is the significant factor causing the reactions to take place and produce the weight loss. The devolatilization step is not instantaneous, as little weight loss occurred at the highest heating rate.

The importance of the temperature history is more significantly noticed among the runs of Pyroprobe experiments where total reaction time in the heatup was short, i.e. a few seconds. Low heating rates produce longer reaction times of the order of minutes, caused more extensive pyrolysis reaction, and therefore resulted in a higher weight loss (or volatile yield).

At temperatures below 150 °C, there is little weight loss, suggesting that no pyrolysis take place. The weight loss takes place in two following stages with two different, distinct patterns of chemical and physical change. In the first stage, a low peak weight loss rate was observed, while

in the second stage a higher peak weight loss rate was observed. These features appear unique to pitch pyrolysis, as they have not been reported for coal or shale pyrolysis.

The total weight loss (volatile yield) decreases slightly with the increase of sample weight over the range studied for both CANMET pitch and Syncrude pitch.

With TGA, more than 80% of residue conversion can be achieved for CANMET pitch, while more than 90% of residue conversion can be achieved for Syncrude pitch.

Table 4.1.1 Experimental Conditions for Runs at Different Sample Weight with TGA

Run#	Heating Rate °C/min	Final Temp °C	Sample Weight mg	$V_{t=0}$ wt%	$V_{t=10}$ wt%
Can11	100	900	4.406	82.8	83.64
Can20	100	900	5.702	82.51	82.82
Can18	100	900	6.441	82.05	83.50
Can45	100	900	7.074	80.60	81.55
Can15	100	900	7.774	79.80	80.47
Can16	100	900	7.981	81.65	81.79
Can17	100	900	10.719	80.27	80.50
Can8	100	900	11.162	79.33	79.57
Can38	100	900	12.034	79.59	79.83
Can19	100	900	13.680	78.70	79.03
Can14	100	900	15.784	79.85	80.03

Table 4.1.2 Experimental Conditions for Runs at Different Sample Weight with TGA

Run#	Heating Rate °C/min	Final Temp °C	Sample Weight mg	$V_{t=0}$ wt%	$V_{t=10}$ wt%
Can28	50	900	4.979	82.89	84.38
Can21	50	900	6.360	82.76	83.32
Can7	50	900	6.723	82.48	86.29
Can27	50	900	8.011	80.51	80.65
Can27	50	900	8.943	81.12	81.38
Can10	50	900	10.179	80.60	81.82
Can25	50	900	11.162	80.25	80.45
Can23	50	900	11.735	80.88	81.02
Can35	50	900	12.022	80.43	80.74
Can22	50	900	12.699	79.97	80.35
Can13	50	900	13.157	80.84	81.71
Can31	50	900	14.042	78.47	78.87
Can24	50	900	14.729	77.85	78.26
Can30	50	900	15.596	78.49	78.87
Can12	50	900	17.175	79.10	80.07

Table 4.1.3 Experimental Conditions for Runs at Different Heating Rates with TGA

Run#	Heating Rate °C/min	Final Temp. °C	Sample Weight mg	Volatile wt %
Can54	25	700	9.368	81.78
Can61	50	700	8.835	80.66
Can53	100	700	7.896	79.74
Can60	150	700	8.923	79.93
Can48	25	800	8.878	80.84
Can33	50	800	8.224	80.79
Can41	100	800	10.304	79.30
Can58	150	800	9.109	77.59

Table 4.1.4 Experimental Conditions for Runs at Different Heating Rates with Pyroprobe

Run#	Heating Rate °C/min	Final Temp. °C	Sample Weight mg	Volatile wt %
Cam069	600	700	5.0	12.00
Cam051	3,000	700	5.6	10.71
Cam033	30,000	700	5.2	9.62
Cam015	300,000	700	5.3	1.88
Cam070	600	800	5.3	49.06
Cam052	3,000	800	5.8	29.31
Cam034	30,000	800	5.2	7.69
Cam016	300,000	800	5.0	2.00

Table 4.1.5 Experimental Conditions for Runs at Different Final Temperature with TGA

Run#	Heating Rate °C/min	Final Temp. °C	Sample Weight mg	$V_{t=0}$ wt %	$V_{t=10}$ wt%
Can53	100	700	7.896	79.74	80.20
Can42	100	750	9.171	79.54	79.81
Can41	100	800	10.304	79.30	79.72
Can40	100	850	10.723	79.01	79.39
Can38	100	900	12.034	79.59	79.83
Can52	100	950	8.199	81.23	81.58

Table 4.1.6 Experimental Conditions for Runs at Different Sample Weight with TGA

Run#	Heating Rate °C/min	Final Temp. °C	Sample Weight mg	$V_{t=0}$ wt %	$V_{t=10}$ wt %
Syn13	100	700	3.010	92.73	93.51
Syn14	100	700	7.852	90.54	90.84
Syn16	100	700	11.029	90.28	90.60
Syn15	100	700	13.932	89.83	90.40
Syn17	100	800	4.321	91.63	91.89
Syn19	100	800	6.797	91.10	91.39
Syn18	100	800	11.376	90.58	90.94
Syn20	100	800	15.534	90.29	91.36

Table 4.1.7 Experimental Conditions for Runs at Different Heating Rates with TGA and Pyroprobe

Run#	Heating Rate °C/min	Final Temp °C	Sample Weight mg	$V_{t=0}$ wt%	Equipment
Syn43	25	800	10.477	91.03	TGA
Syn29	50	800	11.708	90.70	TGA
Syn18	100	800	11.376	90.59	TGA
Syn8	150	800	10.053	90.62	TGA
Syn070	600	800	4.600	8.70	Pyroprobe
Syn052	3,000	800	2.400	8.33	Pyroprobe
Syn034	30,000	800	3.600	2.78	Pyroprobe
Syn016	300,000	800	4.900	4.08	Pyroprobe

Table 4.1.8 Experimental Conditions for Runs at Different Final Temperature with TGA

Run#	Heating Rate °C/min	Final Temp. °C	Sample Weight mg	$V_{t=0}$ wt %	$V_{t=10}$ wt %
Syn27	50	750	7.604	90.96	91.02
Syn32	50	850	7.134	90.61	90.87
Syn33	50	950	6.942	91.01	91.21
Syn10	150	750	7.606	90.18	90.51
Syn5	150	850	6.920	91.19	91.22
Syn4	150	950	7.262	92.66	93.05

Table 4.1.9 The Pyrolysis Conditions for CANMET Pitch and Syncrude Pitch at Different Temperature and Heating Rates

Run#	Heating Rate °C/min	Final Temp. °C	V* wt %
	CANMET Pitch		
Can48	25	800	80.84
Can33	50	800	80.79
Can41	100	800	79.30
Can58	150	800	77.59
	Syncrude Pitch		
Syn43	25	800	91.03
Syn29	50	800	90.70
Syn18	100	800	90.58
Syn8	150	800	90.62

4.2 Pyroprobe-GC Pyrolysis of CANMET and Syncrude Pitch

CANMET and Syncrude pitches were studied with the Pyroprobe-GC. The yield of volatiles was determined by the difference between the sample weight and residue weight after pyrolysis. The yield of each major group of components was determined following the method outlined in the experiment techniques section in Chapter 3. The experimental conditions are summarized in each of the following sections. The mass balance of each run in this section is in the range of 95 to 105%.

4.2.1 Pyroprobe-GC Pyrolysis of CANMET Pitch

The Pyroprobe-GC pyrolysis of CANMET pitch was performed under different experimental conditions to study the effects of heating rates, pyrolysis reaction temperatures and holding times. The sample weight was kept relatively constant around 5 mg in order to limit the sample size effects. The heating rates are 300000, 30000, 3000 °C/min, the holding times are 10, 5 and 0 s. The combinations of these operating parameters are listed in Table 4.2.1. Each combination of these parameters was performed at the final temperatures of 500, 600, 700, 800, 900, 1000 °C.

Table 4.2.1 Experimental Conditions for Runs at Different Holding Times

Holding Time s	Heating Rate °C/min
10.0	300,000
5.0	300,000
0.0	300,000
10.0	30,000
5.0	30,000
0.0	30,000
10.0	3,000
5.0	3,000
0.0	3,000

4.2.1.1 Effect of Experimental Conditions on the Total Weight Loss

The total weight loss vs. holding time is an important characteristic in hydrocarbon pyrolysis. The effect of holding times on the total weight loss is shown in Figures 4.2.1 to 4.2.3.

Figures 4.2.1 to 4.2.3 show that the weight loss (volatile yield) generally increases as the increase of temperature, with maximum weight loss observed at heating rate 30,000 and 3,000 °C/min. At the heating rate of 300,000 °C/min as shown in Figure 4.2.1, higher weight loss is observed for a longer holding time at temperatures below 800 °C, i. e., more weight loss is observed after 10 s than 5 or 0 s. At temperatures higher than 800 °C, however, about the same amount of weight loss is observed at 10 and 5 s. That may indicate that the pyrolysis is nearly complete at these conditions. Little weight loss is observed at 0 s.

At heating rate of 30,000 °C/min as shown in Figure 4.2.2, it is observed that the weight loss vs. temperature at different holding times is not linear. The maximum weight loss is reached at 900 °C for holding time 10 and 5 s. Higher weight loss is also observed under longer holding time. About 5% more weight loss is observed at 10 s holding time than 5 s holding time.

At heating rate of 3000 °C/min as shown in Figure 4.2.3, it is observed that the weight loss vs. temperature at different holding times is not linear. The maximum weight loss is observed at 700 °C for holding time 10 s, and at 800 °C for 5 s. At temperatures lower than 800 °C, more weigh loss is observed under a longer holding time. At temperatures higher than 900 °C, weight loss becomes less sensitive to the holding time. More weight loss is observed at 0 s for heating rate 3000 °C/min than that for 300,000 and 30,000 °C/min. 50.9% weight loss is observed at 1000 °C and 0 s for heating rate 3000 °C/min, while less than 5% weight loss is observed for both 300,000 and 30,000 °C/min at the same temperature. This further indicates the importance of holding times. To reach 1000 °C, it takes 19, 1.9 and 0.19 s for 3000, 30,000 and 300,000 °C/min respectively.

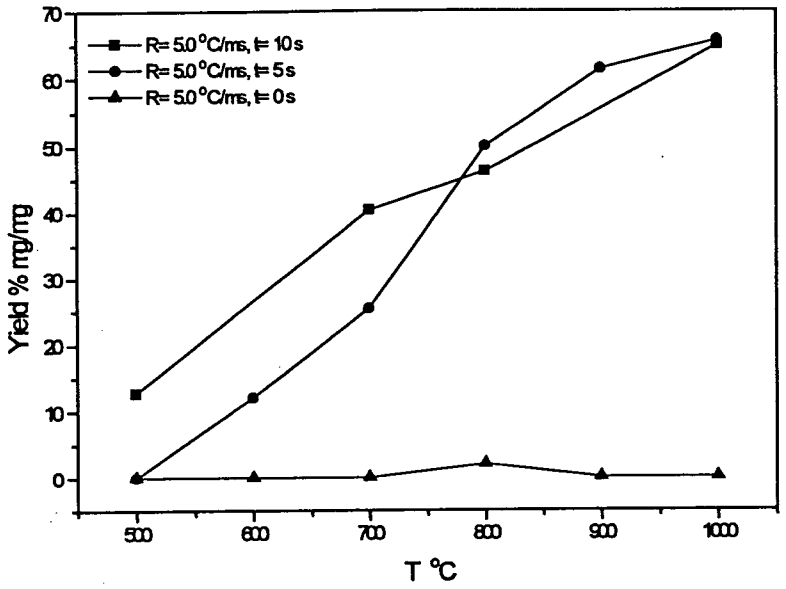

Figure 4.2.1 CANMET pitch pyrolysis total loss (yield) vs. temperature at different pyrolysis holding times with heating rate 300,000 °C/min

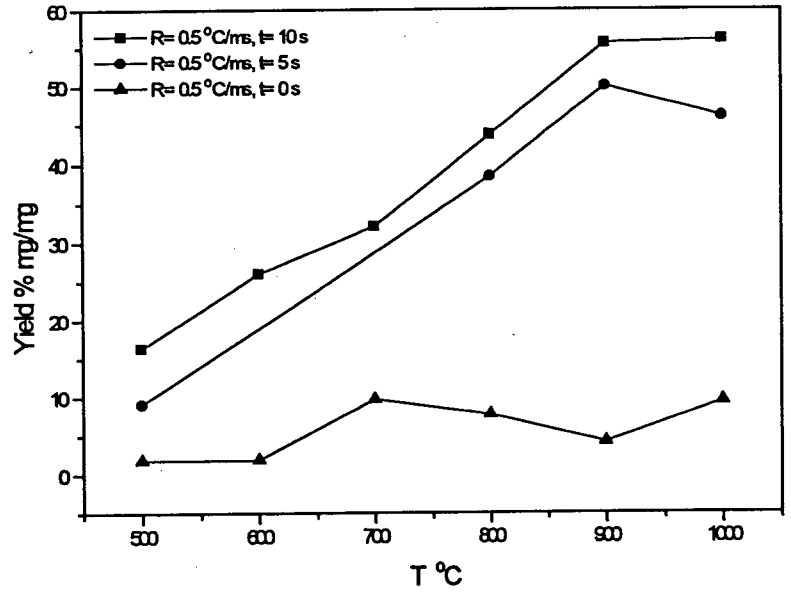

Figure 4.2.2 CANMET pitch pyrolysis total loss (yield) vs. temperature at different pyrolysis holding times with heating rate 30,000 °C/min

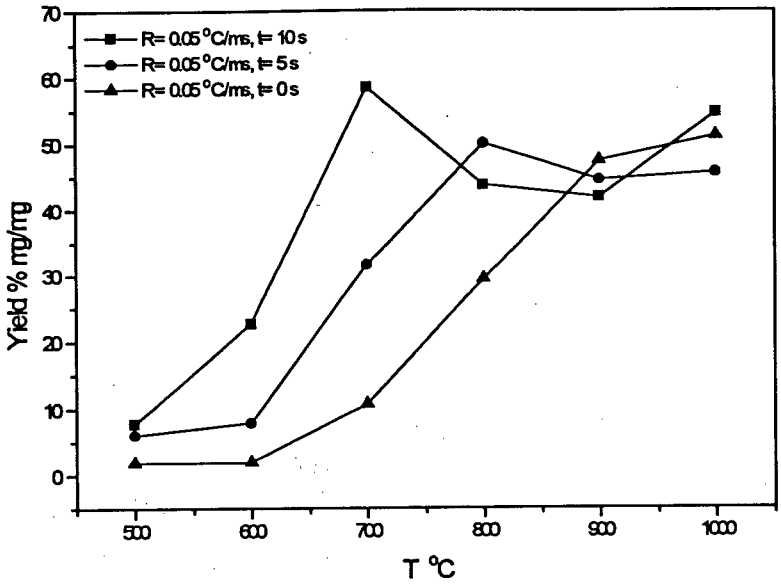

Figure 4.2.3 CANMET pitch pyrolysis total loss (yield) vs. temperature at different pyrolysis holding times with heating rate 3000 °C/min

4.2.1.2 Effect of Experimental Conditions on the C_7 Yield

Figures 4.2.4 to 4.2.6 show that the C_7 yield generally increases as the increase of temperature, while maximum yield was observed at 3000 °C/min. At the heating rate of 300,000 °C/min as shown in Figure 4.2.4, higher C_7 yield is observed at a longer holding time in the temperature range studied. The C_7 yield is 54.46%, 27.92% and 0% at 1000 °C for holding time 10, 5 and 0 s respectively.

At heating rate 30,000 °C/min as shown in Figure 4.2.5, it is observed that the C_7 yield vs. temperature at different holding times is not linear. It is also observed that the C_7 yield at 10 second holding time is very close to that at 5 second holding time. A maximum C_7 yield, 40.94%, is observed at 900 °C for holding time 5 s. C_7 yield reached 47.77% and 39.19% at 1000 °C for 10 and 5 second holding time respectively. The C_7 yield at 0 s is negligible, as also observed in Figure 4.2.4.

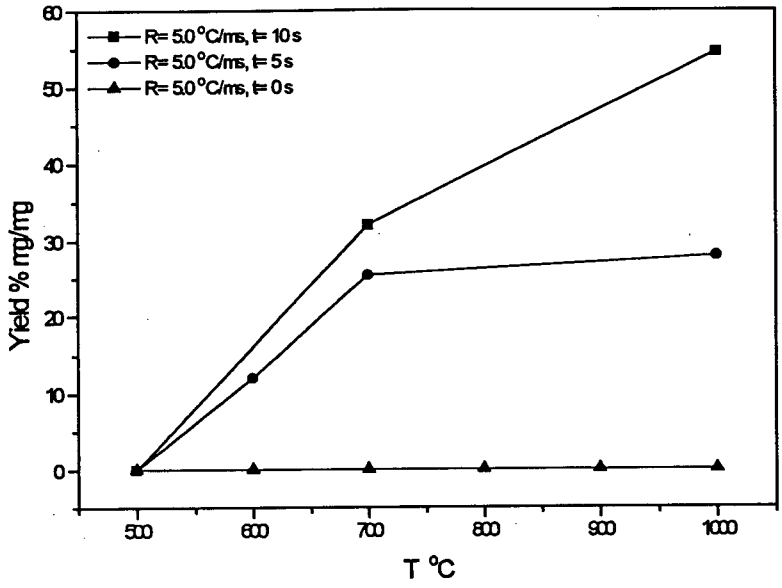

Figure 4.2.4 CANMET pitch pyrolysis C_7 yield vs. temperature at different pyrolysis holding times with heating rate 300,000 °C/min

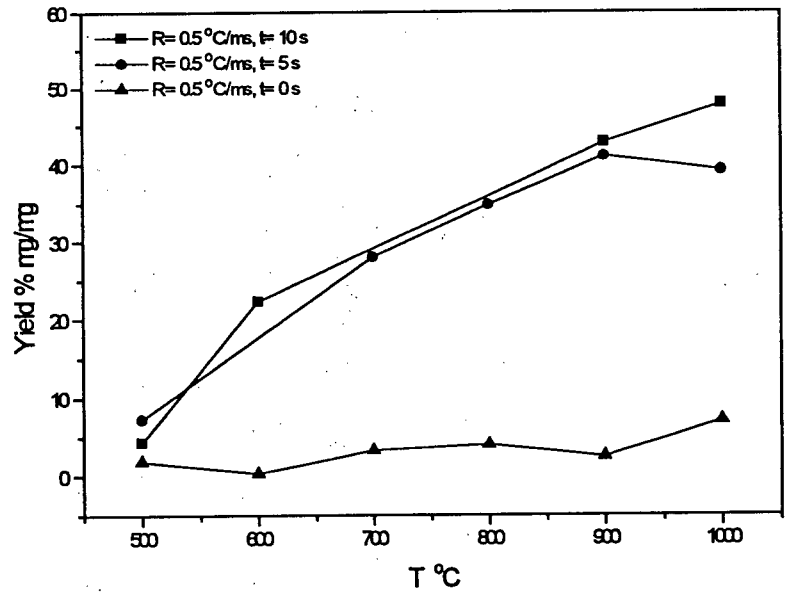

Figure 4.2.5 CANMET pitch pyrolysis C_7 yield vs. temperature at different pyrolysis holding times with heating rate 30,000 °C/min

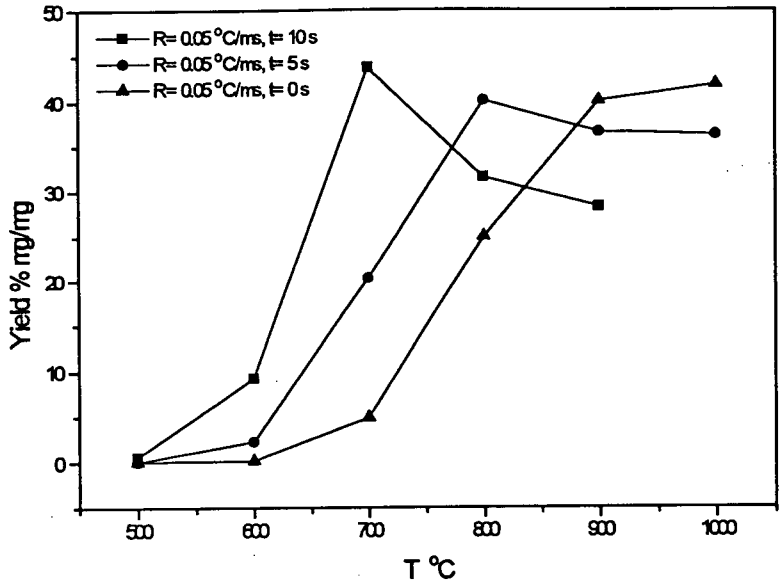

Figure 4.2.6 CANMET pitch pyrolysis C_7 yield vs. temperature at different pyrolysis holding times with heating rate 3000 °C/min

At heating rate of 3000 °C/min as shown in Figure 4.2.6, it is observed that the C_7 yield vs. temperature is not linear. It is also observed that maximum C_7 yield is reached at different temperature for different holding times. Maximum C_7 yield is reached at a lower temperature for a longer holding time. Maximum C_7 yield, 43.75%, is reached at 700 °C for 10 second holding time, while maximum C_7 yield, 40.14% and 41,75%, is reached at 800 °C and 1000 °C for holding time 5 and 0 s respectively. Secondary pyrolysis is clearly observed for the C_7 lump of compounds. At temperature lower than 750 °C, it is observed that longer holding time resulted in higher C_7 yield, while at temperature higher than 900 °C, longer holding time resulted in lower C_7 yield. It is also observed that C_7 yield increased dramatically at temperatures above 700 °C for 0 second holding time and 41.75% is obtained at 1000 °C for holding time 0 s. The maximum C_7 yields at different conditions is essentially the same and may indicate the secondary reactions of some of the components in the sample.

4.2.1.3 Effect of Experimental Conditions on the C_{10} Yield

Figures 4.2.7 to 4.2.9 show that C_{10} yield generally increases as temperature, with the maximum yield observed at 800 to 900 °C. At heating rate 300,000 °C/min as shown in Figure 4.2.7, higher C_{10} yield is observed at higher heating rate in the temperature range studied. The C_{10} yield is not sensitive to temperatures lower than 600 °C. As also observed in Figure 4.2.5, C_{10} yield is negligible for 0 s in the temperature range studied. Maximum C_{10} yield is also observed at 800 °C for holding time 10 s.

At heating rate 30,000 °C/min as shown in Figure 4.2.8, it is observed that the C_{10} yield vs. temperature at different holding times is not linear. It is also observed that the C_{10} yield at 10 second holding time is very close to that at 5 second holding time. A maximum C_{10} yield, 2.3% and 2.2%, is observed at 900 °C for holding time 10 and 5 s respectively. The C_{10} yield at 0 s is, as also observed in Figure 4.2.7, negligible.

At heating rate of 3000 °C/min as shown in Figure 4.2.9, it is observed that the C_{10} yield vs. temperature is not linear. It is also observed that maximum C_{10} yield is reached at different temperature for different holding times. Maximum C_{10} yield is reached at about the same temperature 900 °C for holding time 10 and 5 s respectively. The maximum C_{10} yield is 1.8% and 1.7% for holding time 10 and 5 s respectively. At temperature lower than 600 °C, it is observed that C_{10} yield is not sensitive to the temperature. It is also observed that C_{10} yield for holding time 10 s is close to that for holding time 5 s in the temperature range from 600 to 900 °C. C_{10} yield increased significantly at temperature higher than 800 °C and reached maximum yield 1.6% at 900 °C for holding time 0 s.

Secondary pyrolysis of C_{10} lump is also evident as shown in Figures 4.2.7, 4.2.8 and 4.2.9.

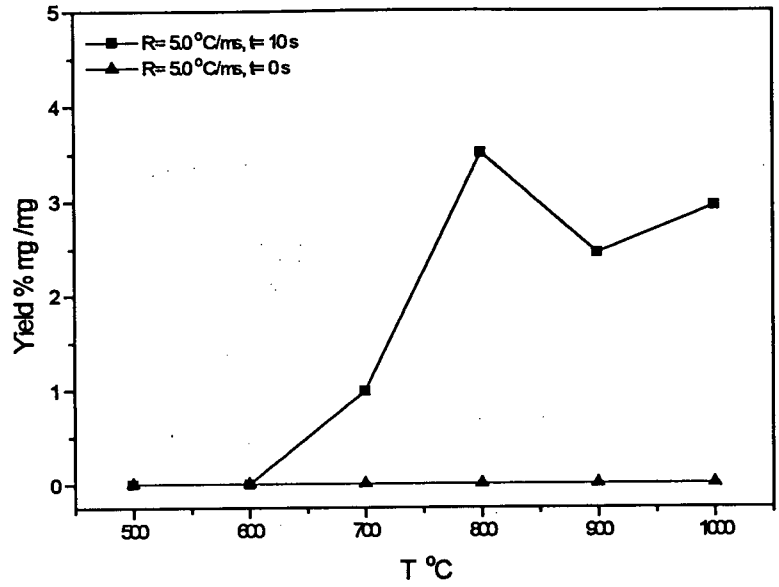

Figure 4.2.7 CANMET pitch pyrolysis C_{10} yield vs. temperature at different pyrolysis holding times with heating rate 300,000°C/min

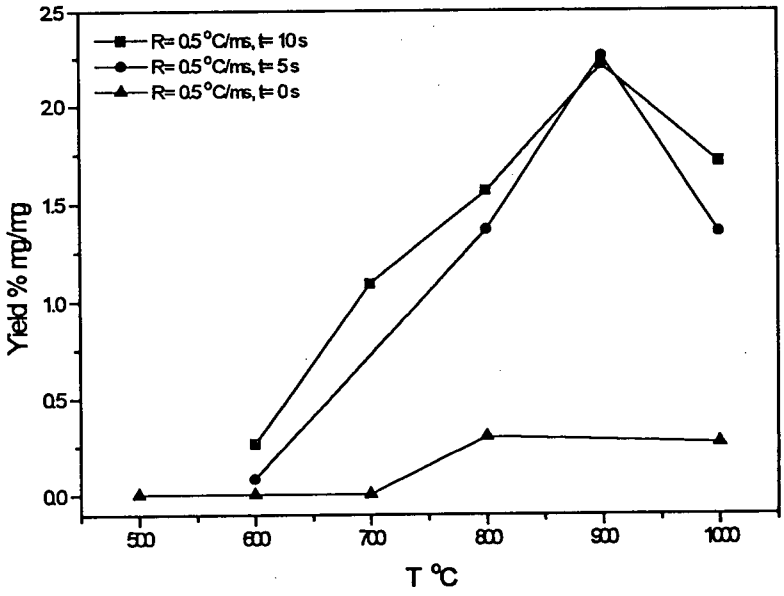

Figure 4.2.8 CANMET pitch pyrolysis C_{10} yield vs. temperature at different pyrolysis holding times with heating rate 30,000 °C/min

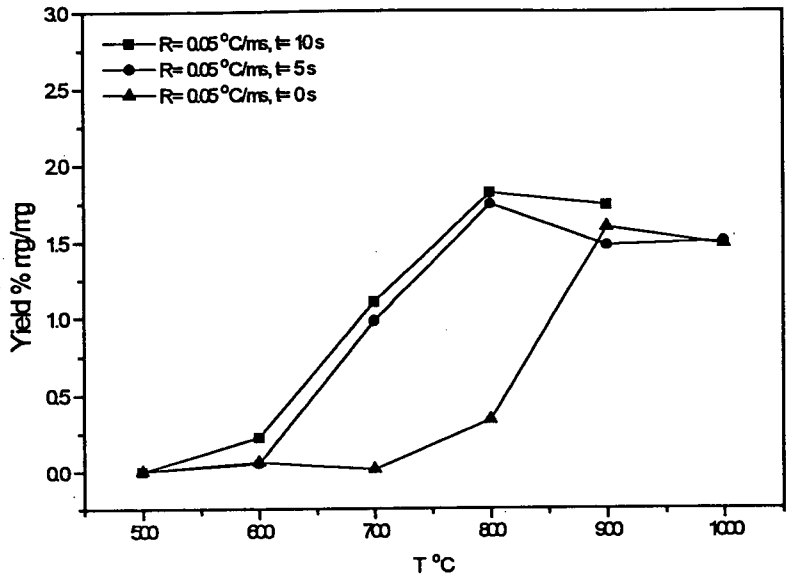

Figure 4.2.9 CANMET pitch pyrolysis C_{10} yield vs. temperature at different pyrolysis holding times with heating rate 3000 °C/min

4.2.1.4 Effect of Experimental Conditions on the C_{11} Yield

Figure 4.1.10 shows that the C_{11} yield generally increases to 800 °C and then decreases as temperature at the heating rate of 300,000 °C/min, with maximum C_{11} yield observed at 800 °C. Maximum C_{11} yield of 2.7% and 1% is obtained at 800 °C for holding time 10 and 0 s respectively. There is no C_{11} observed at temperatures lower than 600 °C for holding time 10 s, and 700 °C for holding time 0 s. It is worth noting that the C_{11} yield is negligible at 1000 °C for holding time 10 s and temperatures higher than 900 °C for holding time 0 s, indicating that the C_{11} lump depleted due to further pyrolysis (i.e. secondary reactions).

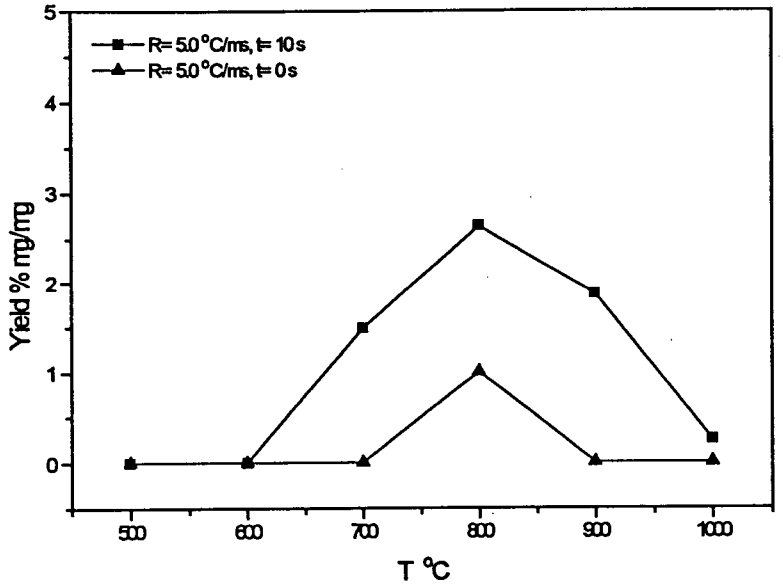

Figure 4.2.10 CANMET pitch pyrolysis C_{11} yield vs. temperature at different pyrolysis holding times with heating rate 300,000 °C/min

4.2.1.5 Effect of Experimental Conditions on the C_{12} Yield

Figure 4.2.11 shows that the C_{12} yield generally increases to 800 °C and then decreases as temperature at the heating rate of 300,000 °C/min, with maximum C_{12} yields observed at 800 °C. Maximum C_{12} yield of 3.7% and 1% is obtained at 800 °C for holding times 10 and 0 s respectively. There is no C_{12} observed at temperature lower than 600 °C for holding time 10 s, 700 °C for holding time 0 s. It is also worth noting that the C_{12} yield depleted at 900 °C due to its further pyrolysis at 0 second holding time and also significantly decreased at temperatures above 800 °C for 10 second holding time.

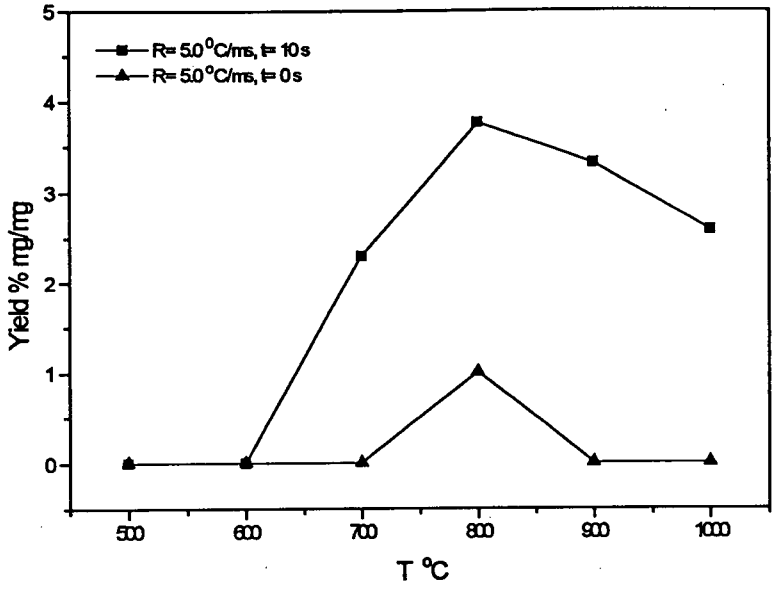

Figure 4.2.11 CANMET pitch pyrolysis C_{12} yield vs. temperature at different pyrolysis holding times with heating rate 300,000 °C/min

4.2.1.6 Effect of Experimental Conditions on the C_{13} Yield

Figure 4.2.12 shows the C_{13} yield generally increases to 700 °C and then decreases as temperature at the heating rate of 30,000 °C/min, with the maximum C_{13} yield observed 700 °C for the holding time studied. Higher C_{13} yield is also observed at a longer holding time. The maximum C_{13} yield, observed at 700 °C, is 2.9%, 2.4% and 2.1% for holding times 10, 5 and 0 s. C_{13} yield decreased as further increase of temperature. This again indicates secondary pyrolysis of C_{13} lump at higher temperature.

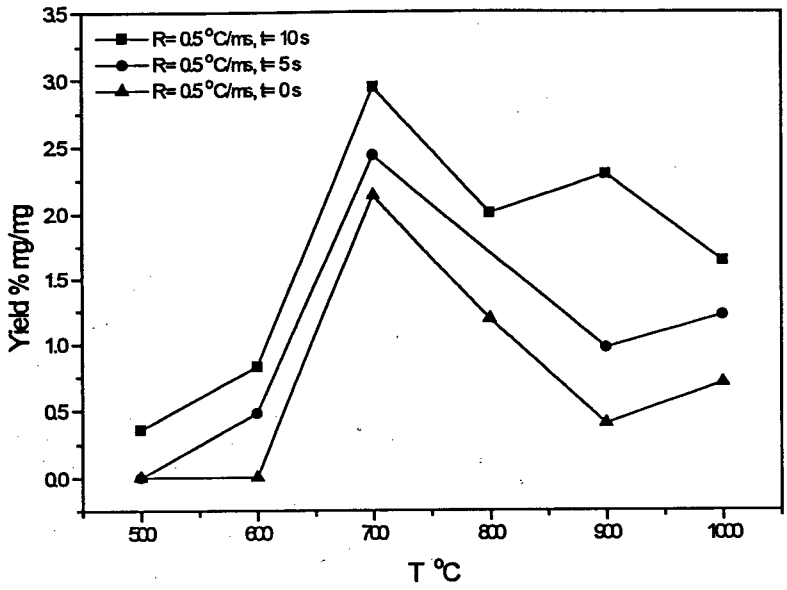

Figure 4.2.12 CANMET pitch pyrolysis C_{13} yield vs. temperature at different pyrolysis holding times with heating rate 30,000 °C/min

4.2.1.7 Effect of Experimental Conditions on the C_{14} Yield

Figures 4.1.13 and 4.1.14 show that the C_{14} yield generally increases to certain temperatures and then decreases as temperature. At the heating rate of 300,000 °C/min as shown in Figure 4.2.13, maximum C_{14} yield is obtained at 800 °C for holding time 10 s and 900 °C for holding time 5 s. The maximum yields are 1.7% and 1.3% respectively. There is no C_{14} observed at the temperature range studied for holding time 0 s.

At heating rate 30,000 °C/min as shown in Figure 4.2.14, it is observed that the C_{14} yield vs. temperature at different holding times is not linear. Maximum C_{14} yield is observed at 700 °C for holding times 10 and 5 s. The maximum yields are 3.89% and 3.91% respectively. C_{14} yield increased as temperature in the range from 500 to 700 °C, decreased in the range from 700 to 1000 °C. C_{14} yield for holding time 10 s is close to that for holding time 5 s at the same temperature. Secondary reaction is also evident for C_{14} as shown in Figures 4.2.13 and 4.2.14.

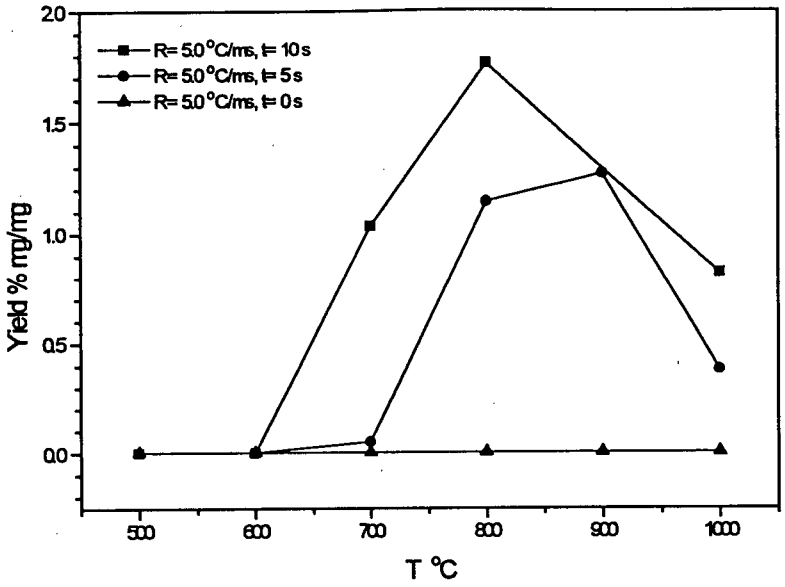

Figure 4.2.13 CANMET pitch pyrolysis C_{14} yield vs. temperature at different pyrolysis holding times with heating rate 300,000 °C/min

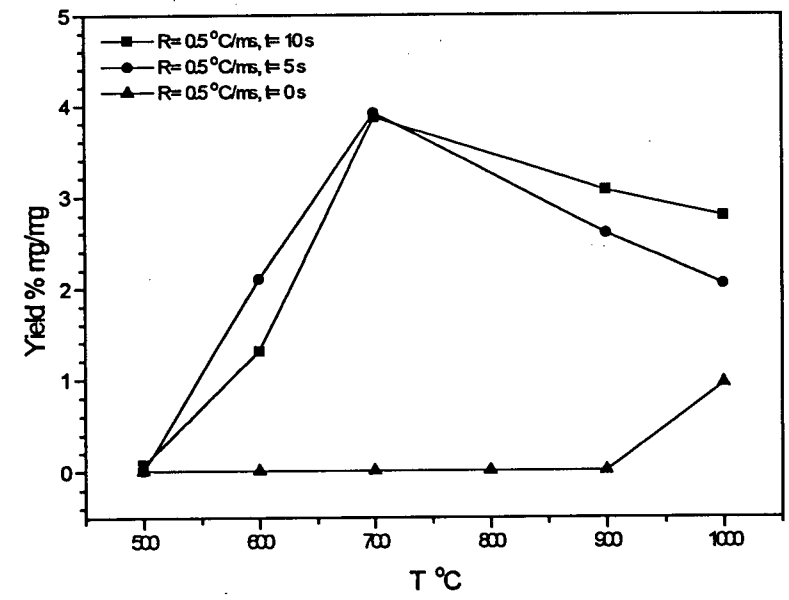

Figure 4.2.14 CANMET pitch pyrolysis C_{14} yield vs. temperature at different pyrolysis holding times with heating rate 30,000 °C/min

4.2.2 Pyroprobe-GC Pyrolysis of Syncrude Pitch

The Pyroprobe-GC pyrolysis of Syncrude pitch was again performed under different experimental conditions to study the effects of heating rates, pyrolysis reaction temperatures and holding times. The sample weight was kept relatively constant around 5 mg in order to limit the sample size effect. The heating rates are 300,000, 30,000, 3000, 600 °C/min, the holding time is 10, 5 and 0 s. The combinations of these operating parameters are listed in Table 4.2.2. Each combination of these parameters was performed at the final temperatures of 500, 600, 700, 800, 900, 1000 °C.

Table 4.2.2 Experimental Conditions for Runs at Different Holding Times

Holding Time s	Heating Rate °C/min
10.0	300,000
5.0	300,000
0.0	300,000
10.0	30,000
5.0	30,000
0.0	30,000
10.0	3000
5.0	3000
0.0	3000
10.0	600
5.0	600
0.0	600

4.2.2.1 Effect of Experimental Conditions on the Total Weight Loss

The total weight loss vs. holding time is an important character for Syncrude pitch pyrolysis as well. The effect of holding times on the total weight loss is shown in Figure 4.2.15.

Figure 4.2.15 shows that the weight loss generally increases as the increase of temperature at 300,000 °C/min, with maximum yield observed for 5 s holding time. Higher weight loss is observed for 10 s than 5 s or 0 s. It is also noted that the weight loss is not significant at holding time 0 s.

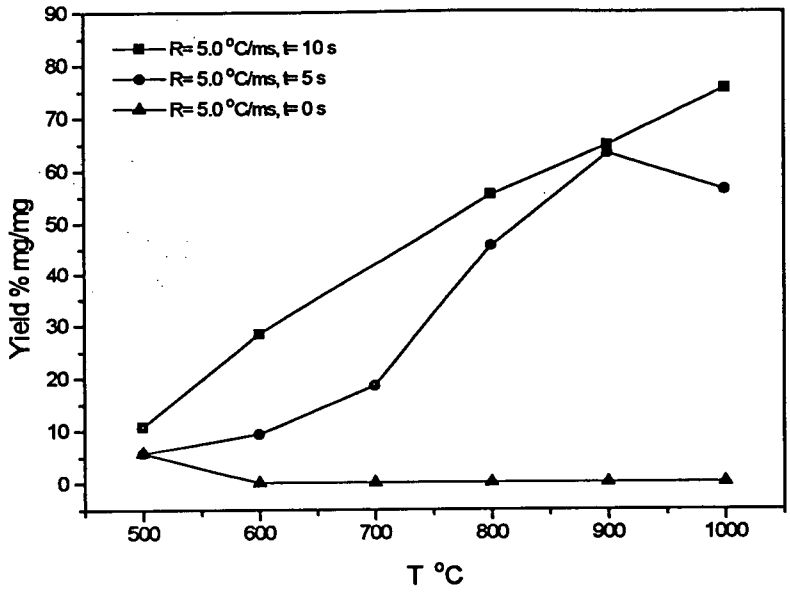

Figure 4.2.15 Syncrude pitch pyrolysis total weight loss vs. temperature at different pyrolysis holding times with heating rate 300,000 °C/min

4.2.2.2 Effect of Experimental Conditions on the C_7 Yield

Figure 4.16 shows that the C_7 yield increases as temperature at the heating rate of 300,000 °C/min, with maximum yield observed for 5 s holding time. Higher C_7 yield is observed at a longer holding time. The C_7 yield reached 75% and 60% at 10 and 5 s holding time respectively, while no C_7 was detected at all at 0 s. Comparison with Figure 4.1.5 shows that at high heating rates the C_7 lump comprises essentially all the weight loss.

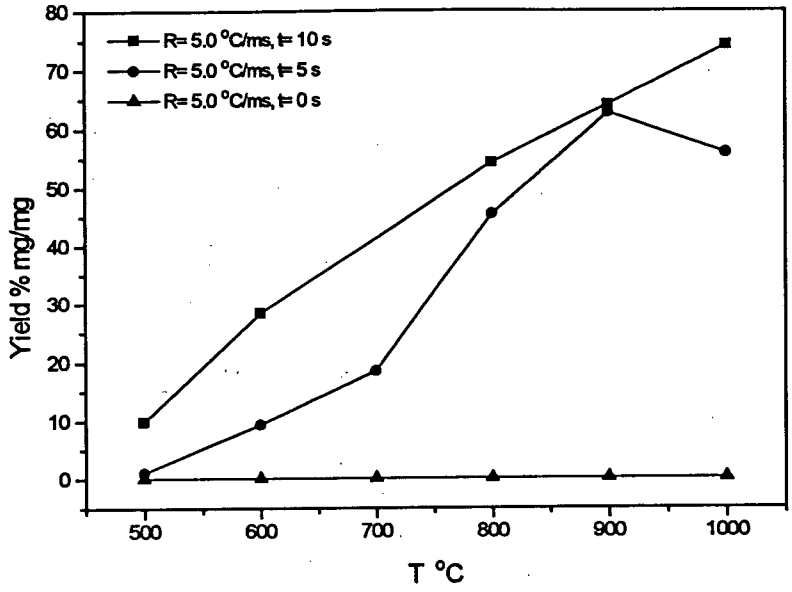

Figure 4.2.16 Syncrude pitch pyrolysis C_7 yield vs. temperature at different pyrolysis holding times with heating rate 300,000 °C/min

4.2.2.3 Effect of Experimental Conditions on the C_{10}, C_{11}, C_{12}, C_{13}, and C_{14} Yield

Higher yield of C_{10} and C_{11} is generally obtained at a lower holding time and higher temperature at the heating rate of 300,000 °C/min. However, the yields of these lumps are rather small. The C_{10} yield reached only 0.7% and 0.5% at holding time of 10 and 5 s respectively, while the C_{11} yield reached only 0.225% and 0.07% for holding time 10 and 5 s. At heating rate 600, 3000, 30,000 °C/min, little C_{10} and C_{11} was detected.

The heating rate effect is not an important parameter for C_{12}, C_{13}, C_{14} yield. The increase of heating rates did not show any significant effect on C_{12}, C_{13}, C_{14} yield as observed in the CANMET pitch pyrolysis. The quantity of each of the lumps is not abundant to determine accurately.

4.2.3 Discussion and Conclusion

It is shown that under Pyroprobe pyrolysis conditions, the pyrolysis reaction time is a very important operating parameter. At the highest heating rate (300,000 °C/min) employed in this study, there is little pyrolysis, i.e. weight loss, is observed for both CANMET and Syncrude pitches, while at heating rate of 3000 °C/min, the weight loss is rather significant when the final temperature is just reached (0 s isothermal reaction time). In the latter case, some 10 to 50% of volatile yield was observed at different final temperature. The latter case is somewhat similar to the TGA experiment results, and the effect of the heating period on the pyrolysis of either CANMET or Syncrude pitch should not be ignored. At heating rate of 30,000 °C/min, the weight loss results are rather close to those at 300,000 °C/min, while they are generally higher than those at 3000 °C/min. The effect of the heating rate combined with the final temperature is therefore expected to be interrelated and remains as a topic of research for high heating rate pyrolysis. However, a different pyrolysis mechanism is also expected for the high heating rate pyrolysis.

The most abundant component of the volatile is shown experimentally the hydrocarbons with less than 10 carbons, which is grouped as single lump as C_7 in this study. At each heating rate and final temperature, the amount of C_7 is becoming significant at temperatures higher than 700 °C. As high as 50% volatile yield of this group was detected for CANMET pitch and secondary reaction is observed at heating rate 3000 °C/min. At the Pyroprobe pyrolysis conditions, the volatile may undergo secondary pyrolysis when being purged through the quartz tube. Similar trend is also observed for Syncrude pitch pyrolysis with Pyroprobe-GC.

The yield of C_{10} compounds is very strongly influenced by the heating rates. At the highest heating rate (300,000 °C/min), less than 5% volatile yield of this group of components was detected, while as high as 23% volatile yield of the group was detected at 30,000 °C/min. This again attests the influence of the reaction time and heating rates. The amount of C_{10} detected from

Syncrude pitch pyrolysis with Pyroprobe-GC is much less than that of CANMET pitch. This is in agreement with the difference of "chemical structure" or "chemical makeup" of these two pitches, where proximate analysis, ultimate analysis and fractionation also show that Syncrude pitch contains more low molecular components than CANMET pitch.

Higher yields of C_{11}, C_{12}, C_{13} and C_{14} groups was also detected at lower heating rates, a similar trend as that of C_{10} group. While the yield of C_{14} is much less that those of C_{11}, C_{12} and C_{13}. C_{14} is the heaviest group of compound detected in the Pyroprobe-GC pyrolysis. This may indicate that the volatile is mostly compounds lighter than C_{14}. The yield of these groups from Syncrude pitch pyrolysis with Pyroprobe-GC is also significantly less than those from CANMET pitch pyrolysis. This is in agreement with the C_{10} yield.

The different yields of each lumped group between CANMET pitch and Syncrude pitch is in good agreement with the difference of the chemical nature of these two pitch samples. This is also in agreement with the TGA pyrolysis results in which the TGA pyrolysis curves showed different patterns between the above two samples.

Secondary reaction of the product lumps is evident for both CANMET and Syncrude pitch. At high temperatures, heavy lumps such as C_{14}, are prone to pyrolysis into smaller molecules before leaving the quartz tube.

Chapter 5 Modeling of Experimental Results

5.1 Introduction of Pyrolysis Kinetic Models

A number of mechanisms which have been proposed in the literature for pyrolysis were described in the literature review. However, the single overall first order reaction mechanism has been accepted most widely due to its simplicity and adequacy to explain the pyrolysis behavior and to model the process mathematically. The single overall first order reaction model assumed that de-volatilization takes place as a single first order reaction and the mechanism does not change during pyrolysis process. It is widely used to describe and explain the pyrolysis processes of coal, oil shale, bitumen, biomass and other hydrocarbons, due to its mathematical simplicity. A number of first order reaction models were thus proposed to that effect.

The general expression for the first order mechanism is given as:

$$\frac{dV}{dt} = k_o e^{-E/RT}\left(V^* - V\right) \tag{5.1}$$

Under nonisothermal conditions, such as those in the TGA experiments, the temperature at any time during the heating period is given by the following expression;

$$T=Ct+T_o \tag{5.2}$$

where T_o is the initial temperature of the experiment. Substituting time term dt with temperature dT, i.e. dT=C*dt, the general expression is then given as:

$$\frac{dV}{dT} = \frac{k_o}{C} e^{-E/RT}\left(V^* - V\right) \tag{5.3}$$

where:

V^*	maximum volatile content released at the final temperature, wt%
T	pyrolysis temperature, K
V	volatile content released at temperature T, wt%
t	pyrolysis reaction time, min.

E activation energy of the single overall first order reaction, J/mol

k_o pre-exponential factor of the single overall first order reaction, min^{-1}.

R gas constant, 8.314 J/mol.K

C pyrolysis heating rate, K/min.

5.1.1 Overall First Order Reaction Model

A number of methods have been suggested to extract values of k_o and E for Equation 5.3 from experiments in which V is measured as a function of T at constant heating rate. Since they use the experimental data in different forms, they tend to give different results for the reaction parameters.

5.1.1.1 Integral Method

This method estimates the values of E and k_o of a reaction from the overall volatile yield vs. temperature curves. Shih and Sohn [108] used this method to determine the kinetic parameters for oil shale pyrolysis. The general expression is rearranged as:

$$\frac{dV}{V^* - V} = \frac{k_o}{C} e^{-E/RT}\, dT \tag{5.4}$$

Integrating the above expression in the temperature range of interest, we then get

$$\int_0^V \frac{dV}{V^* - V} = \int_{T_o}^{T} \frac{k_o}{C} e^{-E/RT} dT \tag{5.5}$$

where T_o is the initial temperature. In the current study the T_o is chosen as 50 °C, and the rate as well as the total volatile yield at this temperature is negligible; therefore the temperature limit T_o can be by replaced by 0.

Integration of the above equation gives, with T_o assumed to be 0 K.

$$-\ln\left(\frac{V^* - V}{V^*}\right) = \frac{k_o}{C}\left[T e^{-E/RT} + \frac{E}{R} E_i\left(-\frac{E}{RT}\right)\right] \tag{5.6}$$

The exponential integral E_i (-E/RT) can be approximated by (Appendix C):

$$E_i\left(-\frac{E}{RT}\right)=-\frac{e^{-E/RT}}{E/RT}\left(1-\frac{1!}{E/RT}+\frac{2!}{(E/RT)^2}-\cdots\right) \tag{5.7}$$

If the first three terms of the approximation are used, the above integration becomes:

$$-\ln\left(\frac{V^*-V}{V^*}\right)\approx\frac{k_o RT^2}{CE}\left(1-\frac{2RT}{E}\right)e^{-E/RT} \tag{5.8}$$

Dividing both sides of the above equation by $RT^2(1-2RT/E)/C$ and taking the logarithm, then

$$\ln\left(\frac{-C\ln\left(1-\frac{V}{V^*}\right)}{RT^2}\right)-\ln\left(1-\frac{2RT}{E}\right)\approx\ln\frac{k_o}{E}-\frac{E}{RT} \tag{5.9}$$

The values of E and k_o can be obtained by repeated least squares fit of the above equation to the experimental data. By first using an approximate E in the left hand side of the above equation, the least squares fit can therefore be performed with the FORTRAN program in Appendix D. The value of E thus obtained is then used as the new value on the left hand side and successively a more accurate value of E is obtained until no improvement in the value of E takes place. The values of E and k_o are therefore obtained.

From the above equation, the volatile yield V (Appendix C) can be obtained as

$$V=V^*\left\{1-\exp\left[-\frac{k_o RT^2}{CE}e^{-E/RT}\left(1-\frac{2RT}{E}\right)\right]\right\} \tag{5.10}$$

5.1.1.2 Friedman Method

This method determines the values of E and k_o from the ratio dV/dT vs. temperature. Rewriting the general expression (Equation 5.3) as:

$$\frac{C}{V^*}\frac{dV}{dT}=k_o e^{-E/RT}\frac{(V^*-V)}{V^*} \tag{5.11}$$

Taking the logarithm and rearranging,

$$\ln\left(\frac{C}{V^*}\frac{dV}{dT}\right)-\ln\left(1-\frac{V}{V^*}\right)=\ln k_o-\frac{E}{RT} \qquad (5.12)$$

The values of E and k_o can be obtained by fitting the above equation to the experimental data, using least squares fitting program in Appendix D. The values of dV/dT are calculated by using two adjacent pairs of the volatile and temperature data:

$$\left(\frac{dV}{dT}\right)_i=\frac{V_{i+1}-V_i}{T_{i+1}-T_i} \qquad (5.13)$$

Where i=1, n-1. The number of data points in a run is n, and $(dV/dT)_n=(dV/dT)_{n-1}$.

The volatile yield can then be calculated from Equation 5.10 with the values of E and k_o obtained.

5.1.1.3 Coats-Redfern Method

This method is the same as the integral method except that the term of 2RT/E is ignored in Equation 5.9. This simplifies the mathematical procedure, and is based on the assumption of $2RT/E \ll 1$.

$$\ln\left(\frac{-C\ln\left(1-\frac{V}{V^*}\right)}{RT^2}\right)=\ln\frac{k_o}{E}-\frac{E}{RT} \qquad (5.14)$$

The values of E and k_o can be obtained by fitting the above equation to the experimental data, using the program in Appendix D. The volatile yield can be obtained from Equation 5.10 by using the E and k_o values thus obtained.

5.1.1.4 Chen-Nuttall Method

This method assumed the initial temperature to be zero K. The initial temperature of this investigation (50 °C) was taken to be close enough to 0 such that the rate as well as the volatile yield was negligible. The general expression is then given as:

$$\int_0^V \frac{dV}{V^* - V} = \int_0^T \frac{k_o}{C} e^{-E/RT} dT \qquad (5.15)$$

Integration of the above equation gives:

$$\ln\left(1 - \frac{V}{V^*}\right) = -\frac{k_o}{C} \frac{RT^2}{E + 2RT} e^{-E/RT} \qquad (5.16)$$

Multiplying both sides of the above equation by $-C(E+2RT)/RT^2$ and taking logarithms gives:

$$\ln\left(\frac{-C(E+2RT)}{RT^2} \ln\left(1 - \frac{V}{V^*}\right)\right) = \ln k_o - \frac{E}{RT} \qquad (5.17)$$

The values of E and k_o can be obtained by repeated least squares fit of the above equation to the experimental data with the same procedure as that of the integral method. By first using an approximate E in the left hand side of the above equation, the least squares fit can therefore be performed with the FORTRAN program in Appendix D and the value of E thus obtained is used in the calculation of the values of the left hand side of the equation and successively a more accurate value of E is obtained until no improvement in the value of E takes place. The values of E and k_o are therefore obtained. The volatile yield can also be calculated from Equation 5.10 with the values of E and k_o obtained.

5.1.2 Multi-First-Order Reaction Model

One of the principal shortcomings of the above four methods is the tacit assumption that a single activation energy and a single pre-exponential factor can adequately describe the evolution of the pyrolysis products. For the case of fossil fuel and especially pitch pyrolysis it is physically

realistic to expected evolution of products (for example CH_4 and H_2) from a wide range of chemically nonequivalent sources. Hence more than one rate constant would be required to describe the pyrolysis process. Anthony and Howard [30] proposed a model to deal with this situation in an attempt to explain the coal devolatilization mechanism. Their model describes the evolution of products by a number of parallel, first order rate processes, each represented by a rate constant k. To simplify the problem, Anthony and Howard [30] assumed that the rate constants have the same pre-exponential factor, and differ only in activation energy, and that the number of parallel reactions is sufficiently large for the activation energies to be described by a Gaussian distribution function. The model and its assumptions have been described in the literature review section in more detail.

Integration of the general expression in the activation range of 0 to ∞ gives:

$$V = V^*\left(1-\frac{1}{s(2\pi)^{0.5}}\int_0^{\infty}\exp\left\{\frac{k_o RT^2}{CE}\left[\exp\left(-\frac{E}{RT}\right)\left(1-\frac{2RT}{E}\right)\right]\right\}\exp\left[-0.5\left(\frac{E-E_0}{s}\right)^2\right]dE\right) \tag{5.18}$$

Due to the complex and nonlinear nature of the model function, nonlinear regression must be used to fit the experimental data for E_o, k_o and s. The Levenberg-Marquart method is thus used in this work. This method adjusts k_o, E_o and s within the calculation. Some authors [52] used a fixed k_o value to simplify the mathematical process and reduce the computing time. However their approach resulted in questionable kinetic parameters. This Levenberg-Marquart method is proven a good nonlinear method. It requires the derivatives of V with respect to each of the three parameters: k_o, E_o and s. In order to use the Levenberg-Marquart method, the derivatives with respect of each parameter must be derived in a specific range of activation energy, using the following general mathematical formula [109]:

$$\frac{d}{dt}\int_{a(t)}^{b(t)} f(x,t)\,dx = \int_{a(t)}^{b(t)} f_t'(x,t)dt + f(b,t)\frac{db}{dt} - f(a,t)\frac{da}{dt}$$

The range of the activation energy is selected as E_o-4s to E_o+4s. Further increases in the range of activation energy did not improve the precision of parameters and the accuracy of the volatile prediction. These derivatives have been derived as part of this work as is shown below:

$$\begin{aligned}\frac{dV}{dE_0} = -\frac{V^*}{s(2\pi)^{0.5}}\Big[\int_{E_0-4s}^{E_0+4s}&\exp\left\{-\frac{k_o RT^2}{CE}\exp(-\frac{E}{RT})(1-\frac{2RT}{E})\right\}\exp\left\{-0.5(\frac{E-E_0}{s})^2\right\}\\ &(\frac{E-E_0}{s^2})dE + \exp(-8)\exp\left\{-\frac{k_o RT^2}{C(E_0+4s)}\exp(-\frac{E_0+4s}{RT})(1-\frac{2RT}{E_0+4s})\right\}\\ &-\exp(-8)\exp\left\{-\frac{k_o RT^2}{C(E_0-4s)}\exp(-\frac{E_0-4s}{RT})(1-\frac{2RT}{E_0-4s})\right\}\Big]\end{aligned} \tag{5.19}$$

$$\begin{aligned}\frac{dV}{ds} = &\frac{V^*}{s^2(2\pi)^{0.5}}\int_{E_0-4s}^{E_0+4s}\exp\left\{-\frac{k_o RT^2}{CE}\exp(-\frac{E}{RT})(1-\frac{2RT}{E})\right\}\exp\left\{-0.5(\frac{E-E_0}{s})^2\right\}dE\\ &-\frac{V^*}{s(2\pi)^{0.5}}\int_{E_0-4s}^{E_0+4s}\exp\left\{-\frac{k_o RT^2}{CE}\exp(-\frac{E}{RT})(1-\frac{2RT}{E})\right\}\exp\left\{-0.5(\frac{E-E_0}{s})^2\right\}\frac{(E-E_0)^2}{s^3}dE\\ &-\frac{4V^*}{s(2\pi)^{0.5}}\exp(-8)\exp\left\{-\frac{k_o RT^2}{C(E_0+4s)}\exp(-\frac{E_0+4s}{RT})(1-\frac{2RT}{E_0+4s})\right\}\\ &-\frac{4V^*}{s(2\pi)^{0.5}}\exp(-8)\exp\left\{-\frac{k_o RT^2}{C(E_0-4s)}\exp(-\frac{E_0-4s}{RT})(1-\frac{2RT}{E_0-4s})\right\}\end{aligned} \tag{5.20}$$

$$\begin{aligned}\frac{dV}{dk_o} = -\frac{V^*}{s(2\pi)^{0.5}}&\int_{E_0-4s}^{E_0+4s}\exp\left\{-\frac{k_o RT^2}{CE}\exp(-\frac{E}{RT})(1-\frac{2RT}{E})\right\}\\ &(-\frac{RT^2}{CE})\exp(-\frac{E}{RT})(1-\frac{2RT}{E})\exp\left\{-0.5(\frac{E-E_0}{s})^2\right\}dE\end{aligned} \tag{5.21}$$

A FORTRAN program was written to solve the above ODEs and the procedures outlined in Numerical Recipe [110] were followed. The FORTRAN program is listed in Appendix D.

5.1.3 Mathematical Methods for Overall Single First Order Reaction Model

In order to use the first order model to fit the parameters, the experimental data, i.e. the measured volatile contents need to be converted according to each method into the form:

$$Y = a + bX \tag{5.22}$$

Y is the LHS of each of the single overall first order reaction methods, b is equal to -E/R, and X is the reciprocal of temperature 1/T in K. The Y and a for each method are listed in Table 5.1.

Table 5.1 Y and a Formulas for the Overall Single First Order Reaction Model

Methods	Y	a
Integral	$Y = \ln\left(\frac{-C\ln\left(1-\frac{V}{V^*}\right)}{RT^2}\right) - \ln\left(1-\frac{2RT}{E}\right)$ (5.23)	$a = \ln(k_o/E)$ (5.23a)
Friedman	$Y = \ln\left(\frac{C}{V^*}\frac{dV}{dT}\right) - \ln\left(1-\frac{V}{V^*}\right)$ (5.24)	$a = \ln k_o$ (5.24a)
Coats-Redfern	$Y = \ln\left(\frac{-C\ln\left(1-\frac{V}{V^*}\right)}{RT^2}\right)$ (5.25)	$a = \ln(k_o/E)$ (5.25a)
Chen-Nuttall	$Y = \ln\left(\frac{-C(E+2RT)}{RT^2}\ln\left(1-\frac{V}{V^*}\right)\right)$ (5.26)	$a = \ln k_o$ (5.26a)

The Y values for the integral method and Chen-Nuttall method were calculated with the first guess of E, and then iterated for the best fit for the activation E and pre-exponential factor k_o. The values of E and k_o for the Friedman and Coats-Redfern methods are obtained by using least squares to fit the above equations to experimental data.

5.2 Testing of the Basic Models

The volatile yield was checked against the prediction of the four different methods and one model described in the previous section. Each method was used to fit to the experimental data for the pre-exponential factor, the activation energy as well as standard activation energy distribution

for the Anthony and Howard model. The values of the k_o, E, as well as s were then used to predict the volatile yield. These values are listed for CANMET pitch, along with the results of kinetic parameters for Moroccan oil shale pyrolysis [111] in Table 5.2.

Table 5.2 Kinetic Parameters for the Nonisothermal Pyrolysis of CANMET Pitch at 50 °C/min. and 700 °C Compared with Literature

Model/Method	Feed	k_o $min.^{-1}$	E kJ/mol	s kJ/mol	s.e.e.
Integral	Pitch	151.0	33.1		6.57
Friedman	Pitch	130.0	32.5		6.12
Coats-Redfern	Pitch	59.1	30.8		9.33
Chen-Nuttall	Pitch	104.0	32.0		5.40
Coats-Redfern[111]	Shale	56.4	32.9		5.3
Chen-Nuttall[111]	Shale	37.7	31.6		5.4
Anthony-Howard	Pitch	$5.0x10^8$	114.9	14.9	6.22
Anthony-Howard[111]	Shale	$5.8x10^5$	90.4		4.6

There is a close agreement between the values obtained in this study and those obtained by Thakur and Nuttall [111] except for the k_o value of the Anthony Howard model. The kinetic parameters also compare favorably with the literature [112-115] for kerogen pyrolysis to bitumen.

Having obtained the kinetic parameters, the volatile yields can then be predicted using Equation 5.10, which were computed using the program in the Appendix D. The predicted and experimental results are plotted in Figure 5.1. It is clear that these models all failed to predict the volatile contents at temperatures higher than 200 °C even though the values of the kinetic parameters are well within the expected range for hydrocarbon pyrolysis and agree well with the literature, and the standard deviation (s.e.e.) is small enough. However, the s.e.e. is misleading because it is the average error (Equation 5.31). The difference between experimental data and the model prediction, is up to 30 % as is observed in Figure 5.1. It comes as no surprise that these models failed. The fact that the chemical nature of the "pitch" is changing continuously as the pyrolysis progresses has long been overlooked. Schuckler [116] reported that the activation energy increases markedly with the increase of fractional volatilization V/V^*. This drastic change

in activation energies coupled with the unusually high preexponential factors at V/V^* of 0.8 and 0.9 suggested a significant change in the pyrolysis mechanism at high volatile levels. The discrepancy at high temperature in Figure 5.1 is also supported by Thakur and Nuttall [111], who reported that two sets of kinetic parameters are required to fit their experimental data over the whole range.

The Anthony and Howard [30] model takes account of the expected change of activation energy in the fashion of a Gaussian distribution with a constant pre-exponential factor. Although this assumption reflects the fact that the activation energy increases in the pyrolysis process, it does not adequately reflect the rate constant change of either CANMET pitch or Syncrude pitch pyrolysis quantitatively and mechanistically. The additional parameter, s, is insufficient to fit the experimental results.

In examining the Y values for each overall single reaction model, it is clear that the assumption of the linear relation between Y values and X is not valid for each of the methods, as shown in Figures 5.2, 5.3, 5.4, and 5.5. Inflection points are observed at X value of 0.0014 (450 °C). This observation is in accordance to the fact that the ratio of pyrolysis dV/dT is dramatically increased at 450 °C as shown in Figures 4.1.15 and 4.1.19 in Chapter 4. Single step reaction models applied to CANMET pitch over the whole temperature range failed to predicted this basic feature. The fitting results of these models to Syncrude pitch showed similar results, in that the single step model failed to predict the change of pyrolysis rate and volatile yield. The results obtained in the present study indicate that the thermal pyrolysis reactions of pitches are complex to the extent that they can not be described as a single overall first order reaction. Hence the above models (the overall single reaction model analyzed with four different mathematical methods, the Anthony and Howard model analyzed with the Levenberg-Marquart nonlinear

regression method) can not be used to fit the TGA data of CANMET and Syncrude pitch pyrolysis.

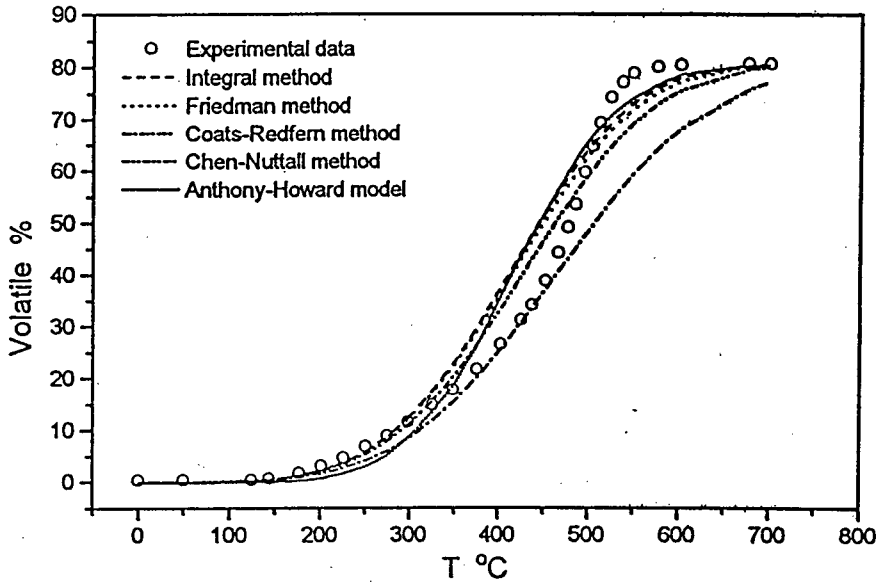

Figure 5.1 Comparison of model prediction and experimental volatile for CANMET pitch at 50 °C/min. and 700 °C with first order reaction models

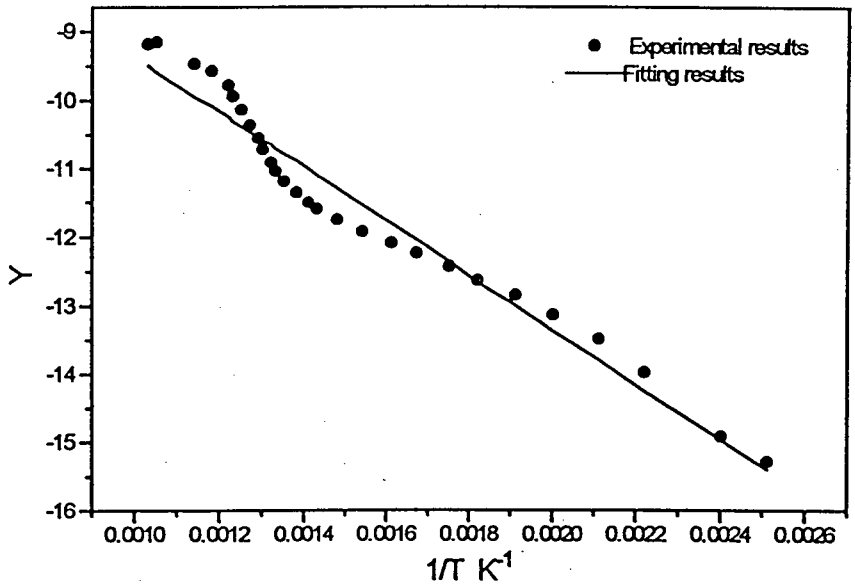

Figure 5.2 Comparison of model predicted Y results and experimental Y results for CANMET pitch at 50 °C/min. and 700 °C with integral method

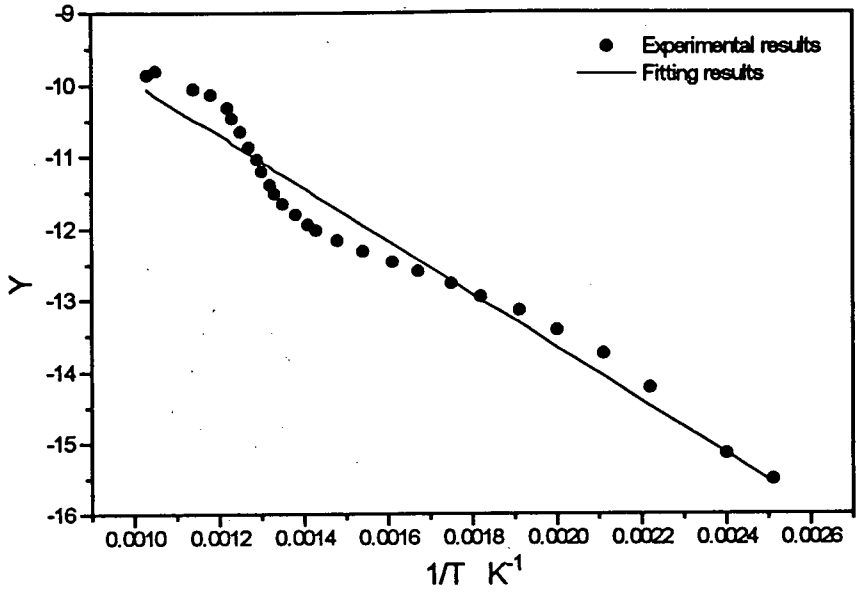

Figure 5.3 Comparison of model predicted Y results and experimental Y results for CANMET pitch at 50 °C/min. and 700 °C with Coats-Redfern method

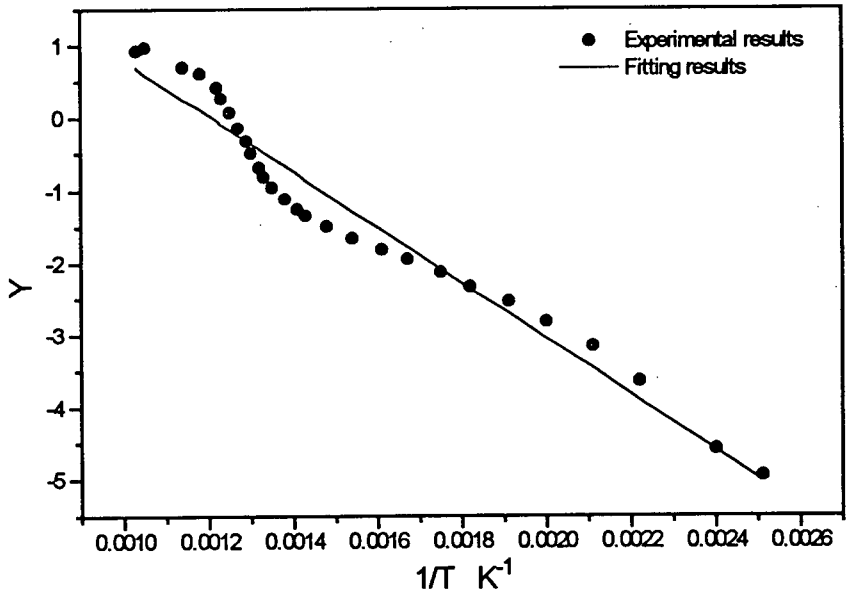

Figure 5.4 Comparison of model predicted Y results and experimental Y results for CANMET pitch at 50 °C/min. and 700 °C with Chen-Nuttall method

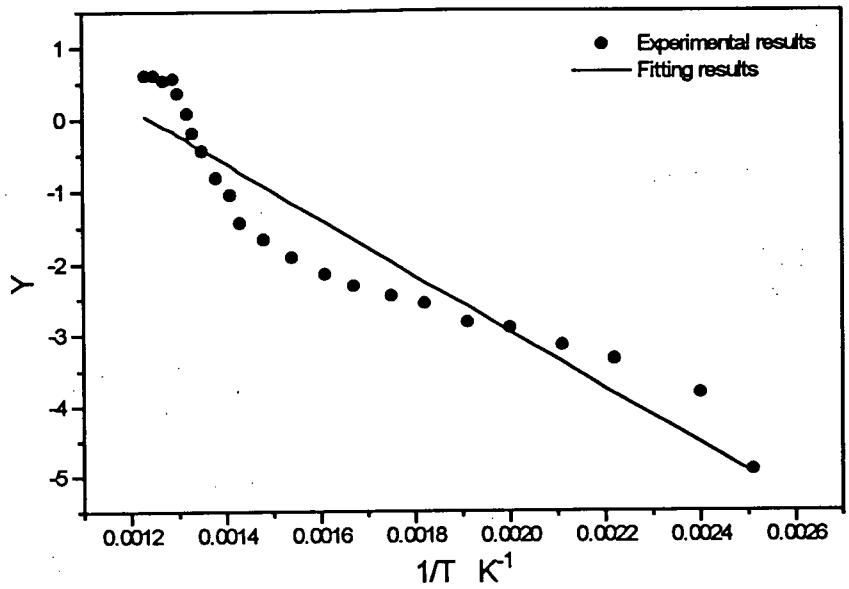

Figure 5.5 Comparison of model predicted Y results and experimental Y results for CANMET pitch at 50 °C/min. and 700 °C with Friedman method

5.3 2-Stage First Order Reaction Model

Multi-step behavior has been clearly identified in the present data as well as results of Rajeshwar [113], Thakur and Nuttall [111] and Schuckler [116]. Rajeshwar [113], Thakur and Nuttall [111] analyzed their oil shale pyrolysis data with the assumption that the thermal decomposition proceeds in two consecutive steps via a soluble bitumen intermediate, while Schuckler [116] analyzed pyrolysis data of heavy residuum fractions within several volatile conversion intervals to evaluate the kinetic parameters, which indicated a multiple step mechanism instead. Campbell et al. [117] employed nonlinear least squares fit of nonisothermal thermogravimetry data to derive kinetic parameters for a Colorado oil shale sample. Herrell and Arnold [118] report the use of nonisothermal TGA for the study of Chattanooga shale. In both these studies the kinetic data have been interpreted in terms of single step decomposition mechanisms. Such an interpretation, however seems to be contradictory to the conclusions

reached in most of the early studies which indicate that the thermal decomposition of oil shale kerogen proceeds in two consecutive steps. It is noted however, that the concept of reaction order and pre-exponential factor in solid-state kinetics assumes a different significance from that adopted in homogenous reaction kinetics. Topochemical considerations restrict values of the reaction order to 0, 1/2, 2/3, and 1 in solid state kinetics [119, 120]. Normally the order of pyrolysis of a sufficiently small sample is considered to be unity [121]. However, a model for a multi-step process such as that identified in the pyrolysis/thermal decomposition process is not yet available. In order to describe the pitch pyrolysis and take into account the activation energy change in the model, it is important that the model reflect those features as shown in Figures 5.6 and 5.7.

Figure 5.6 shows the ratio dV/dT and the rate dV/dt vs. the remaining volatile content V*-V for different heating rates at the final temperature 800 °C for CANMET pitch. It is shown that the ratio dV/dT increase linearly with the increase of the remaining volatile content, up to 25% remaining volatile content, and then decreases approximately linearly with the increase of the remaining volatile content. It is also noted that the heating rate does not show any influence on the volatile yield rate, i.e. the reaction mechanism. The same value of maximum dV/dT is reached at about 25% remaining volatile content for each heating rate. This suggests that the pyrolysis process of CANMET pitch is chemically controlled. This further indicates that the pyrolysis takes place in two stages with differing mechanisms. In the beginning of the pyrolysis, the rate increases with temperature, and the decrease of the remaining volatile content, up to the maximum value which occurs at the remaining volatile content of 25%. Then the ratio dV/dT decreases with increasing temperature, and the decrease of remaining volatile content.

Figure 5.7 shows the ratio dV/dT and the rate dV/dt vs. the remaining volatile content V*-V for different heating rates at the final temperature 800 °C for Syncrude pitch. The ratio dV/dT

increases roughly linearly with the increase of the remaining volatile content, up to about 25% remaining volatile content, which is the amount of the remaining volatile content also observed for the CANMET pitch pyrolysis. However unlike the CANMET pitch pyrolysis, the ratio dV/dT vs. the remaining V*-V does not show a single linear relationship to the end of the pyrolysis process. Instead, the ratio dV/dT vs. the remaining volatile content V*-V decreases approximately linearly to 55% remaining volatile content, then maintains a steady value dV/dT up to 75% remaining volatile content, and then decreases to nil. This is because there are more lower molecular weight components in the Syncrude pitch than in the CANMET pitch shown by the lower pentane solubles and higher H/C atomic ratio in Table 3.1. At the beginning of pyrolysis of the Syncrude pitch, the value increases with the temperature and the decrease of the remaining of the volatile content, then the ratio dV/dT maintains a steady value in the range of remaining volatile content of 55% to 70%. This suggests that lower molecular components undergo mild and rather quick chemical changes in the narrow temperature interval of 300 °C to 450 °C. The steady value in dV/dT is unlikely to be caused by physical changes, such as distillation, because the temperature is too high for distillation of most components existing in pitch samples. The relationship of dV/dT vs. V*-V of Syncrude pitch shows some similarities to that of CANMET pitch, suggesting a similar pyrolysis pathway, at least up to remaining volatile content of 45%.

Similar patterns as that observed from results of dV/dT are also observed in the pyrolysis rate dV/dt plots Figure 5.6b and Figure 5.7b. The difference in these two graphs as a function of heating rate is as expected, and is caused by the difference of time scale of the pyrolysis process.

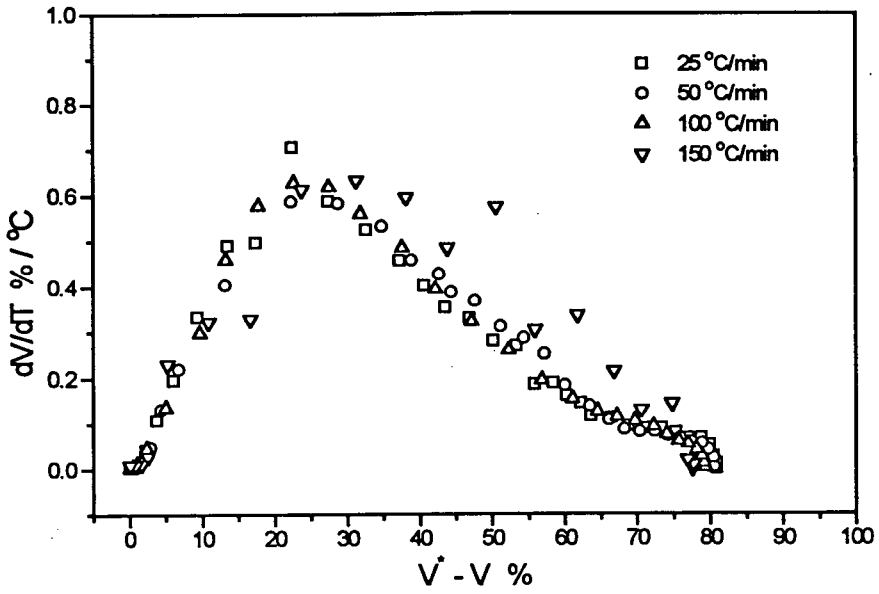

Figure 5.6 The devolatilization ratio dV/dT vs. the remaining volatile at different heating rates and 800 °C for CANMET pitch

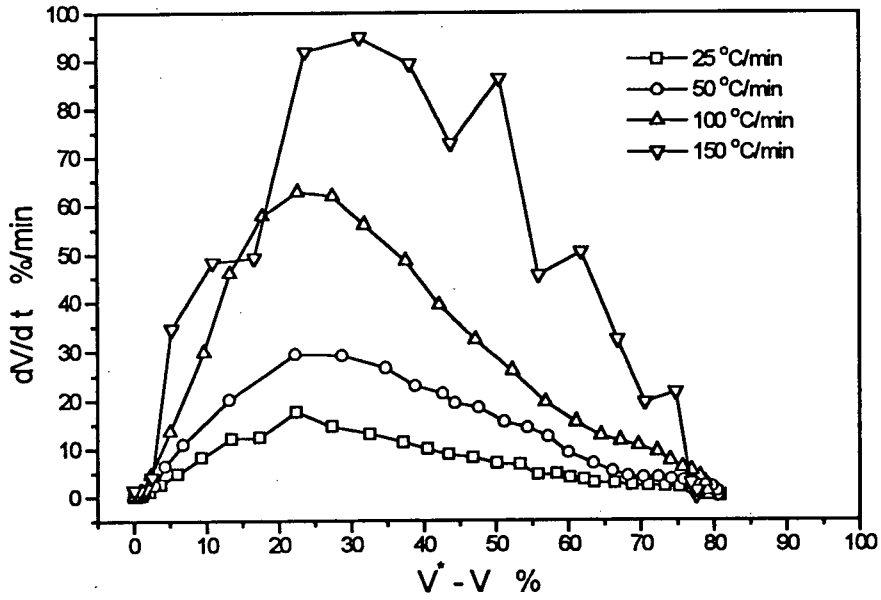

Figure 5.6b The devolatilization rate dV/dt vs. the remaining volatile at different heating rates and 800 °C for CANMET pitch

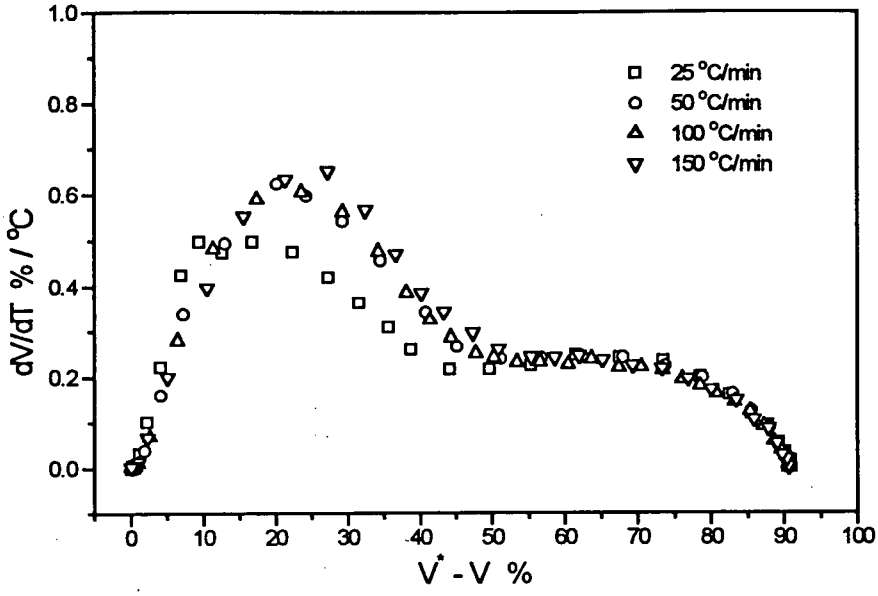

Figure 5.7 The devolatilization ratio dV/dT vs. the remaining volatile at different heating rates and 800 °C for Syncrude pitch

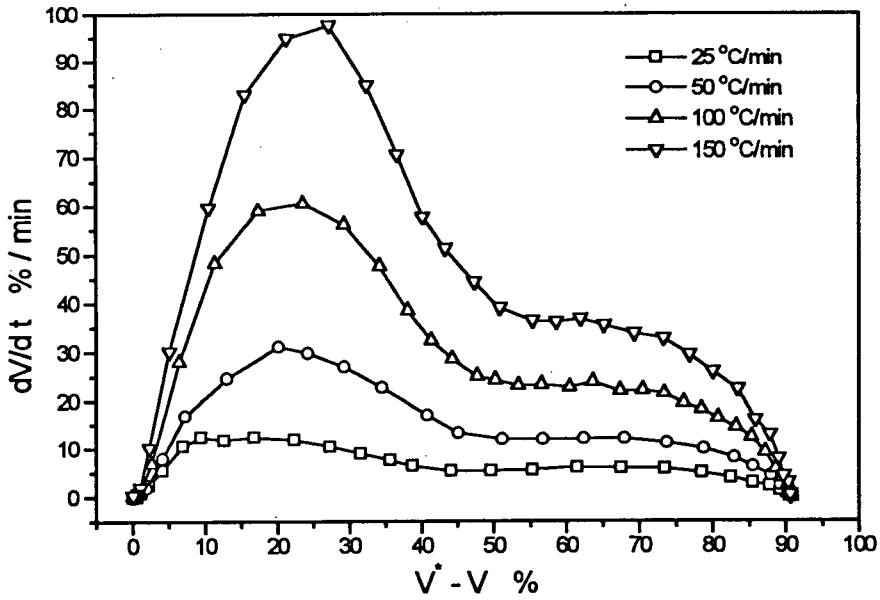

Figure 5.7b The devolatilization rate dV/dt vs. the remaining volatile at different heating rates and 800 °C for Syncrude pitch

5.3.1 Multi-Stage First Order Reaction Model and its Assumptions

In order to model the pitch pyrolysis data, it is assumed that the pyrolysis of the pitch samples takes place as a multi-step first order thermal decomposition with regard to the volatile content remaining in the "residue" and is a chemically controlled process. It is also assumed that at some critical temperature, the kinetic parameters undergo change as the "reaction" shifts from one stage to the other stage of the pyrolysis process. In each stage, only one type of reaction dominates, and the kinetics parameters remain relatively constant. Therefore each stage of the reaction can be modeled as a single overall first order reaction. As the reaction proceeds and the temperature increases, the chemical nature of the "active reacting matrix" gradually undergoes change due to the depletion of the "component" which dominated the reaction behavior in that stage. This causes the significant change of the reaction behavior. The critical temperatures at which the subsequent stage begins should be identifiable from the pyrolysis rate or weight loss ratio in the case of TGA experiments, such as are shown in Figures 5.6 and 5.7. With these assumptions in mind, the total volatile content can therefore be given by the following expression:

$$\frac{dV}{dt} = \sum_{i=1}^{n} \alpha_i k_{oi} e^{-E_i/RT} \left(V^* - V\right) \tag{5.27}$$

$$T = Ct + 323.16 \tag{5.28}$$

therefore:

$$\frac{dV}{dT} = \sum_{i=1}^{n} C\alpha_i k_{oi} e^{-E_i/RT} \left(V^* - V\right) \tag{5.29}$$

where:

n	no. of reaction stages which are first order reaction
α_i	constant used to characterize the gradual change of the chemical structure of reacting residue.

α_i =1 when $T_{i-1} \leq T < T_i$, otherwise α_i =0

T_i critical temperature, at which reaction behavior is undergoing visible change in terms of the ratio dV/dT or rate dV/dt due to the change of reacting residue, K

E_i activation energy of ith stage of reaction, J/mol

k_{oi} pre-exponential factor of ith stage reaction, min^{-1}.

5.3.2 Application of the Multi-Stage Model

As observed in the TGA results of CANMET and Syncrude pitch pyrolysis, the pyrolysis behavior is shifted at about 450 °C into a second stage as shown in the rate plots and weight loss plot. This two step feature is also observed by Rajeshwar [113] and Thakur and Nuttall [111] for oil shale pyrolysis, and Schuckler [116] for vacuum residuum pyrolysis. The need for a two stage reaction analysis was evident by their results, but two stage analysis was not implemented. The multi-stage expression can therefore be simplified to a 2-stage pyrolysis mechanism as follows:

$$\frac{dV}{dT} = \sum_{i=1}^{2} C\alpha_i k_{oi} e^{-E_i/RT}\left(V^* - V\right) \qquad (5.30)$$

where α_1=1, α_2=0 when T < 450 °C

α_1=0, α_2=1 when T ≥ 450 °C

This approach which was developed in this work, differs from the multi-parallel reactions discussed in Section 2.3: previous works have assumed that the reactions take place as mutually competing first order reactions. The 2-stage first order reaction model was applied to the overall single first order reaction methods described earlier, and fitted to experimental data of both CANMET and Syncrude pitch. The TGA data have been divided into two stages: stage 1 corresponding to the first stage of the pyrolysis reaction in the temperature range 50 °C (initial

TGA pyrolysis temperature) to 450 °C, and stage 2 corresponding to the second stage of pyrolysis reaction in the temperature range of 450 °C to the final pyrolysis temperature. Each stage was fitted to the model for the kinetic parameters for CANMET pitch and Syncrude pitch pyrolysis with the FORTRAN program, listed in Appendix E. One run was initially chosen for each pitch. The kinetic parameters are listed in Table 5.3 for runs at 25 °C/min and 800 °C:

Table 5.3 Kinetic Parameters for the Nonisothermal Pyrolysis of CANMET Pitch and Syncrude Pitch at 25 °C/min. and 800 °C

	First stage		Second stage		
	E_1 kJ/mol	k_{o1} min^{-1}	E_2 kJ/mol	k_{o2} min^{-1}	s.e.e.
Run# Can48		CANMET Pitch			
2-Integral	21.89	5.534	71.34	$4.448*10^4$	1.42
2-Coats-Redfern	18.31	1.207	69.93	$2.865*10^4$	8.66
2-Chen-Nuttall	19.81	2.663	70.91	$4.004*10^4$	4.46
2-Friedman	18.35	2.169	39.42	$2.221*10^2$	5.68
Run# Syn43		Syncrude Pitch			
2-Integral	30.82	51.80	67.66	$2.555*10^4$	1.94
2-Coats-Redfern	28.92	22.28	66.14	$1.597*10^4$	5.23
2-Chen-Nuttall	29.96	38.04	67.18	$2.271*10^4$	2.06
2-Friedman	22.43	7.251	101.5	$3.875*10^6$	9.74

The values of the E_1, k_{o1}, E_2, k_{o2}, i.e. the kinetic parameters determined by each of the 2-stage reaction methods, are in reasonable agreement except for Friedman method. The 2-stage integral method gives the best fit for both CANMET and Syncrude pitch. Table 5.3 also indicates the significant change of kinetic parameters between the first stage and second stage reactions, as expected. The activation energies of the second stage are about 2 to 4 times those of the first stage. Having obtained these parameters, the volatile contents were calculated according to each method and the predicted results (Appendices E and F) were plotted, along with experimental results in Figures 5.10 and 5.13. Only the 2-stage integral method gave good predictions of the volatile content over the complete range. The other three 2-stage methods failed to predict the volatile content reasonably. The effect of the number of significant digits and a change of k in the range of ±2% was examined (Appendix I). A change of the number of significant digits or k did not affect the fitting results and the superiority of integral method to other methods. The kinetic parameters were then reported in four significant digits and the s.e.e. in three significant digits.

Examination of the fitted Y values for each 2-stage reaction method revealed that only the 2-stage integral method fitted the Y value calculated from experimental results as shown in Figures 5.8, 5.9, 5.11 and 5.12.

The 2-stage Coats-Redfern method analysis was performed by fitting Equation 5.14 to the 2 stages of TGA experimental data, with the term 2RT/E ignored. This term, ranging from 0.293 to 0.656 for the first stage reaction and from 0.172 to 0.255 for the second stage reaction of CANMET pitch pyrolysis and from 0.186 to 0.416 for the first stage reaction and from 0.182 to 0.270 for the second reaction of Syncrude pitch pyrolysis, is not small enough to be ignored in the linear regression fitting for the kinetic parameters. To do so, introduces a large error, and results in erroneous kinetic parameters and therefore wrong volatile yield predictions. Given a small value of 2RT/E of 0.05, the activation energy E is 423.4 kJ/mol at 1000 °C, and 107.4 kJ/mol at 50 °C. The error thus introduced to the predicted volatile content would be negligible for this case. However, the obtained activation energy of 423.4 kJ/mol is unrealistically high. The simplification may be quite satisfactory when the thermal energy RT is significantly less than the activation energy. This case is often found for thermal decomposition of solids where either the temperature is low or the activation energy of the process is greater than RT. However, if RT tends to E, as is observed in this study, i.e., with low activation barriers and high temperatures, it is necessary to take a great number of terms in the integral analytical solution. It is clearly indicated that the assumption of $2RT/E \ll 1$ is not valid for the case of pitch pyrolysis. The results obtained in the present study indicate that the thermal pyrolysis reactions of pitches are complex to the extent that they can not be described by the 2-stage Coats-Redfern method.

The 2-stage Friedman method analysis was performed by fitting Equation 5.15 to the 2 stages of the TGA experimental data, with the dV/dT calculated with experimental data in each stage by Equation 5.13. However the value of dV/dT has been noted to be a sensitive index of the

reaction rate. The error introduced into the method is even significant at the second stage of reaction. Nonlinear behavior was observed for both CANMET pitch and Syncrude pitch as shown in Figures 5.9 and 5.12. In the second stage, the rate of the weight loss changes dramatically as the temperature is increased, and the ratio dV/dT is less accurate. The standard error of deviation is observed as high as 5.68 for CANMET pitch and 9.74 for Syncrude pitch. The difference between the predicted and experimental volatile content is observed as high as 20% for CANMET pitch and 25% for Syncrude pitch as shown in Figures 5.10 and 5.13. The Friedman method is handicapped by the necessity of differentiating the raw TGA data, which is prone to error. Application of this method for the analysis of nonisothermal TGA data for pitch pyrolysis would lead, therefore, to incomplete, even wrong, information on the pyrolysis parameters.

The 2-stage Chen-Nuttall method analysis was performed by fitting Equation 5.17 to the 2 stages of the TGA experimental data, with the iterative linear regression technique. However, the Y values for this method are rather sensitive to the activation energy. The results indicate less satisfactory fitting than the integral method, even though the standard deviation s.e.e. of this method is rather close to that of 2-stage integral method for Syncrude pitch pyrolysis.

In the derivation of the Least Squares Fitting Equation 5.22, it is assumed that all measurements have the same standard deviation, s.e.e., and that the equation does fit well, then fitting for the parameters to minimize this deviation error and finally recomputing the standard deviation s.e.e.

$$s.e.e. = \sqrt{\sum_{i=1}^{n}\left(V_{i\exp} - V_{i\,fit}\right)^2 / (n-2)} \qquad (5.31)$$

Where $V_{i\ exp}$ is the experimental volatile content, $V_{i\ fit}$ is the model predicted volatile content at data point i and n is the total number of data points.

Obviously, this approach prohibits assessment of goodness-of-fit, a fact frequently missed. When the standard deviation is too large, it indicates that the fitting is not successful, as can be seen in Table 5.2 and Figure 5.1. However, a small s.e.e. does not suggest any goodness-of-fit when the standard deviation is well within the experimental error. Further examination is always necessary to ensure the validity of the modeling results, as well as of the kinetic parameters.

The 2-stage integral method does not have the shortcomings mentioned above. The Y values calculated from the experimental data fitted linearly to 1/T for both CANMET and Syncrude pitches, as shown in Figures 5.8 and 5.11. The predicted volatile contents compare closely to the experimental results for both CANMET pitch and Syncrude pitch at all the temperature investigated in this study as shown in Figures 5.10 and 5.13, with s.e.e. 1.4 and 1.9 respectively. The results obtained therefore suggest that the thermal pyrolysis reactions of these pitches can best be described by a 2-stage integral method. This analysis method is further tested for different pyrolysis conditions for its validity.

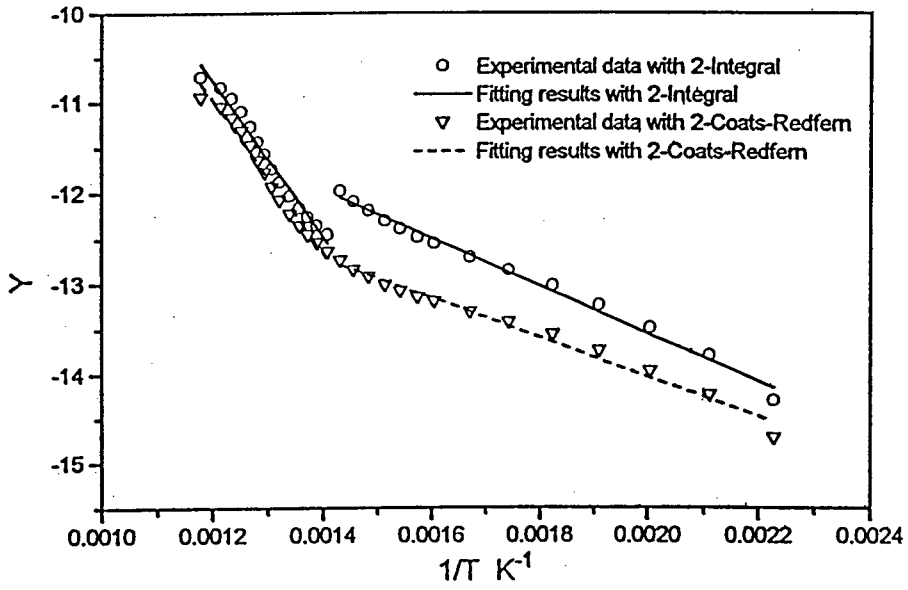

Figure 5.8 Comparison of model predicted Y results and experimental Y results for CANMET pitch at 25 °C/min. and 800 °C with 2-stage model

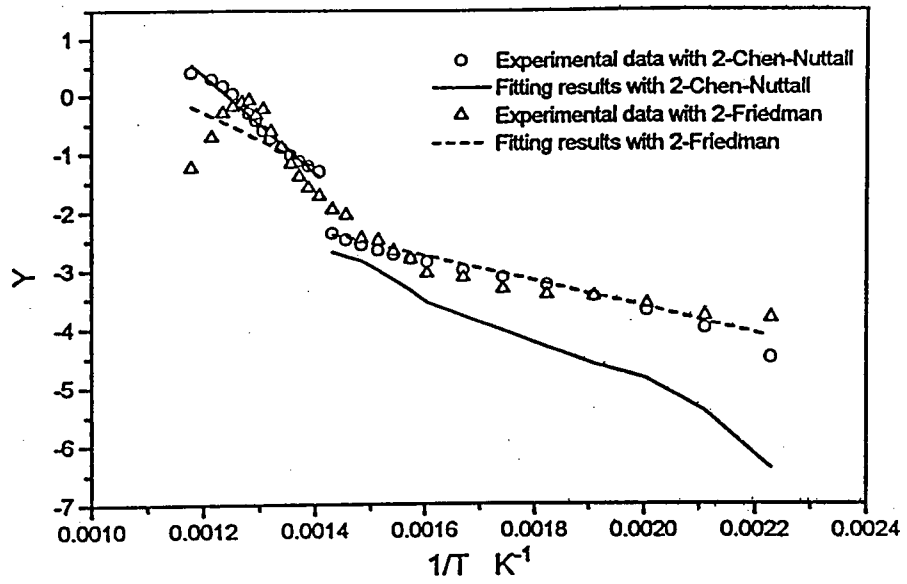

Figure 5.9 Comparison of model predicted Y results and experimental Y results for CANMET pitch at 25 °C/min. and 800 °C with 2-stage model

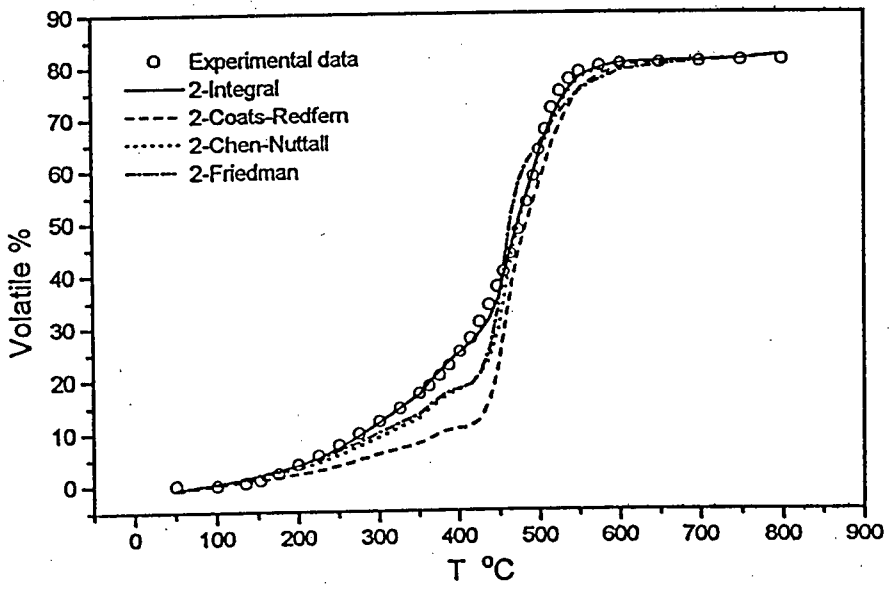

Figure 5.10 Comparison of model prediction and experimental volatile for CANMET pitch at 25 °C/min. and 800 °C with 2-stage first order reaction model

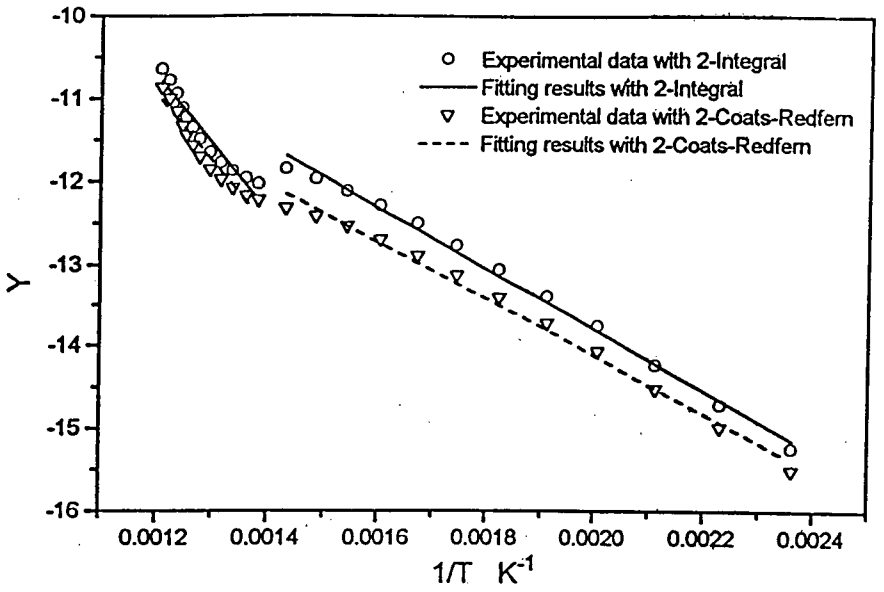

Figure 5.11 Comparison of model predicted Y results and experimental Y results for Syncrude pitch at 25 °C/min. and 800 °C with 2-stage model

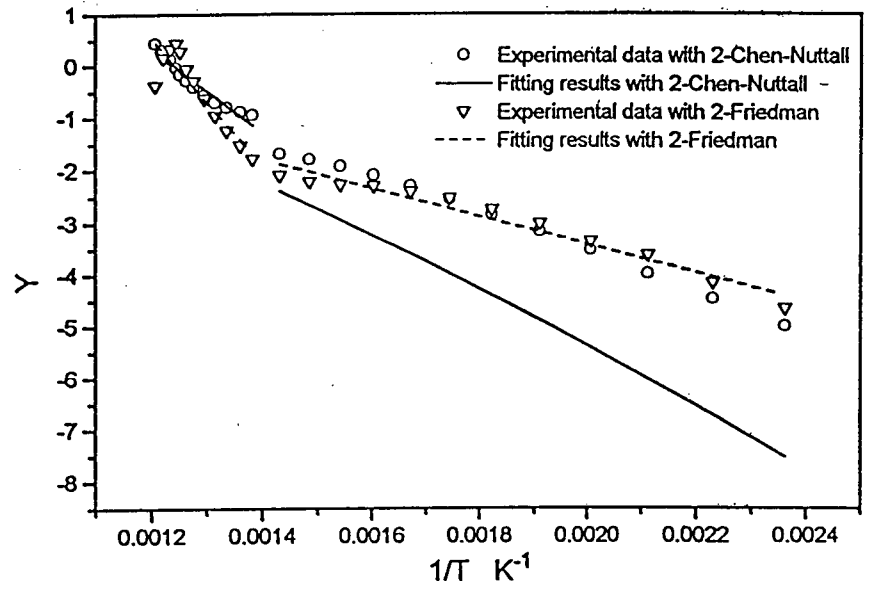

Figure 5.12 Comparison of model predicted Y results and experimental Y results for Syncrude pitch at 25 °C/min. and 800 °C with 2-stage model

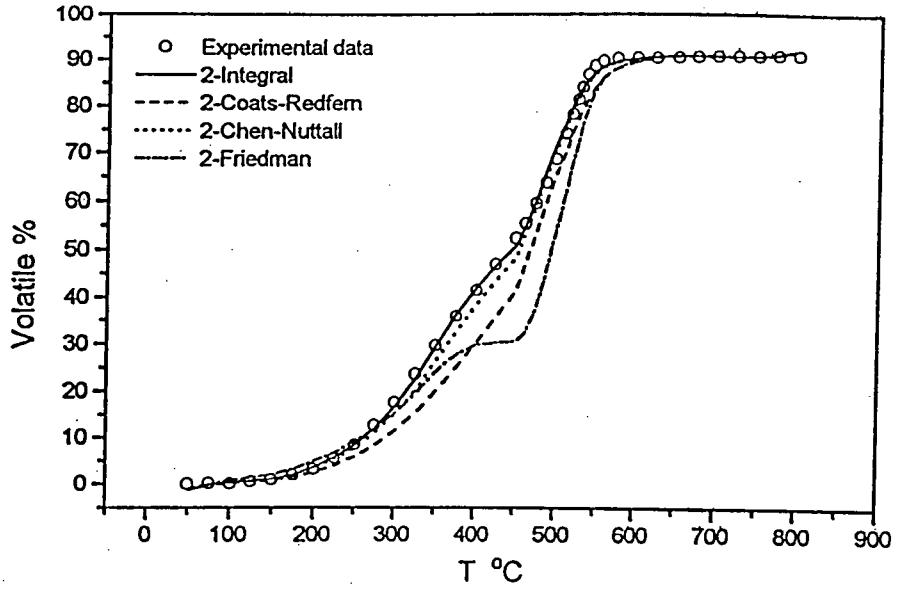

Figure 5.13 Comparison of model prediction and experimental volatile for Syncrude pitch at 25 °C/min. and 800 °C with 2-stage first order reaction model

5.4 2-Stage First Order Reaction Model for Pitch Pyrolysis

Using the least squares curve fitting of experimental data to the 2-stage integral method, the kinetic parameters E_1, k_{o1}, E_2, k_{o2}, and s.e.e. were computed using iterative techniques for a number of different experiments. The values of these parameters are listed in Table 5.4.

Table 5.4 Kinetic Parameters for the Nonisothermal Pyrolysis of CANMET Pitch and Syncrude Pitch at 800 °C and Different Heating Rates with 2-Integral Method

		First stage		Second stage		
Run#	°C/min.	E_1 kJ/mol	k_{o1} min.$^{-1}$	E_2 kJ/mol	k_{o2} min.$^{-1}$	s.e.e.
			CANMET Pitch			
Can48	25	21.89	5.534	71.34	$4.448*10^4$	1.42
Can33	50	20.90	7.649	64.47	$2.444*10^4$	2.12
Can41	100	26.91	39.63	72.11	$1.111*10^5$	1.44
Can58	150	46.64	552.3	96.65	$3.511*10^6$	0.97
			Syncrude Pitch			
Syn43	25	30.82	51.80	67.66	$2.554*10^4$	1.94
Syn29	50	37.57	298.2	76.57	$1.964*10^5$	2.07
Syn18	100	44.16	$1.326*10^3$	65.51	$3.523*10^4$	2.97
Syn8	150	46.14	$2.549*10^3$	69.80	$1.031*10^5$	2.85

Having obtained the values of E_1, k_{o1}, E_2, k_{o2}, from this table, the volatile content and the Y values for both CANMET pitch and Syncrude pitch predicted by the 2-stage integral method were computed using Equation 5.22 and Equation 5.23 respectively.

The Y values obtained experimentally and predicted by the 2-stage integral method for runs at different heating rates are plotted in Figures 5.14 and 5.15, as a function of 1/T. The 2-stage integral method fits adequately and linearly the Y versus 1/T data for both CANMET pitch and Syncrude pitch. It is also noted that it is not safe to fit all the data from different runs to find a set of unique activation energy E and pre-exponential factor k_o, regardless of the heating rates. The scatter of the data points prohibits this. It is more evidently noted in Figure 5.14 for CANMET pitch pyrolysis at low temperatures. However the heating rate did not show a systematic influence.

Similarly, the prediction of the 2-stage integral method for the volatile content is shown in Figures 5.16 and 5.17 as a function of pyrolysis time and in Figures 5.18 and 5.19 as a function of pyrolysis temperature for runs at different heating rates, for CANMET pitch and Syncrude pitch respectively. The experimental data fitted the 2-stage integral method well at different heating rates over the entire temperature range. The close agreement between the experimental volatile contents and the predicted volatile contents suggests that the 2-stage integral method describes the pitch pyrolysis adequately. The magnitude of the standard deviation also supports this observation.

The volatile yield rate dV/dt is also computed with the kinetic parameters obtained as shown in Table 5.4 and compared with the yield rate dV/dt calculated from the experimental data. The results are plotted in Figures 5.20 and 5.21. The close agreement between the predicted volatile yield rate and the rate calculated from experimental data is in accordance with that of the volatile content versus t curve, but is a more rigorous test.

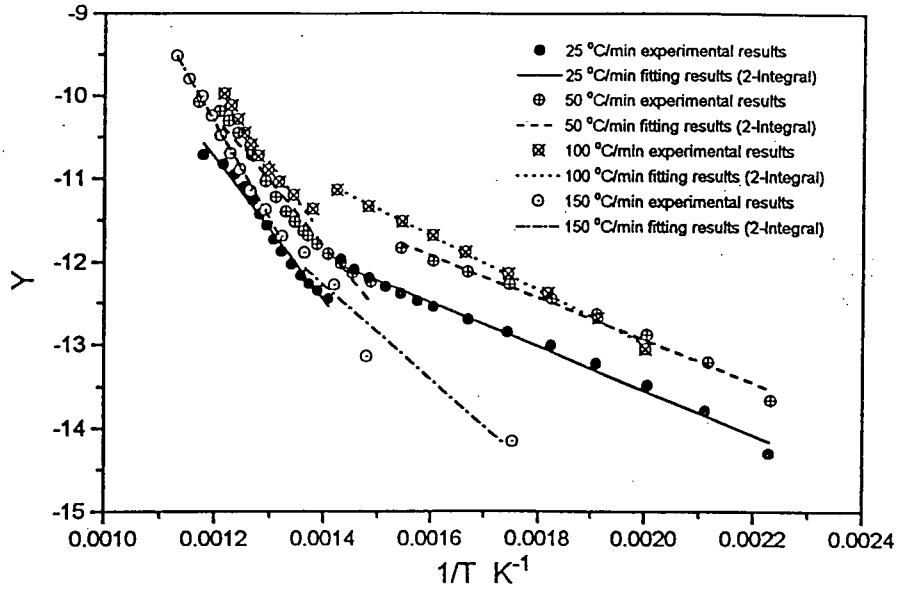

Figure 5.14 Comparison of model predicted Y results and experimental Y results for CANMET pitch at different heating rates and 800 °C with 2-stage integral method

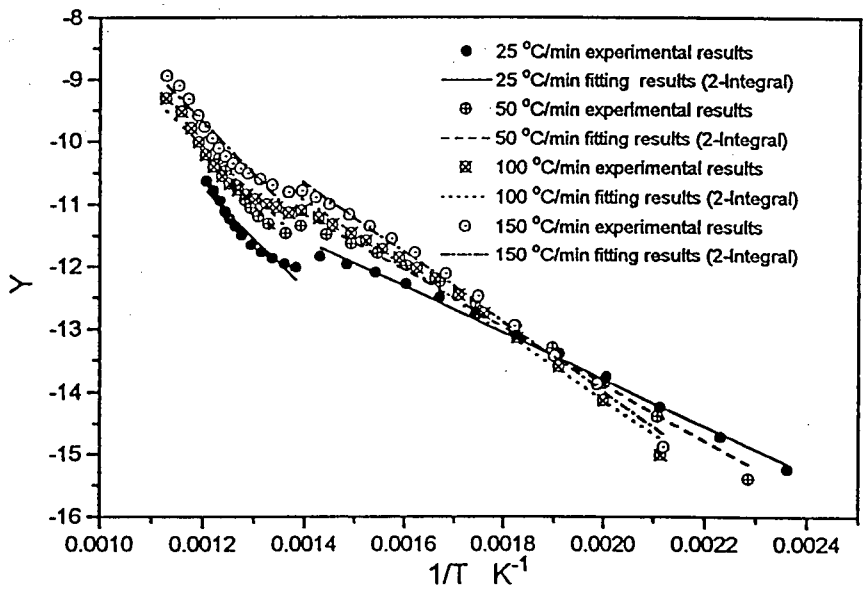

Figure 5.15 Comparison of model predicted Y results and experimental Y results for Syncrude pitch at different heating rates and 800 °C with 2-stage integral method

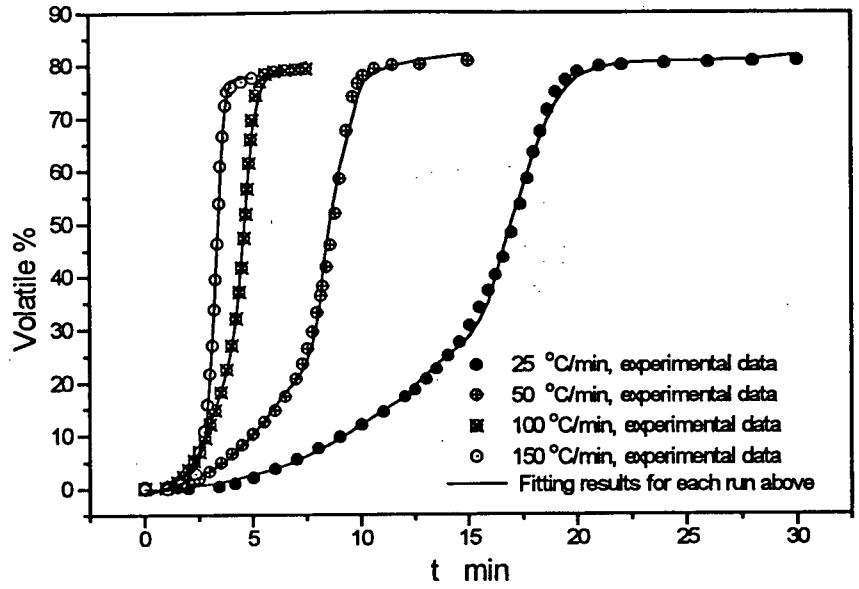

Figure 5.16 Comparison of model prediction and experimental volatile for CANMET pitch at different heating rates and 800 °C with 2-stage integral method

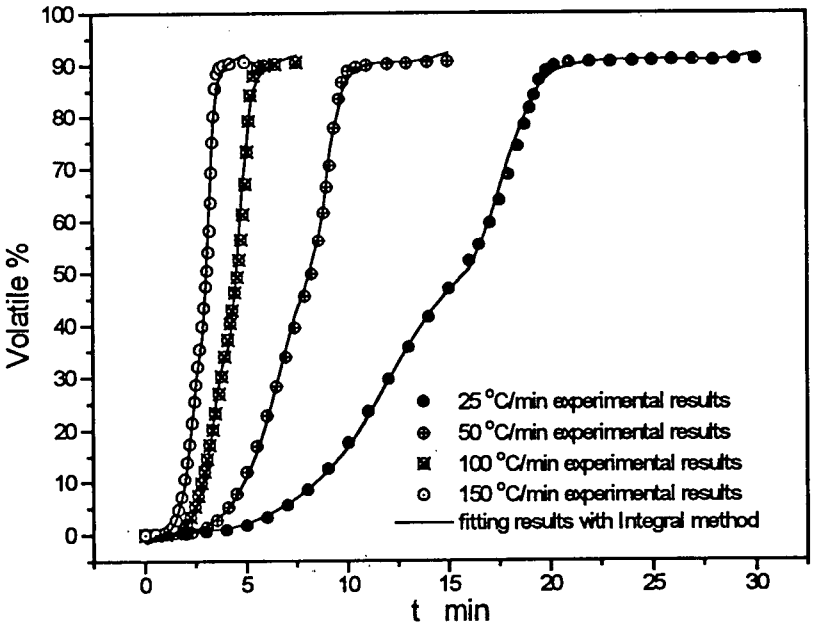

Figure 5.17 Comparison of model prediction and experimental volatile for Syncrude pitch at different heating rates and 800 °C with 2-stage integral method

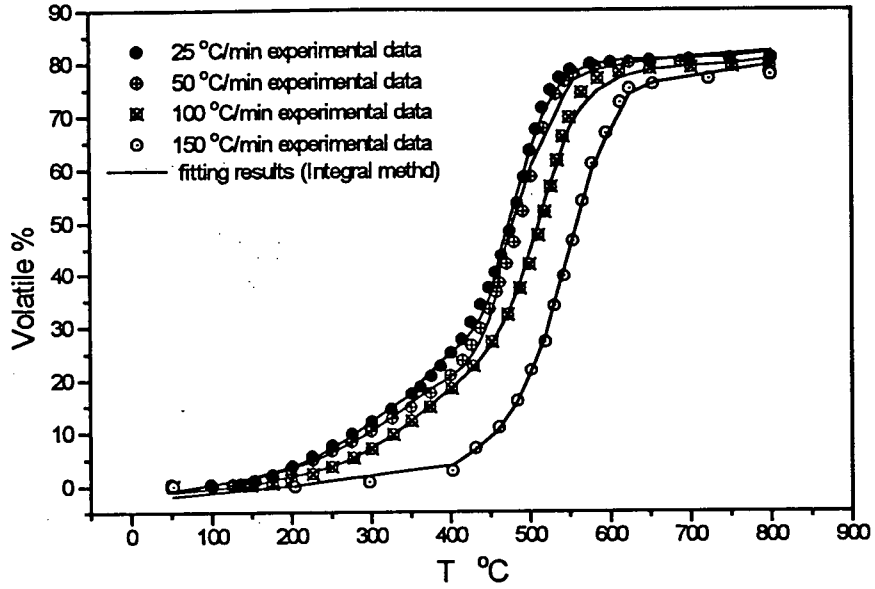

Figure 5.18 Comparison of model prediction and experimental volatile for CANMET pitch at different heating rates and 800 °C with 2-stage integral method

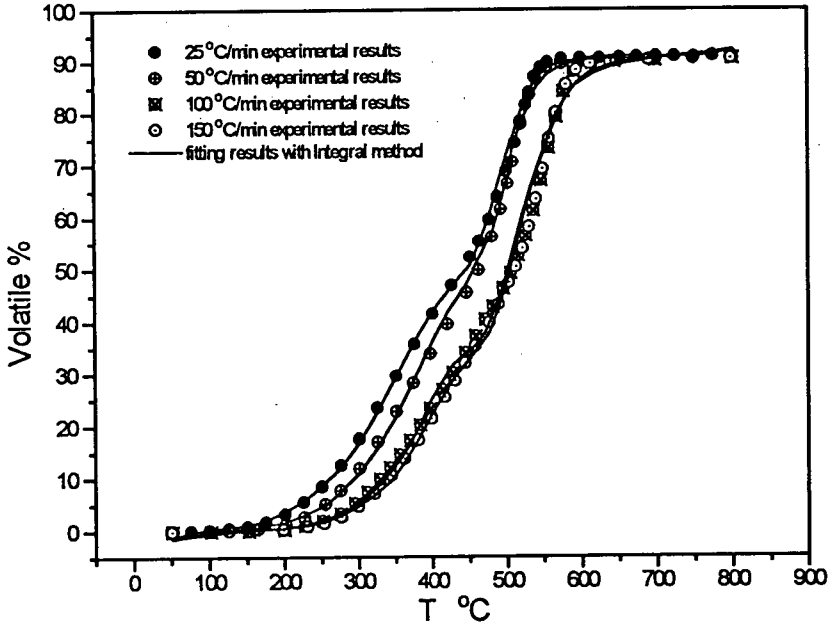

Figure 5.19 Comparison of model prediction and experimental volatile for Syncrude pitch at different heating rates and 800 °C with 2-stage integral method

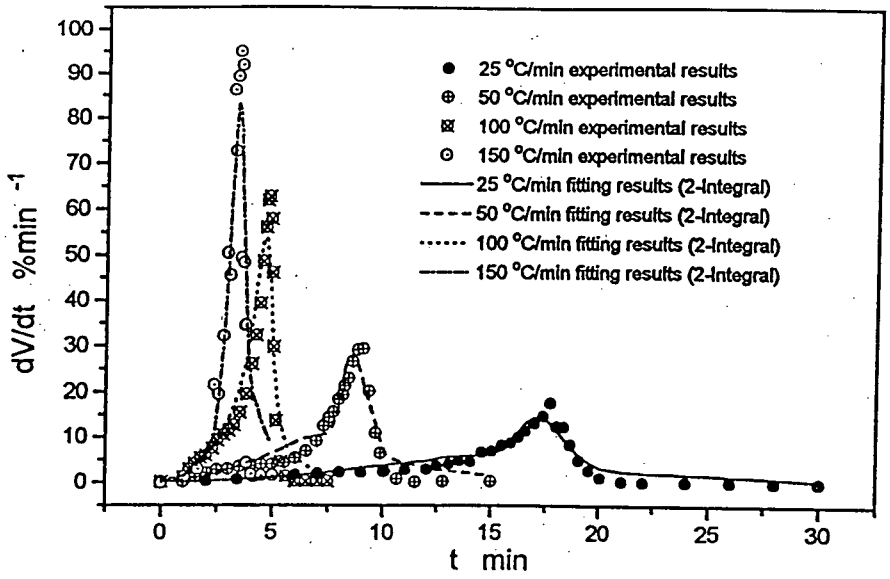

Figure 5.20 Comparison of model prediction dV/dt and experimental dV/dt for CANMET pitch at different heating rates and 800 °C with 2-stage integral method

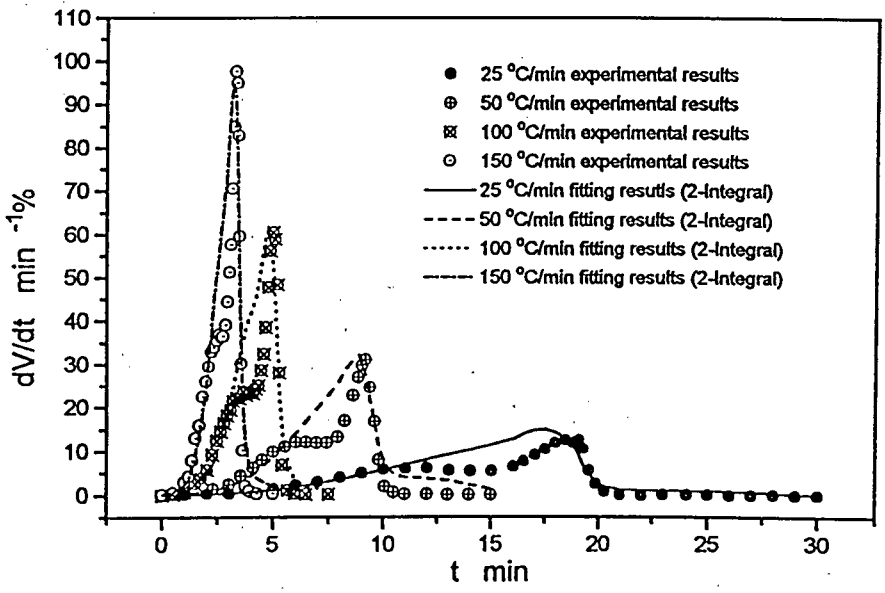

Figure 5.21 Comparison of model prediction dV/dt and experimental dV/dt for Syncrude pitch at different heating rates and 800 °C with 2-stage integral method

5.5 Testing of the 2-Stage Integral Method

In order to further examine the validity of the 2-stage integral method, it was used to predict the volatile yield at different pyrolysis conditions, other than the runs used to fit for the kinetic parameters. The kinetic parameters obtained at conditions of 25, 50, 100 and 150 °C/min and final temperature 800 °C were used to fit runs at the same heating rates but different final temperature ranging from 750 °C to 950 °C for CANMET pitch and Syncrude pitch respectively. The kinetic parameters at heating rate 100 °C/min and final temperature 800 °C were used to predict the volatile yield for CANMET pitch runs at the same heating rate but different final temperature 750, 850 and 950 °C, while the kinetic parameters at heating rate 50 °C/min and 800 °C were used to predict the volatile yield for Syncrude pitch runs at the same heating rate but final temperature of 750, 850 and 950 °C. The experimental conditions are listed in Table 5.5. The s.e.e. values are also listed in the table as the indication of the goodness of the model prediction. The s.e.e values calculated with other methods are also listed in the table for comparison.

Table 5.5 Experimental Conditions and Model Predicted Results of CANMET Pitch and Syncrude Pitch Pyrolysis

			s.e.e.			
Run#	T °C	V*	Integral	C-R	C-N	FM
		CANMET Pitch at 100 °C/min				
Can42	750	79.54	2.05	4.24	1.95	4.60
Can40	850	79.01	4.87	2.70	4.09	3.12
Can52	950	81.23	1.39	5.25	2.28	4.94
		Syncrude Pitch at 50 °C/min				
Syn27	750	90.96	2.57	5.38	2.63	9.07
Syn32	850	90.61	2.04	5.15	2.01	8.64
Syn33	950	91.01	4.49	8.75	5.26	12.19

Integral=2-stage integral method, C-R=2-stage Coats-Redfern method, C-N= 2-stage Chen-Nuttall method, FM= 2-stage Friedman method

It is observed from the s.e.e. values that the prediction is in good agreement with the experimental volatile content. Further examination of Figure 5.22 to Figure 5.27 proved that the

model indeed predicted the volatile content well. The prediction of CANMET pitch pyrolysis volatile content was calculated with the kinetic parameters obtained at 100 °C/min and 800 °C and plotted in Figures 5.22, 5.23, and 5.24, along with the experimental volatile content for comparison. The prediction of Syncrude pitch pyrolysis volatile content was calculated with the kinetic parameters obtained at 50 °C/min and 800 °C and plotted in Figures 5.25, 5.26, 5.27, along with the experimental volatile contents for comparison. It is shown that the agreement between the prediction and experimental data is very good, which is supported by the s.e.e. values. This indicates that the 2-stage integral method can describe the pitch pyrolysis, and the kinetic parameters derived from this model are independent of pyrolysis conditions such as final temperature. The results thus support the assumption that pyrolysis is a chemical reaction controlled process.

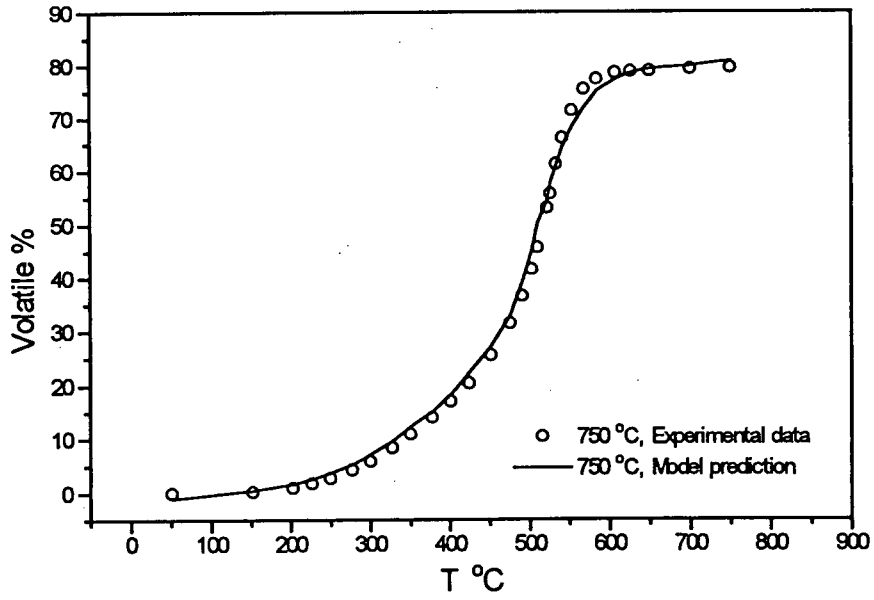

Figure 5.22 Comparison of model prediction and experimental volatile for CANMET pitch at 100 °C/min and 750 °C with 2-stage integral method

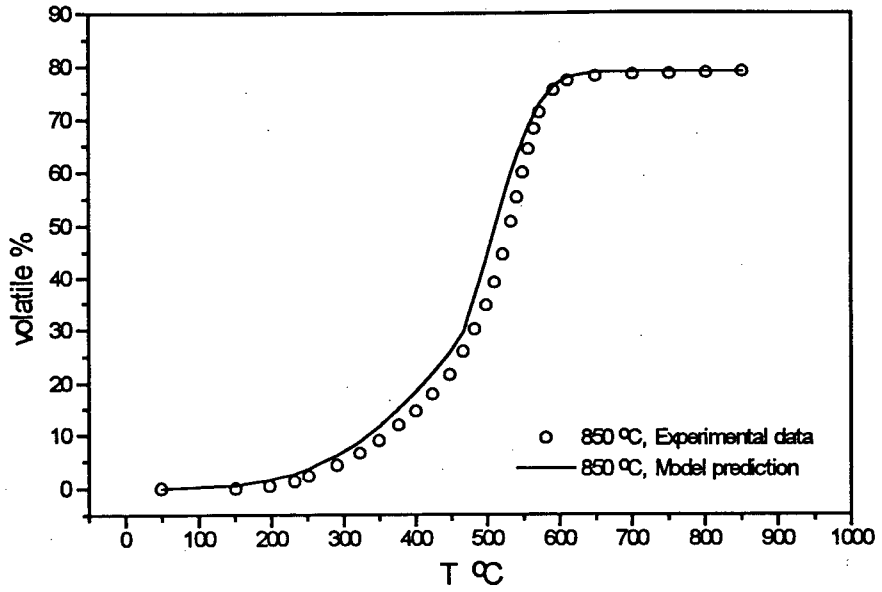

Figure 5.23 Comparison of model prediction and experimental volatile for CANMET pitch at 100 °C/min and 850 °C with 2-stage integral method

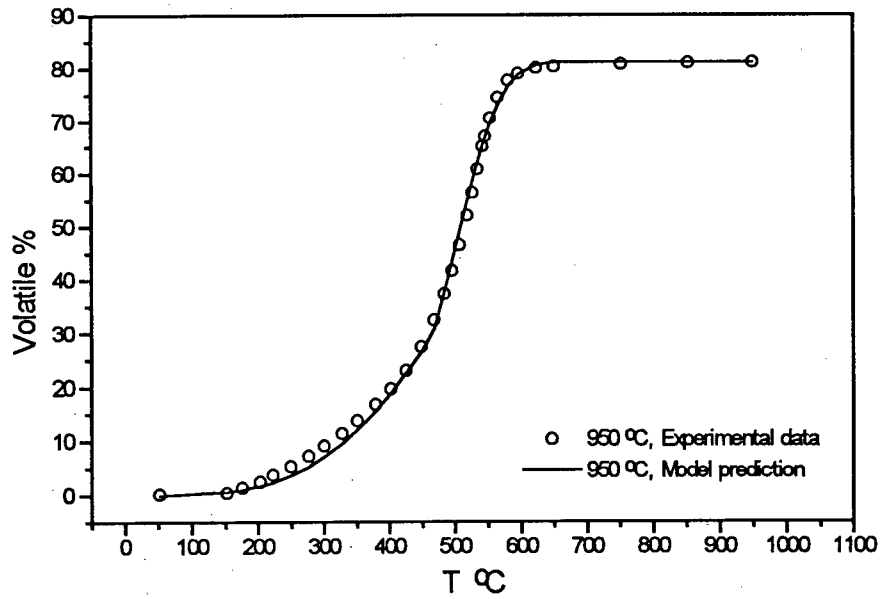

Figure 5.24 Comparison of model prediction and experimental volatile for CANMET pitch at 100 °C/min and 950 °C with 2-stage integral method

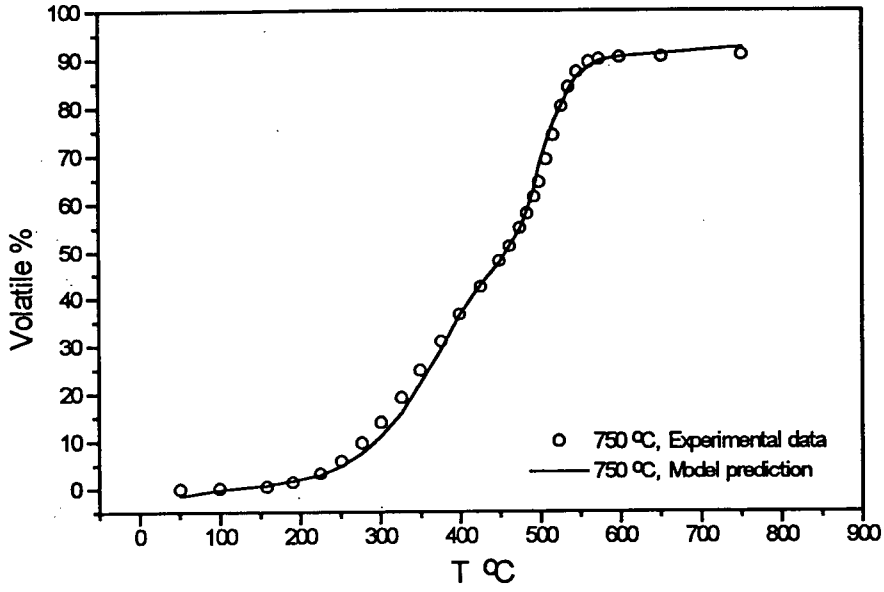

Figure 5.25 Comparison of model prediction and experimental volatile for Syncrude pitch at 50 °C/min and 750 °C with 2-stage integral method

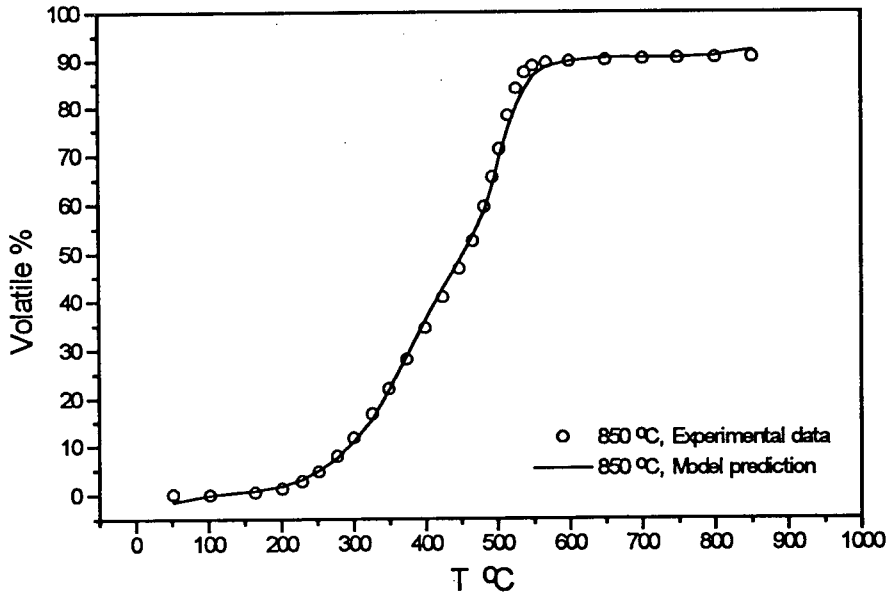

Figure 5.26 Comparison of model prediction and experimental volatile for Syncrude pitch at 50 °C/min and 850 °C with 2-stage integral method

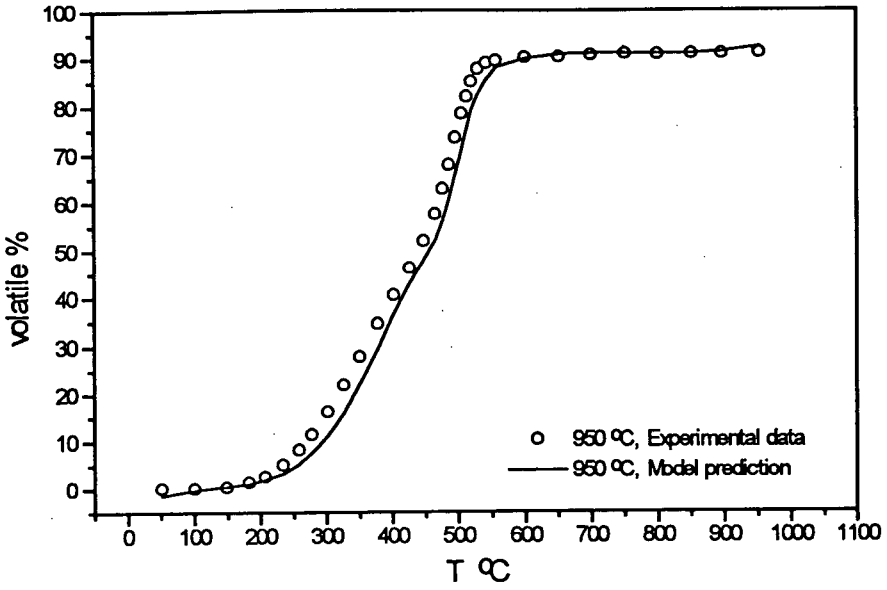

Figure 5.27 Comparison of model prediction and experimental volatile for Syncrude pitch at 50 °C/min and 950 °C with 2-stage integral method

5.6 Discussion and Conclusions

Although the pattern of volatile release for pitches pyrolyzed under TGA conditions is complex, an adequate description of the kinetics is possible. The pyrolysis takes place in 2 stages, with a first stage of low activation energy barrier and lower pre-exponential factor, and the second stage of higher activation energy and pre-exponential factor. It is recommended that the process be modeled with a 2-stage reaction model with the integral method analysis. It is demonstrated that the overall single stage reaction model with analysis by the integral, Coats-Redfern, Chen-Nuttall and Friedman methods, as well as Anthony and Howard's distributed activation energy model, are not sufficient to fit the TGA pyrolysis data and predict the course of the pitch pyrolysis process. It is also found that the single stage reaction model analyzed with these methods does not reproduce the values of activation energy and pre-exponential factors when the pitch TGA pyrolysis data at different conditions are taken for computation. This

phenomena has also been observed by Dahr [122], Natu [123] and Carrasco [62]. By contrast, the two-stage first order model with constants fitted by the integral analysis method provides a good description of the volatilization behavior.

The kinetic expressions obtained represent the global process, and are intended for numerical modeling or engineering calculations. These parameters have only limited validity and can not be used to pin-point the rate controlling mechanism. The true reaction chemistry undoubtedly is much more complex than the multiple stage first order reactions assumed above. It is known that the pyrolysis of any hydrocarbon residual is a very intricate and complex phenomena composed of various elementary reactions that are different to analyze separately and whose quantitative contributions to the global pyrolysis process are virtually impossible to evaluate. For these reasons, even if the overall process has no ideal significance with regard to the reaction mechanism, it is useful as a means of quantifying the rate of reaction and for design purposes. Caution must therefore be used to avoid over-interpreting these rate equations in terms of the fundamental microscopic chemistry of the system.

The apparent activation energies calculated from this study for pitch fall approximately midway between values reported by others for oil shale decomposition. Values of 31.6 kJ/mol, 38.4 kJ/mol and 62.3 kJ/mol [111], 108.10 kJ/mol and 209.50 kJ/mol [113] are reported. Since the strength of typical single bonds to carbon are about 335-420 kJ/mol, the question often arises as to why the activation energies for thermal decomposition of such residues are so much lower. The answer is that the activation energies for decomposition of heterogeneous organic material can not generally be interpreted in terms of a specific bond-breaking process (e.g. C-C vs. C-H vs. C-O etc.). Often, activation energies in the ranges of 42-84 kJ/mol are reported with an indication that these are essentially effective activation energies for a sum of different reactions that occur simultaneously. When there are radicals involved in the pyrolysis, the activation energy

can be reduced to as low as 21-42 kJ/mol [22]. The activation energies for each reaction may be much higher. As a result, the development of a detailed mechanistic picture on the basis of a few effective activation energies is usually fruitless.

Heck and DiGuiseppi [124] observed that the critical element of 2-stage hydrocracking of residuum is believed to be the balancing of the cracking and hydrogenation activities during the initial 50% conversion. It is during this initial conversion that the residuum is most active, free radicals are formed at the highest rate and hydrogen demand is highest. Gray et al. [125] found that the initial conversion of asphaltenes occurs largely as a result of cracking relatively long aliphatic fragments away from a largely aromatic core. The aliphatic/aromatic bonds broken during this initial conversion process are relatively facile, especially when the aliphatic chains are longer than one or two carbon atoms. The conversion path is best illustrated [124] by the relatively rapid decrease in average molecular size and increase in aromaticity that occurs during the initial cracking of the large aliphatic moieties away from the largely aromatic core. The remaining conversion, which proceeds more slowly, involves the cracking away of smaller aliphatic moieties. Stubington's results [126] using bagasse suggested that the pyrolysis mechanism changed at certain pyrolysis level, which can be expressed as time, conversion of carbon or the remaining volatile content. At a certain devolatilization level, a set of different kinetic parameters is required to describe the change of the pyrolysis mechanism. These findings support the 2-stage pitch pyrolysis mechanism with the low activation energy barrier for the first stage and high activation energy barrier for the second stage.

The 2-stage model reflects changes in the chemical constitution or structures as conversion proceeds by using two values of activation energy and pre-exponential factor. This feature is essential to describe pitch dependence of devolatilization rates on the remaining volatile content. The abundance of radicals in the bridges of non-aromatics accelerates their conversion

rates, which has two ramifications: First, gases are expelled rapidly at low temperature and, second, extensive cross-linking inhibits the production of tar precursors [127]. In contrast, bridges in aromatics have very little radical content, so they decompose at relatively high temperatures at significantly slower rates. The transition between these two limiting cases is a sharp one, occurring at a certain temperature (remaining volatile content) level. Consequently for non-aromatic and aromatic components, small differences in the radical content causes appreciable difference in rates and yields, compounding the acute sensitivity of the labile bridge fraction to carbon content. These findings in the present study clearly demonstrated that the chemical constitution of pitch affects product evolution rates and yield at any stage of devolatilization.

The magnitude of the activation energies in both stages suggests that the pyrolysis of pitch was kinetically controlled under the reaction conditions studied. The dependence of dV/dT on V*-V is also in accordance with that.

In summary, the overall single first order model and the Gaussian distributed activation energy model are not adequate to describe pyrolysis of CANMET and Syncrude pitches due to the mechanism change of the pitch pyrolysis at an intermediate temperature, and high volatile yield. These models have been developed for relatively low volatile content material and processes such as coal pyrolysis. The 2-stage first order reaction model with the integral analysis method is proven adequate to describe the pitch pyrolysis process and gives lower activation energy and preexponential factor for the first stage, and higher activation energy and preexponential factor for the second stage of pyrolysis. These kinetic parameters can be extrapolated to different temperature range. However, the compensation effect of the kinetic parameters is observed and is discussed in the next chapter.

Chapter 6 Compensation Effect of the Kinetic Parameters

It was noted in applying the different analysis methods to the pyrolysis kinetics, that when the activation energy was low, the pre-exponential factor was also low. The mutual dependence of the activation energy E and the pre-exponential factor k_o, termed the compensation effect, has been reported for catalytic kinetics [68, 69], thermal aging process of polymers [128-130], and some $CaC_2O_4 \bullet H_2O$ pyrolysis processes [86] as described in Chapter 2. The mutual dependence of the kinetic parameters does not occur in simple reactions. The compensation effect is associated with the following two criteria:

A) The logarithm of the pre-exponential factor, $\ln k_o$, is linearly proportional to the activation energy E, given by the following equation, where the α and β are the compensation constants:

$$\ln k_o = \alpha + \beta E \qquad (6.1)$$

B) The logarithm of the reaction rate constant, lnk, is linearly proportional to the reciprocal of the reaction temperature 1/T, and all the lnk vs. 1/T lines generated in different temperature programmed experiments intersect at one point T_i, the isokinetic temperature. This results in the following equation, where the a and b are isokinetic constants:

$$\ln k = a + b\frac{1}{T} \qquad (6.2)$$

As pointed out in the literature review, the second criterion is a special case of the first one. The existence of the second criterion guarantees the existence of the first criterion and the compensation effect. However, the existence of the first criterion guarantees the existence of the compensation effect, but not the second criterion.

The most common identification of a compensation effect comes from the observation of a linear correlation between the activation energy and the logarithm of the pre-exponential factor

[66]. The application of statistical methods to the recognition of a linear relationship between values of the activation energy and the logarithm of the pre-exponential factor has been described by Exner [100], who suggests that a single point of intersection in the lnk vs. 1/T plots could be used for a sound statistical test, since lnk and T are statistically independent. This is the basis of the isokinetic relationship. It is evident that for a set of experimental data one may infer from such a point of intersection the linearity between the activation energy and the logarithm of the pre-exponential factor, but the reverse may not be true.

In this work, the compensation effect was investigated at different pyrolysis conditions and for different single overall first reaction models and 2-stage first order model for both CANMET and Syncrude pitch. The accuracy of the kinetic parameters was also examined, comparing the resulting standard deviation error (s.e.e.). The possibility of the existence of one unique set of these kinetic parameters was therefore investigated.

6.1 Compensation Effect of Kinetic Parameters Derived from Overall First Order Model

Since the single overall first order reaction model (analyzed with integral, Coats-Redfern, Chen-Nuttall and Friedman methods) was inadequate to describe the pyrolysis kinetics, results on compensation effect are not discussed in detail. Figures 6.1 and 6.2 show that a good linear correlation of Equation 6.1 was obtained, however, Equation 6.2 was not met since an isokinetic temperature within the operating temperature range was not found. This compensation effect has also been observed in the studies of thermal degradation of polymers with different mathematical methods [130]. The single overall first order model analyzed by the different mathematical methods in this work did not reproduce the kinetic parameters, and these parameters derived from each of these methods follow the compensation effect.

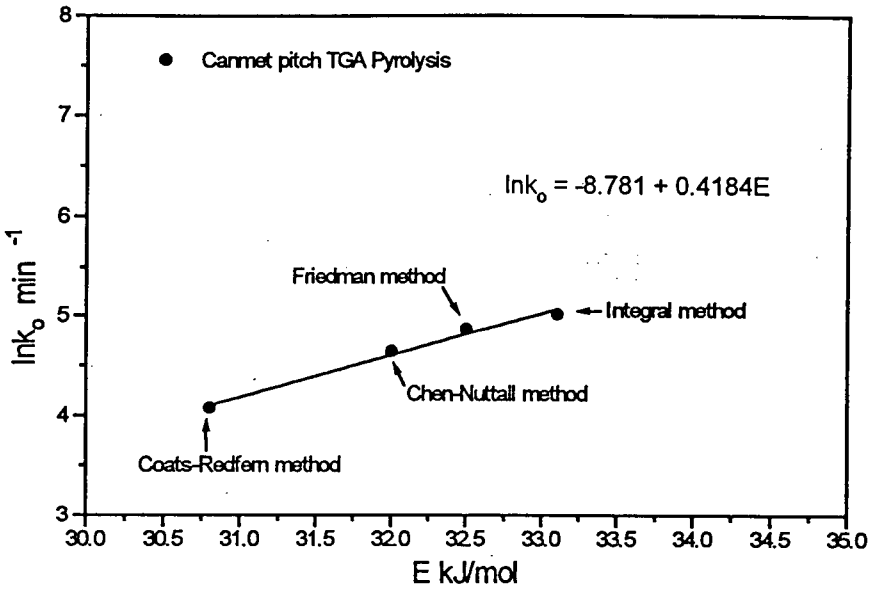

Figure 6.1 CANMET pitch TGA pyrolysis kinetic parameters at 50 °C/min and 700 °C with different methods (overall first order)

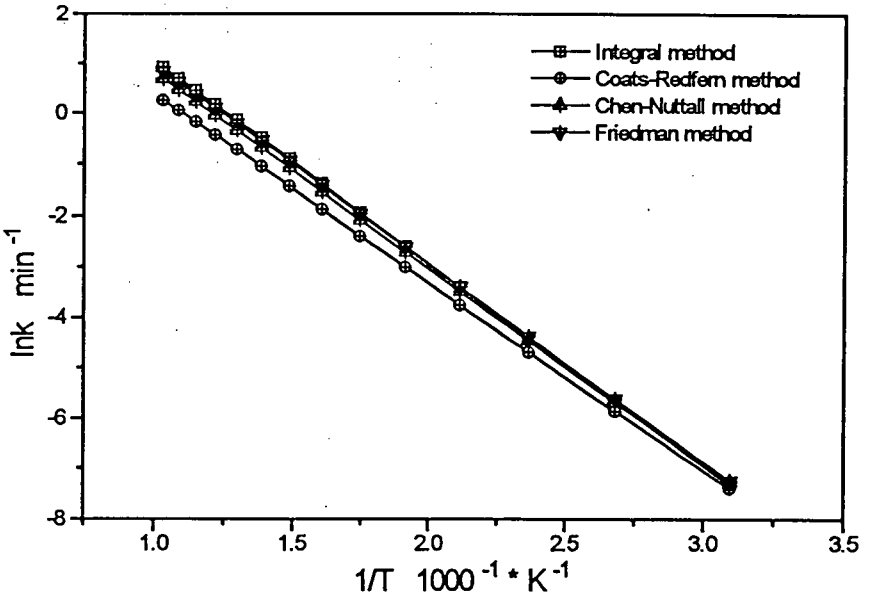

Figure 6.2 CANMET pitch pyrolysis reaction rate constant as a function of temperature at heating rate 50 °C/min and final temperature 700 °C

6.2 Compensation Effect of Kinetic Parameters Derived from 2-Stage Reaction Model

The compensation effect for the 2-stage reaction model analyzed with different methods, at different heating rates such as 25, 50, 100 and 150 °C/min and final temperature of 800 °C, was investigated and the values of the compensation effect parameters (Equation 6.1) for the first stage: α_1 and β_1, for the second stage α_2 and β_2, are listed in Tables 6.1 and 6.2 for CANMET and Syncrude pitch. The square of the regression coefficients, R^2, are also listed in these tables indicting the linearity of the fitting. Four data points derived via each 2-stage method were used in the fitting of each run.

Table 6.1 Compensation Parameters for CANMET Pitch Pyrolysis at Different Heating Rates and 800 °C

	First stage			Second stage		
Method	α_1	β_1*10^{-4}	R^2	α_2	β_2*10^{-4}	R^2
Integral	-1.544	1.711	0.952	0.008	1.558	0.978
Coats-Redfern	-2.824	1.930	0.959	-0.406	1.586	0.980
Chen-Nuttall	-2.128	1.826	0.956	-0.087	1.566	0.979
Friedman	-2.444	1.980	0.984	-1.169	1.693	0.999
All methods	-2.360	1.903	0.957	-0.789	1.650	0.991

Table 6.2 Compensation Parameters for Syncrude Pitch Pyrolysis at Different Heating Rates and 800 °C

	First stage			Second stage		
Method	α_1	β_1*10^{-4}	R^2	α_2	β_2*10^{-4}	R^2
Integral	-3.718	2.492	0.998	-1.220	1.761	0.795
Coats-Redfern	-4.367	2.591	0.998	-1.554	1.781	0.809
Chen-Nuttall	-3.923	2.530	0.998	-1.278	1.765	0.801
Friedman	-4.361	2.852	0.998	0.705	1.471	0.977
All methods	-3.308	2.384	0.979	0.516	1.497	0.961

Figures 6.3 and 6.4 show that the compensation effect Equation 6.1 fits data for each method at each stage of pyrolysis adequately. For all the cases investigated for CANMET pitch the R^2 coefficient is greater than 0.95, whereas for Syncrude pitch the R^2 is greater than 0.998 for the first stage and greater than 0.795 for the second stage.

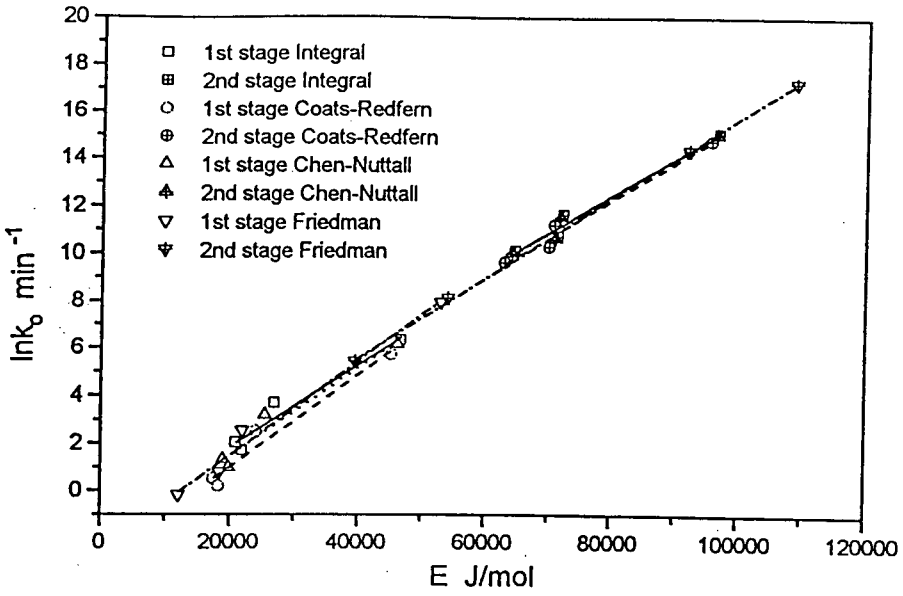

Figure 6.3 CANMET pitch TGA pyrolysis kinetic parameters at different heating rates and 800 °C with 2-stage first order model analyzed with different methods

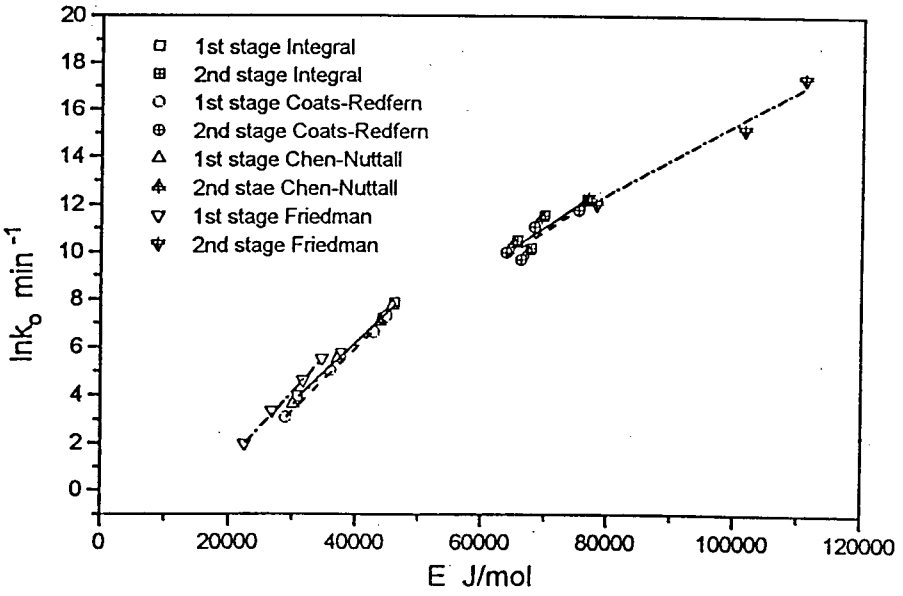

Figure 6.4 Syncrude pitch TGA pyrolysis kinetic parameters at different heating rates and 800 °C with 2-stage first order model analyzed with different methods

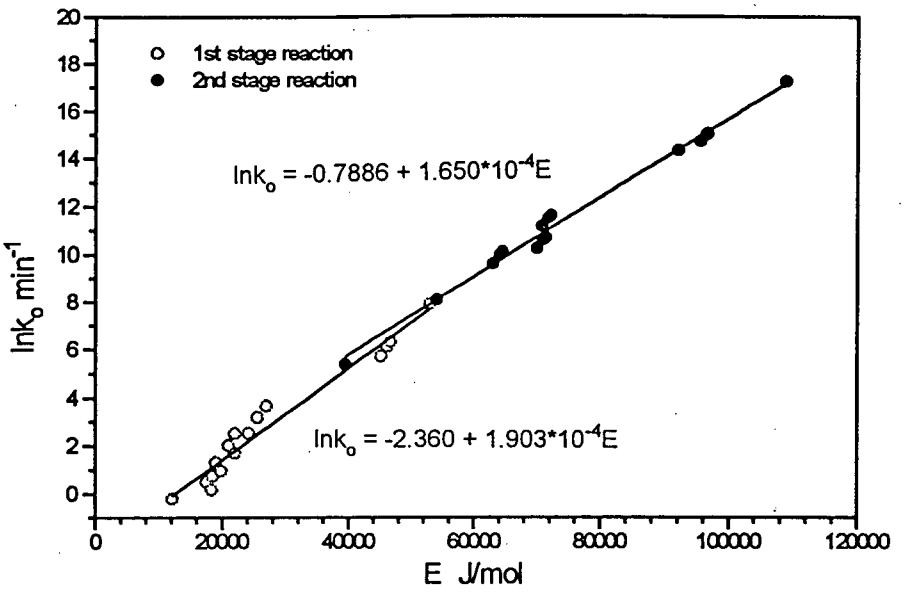

Figure 6.5 CANMET pitch TGA pyrolysis kinetic parameters at different heating rates and 800 °C with 2-stage first order model

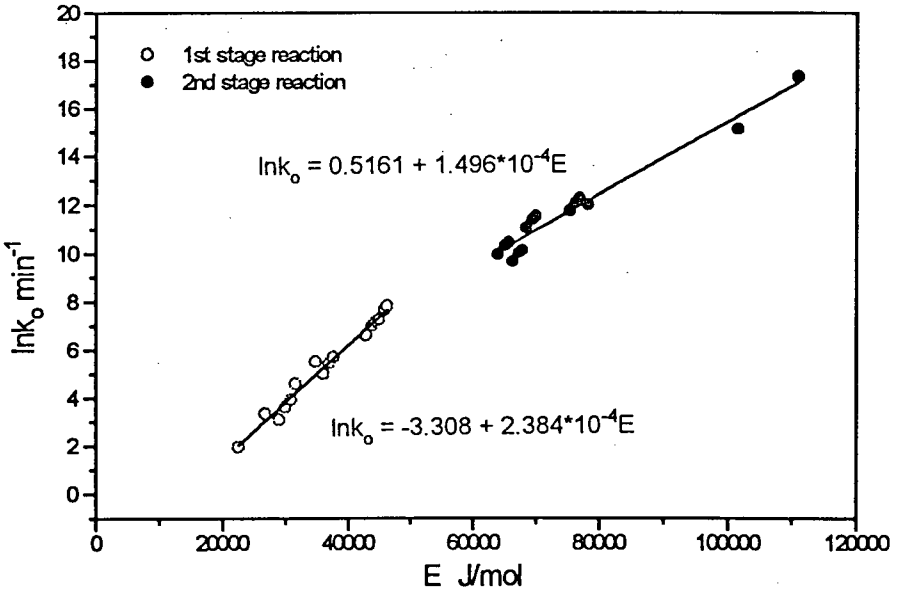

Figure 6.6 Syncrude pitch TGA pyrolysis kinetic parameters at different heating rates and at 800 °C with 2-stage first order model

The regression results for parameters via 2-stage model are plotted in Figure 6.5 and Figure 6.6 for CANMET and Syncrude pitch respectively. Clearly one set of constants fits data from all methods in each stage, with R^2 coefficient is greater than 0.957 for all the cases investigated.

The physical meaning of the compensation effect parameters α and β has been a topic of research and it is beyond the scope of this research to explore it in detail. However, it is noticed that the parameter β is rather constant for each stage of the pyrolysis and the parameter β of the first stage is larger than the β parameter of the second stage, for both of the two pitches studied. By contrast the parameter α changes with the model over a large range. For decarboxylation of solids, Muraishi [65] has stated that whereas the parameter β is related to the bond strength of the metal leaving group in the three dicarboxylates investigated in his work, the parameter α is related to the structure of and defects in the starting material or to the mobility of the crystal lattice in the dicarboxylate thermal decomposition. The parameter α obtained in the present work showed complex tendencies among the 2-stage of pyrolysis process and different mathematical methods used with the 2 stage model to derive the kinetic parameters. However, the parameter α of the first stage of the pyrolysis process of both pitches studied is smaller than that of the second stage of the pyrolysis process, which may suggest the chemical structure difference between these two stages. This difference of the chemical structure at different level of pyrolysis has been also observed experimentally [125]. Although there are slight differences in the parameter β obtained from the different methods, the parameter β obtained may indicate similar " bond strength" and therefore suggest there is one type of reaction dominant in each stage. The bond strength is therefore different according to the parameter β between the first stage and second stage.

The R^2 coefficient of the first stage of Syncrude pitch is the highest in all the cases studied. This is in good agreement with the results as shown in Figure 5.7 in Chapter 5. The experimental results clearly show a consecutive pyrolysis process: at the beginning of the pyrolysis, the ratio dV/dT increases with the decrease of the V*-V and up to a point where dV/dT kept roughly the same before going into the next stage of pyrolysis. In the modeling process, this consecutive process was not divided into more detailed stages for the simplicity of modeling and limiting the parameters introduced into the kinetic model due to the fact that the yield of volatile at this stage is much less than that at lower V*-V. This experimental evidence supports a common belief that a consecutive process is one of causes of the compensation effect. This is further supported by the results with CANMET pitch. When the pyrolysis process was fitted with the overall single first order model, the linear regression of the kinetic parameter k_o and E to the compensation equation resulted in a R^2 of 0.986. When the pyrolysis experimental results were fitted with 2-stage model, the linear regression of the kinetic parameter k_o and E for each stage and each method resulted in R^2 coefficient from 0.952 to 0.999. The R^2 coefficient is smaller than that obtained from the overall single first order model, except for the second stage of the Friedman method for CANMET pitch pyrolysis. It is, therefore, evident that the 2 stage behavior in the overall single first order model resulted in the higher R^2 coefficient. Similarly the lower R^2 coefficient derived for the second stage kinetic parameters k_o and E of Syncrude pitch pyrolysis suggests a lesser degree of multi-stage behavior, i.e., lesser heterogeneity of reactions. The activation energy of the second stage of Syncrude pitch pyrolysis changes over a very small range with changes of pyrolysis conditions and methods used to derive this parameter.

The compensation effect was also assessed via Equation 6.2, and the results calculated with the kinetic parameters derived from 2-stage reaction model analyzed with integral method are shown in Figure 6.7 and Figure 6.8 for CANMET and Syncrude pitch respectively, as a

function of the reciprocal of the pyrolysis temperature 1/T. The logarithm of reaction rate constants at different heating rates shows linear relationship with the reciprocal temperature 1/T in each temperature range, however the lines of lnk ~ 1/T do not intersect at one single point for either pitch in both stages. The isokinetic temperature was therefore not observed. This suggests that the second criterion for the compensation effect does not hold for CANMET and Syncrude pitch pyrolysis. As described by Kral [68, 69], the second criterion is a special case, and the existence of the compensation effect does not guarantee it to be true.

Similarly, calculations were done with the kinetic parameters derived from Coats-Redfern, Chen-Nuttall and Friedman methods as found in Appendix G. As before, the isokinetic temperature was not clearly observed. The inaccuracy of these methods used to derive the kinetic parameters has been cited as a cause of the compensation effect, however the less accurate models did not result in an isokinetic temperature. It is worth noting that although the lnk ~ 1/T lines appeared to intersect at a single point during the first stage pyrolysis of Syncrude pitch, with all 2-stage methods, a narrow temperature range was observed rather than a single point.

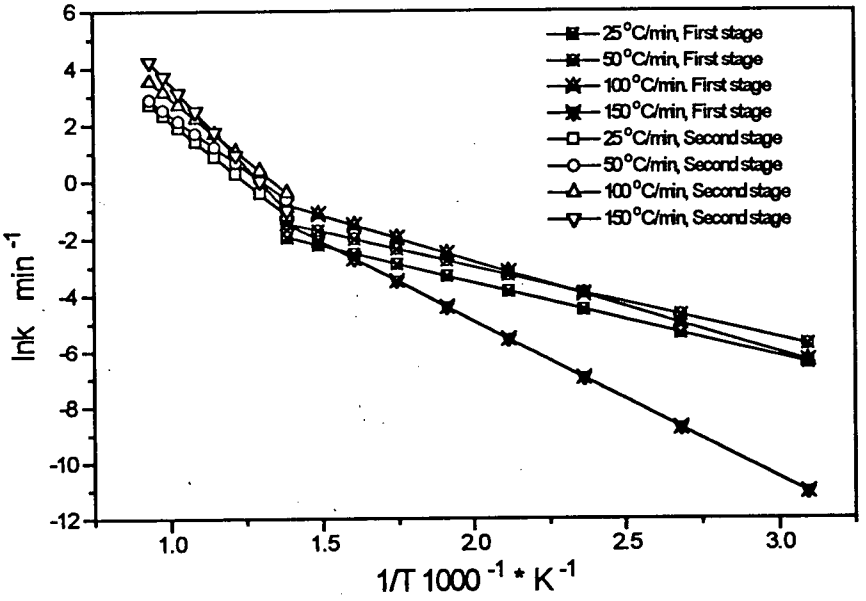

Figure 6.7 CANMET pitch pyrolysis reaction rate constant as a function of temperature at different heating rates and final temperature 800 °C with 2-stage reaction model analyzed with integral method

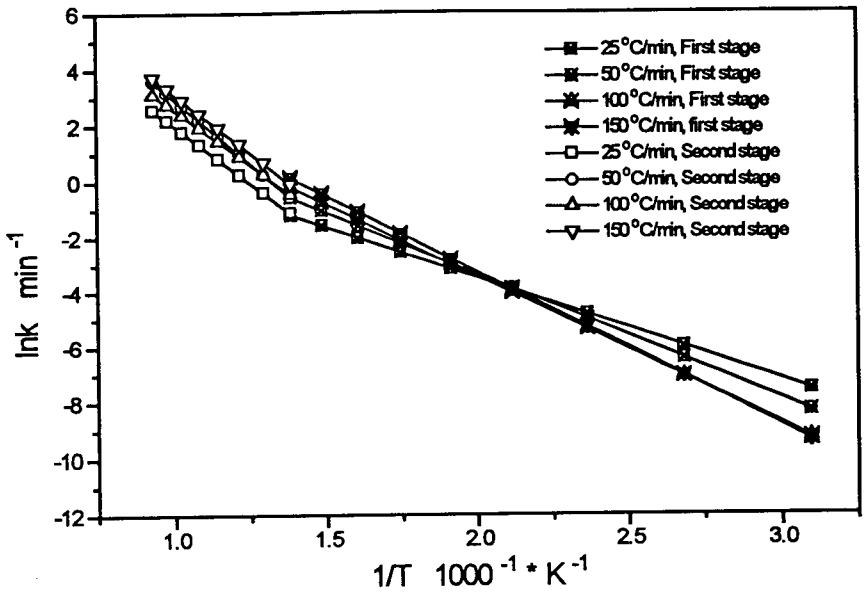

Figure 6.8 Syncrude pitch pyrolysis reaction rate constant as a function of temperature at different heating rates and final temperature 800 °C with 2-stage reaction model analyzed with integral method

6.3 The Relationship of Standard Errors and Kinetic Parameters

Even though the kinetic parameters $\ln k_o$ and E follow a linear relationship, the standard deviation errors (s.e.e.) of the experimental volatile content and the model predicted volatile yield via different pairs of the kinetic parameters were not identical. The standard deviation error was calculated with the related model and the kinetic parameters (Appendix E), and is plotted against the activation energy obtained with the different analysis methods and at different pyrolysis conditions in Figures 6.9 and 6.10. For CANMET pitch (Figure 6.9), the s.e.e. for the first stage decreases with the increase of the activation energy and passes through a weak minimum. This minimum is not really well defined. For the second stage pyrolysis of CANMET pitch pyrolysis, a minimum was also observed. It is evident that there is an optimal value of activation energy for each stage of pyrolysis reaction at which minimum s.e.e. can be achieved. Because $\ln k_o$ is linearly

proportional to E, there exists a relative value of k_o. Therefore there is an unique set of optimal values of E and k_o for the first and second stage reaction which minimize the s.e.e. For CANMET pitch these minimal values for the pyrolysis kinetic parameters obtained from Figure 6.9 are:

E_1=40.2 kJ/mol, k_{01}=197.4 min^{-1}, E_2=86.6 kJ/mol, k_{02}=7.31*10^5 min^{-1}.

It should be noted that for the first stage, a range of values of E could be applied. For Syncrude pitch pyrolysis process as shown in Figure 6.10, the trends are different in that no minima are evident, but optimal values for the pyrolysis kinetic parameters can be obtained as:

E_1=45.7 kJ/mol, k_{01}=1.96*10^3 min^{-1}, E_2=67.6 kJ/mol, k_{02}=4.19*10^4 min^{-1}.

The activation energy values are within the wide range of published kinetic parameters [127] in which an activation energy range of 42-84 kJ/mol was reported for kerogen-to-bitumen pyrolysis. It is also worth noting that these values are very close to the kinetic parameter values derived with integral method for each stage.

With the above kinetic parameters, the volatile yields were calculated for different pyrolysis conditions with Equation 5.10 in Chapter 5 and the results are listed in Appendix H and plotted in Figures 6.11 to 6.14. With the predicted volatile yield, the s.e.e. can therefore be calculated. The results are listed in Tables 6.3 and 6.4 are plotted in Figures 6.11 to 6.14.

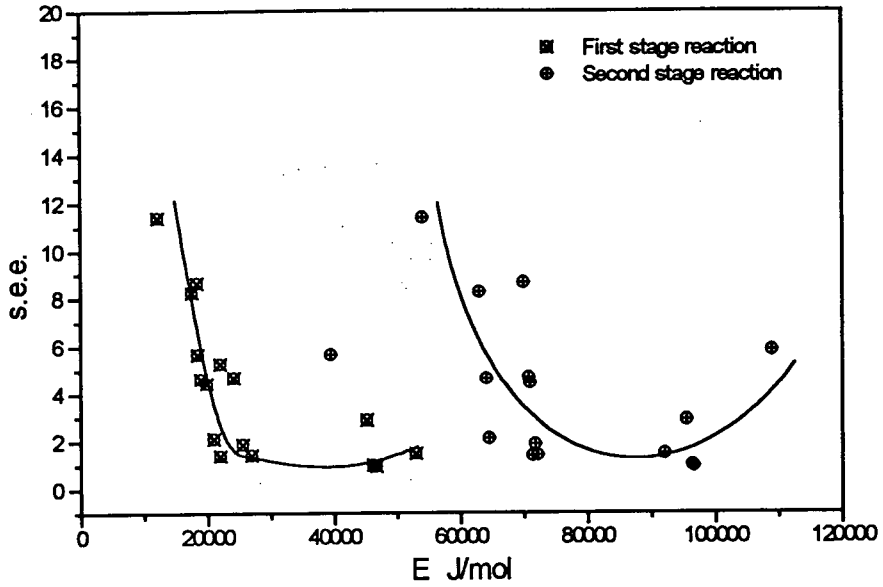

Figure 6.9 CANMET pitch TGA pyrolysis s.e.e. as a function of E at different conditions and with different methods

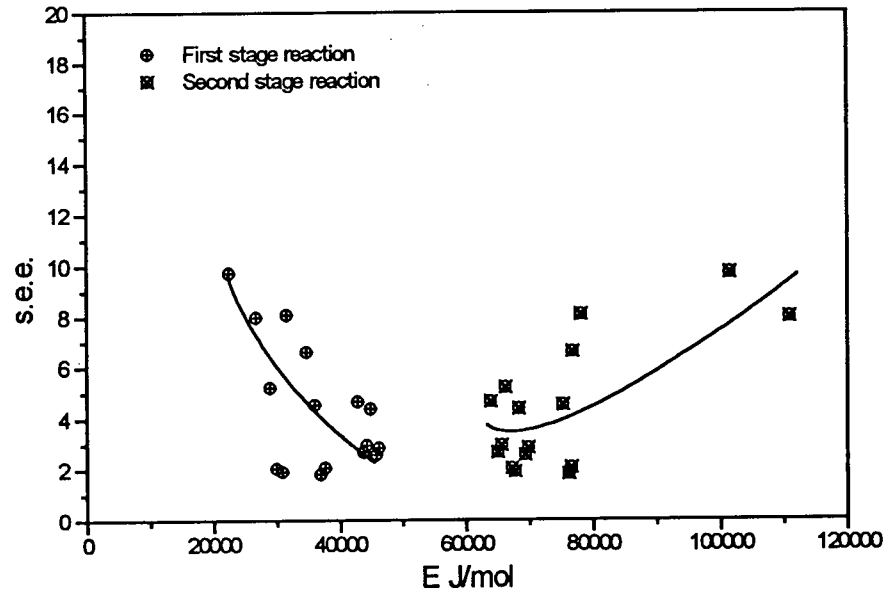

Figure 6.10 Syncrude pitch TGA pyrolysis s.e.e. as a function of E at different conditions and different methods

Figures 6.11 and 6.12 show that the predicted volatile contents at high heating rates and high temperature are in very good agreement with the experimental values, while the prediction at low temperatures for both samples and at the low heating rate of 25 °C/min for CANMET pitch is acceptable. Figures 6.13 and 6.14 also show that at different final temperatures the predicted volatile contents at high temperature for each run are in very good agreement with the experimental volatile yields. The prediction is generally better than that shown in Figures 6.11 and 6.12, and much better than the prediction of the overall single reaction model as shown in Figure 5.1. It is therefore possible to predict the volatile content with one set of unique kinetic parameters for the 2 stage reaction model regardless of the pyrolysis conditions and the methods used to fit the experimental results.

Table 6.3 Experimental Conditions and Model Predicted Results of CANMET Pitch and Syncrude Pitch Pyrolysis

Run#	Heating Rate °C/min	V* %	One set k_o E, s.e.e	Integral s.e.e
	CANMET pitch at 800 °C			
Can48	25	80.84	4.10	1.42
Can33	50	80.79	5.62	2.12
Can41	100	79.30	8.69	1.44
Can58	150	77.59	1.57	0.97
	Syncrude Pitch at 800 °C			
Syn43	25	91.03	10.45	1.94
Syn29	50	90.07	5.62	2.07
Syn18	100	90.58	4.01	2.97
Syn8	150	90.62	9.98	2.85

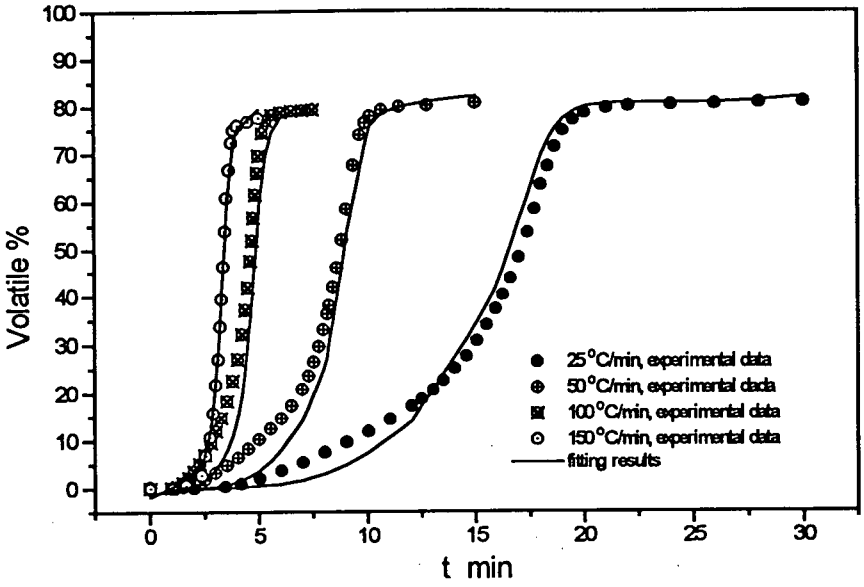

Figure 6.11 Comparison of experimental data and model prediction for CANMET pitch at different heating rates and 800 °C with a single set of kinetic parameters

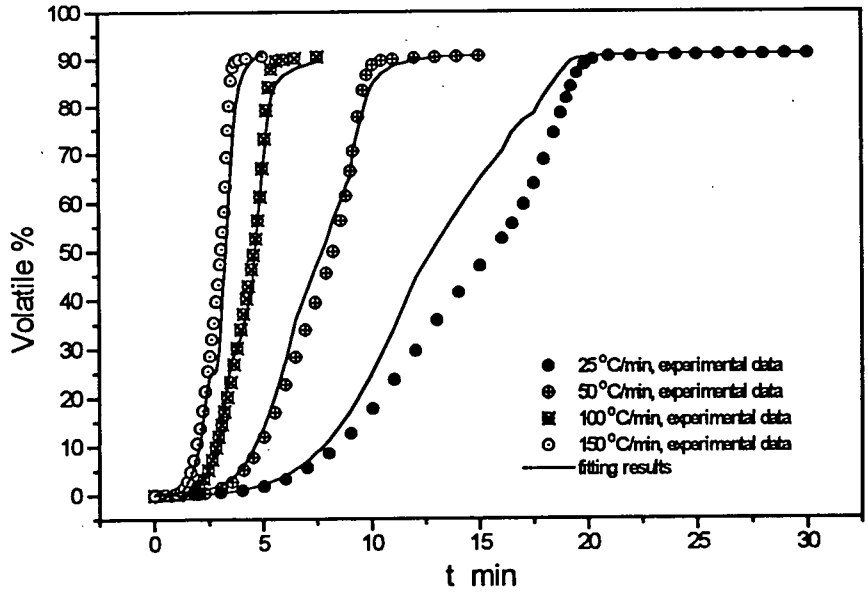

Figure 6.12 Comparison of experimental data and model prediction for Syncrude pitch at different heating rates and 800 °C with a single set of kinetic parameters

Table 6.4 Experimental Conditions and Model Predicted Results of CANMET Pitch and Syncrude Pitch Pyrolysis

Run#	T °C	V* %	One set k_o E, s.e.e.	Integral s.e.e
	CANMET Pitch at 100 °C/min			
Can42	750	79.54	8.13	2.05
Can40	850	79.01	4.34	4.87
Can52	950	81.23	8.93	1.39
	Syncrude Pitch at 50 °C/min			
Syn27	750	90.96	5.40	2.57
Syn32	850	90.61	5.94	2.04
Syn33	950	91.01	5.97	4.49

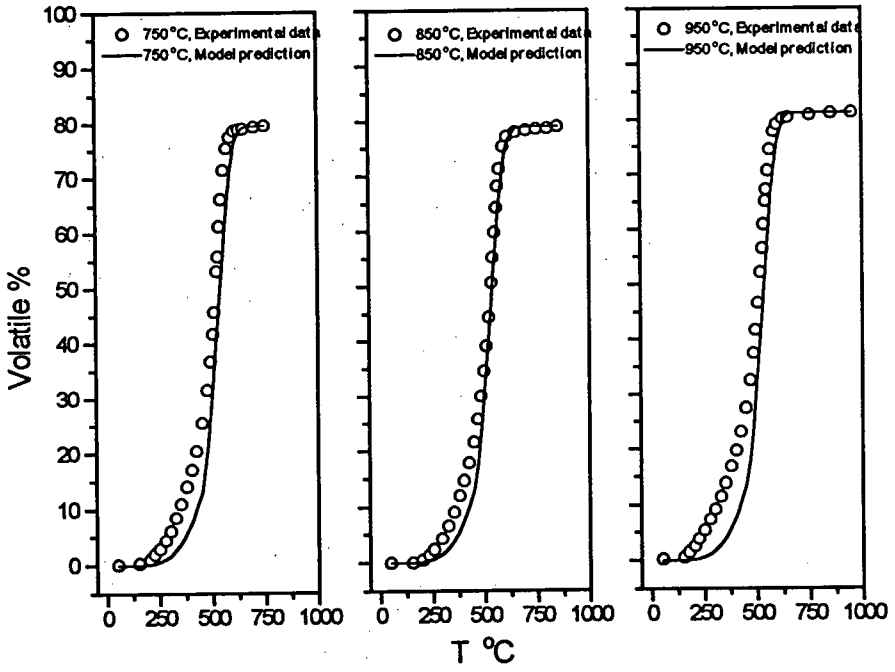

Figure 6.13 Comparison of model prediction and experimental volatile content for CANMET pitch at 100 °C/min and 750 °C, 850 °C, and 950 °C respectively

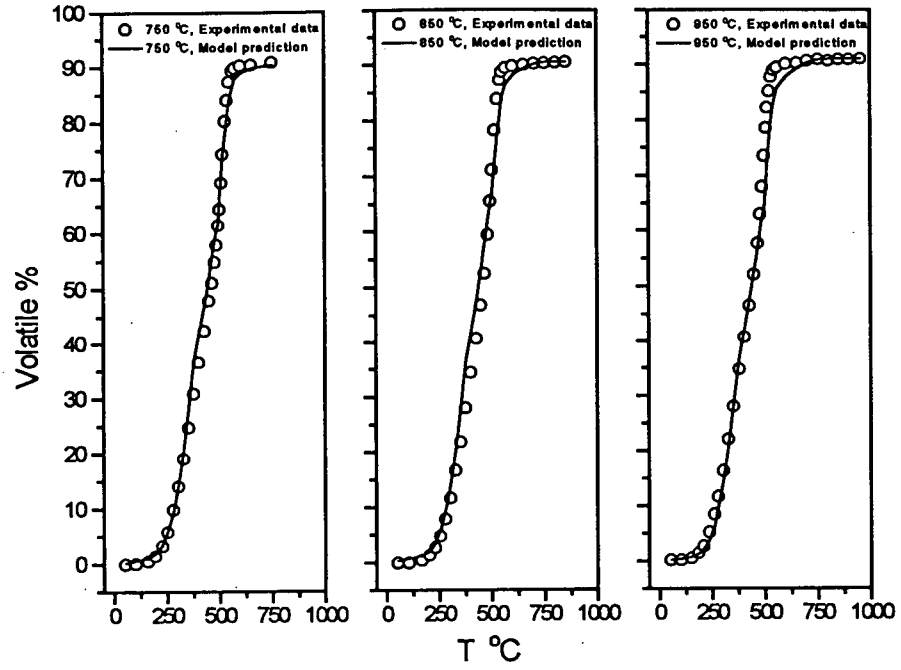

Figure 6.14 Comparison of model prediction and experimental volatile content for Syncrude pitch at 50 °C/min and 750 °C, 850 °C and 950 °C respectively

6.4 Discussion and Conclusion

Clearly for both CANMET and Syncrude pitches, evidence for the compensation effect Equation 6.1 was obtained for the kinetic parameters derived from the single first order reaction model, and the kinetic parameters derived from each stage of the 2-stage kinetic model with different mathematical methods. It seems that the compensation effect is caused by the heating rates for each method used to analyzed the kinetic model equation, as shown in Figures 6.3 and 6.4. Since for these experiments were performed at the same atmosphere and roughly the same sample weight for each pitch type, these physico-chemical factors are therefore excluded. However, one set of compensation effect constants was found to be able to fit all the kinetic parameters derived from the 2-stage kinetic model with all the mathematical methods, as shown in Figures 6.5 and 6.6. This further indicates that the effects of heating rates and mathematical

methods are inseparable factors causing the kinetic compensation effect. Equation 6.2 was not met in the temperature range studied. The isokinetic temperature T_i was therefore not observed as a result. Such an isokinetic temperature was not observed either for TVC-70 polymer thermal degradation [129]. The isokinetic temperature is more commonly observed in the catalysis kinetics and is often explained in terms of the temperature at which the catalyst was prepared [68, 69]. It is not surprising that the isokinetic temperature is not observed in pitch pyrolysis kinetics, since the temperature at which the pitch was prepared, has a totally different meaning. It seems safe to say that the measuring conditions and the methods used to analyze the kinetic models cause the kinetic compensation effect in this work and these factors are inseparable. This work however is not intended to investigate this effect in detail and identify the underlying factors as well as the mechanism of the kinetic compensation effect.

The Arrhenius equation of the kinetic parameters, which is rigorously valid for homogeneous reactions, is widely used for heterogeneous reactions, such as hydrocarbon pyrolysis, although such an extrapolation is not justified. Indeed, heterogeneous systems are characterized by supplementary problems due to complication of heterogeneous reactions. It has been shown [130] that for a series of related heterogeneous reactions, the compensation effect holds between the activation energy and pre-exponential factors. Compensation effects occur either for a series of reactions or for a given reaction when the operational parameters are changed. According to Garn [131-133], the common element of the reported cases of compensation effects is the existence of a main reaction which remains unaltered, in which a parameter regarded as a secondary factor changes the modification of the reaction rate with temperature. Audouin and Verdu [128] reported that a compensation effect appears only when the overall kinetic equation for thermal degradation is composed of many steps. It has been suggested that for such system at each moment a new material undergoes degradation and that

each reaction is characterized by a specific value of the activation energy. In catalytic reactions, the reaction rates have been proven associated with the distribution and concentration of active sites [134, 135].

For pyrolysis, the activation energy E value has been observed to change with its conversion in nonisothermal experiments with oil shale [116], and in the two stages of pyrolysis in the present study. Pitch pyrolysis is such a process in which a series of reactions occur consecutively and/or concurrently, in the meantime the concentration of the active radicals decreases with the extent of reaction. When an inappropriate method is used to derive the two kinetic parameters, the error of one parameter caused by the method would be dumped to the other. However, these two parameters are related through the Arrhenius relationship. Since the pyrolysis rate is dependent on the remaining volatile content (or the reactive residue structure), the pyrolysis rate constants should be independent of the mathematical methods. The change of one parameter would be compensated to give the same rate. The existence of the compensation effect can therefore be attested. Similarly at different heating rates, the same "component" may undergo pyrolysis at different temperatures under TGA conditions. When one method is used to derive the kinetic parameters, the accuracy of the parameters to reflect the "true kinetics of that component" may be affected. Again the average kinetic behavior is retained by the Arrhenius relationship and consequently causing the compensation effect. However, the importance of the compensation effect may lie in the fact that the kinetic parameters k_o and E are interrelated for the pitch pyrolysis. This requires that the kinetic parameters of pitch pyrolysis be interpreted and compared with as a pair. One of the parameters may not be able to describe the whole picture of the pitch pyrolysis process. Care must also be exercised when using the reported kinetic parameters in research or design work.

It is also noted that these methods did not reproduce the kinetic parameters k_o and E at the operating conditions studied. The standard deviation caused by each pair of these parameters is not identical and it is possible to minimize the standard deviation through choosing the best pair of kinetic parameters k_o and E.

Chapter 7 Conclusions and Recommendations

At the onset of the research, no adequate data were available for the kinetics of the pitch pyrolysis and no mathematical models were available for the pitch pyrolysis mechanism. The primary goal of this research has been fulfilled in that the kinetic data for these processes have been outlined and a relevant kinetic model proposed.

7.1 SUMMARY OF FINDINGS

The principal observations and conclusions resulting from this study are listed below:

1. Heating rates were found to slightly affect the weight loss at a given temperature. The temperature history is the significant factor governing the extent to which the reactions take place and produce the weight loss. The devolatilization step is not instantaneous, as little weight loss occurred at the highest heating rates where the heating time took of the order of a few seconds.
2. The pyrolysis takes place in stages. At temperatures below 150 °C, there is little weight loss. The weight loss takes place in two following stages with two different, distinct patterns of chemical and physical change. In the first stage, the rate of the total weight loss increased with the temperature. In the second stage, the rate decreased with the temperature. These features appear unique to pitch pyrolysis, as they have not been reported for coal or shale pyrolysis.
3. The total weight loss (volatile yield) using thermogravimetric analysis decreased slightly with the increase of sample weight over the range of 3 to 17 mg for both CANMET pitch and Syncrude pitch. More than 80% of residue conversion was achieved for CANMET pitch, while more than 90% of residue conversion was achieved for Syncrude pitch.

4. Under Pyroprobe pyrolysis conditions, the pyrolysis time is a very important operating parameter. At the highest heating rate (300,000 °C/min) employed in this study, little pyrolysis was observed for both CANMET and Syncrude pitches up to 700 °C, while at heating rate of 600 °C/min, the weight loss was rather significant when the final temperature was just reached (0 min isothermal reaction time). Higher heating rates exhibit complex effects on the weight loss and the secondary pyrolysis of the volatiles.
5. The most abundant component of the volatiles is shown experimentally to be hydrocarbons with less than the 10 carbons, which is grouped as single lump, C_7, in this study. At each heating rate and final temperature, the amount of C_7 became significant at temperatures higher than 700 °C. As high as 50% volatile yield of this group in the total volatiles was detected for CANMET pitch and secondary reaction is observed at heating rate 3000 °C/min. At the Pyroprobe pyrolysis conditions, the volatiles may undergo secondary pyrolysis when being purged through the quartz tube. A similar trend is also observed for Syncrude pitch pyrolysis with the Pyroprobe-GC.
6. The yield of C_{10} compounds is very strongly influenced by the heating rates. At the highest heating rate (300,000 °C/min), less than 5% volatile yield of this group of components was detected, while as high as 25% volatile yield of C_{10} was detected at lower heating rates. This again attests to the influence of the reaction time and heating rates. The amount of C_{10} detected from Syncrude pyrolysis with Pyroprobe-GC is much less than that of CANMET pitch, which is in agreement with the differences of chemical structure or makeup of these two pitches. Higher yields of C_{11}, C_{12}, C_{13} and C_{14} groups were also detected at lower heating rates, a similar trend as that of C_{10} group. The yield of C_{14} is much less that those of C_{11}, C_{12} and C_{13}. C_{14} is the heaviest group of compounds detected in the Pyroprobe-GC pyrolysis, which suggests that the volatiles are mostly compounds lighter than C_{14}. The yield of these

groups from Syncrude pitch pyrolysis with Pyroprobe-GC is also significantly less than those from CANMET pitch pyrolysis. This is in agreement with the C_{10} yield.

7. Although the pattern of volatile release for pitches pyrolyzed under TGA conditions is complex, an adequate description of the kinetics is possible by methods developed in this work. The pyrolysis takes place in 2 stages, with a first stage of low activation energy barrier and lower pre-exponential factor, and the second stage of higher activation energy and pre-exponential factor. It is recommended that the process be modeled with a 2-stage first order reaction model using integral analysis method. It is demonstrated that the overall single stage reaction model using integral, Coats-Redfern, Chen-Nuttall and Friedman methods as well as Anthony and Howard's distributed activation energy model, are not sufficient to fit the TGA pyrolysis data and predict the course of the pitch pyrolysis process over the full range of conversion. It is also found that these single stage methods do not give similar values of activation energy and pre-exponential factors when data at different TGA conditions are taken for computation.
8. The 2-stage model reflects changes in the chemical constitution or structures as conversion proceeds by using two sets of activation energy. This feature is essential to describe pitch dependence of devolatilization rates on the remaining volatile content. The transition between these two stages is a sharp one, occurring at 450 °C for both CANMET and Syncrude pitches. The magnitude of the activation energies suggests that the pyrolysis of pitch was kinetically controlled under the reaction conditions studied. The dependence of dV/dT on V*-V is also in accordance with that. The activation energy of the second stage is higher than that of the first stage.
9. For both CANMET and Syncrude pitches, correlation between k_o and E values obtained via the different methods was observed. One set of compensation effect constants was found to

be able to fit all the kinetic parameters derived from all the 2-stage kinetic analysis methods. An isokinetic temperature T_i was not observed. These methods did not give similar kinetic parameters k_o and E at the operating conditions studied. The standard deviation caused by each pair of these parameters was not identical and it was possible to minimize the standard deviation through choosing the best pair of kinetic parameters k_o and E.

7.2 RECOMMENDATIONS

The following recommendations are offered for further work and future application:

1. To achieve more detailed GC analysis of the Pyroprobe pyrolysis products, a longer column should be used and the gaseous and liquid components should be analyzed separately using cryogenic focus. The C_7 should also be analyzed in detail with GC for gas components since it is the major lump for both CANMET and Syncrude Pitch.
2. To correlate the volatile yield with operating conditions such as heating rates, final temperature, and sample weights, a wider heating rate range should be used, such as heating rates as low as a few degrees per minute. Large sample weight (>18mg) should also be used to study the internal mass transfer effect.
3. The critical temperature, dividing the two pyrolysis stage of pitch pyrolysis should be further studied with a variety of pitch samples of different origin. This temperature may be dependent on the pitch sample used.
4. To achieve a higher conversion and more light volatile yields, reactive pyrolysis environments such as hydrogen or steam should be used.
5. The use of a pilot-scale pyrolyzer is needed to explore the applicability of the 2-stage mechanism and the related 2-stage first order integral method.

6. The application of the kinetic parameters of pitch pyrolysis should be concerned with the methods used to derived these values and the accuracy of the model predictions. The kinetic parameters k_o and E should be compared with and used as a pair. The magnitude of one of these parameters may not be adequate to describe the characteristics of a pitch pyrolysis process.

REFERENCES

1. Solomon, P. and G. Hamblen, 'Pyrolysis", in 'Chemistry of Coal Conversion", Richard H. Schlosberg, Eds., Plenum Press, New York and London (1985), pp. 122.

2. Solomon, P. and G. Hamblen, 'Pyrolysis", in 'Chemistry of Coal Conversion", Richard H. Schlosberg, Eds., Plenum Press, New York and London (1985), pp. 121.

3. Solomon, P. and G. Hamblen, 'Pyrolysis", in 'Chemistry of Coal Conversion", Richard H. Schlosberg, Eds., Plenum Press, New York and London (1985), pp. 127.

4. Howard, J. B., 'Chemistry of Coal Utilization", Secondary Supplementary Volume, M. A. Elliott, Eds., Wiley Press, New York (1981), pp. 625-784.

5. Serio, M. A., W. A. Peters and J. B. Howard, 'Kinetics of Vapor Phase Secondary Reactions of Prompt Coal Pyrolysis Tars", Ind. Eng. Chem. Res. **26**, 1831-1838 (1987).

6. Hebden, D. and Henry J. F. Strout, 'Chemistry of Coal Utilization", Secondary Supplementary Volume, M. A. Elliott, Eds., Wiley Press, New York (1981), pp. 1599-1800.

7. Maa, P. S., Ken L. Trachete and Richard D. Williams, 'Solvent Effects in Exxon Donor-Solvent Coal Liquefaction", in 'Chemistry of Coal Conversion", Richard H. Schlosberg, Eds., Plenum Press, New York and London (1985), pp. 317-330.

8. Furimsky, E., 'Pyrolysis of Virgin Pitch and Thermally Hydrocracked Pitch Derived from Athabasca Bitumen", Ind. Eng. Chem. Prod. Res. Dev. **22**, 637-642 (1983).

9. Howard, J. B., 'Chemistry of Coal Utilization", Secondary Supplementary Volume, M. A. Elliott, Eds., Wiley Press, New York (1981), pp. 669.

10. Legros, R, J. R. Grace, C. M. H. and C. J. Lim, 'Circulating Fluidized Bed Combustion of Pitches", Research Report, Department of Chemical Engineering, UBC (1990).

11. Watkinson, A. P., Personal File, (1992).

12. Menzies, M. A., A. E. Siliva and J. M. Denis, 'Hydrocracking without Catalysis Upgrades Heavy Oil", Chem. Eng. **88**(4) 46-47 (1981).

13. Pruden, B. B., 'Hydrocracking of Bitumen and Heavy Oils at CANMET", Can. J. Chem. Eng. **56**, 277-280 (1978).

14. Pruden, B. B., 'Upgrading of Cold Lake Heavy Oil in the CANMET Hydrocracking Demonstration Plant", The Fourth Unitar/UNDP International Conference on Heavy Crude and Tar Sands", Proceedings volume **5**, Extraction, Upgrading, Transportation, August 7-12, Edmonton, Alberta, Canada (1988) pp. 249-254.

15. Reich, A., W. Bishop and M. Veljkovic, 'LC-Finer Commercial Experience and Hydroprocessing Future Direction", Oil Sands:Our Petroleum Future Conference April 4-7, Edmonton, Alberta, Canada (1993)

16. Lowry, H. H., Eds., 'The Chemistry of Coal Utilization", Supplementary Volume, John Wiley and Sons, Inc., New York (1963).

17. Van Krevelen, D. W., "Coal", Elsevier, Amsterdam (1981), pp. 514-516.

18. Komatsu, N and T. Nishizawa, 'Ext. Abstracts 17th Biennial Conference on Carbon", Lexington, Kentucky, 16-21 June 1985 pp. 342-343.

19. Mazza, A. G., 'Modeling of the Liquid Phase Thermal Cracking Kinetics of Athabasca Bitumen and Its Major Chemical Fractions", Ph.D. Thesis, Department of Chemical Engineering and Applied Chemistry, University of Toronto, Toronto, Canada (1987).

20. Reynolds, J. G., 'Effect of Prehydrogenation on Hydroconversion of Maya Residuum, Part III: Predicting Residuum Processibility by the SARA Separation Method". AIChE Symp. Ser. **87**, 62-71 (1991).

21. Sanford, E., 'Molecular Approach to Understanding Residuum Conversion", Ind. Eng. Chem. Res. **33**, 109-117 (1994).

22. Fitzer, E., K. Mueller and W. Schaefer, 'Conversion of Organic Compounds to Carbon", in "Chemistry and Physics of Carbon" **7**, 238-283 (1971).

23. Mazza, A. G. and Donald E. Cormack, 'Thermal Cracking of the Major Chemical Fractions of Athabasca Bitumen", AOSTRA J. Res. **4**, 193-208 (1988).

24. Selucky, M. L., S. S. Kim, K. Skinner and O. P. Strausz, 'Structure-Related Properties of Athabasca Asphaltenes and Resins as Indicated by Chromatographic Separation", in 'The Chemistry of Asphaltenes", J. W. Bunger and N. Li, Eds., Am. Chem. Soc. Advances in Chemistry Series **195** (1981), pp. 83.

25. Gould, K. A., 'Influence of Thermal Processing on the Properties of Cold Lake Asphaltenes, 2. Effect of Steam Treatment During Oil Recovery", Fuel **62**, 370- 372 (1983).

26. Speight, J. G., 'Thermal Cracking of Athabasca Bitumen, Athabasca Asphaltenes and Athabasca Deasphalted Heavy Oil", Fuel **49**, 134-145 (1970).

27. Mojelsky, T. W., and O. P. Strausz, 'Detection of Alkylated Fluorenes in Athabasca Oil Sand Bitumens", Organic Geochemistry **9**, 39-45 (1986).

28. Selucky, M. L., Y. Chu, T. Ruo and O. P. Strausz, 'Chemical Composition of Athabasca Bitumen", Fuel **56**, 369-381 (1977).

29. Hayashitani, M., Ph.D. Thesis, University of Calgary, Calgary, Alberta, Canada (1978).

30. Anthony, D. B. and J. B. Howard, "Coal Devolatilization and Hydrogasification", AIChE **22**, 625-656 (1976).

31. Smoot, L. D., "Pulverized Coal Diffusion Flames, A perspective through Modeling", 18th Symposium (international) on Combustion, The Combustion Institute (1981), pp. 1185-1202.

32. Smoot, L. D. and D. T. Pratt, "Pulverized Coal Combustion and Gasification", Plenum Press , New York (1979).

33. Trimm, D. L. and C. J. Turner, "The Pyrolysis of Propane. I. Production of Gases, Liquids and Carbon", J. Chem. Tech. Biotechnol. **31**, 195-204 (1981).

34. Sundaram, K. M. and G. F. Froment, "Kinetics of Coke Deposition in Thermal Cracking of Propane", Chem. Eng. Sci. **34**, 635-644 (1979).

35. Kumar, P. and D. Kunzru, "Modeling of Naphtha Pyrolysis", Ind. Eng. Chem. Process Des. Dev. **24**, 774-782 (1985).

36. Jamaluddin, A. S., T. F. Wall and J. S. Truelove, "Modeling of Devolatilization and Combustion of Pulverized Coal under Rapid Heating Condition", in "Coal Science and Chemistry", A. Volborth, Eds., Elsevier Science Publishers B. V., Amsterdam (1987), pp. 61-106.

37. Suuberg, E. M., "Mass Transfer Effects in Pyrolysis of Coals: A Review of Experimental Evidence and Models", in "Chemistry of Coal Conversion", R. H. Schlosberg, Eds., Plenum Press (1985), pp. 67-117.

38. Baum, M. M. and P. J. Street, "Predicting the Combustion Behavior of Coal Particles", Combustion Science and Technology **3**, 231-243 (1971).

39. Lochwood, F. C., S. M. A. Rizvi, G. K. Lee and H. Whaley, "Coal Combustion Model Validation Using Cylindrical Furnace Data", 20th Symposium (International) on Combustion, The Combustion Institute (1984), pp. 513-522.

40. Badzioch, S. and P. G. W. Hawksley, "Kinetics of Thermal Decomposition of Pulverized Coal Particles", Ind. Eng. Chem. Process Des. Dev. **9**, 521-530 (1970).

41. Kobayashi, H., J. B. Howard and A. F. Sarofim, "Coal Devolatilization at High Temperatures", 16th Symposium (international) on Combustion, The Combustion Institute (1977), pp. 411-425.

42. Ubhayakar, S. K., D. B. Stickler, C. W. V. Rosenberg and R. E. Gannon, "Rapid Devolatilization of Pulverized Coal in Hot Combustion Gases", 16th Symposium (International) on Combustion, The Combustion Institute (1977), pp. 427-436.

43. Wen, C. Y. and S. Dutta, 'Rates of Coal Pyrolysis and Gasification Reactions", in 'Coal Conversion Technology", C. Y. Wen and E. S. Lee, Eds., Addison Wesley Publishing Co., New York (1979).

44. Niksa, S., H. E. Heyd, W. B. Russel and D. A. Saville, 'On the Role of Heating Rate and Rapid Coal Devolatilization", 20th Symposium (International) on Combustion, The Combustion Institute (1984), pp. 1445-1453.

45. Jüntgen, H. and K. H. Van Heek, 'Gas Release from Coal as a Function of the Rate of Heating", Fuel **47**, pp. 103-117 (1968).

46. Jüntgen, H. and K. H. van Heek, "An Update of German Non-Isothermal Coal Pyrolysis Work", Fuel Processing Technology **2**, 261-293 (1979).

47. Nsakala, N. Y., R. H. Essenhigh and P. L. Walker Jr., 'Studies on Coal Reactivity: Kinetics of Lignite Pyrolysis in Nitrogen at 808 °C", Combustion Science and Technology **16**, 153-163 (1977).

48. Pitt, G. J., 'The Kinetics of the Evolution of Volatile Products from Coal", Fuel **41**, 267-276 (1962).

49. Anthony, D. B., J. B. Howard, H. C. Hottel and H. P. Meissner, 'Rapid Devolatilization and Hydrogasification of Bituminous Coal", Fuel **55**, 121-128 (1976).

50. Anthony, D. B. and J. B. Howard, 'Coal Devolatilization and Hydrogasification", AIChE **22**, 625-656 (1976).

51. Lakshmanan, C. C. and N. White, "A New Distribution Activation Energy Model Using Weibull Distribution for the Representation of Complex Kinetics", Energy & Fuels **8**, 1158-1167 (1994).

52. Miura, K., "A New and Simple Method to Estimate f(E) and $k_o(E)$ in the Distributed Activation Energy Model from Three Sets of Experimental Data", Energy & Fuels **9**, 302-307 (1995).

53. Antal, M. J., E. G. Plett, T. P. Chung and Summerfield, 'Recent Progress in Kinetic Models for Coal Pyrolysis", ACS Divn. of Fuel Chemistry Prprints **22**, 137-148 (1977).

54. Reidelbach, H. and M. Summerfield, 'Kinetic Model for Coal Pyrolysis Optimization", ACS Divn. of Fuel Chemistry Preprints **20**, 161-202 (1975).

55. Antal, M. J., E. G. Plett, T. P. Chung and M. Summerfield, 'Recent Progress in Kinetic Models for Coal Pyrolysis", ACS Div. of Fuel Chemistry Preprints **22**, 137-148 (1977).

56. Suuberg, E. M., W. M. Peters and J. B. Howard, 'Product Composition and Kinetics of Lignite Pyrolysis", Ind. Eng. Chem. Process Des. Dev. **17**, 37 (1978).

57. Suuberg, E. M., 'Rapid Pyrolysis and Hydropyrolysis of Coal", Sc.D. Thesis, Department of Chemical Engineering, MIT, Cambridge, Mass (1977).

58. Suuberg, E. M., W. A. Peters and J. B. Howard, 'Product Compositions and Formation Kinetics in Rapid Pyrolysis of Pulverized Coal Implications for Combustion", Symposium (International) on Combustion, The Combustion Institute (1979), pp. 117-130.

59. Hajaligol, M., J. B. Howard and W. A. Peters, 'Product Composition and Kinetics for Rapid Pyrolysis of Cellulose", I&EC Process Des. Dev. **21**, 457- 567 (1982).

60. Kizler, F. J. and A. Broidio, 'Speculation on the Nature of Cellulose Pyrolysis", Pyrodynamics **2**, 151-162 (1965).

61. Milosavljevic, I. and E. Suuberg, 'Cellulose Thermal Decomposition Kinetics: Global Mass Loss Kinetics", Ind. Eng. Chem. Res. **34**, 1081-1091 (1995).

62. Carrasco, F., 'The Evaluation of Kinetic Parameters from Thermogravimetric Data: Comparison between Established Methods and the General Analytical Equation", Thermochim Acta **213,** 115-134 (1993).

63. Pysiak, J. and B. J. Sabalski, 'Compensation Effect and Isokinetic Temperature in Thermal Dissociation Reactions of the Type $A_{solid} \leftrightarrow B_{slod} + C_{gas}$: Interpretation of the Arrhenius Equation as a Projection Correlation", J. Therm. Anal. **17**, 287-303 (1979).

64. Constable, F. H., 'The Mechanism of Catalytic Decomposition", Proc. Roy. Soc. London, Ser. A **108**, 355-385 (1925).

65. Muraishi, K. and H. Yokobayashi, 'Kinetic Compensation Effect for the Thermal Solid State Reactions of Lanthanide Oxalate, Malonate and Succinate Hydrates and their Anhydrides", Thermochim. Acta **209**, 175-188 (1992).

66. Galwey, A. K., 'Compensation Effect in Heterogeneous Catalysis", Advance in Catalysis **26**, 247-322 (1977).

67. Koga, N., "A Review of the Mutual Dependence of Arrhenius Parameters Evaluated by the Thermoanalytical Study of Solid Reactions: the Kinetic Compensation Effect", Thermochim Acta **244**, 1-20 (1994).

68. Kral, H., 'Thermal Deactivation of Heterogeneous Catalysts, Part 1. The Theta-Rule, A Critical Review", Chem. Eng. Technol. **11**, 113-119 (1988).

69. Kral, H., 'Thermal Deactivation of Heterogeneous Catalysts, Part 2. The Compensation Effect and the Catalytic Paradox", Chem. Eng. Technol. **11**, 228-236 (1988).

70. Lesnikovich, A. I. and S. Levchik, 'Isoparametric Kinetic Relations for Chemical Transformations in Condensed Substances (Analytical Survey). I. Theoretical Fundamentals ", J. Therm. Anal. **30**, 237-262 (1985).

71. Norwisz, J., Z. Smieszek and Z. Kolenda, "Apparent Linear Relationship, Compensation Law and Others: Part I", Thermochim Acta **156**, 313-320 (1989).

72. Zawadski, J. and S. Bretzsnajder, "The Temperature Increament of the Reaction Velocity of Reactions of the Type A Solid $\rightarrow$B Solid + C Gas", Z. Elektrochem. **41**, 215-223 (1935).

73. Gallagher, P. K. and D. W. Johnson, "The Effects of Sample Size and Heating Rate on the Kinetics of the Thermal Decomposition of $CaCO_3$", Thermochim. Acta **6**, 67-83(1973).

74. Pavlyuchenko, M. M. and E. A. Prodan, "The Role of Chemical and Crystallization Processes in Reversible Topochemical Reactions", Doklady Akad. Nauk. S.S.S.R. **136**, 651-653 (1961).

75. Wist, A. O., in R. F. Schwenker, Jr. and P. D. Garn, Eds., "Thermal Analysis (Proc. 2nd ICTA)", Academic Press, New York (1969), pp. 1095.

76. Roginski, S. Z. and J. L. Chatji, Izv. Acad. Sci. USSR Ser. Khim (1961), pp. 771.

77. Pysiak, J., "Influence of Some Factors on Thermal Dissociation of Solids", Thermochim Acta **148**, 165-171 (1989).

78. Zsakó, J. and H. E. Arz, "Kinetic Analysis of the Thermogravimetric Data: VII Thermal Decomposition of Calcium Carbonate", J. Therm. Anal. **6**, 651-656 (1974).

79. Zsakó, J., C. Várhelyi and G. Liptay, "Kinetic Analysis of Thermogravimetric Data. XXVIII. Thermal Decomposition of Some Metal and Ammonium Salts of Hexabromoplatinic Acid", J. Therm. Anal. **38,** 2301-2310 (1992).

80. Muraishi. K. and H. Yokobayashi, "Kinetic Compensation Effect for the Thermal Solid State Reactions of Lanthanide Oxalate, Malonate and Succinate Hydrates and Their Anhydrides", Thermochim. Acta **209**, 175-188 (1992).

81. Dollimore, D. and P. F. Rogers, "The Appearance of a Compensation Effect in the Thermal Decomposition of Manganese (II) Carbonates, Prepared in the Presence of Other Metal Ions", Thermochim. Acta **30**, 273-280 (1979).

82. Bordas, S., M. T. Clavaguera-Mora and N. Clavaguera, "Glass Formation and Crystallization Kinetics of Some Germanium-Antimony-Selenium Glasses", J. Non-Cryst. Solids **107**, 232-237 (1990).

83. MacCallum, J. R. and M. V. Munro, "The Kinetic Compensation Effect for the Thermal Decomposition of Some Polymers", Thermochim. Acta **203**, 457-463 (1992).

84. Guarini, G. G. T., R. Spinicci, F. M. Carlini and D. Donati, "Some Experimental Aspects of DSC Determination of Kinetic Parameters in Thermal Decomposition of Solids", J. Therm. Anal. **5**, 307-314 (1973).

85. Simon, J., 'Some Considerations Regarding the Kinetics of Solid-State Reactions", J. Therm. Anal. **5**, 271-284 (1973).

86. Szekely, T., G. Varhegyi, F. Till, P. Szabo and E. Jakab, 'The Effects of Heat and Mass Transport on the Results of Thermal Decomposition Studies. Part 1. the Three Reactions of Calcium Oxalate Monohydrate", J. Anal. Appl. Pyrol. **11**, 71-81 (1987).

87. Tanaka, H. and N. Koga, 'Kinetics of Thermal Decomposition of MC_2O_4 to MCO_3 (M=Ca, Sr and Ba)", J. Therm. Anal. **32**, 1521-1529 (1987).

88. Ninan, K. N., 'Kinetics of Solid State Thermal Decomposition Reactions", J. Therm. Anal. **35**, 1267-1278 (1989).

89. Flynn, J., 'Thermal Analysis Kinetics: Problems, Pitfalls and How to Deal with Them", J. Therm. Anal. **34**, 367-381 (1988).

90. Czarnecki, J. P., N. Koga, V. Sesták and J. Sesták, 'Factors Affecting the Experimentally Resolved Shapes of TG Curves", J. Therm. Anal. **38**, 575-582 (1992).

91. Criado, J. M. and M. Gonzalez, 'The Method of Calculation on Kinetic Parameters as a Possible Cause of Apparent Compensation Effects", Thermochim. Acta **46**, 201-207 (1981).

92. Criado, J. M., D. Dollimore and G. R. Heal, "A Critical Study of the Suitability of the Freeman and Carroll Method for the Kinetic Analysis of Reactions of Thermal Decomposition of Solids", Thermochim. Acta **54**, 159-165 (1982).

93. Criado, J. M. and A Ortega, 'Errors in the Determination of Activation Energies of Solid-State Reactions by the Piloyan Method, as a Function of the Reaction Mechanism", J. Therm. Anal. **29**, 1075-1082 (1984).

94. Vyazovkin, S. V. and A. I. Lesnikovich, 'Errors in Determining Activation Energy Caused by the Wrong Choice of Process Model", Thermochim. Acta **165**, 11-15 (1990).

95. Somasekharan, K. M. and V. Kalpagam, 'Use of a Compensation Parameter in the Thermal Decomposition of Copolymers", Thermochim. Acta **107**, 379-382 (1986).

96. Arnold, M., G. E. Veress, J. Paulik and F. Paulik, 'Problems of the Characterization of Thermoanalytical Process be Kinetic Parameters, Part I", J. Therm. Anal. **17**, 507-528 (1979).

97. Hulett, J. R., "Deviations from the Arrhenius Equations", Q. Rev **18**, 227-230 (1964).

98. Sesták, J., 'Errors of Kinetics Data Obtained from Thermogravimetric Curves at Increasing Temperature", Talanta **13**, 567-579 (1966).

99. Zsakó, J., "The Kinetic Compensation Effect", J. Therm. Anal. **9**, 101-108 (1976).

100. Exner, O., "Determination of the Isokinetic Temperature", Nature **227**, 366-367 (1970).

101. Agrawal, R. K., "Compensation Effect: a Fact or a Fiction", J. Therm. Anal. **35**, 909-917 (1989).

102. Sesták, J. and Z. Chvoj, "Thermodynamics and Thermochemistry of Kinetic (Real) Phase Diagram Involving Solids", J. Therm. Anal. **32**, 1465-1650 (1987).

103. Zsakó, J. and K. N. Somasekharan, "Critical Remarks on "On the Compensation Effect"", J. Therm. Anal. **32**, 1277-1281 (1987).

104. Garn, P. D., "Kinetic Parameters", J. Therm. Anal. **13**, 581-593 (1978).

105. Tanaka, H., N. Koga and J. Sesták, "Thermoanalytical Kinetics for Solid State Reactions as Examplified by the Thermal Dehydration of $Li_2SO_4.H_2O$", Thermochim. Acta **203**, 203-220 (1992).

106. Heck, R. H., L. A. Rankel and F. T. DiGuiseppi, "Conversion of Petroleum Resid from Maya Crude: Effects of H-donors, Hydrogen Pressure and Catalyst", Fuel Process Technology **30**, 69-81 (1992).

107. Nguyen, Q. T., "Kinetics of Gasification and Sulphur Capture of Oil Sand Cokes", Ph.D. Thesis, Department of Chemical Engineering, University of British Columbia, Canada, 1988

108. Shih, S. M. and H. Y. Sohn, "Nonisothermal Determination of the Intrinsic Kinetics of Oil Generation from Oil Shale", Ind. Eng. Chem. Process. Des. Dev. **19**, 426-431 (1980).

109. Guo, D., Eds., "University Mathematics Handbook", Shandong Science and Technology Press, Jinan (1985), pp. 202.

110. Press, W. H., S. A. Teukolsky, W. T. Vetterling and B. P. Flannery, "Numerical Recipes in FORTRAN, The Art of Scientific Computing ", 2nd. Ed., Cambridge University Press (1992), pp. 678-683.

111. Thakur, D. S. and H. E. Eric Nuttall Jr., "Kinetics of Pyrolysis of Moroccan Oil Shale by Thermogravimetry", Ind. Eng. Chem. Res. **26**, 1351-1356 (1987).

112. Braun, R. L. and A. Rothman, "Oil Shale Pyrolysis Kinetics and Mechanism of Oil Production", J. Fuel **54**, 129-131 (1975).

113. Rajeshwar, K., "Kinetics of Thermal Decomposition of Green River Shale Kerogen by Nonisothermal Thermogravimetry", Thermochim. Acta **40**, 253-263 (1981).

114. Haddadin, R. A. and F. A. Mizyet, "Thermogravimetric Analysis Kinetics of Jordan Oil Shale", Ind. Eng. Chem. Process Des. Dev. **13**, 332-336 (1974).

115. Haddadin, R. A. and K. M. Tawarah, "DTA Derived Kinetics of Jordan Oil Shale", Fuel **59**, 539-545 (1980).

116. Schucher, R., "Thermogravemetric Determination of the Coking Kinetics of Arab Vacuum Residuum", Ind. Eng. Chem. Process. Des. Dev. **22**, 615-619 (1983).

117. Campbell, J. H., George H Koskinas and Norman D. Stout, "Kinetics of Oil Generation from Colorado Oil Shale", Fuel **57**, 372-376 (1978).

118. Herrell, A. Y. and C. Arnold, Jr., "Preliminary Studies on the Recovery of Oil from Chattanooga Shale", Thermochim. Acta **17**, 165-175 (1976).

119. Jacobs, P. W. M. and F. C. Tompkins, Chap. 7 in "Chemistry of Solid State", W. E. Garner Eds., Butterworths, London (1995), pp. 184-211.

120. Coats, A. W. and J. P. Redfern, "Kinetic Parameters from Thermogravimetric Data", Nature (London) **201**, 68-69 (1964).

121. Caballero, J. A., R. Font, A. Marcilla and J. A. Conesa, "New Kinetic Model for Thermal Decomposition of Heterogeneous Materials", Ind. Eng. Chem. Res. **34**, 806-812 (1995).

122. Dahr, P. S., "A Comparative Study of Different Methods for the Analysis of TGA Curves ", Computers and Chemistry **10**, 293-297 (1986).

123. Natu, G. N., S. B. Kulkarni and P. S. Dahr, "Thermal Studies on Tris-Chelate Complex of Nickel", J. Therm. Anal. **23**, 101-109 (1982).

124. Heck, R. H. and F. T. DiGuiseppi, "Kinetic Effects in Resid Hydrocracking", Energy & Fuels **8**, 557-560 (1994).

125. Gray, M. R., et al., "Role of Catalyst in Hydrocracking of Residues from Alberta Bitumens", Energy & Fuels **6**, 478-485 (1992).

126. Stubington, J. F. and S. Aiman, "Pyrolysis Kinetics of Bagasse at High Heating Rates", Energy & Fuels **8**, 194-203 (1994).

127. Lau, C. W. and S. Niksa, "Impact of Soot on the Combustion Characteristics of Coal Particles of Various Types", Combust. Flame **95**, 1-21 (1993)

128. Audouin, L. and J. Verdu, "Comments on the Electrotechnical Ageing Compensation Effect", Polymer Degradation and Stability **31**, 335-346 (1991).

129. Budrugeac, P. and E. Segal, "The Ageing Compensation Effect on the Thermal Degradation of Some Electrical Insulators", Thermochim. Acta **202**, 121-131 (1992).

130. Budrugeac, P. and E. Segal, "On the Kinetics of the Thermal Degradation of Polymers with Compensation Effect and the Dependence of Activation Energy on the Degree of Conversion", Polymer Degradation and Stability **46**, 203-210 (1994).

131. Garn, P. D., "An Examination of the Kinetic Compensation Effect", J. Therm. Anal. **7**, 475-478 (1975).

132. Garn, P. D., 'Kinetics of Decomposition of the Solid State", Thermochim. Acta **135**, 71-77 (1988).

133. Garn, P. D., 'Kinetics of Thermal Decomposition of the Solid State. II. Delimiting the Homogeneous-Reaction Model", Thermochim. Acta **160**, 135-145 (1990).

134. Yoneda, Y., 'Linear Free Energy Relationships in Heterogeneous Catalysis: IV Regional Analysis for Solid Acid Catalysis", J. Catal. **9**, 51-56 (1967).

135. Li-Quin, S, H. Su, and L. Xuan-Wen, 'Stud. Surf. Sci. Catal", in 'Catalysis by Acids and Bases", B. Imelik, Eds., Elsevier, Amsterdam (1985) pp. 335.

APPENDICES

APPENDIX A Methods Available for Computing Kinetic Parameters

Carrasco [62] has compared the activation energy results obtained by using the general analytical solution with those evaluated by means of established methods which were classified in three categories: integral (Table A.1), differential (Table A.2), and special methods (Table A.3). The comparison of the results and the related methods are summarized in the following tables. The accuracy (inaccuracy) of these methods was considered as the consequences of the simplification. These methods are however of no use due to the inaccuracy and their oversimplification for pitch pyrolysis.

Table A.1 Summary of the Integral Methods [62]

Author	Method	E
Analytical solution	$\ln\left[\frac{1-(1-f)^{1-n}}{(1-n)T^2\sum_{i=1}^{\infty}(-1)^{i+1}i!\left(\frac{RT}{E}\right)^{i-1}}\right]=\ln\left(\frac{A^*R}{\beta E}\right)-\frac{E}{R}\frac{1}{T};\ n\neq 1$ (2.9a) $\ln\left[\frac{1-(1-f)}{T^2\sum_{i=1}^{\infty}(-1)^{i+1}i!\left(\frac{RT}{E}\right)^{i-1}}\right]=\ln\left(\frac{A^*R}{\beta E}\right)-\frac{E}{R}\frac{1}{T};\ n=1$ (2.9b)	100%
van Krevelen et al. (1951)	$\ln\left[\frac{1-(1-f)^{1-n}}{1-n}\right]=\ln\left[\frac{A^*}{\beta}\left(\frac{0.368}{T_m}\right)^{E/RT_m}\frac{1}{\frac{E}{RT_m}+1}\right]+\left(\frac{E}{RT_m}+1\right)\ln T;\ n\neq 1$ (2.10a) $\ln\left[-\ln(1-f)\right]=\ln\left[\frac{A^*}{\beta}\left(\frac{0.368}{T_m}\right)^{E/RT_m}\frac{1}{\frac{E}{RT_m}+1}\right]+\left(\frac{E}{RT_m}+1\right)\ln T;\ n=1$ (2.10b)	108%
Kissinger (1957)	$\ln\left[\frac{\beta}{T_m^2}\frac{1}{n(1-f_m)^{n-1}}\right]=\ln\left(\frac{A^*R}{E}\right)\frac{E}{R}\frac{1}{T_m};\ n\neq 1$ (2.11a) $\ln\left[\frac{\beta}{T_m^2}\right]=\ln\left(\frac{A^*R}{E}\right)\frac{E}{R}\frac{1}{T_m};\ n=1$ (2.11b)	80%

Table A.1 (Continued)

Horowitz and Metzger (1963)	$\ln\left[\frac{1-(1-f)^{1-n}}{1-n}\right]=\frac{E}{RT_s^2}\theta\ ;n\neq 1$ (2.12a) $\ln\left[-\ln(1-f)\right]=\frac{E}{RT_s^2}\theta\ ;n=1$ (2.12b) where: $\theta=T-T_s$ (T_s is T at which f=(1-1/e) for n=1 and $T_s=T_m$ for n≠1 $A=\frac{\beta E}{RT_s^2}\exp\left(\frac{E}{RT_s}\right)$ (2.12c)	116%
Coats and Redfern (1965) (zero-order reaction)	$\ln\left[\frac{f}{T^2\left(1-\frac{2RT}{E}\right)}\right]=\ln\left(\frac{A^*R}{\beta E}\right)-\frac{E}{R}\frac{1}{T}$ (2.13a) $\ln\left[\frac{f}{T^2}\right]=\ln\left(\frac{A^*R}{\beta E}\right)-\frac{E}{R}\frac{1}{T};(when\ RT<<E)$ (2.13b)	94%

Table A.2 Summary of Differential Methods [62]

Author	Method	E
Classical	$\ln\left[\frac{\left(\frac{df}{dT}\right)}{(1-f)^n}\right]=\ln\left(\frac{A^*}{\beta}\right)-\frac{E}{R}\frac{1}{T}$ (2.14)	Close
Multiple linear regression	$\ln\left(\frac{df}{dT}\right)=\ln\left(\frac{A^*}{\beta}\right)+n\ln(1-f)-\frac{E}{R}\frac{1}{T}$ (2.15)	Close
Freeman and Carroll (1958)	$\frac{\Delta\ln\left(\frac{df}{dT}\right)}{\Delta\ln(1-f)}=n-\frac{E}{R}\frac{\Delta\left(\frac{1}{T}\right)}{\Delta\ln(1-f)}$ (2.16)	90% to 110%
Vachusca and Voboril (1971)	$\frac{T^2\left(\frac{d^2f}{dT^2}\right)}{\left(\frac{df}{dT}\right)}=\frac{E}{R}-n\frac{T^2\left(\frac{df}{dT}\right)}{(1-f)}$ (2.17)	110%

Table A.3 Summary of Special Methods [62]

Author	Method		E
Reich (1964)	$E = \dfrac{R \ln\left[\dfrac{\beta_1}{\beta_2}\left(\dfrac{T_1}{T_2}\right)^2\right]}{\dfrac{1}{T_1}-\dfrac{1}{T_2}}$	(2.18)	82%
	T_1 and T_2 are measured at the same conversion value of two different heating rate runs.		
Friedman (1969)	$n = \dfrac{\ln\dfrac{(df/dT)_m}{df/dT}}{\dfrac{T_m(T_m-T)(df/dT)_m}{T(1-f_m)} - \ln\left(\dfrac{1-f}{1-fm}\right)}$	(2.19a)	107%
	$\dfrac{E}{R} = \dfrac{n T_m^2 (df/dT)_m}{1-f_m}$	(2.19b)	
	$A = \dfrac{\beta\left(\dfrac{df}{dT}\right)_m}{(1-f_m)^n}\exp\left(\dfrac{E}{RT_m}\right)$	(2.19c)	
Reich and Stivala (1978)	$\ln\left[\dfrac{1-(1-f_1)^{1-n}}{1-(1-f_2)^{1-n}}\left(\dfrac{T_2}{T_1}\right)^2\right] = \dfrac{E}{R}\left(\dfrac{1}{T_2}-\dfrac{1}{T_1}\right);\ n \neq 1$	(2.20a)	98%
	$\ln\left[\dfrac{\ln(1-f_1)}{\ln(1-f_2)}\left(\dfrac{T_2}{T_1}\right)^2\right] = \dfrac{E}{R}\left(\dfrac{1}{T_2}-\dfrac{1}{T_1}\right);\ n = 1$	(2.20b)	
	$A = \dfrac{\beta\ EK}{(1-n)R};\ n \neq 1$	(2.20c)	
	where lnK is the intercept of the line:		
	$\ln\left[\dfrac{1-(1-f)^{1-n}}{T^2}\right]\ vs\ \dfrac{1}{T}$	(2.20d)	
Popescu and Segal (1983)	$E = R\dfrac{T_{0i}T_{0j}}{T_{0j}-T_{0i}}\ln\left[\left(\dfrac{\Delta T_i}{\Delta T_j}\right)^2\dfrac{\beta_1}{\beta_2}\right]$	(2.21a)	80%
	$\Delta T = T_1 - T_0$	(2.21b)	
	T_0 and T_1 are characteristic temperatures		
	$n = \dfrac{E}{R}\left(\dfrac{T_1-T_m}{T_m^2}\right)$	(2.21c)	
	$A = \dfrac{\beta\ E}{R(\Delta T)^2}\exp\left(\dfrac{E}{RT_0}\right)$	(2.21d)	

APPENDIX B GC Computer Station Method Parameters

```
********************************************************************************
Varian GC Star Workstation - Method Listing   Thu  Jan  05  17:15:06   1995
Method: C:\STAR\PHILIP\PHILIPC.MTH
********************************************************************************

*********************************
      ADC Board
*********************************
Module Address:    16
                          End Time    :   65.00 minutes
                  Autozero at Start   :   Yes
                    Channel  A Name   :   PID
                    Channel  B Name   :   FID
                Channel A Full Scale  :   10 VOLTS
                Channel A Full Scale  :   10 VOLTS

*********************************
      GC  3600
*********************************
Module Address : 17

GC Injector  A
Injector Type                              :  Isothermal
Initial GC Injector Temperature            :  220 degree C
Initial GC Injector Hold Time              :  0.00 minutes
GC Injector Oven On?                       :  Yes

GC Injector B
Injector Type                              :  Isothermal
Initial GC Injector Temperature            :  220 degree C
Initial GC Injector Hold Time              :  0.00 minutes
GC Injector Oven On?                       :  Yes

Coolant To Injector Value On?    :  No
Coolant Timeout                  :  INFINITE

GC Auxiliary
Injector Type                    :  Not used

GC Column
Column Oven On?                  :  Yes
Initial Column Temperate         :  40 degree C
Initial Column Hold Time         :  10.00 minutes
Thermal Stabilization Time       :  3.00 minutes

Coolant To Injector Value On?    :  No
Coolant Timeout                  :  INFINITE

GC Column Program 1
Final Temperature                :  120 degree C
Rate                             :  2.0 degrees C/minute
Hold Time                        :  15.00 minutes

GC Column A Parameters
Installed?                       :  Yes
Length                           :  30 meters
Diameter                         :  255 microns
Carrier Gas                      :  Helium
GC Column B Parameters
Installed?                       :  Yes
```

Length	:	30 meters
Diameter	:	255 microns
Carrier Gas	:	Helium

GC Detector Heater A

Detector Heater On?	:	Yes
Detector Temperature	:	300 degrees C

GC Detector Heater B

Detector Heater On?	:	Yes
Detector Temperature	:	250 degrees C

GC Detector A

Detector Type	:	PID
Detector On?	:	Yes
Attenuation	:	1
Detector Range	:	12
Autozero at GC Ready?	:	Yes

GC Detector B

Detector Type	:	FID
Detector On?	:	Yes
Attenuation	:	1
Detector Range	:	12
Autozero at GC Ready?	:	Yes

Autosampler

Autosampler Type	:	Not used

GC Relays

Relay Time Program	:	Do Not Use

GC Stripchart

Stripchart On?	:	No

****
ADC Board
****

Module Address : 16

Integration Parameters

Run Mode	:	Analysis
Multiplier	:	1.000000
Divisor	:	1.000000
Amount Standard	:	1.000000
Unidentified Peak Factor	:	0.000000
Measurement	:	Peak Area
Calculation	:	External Standard
Report Unidentified Peaks	:	NO
Subtract Blank Baseline	:	Yes
Peak Rejection Value	:	0 Counts
S/N Ratio	:	5
Tangent Height %	:	5%
Initial Peak Width	:	2 sec
Response factor Tolerance	:	Update All Response Factors
Minimum Reference Window	:	0.10 minutes
Percent Reference Window	:	2.0%
Minimum NonReference Window	:	0.10 minutes
Percent NonReference Window	:	2.0%
Unretained Peak Time	:	0.000 minutes

Peak Table

Name	Time	Factor	Amount	Ref.	Std.	RRT
C7	2.370	0.0028412	0.5700000	N	N	N
C10	12.350	0.0094076	0.6083000	N	N	N
C11	21.569	0.0098415	0.6175000	N	N	N
C12	27.979	0.0134153	0.6258000	N	N	N
C13	34.059	0.0128364	0.6308000	N	N	N
C14	40.075	0.0209216	0.6357000	N	N	N

TimeEvents Table

Group Event	:	0.01	until	4.73
Group Event	:	8.84	until	15.86
Group Event	:	19.17	until	23.97
Group Event	:	24.24	until	31.72
Group Event	:	32.11	until	36.01
Group Event	:	37.49	until	42.66
Inhibit Integrate	:	42.67	until	60.00

Report Format

Title	:	Standard Sample GC Analysis
Start Retention Time	:	0.00 minutes
End Retention Time	:	65.00 minutes
Initial Attenuation	:	32
Initial Zero Offset	:	0
Length in Pages	:	1
Initial Chart Speed	:	Off cm/min
Minutes per Tick	:	1.0
Autoscale	:	On
Time Events	:	Off
Chromatogram Events	:	Off
Retention Times	:	On
Peak Names	:	On
Baseline	:	Off
Units	:	mg
Number of Decimal Digits	:	4
Run Log	:	Off
Error Log	:	On
Notes	:	Off
ASCII File Convert	:	Off
Print Chromatogram	:	On
Print Results	:	On
Copies	:	1

Sample Information

Detector Bunch	:	8 points
Monitor Length	:	64 points
Data File Name	:	stan
Channel	:	FID 10 VOLTS

Blank Baseline

Baseline Compression Factor	:	128
Baseline Points	:	152
Baseline Bunch Size	:	8
Baseline Frequency	:	40.00 Hz

APPENDIX C Comparison of Equation 5.5 and Equation 5.6 Evaluated with Different Numbers of Terms of Integral $E_i(-E/RT)$

The accuracy of term V from Equation 5.6 was compared with that from Equation 5.6, using the kinetic parameters derived from CANMET pitch pyrolysis at 50 °C/min and 700 °C. The V term was integrated with Equation 5.5 and calculated with Equation 5.6, in which different numbers of terms of integral (Equation 5.7) were used. The results of V were plotted in Figure C.1. As can be seen that the V term calculated with 3 to 8 terms of integral (Equation 5.7) is very close to that from the integration of Equation 5.5. It is therefore reasonable to use 3 terms of integral to estimate Equation 5.6 and simplify the mathematical process of Equation 5.5, and the accuracy of V thus obtained will not significantly affected.

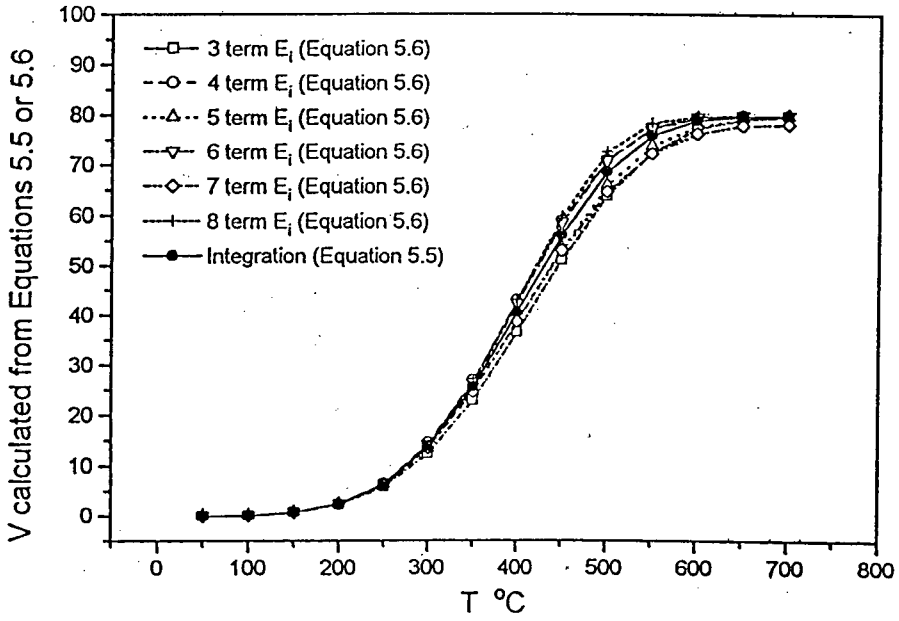

Figure C.1 Comparison of V evaluated for Equation 5.5 and Equation 5.6

APPENDIX D FORTRAN Programs and Calculation Results for TGA Experimental Results Modeling

Single Overall First Order Reaction Model Fitting Program

```
C     M       NO OF EXPERIMENTAL DATA POINTS
C     N       NO OF COEFFICIENTS FOR LINEAR REGRESSION
C     L1      NO OF DATA POINTS OMITTED AT THE BEGINNING OF DV/DT
C     L2      NO OF DATA POINTS OMITTED AT THE END OF DV/DT
C     M1L1    NO OF DATA POINTS OMITTED AT THE END OF DV/DT AFTER LI
C     R       GAS CONSTANT
C     VO      MAX VOLATILE AT CERTAIN HEATING RATE AND FINAL TEMPERATURE
C     C       HEATING RATE
C
C
C     FOLLOWING ARRAYS WITH 1 ARE THOSE WITH SOME END POINTS OMITTED
C     FROM EXPERIMENTAL DATA FOR DIFFERENT MODEL
C
C     V, V1       ARRAY OF EXPERIMENTAL VOLATILE CONTENTS
C     T           ARRAY OF TEMPERATURE IN C
C     X, X1       ARRAY OF 1/T IN 1/K
C     VD          ARRAY OF EXPERIMENTAL DV/DT
C
C     INTEGRAL METHOD
C     Y, Y1           ARRAY OF EXPERIMENTAL DATA
C     YFIT, YFIT1     ARRAY OF FITTED Y
C     A               ARRAY OF FITTED COEFFICIENTS
C     VFIT, VFIT1     ARRAY OF FITTED VOLATILE CONTENTS V
C
C     FRIEDMAN METHOD
C     XD      ARRAY OF X WITH END POINTS OMITTED
C     YD      ARRAY OF EXPERIMENTAL DATA
C     YDD     ARRAY OF YD WITH END POINTS OMITTED
C     YDDF    ARRAY OF FITTED YDD
C     AD      ARRAY OF FITTED COEFFICIENTS
C     VDD     ARRAY OF FITTED VOLATILE CONTENTS V
C
C     COATS-REDFERN METHOD
C     YCR, YCR1     ARRAY OF EXPERIMENTAL DATA
C     ACR           ARRAY OF FITTED COEFFICIENTS
C     YCRF,YCRF1    ARRAY OF FITTED YCR
C     VCR, VCR1     ARRAY OF FITTED VOLATILE CONTENTS V
C
C     CHEN-NUTTALL METHOD
C     YCN, YCN1      ARRAY OF EXPERIMENTAL DATA
C     ACN            ARRAY OF FITTED COEFFICIENTS
C     YCNF, YCNF1    ARRAY OF FITTED YCN
C     VCN, VCN1      ARRAY OF FITTED VOLATILE CONTENTS V
C
C


      IMPLICIT REAL*8(A-H,O-Z)
      PARAMETER (M=30,L1M1=3)
      EXTERNAL NOMIAL
      DIMENSION V(M),T(M),X(M),X1(M),VD(M),VD1(M),YD(M),
     1          Y(M),Y1(M),A(2),YFIT(M),YFIT1(M),VFIT(M),
     2          VFIT1(M),XD(M),AD(2),YDD(M),YDDF(M),VDD(M),
     3          XD1(M),YDD1(M),YDDF1(M),VDD1(M),
     4          YCR(M),YCRF(M),VCR(M),ACR(2),
     5          YCR1(M),YCRF1(M),VCR1(M),
     6          YCN(M),YCNF(M),VCN(M),ACN(2),
     7          YCN1(M),YCNF1(M),VCN1(M)
      DATA V/99.61D0,99.61D0,99.61D0,99.39D0,98.22D0,96.84D0,
```

```
     1       95.19D0,93.11D0,91.01D0,88.39D0,85.18D0,82.21D0,
     2       78.23D0,73.51D0,68.8D0,65.87D0,61.13D0,55.71D0,
     3       50.84D0,46.5D0,40.38D0,35.34D0,30.66D0,25.81D0,
     4       22.86D0,21.25D0,19.99D0,19.66D0,19.36D0,19.36D0/
      DATA T/0.D0,49.85D0,124.5D0,143.15D0,176.35D0,201.2D0,
     1       226.1D0,251.D0,275.D0,298.65D0,325.65D0,
     2       348.45D0,375.4D0,402.35D0,425.15D0,437.6D0,452.1D0,
     3       466.6D0,477.D0,485.3D0,495.65D0,503.95D0,512.25D0,
     4       524.7D0,537.1D0,549.55D0,576.5D0,601.4D0,676.05D0,700.D0/
      DATA MM,N,L1,L2,R,VO,C/2,2,2,2,8.314D0,80.66D0,50.D0/
      OPEN(UNIT = 3, FILE = 'FIT.DAT',
     1     ACCESS = 'SEQUENTIAL', STATUS = 'NEW')
      E=250.D3
      DO 10 I=1,M
      V(I)=100.D0-V(I)
      T(I)=T(I)+273.16D0
      X(I)=1.D0/T(I)
   10 CONTINUE
      DO 12 I=1+MM,M
      X1(I-MM)=X(I)
   12 CONTINUE
C
C     INTERGRAL METHOD
C
   20 EOLD=E
      DO 30 I=1,M
      Y(I)=DLOG(-C*DLOG(1.D0-V(I)/VO)/(R*T(I)*T(I)))
     1     -DLOG(1.D0-2.D0*R*T(I)/E)
   30 CONTINUE
      CALL FLSQP(X,Y,M,N,A,VAR)
      E=-A(2)*R
      IF(DABS(E-EOLD).LT.0.1D-4) THEN
      RA=EXP(A(1))*E
      GOTO 40
      ENDIF
      GOTO 20
   40 CONTINUE
      DO 60 I=1,M
      YFIT(I)=A(1)+A(2)*X(I)
      VFIT(I)=VO*(1.D0-EXP(-RA*R*T(I)*T(I)*EXP(-E/(R*T(I)))*(1.D0-
     1       2.D0*R*T(I)/E)/(C*E)))
   60 CONTINUE

      M1=M-MM
      E1=E
   62 EOLD=E1
      DO 64 I=1+MM,M
      Y1(I-MM)=DLOG(-C*DLOG(1.D0-V(I)/VO)/(R*T(I)*T(I)))
     1        -DLOG(1.D0-2.D0*R*T(I)/E1)
   64 CONTINUE
      CALL FLSQP(X1,Y1,M1,N,A,VAR)
      E1=-A(2)*R
      IF(DABS(E1-EOLD).GE.0.1D-4) GOTO 62
      RA1=EXP(A(1))*E1
      DO 66 I=1,M1
      YFIT1(I)=A(1)+A(2)*X1(I)
   66 CONTINUE
      DO 68 I=1,M
      VFIT1(I)=VO*(1.D0-EXP(-RA1*R*T(I)*T(I)*EXP(-E1/(R*T(I)))
     1      *(1.D0-2.D0*R*T(I)/E1)/(C*E1)))
   68 CONTINUE

C
```

```
C      FRIEDMAN METHOD
C
       MD=M-1
       DO 70 I=1,MD
       VD(I)=(V(I+1)-V(I))/(T(I+1)-T(I))
    70 CONTINUE
       VD(M)=VD(MD)
       DO 80 I=1+L1,M-L2
       YD(I)=DLOG(C/VO*VD(I))-DLOG(1.D0-V(I)/VO)
    80 CONTINUE
       ML=M-L1-L2
       DO 90 I=1,ML
       XD(I)=X(I+L1)
       YDD(I)=YD(I+L1)
    90 CONTINUE
       CALL FLSQP(XD,YDD,ML,N,AD,VARD)
       ED=-AD(2)*R
       RAD=EXP(AD(1))
       DO 100 I=1,ML
       YDDF(I)=AD(1)+AD(2)*XD(I)
   100 CONTINUE
       DO 110 I=1,M
       VDD(I)=VO*(1.D0-EXP(-RAD*R*T(I)*T(I)*EXP(-ED/(R*T(I)))*(1.D0-
      1        2.D0*R*T(I)/ED)/(C*ED)))
   110 CONTINUE
       ML1=ML-L1M1
       DO 112 I=1,ML1
       XD1(I)=XD(I)
       YDD1(I)=YDD(I)
   112 CONTINUE
       CALL FLSQP(XD1,YDD1,ML1,N,AD,VARD)
       ED1=-AD(2)*R
       RAD1=EXP(AD(1))
       DO 114 I=1,ML1
       YDDF1(I)=AD(1)+AD(2)*XD1(I)
   114 CONTINUE
       DO 116 I=1,M
       VDD1(I)=VO*(1.D0-EXP(-RAD1*R*T(I)*T(I)*EXP(-ED1/(R*T(I)))*
      1         (1.D0-2.D0*R*T(I)/ED1)/(C*ED1)))
   116 CONTINUE
C
C      COATS AND REDFERN METHOD
C
       DO 120 I=1,M
       YCR(I)=DLOG(-C*DLOG(1.D0-V(I)/VO)/(R*T(I)*T(I)))
   120 CONTINUE
       CALL    FLSQP(X,YCR,M,N,ACR,VAR)
       ECR=-R*ACR(2)
       RCR=ECR*EXP(ACR(1))
       DO 130 I=1,M
       YCRF(I)=ACR(1)+ACR(2)*X(I)
       VCR(I)=VO*(1.D0-EXP(-RCR*R*T(I)*T(I)*EXP(-ECR/(R*T(I)))*(1.D0-
      1       2.D0*R*T(I)/ECR)/(C*ECR)))
   130 CONTINUE
       DO 132 I=1+MM,M
       YCR1(I-MM)=DLOG(-C*DLOG(1.D0-V(I)/VO)/(R*T(I)*T(I)))
   132 CONTINUE
       CALL FLSQP(X1,YCR1,M1,N,ACR,VAR)
       ECR1=-R*ACR(2)
       RCR1=ECR1*EXP(ACR(1))
       DO 134 I=1,M1
       YCRF1(I)=ACR(1)+ACR(2)*X1(I)
   134 CONTINUE
```

```
      DO 136 I=1,M
      VCR1(I)=VO*(1.D0-EXP(-RCR1*R*T(I)*T(I)*EXP(-ECR1/(R*T(I)))
     1         *(1.D0-2.D0*R*T(I)/ECR1)/(C*ECR1)))
  136 CONTINUE
C
C     CHEN-NUTTAL METHOD
C
      ECN=E
  140 EOLD=ECN
      DO 150 I=1,M
      YCN(I)=DLOG(-C*(ECN+2.D0*R*T(I))*DLOG(1.D0-V(I)/VO)/(T(I)*T(I)*R))
  150 CONTINUE
      CALL  FLSQP(X,YCN,M,N,ACN,VAR)
      ECN=-R*ACN(2)
      IF(DABS(ECN-EOLD).GE.0.1D-4) GOTO 140
      RCN=EXP(ACN(1))
      DO 160 I=1,M
      YCNF(I)=ACN(1)+ACN(2)*X(I)
      VCN(I)=VO*(1.D0-EXP(-RCN*R*T(I)*T(I)*EXP(-ECN/(R*T(I)))*(1.D0-
     1        2.D0*R*T(I)/ECN)/(C*ECN)))
  160 CONTINUE
      ECN1=E1
  162 EOLD=ECN1
      DO 164 I=1+MM,M
      YCN1(I-MM)=DLOG(-C*(ECN1+2.D0*R*T(I))*DLOG(1.D0-V(I)/VO)/(T(I)*
     1         T(I)*R))
  164 CONTINUE
      CALL FLSQP(X1,YCN1,M1,N,ACN,VAR)
      ECN1=-R*ACN(2)
      IF(DABS(ECN1-EOLD).GE.0.1D-4)  GOTO 162
      RCN1=EXP(ACN(1))
      DO 166 I=1,M1
      YCNF1(I)=ACN(1)+ACN(2)*X1(I)
  166 CONTINUE
      DO 168 I=1,M
      VCN1(I)=VO*(1.D0-EXP(-RCN1*R*T(I)*T(I)*EXP(-ECN1/(R*T(I)))*
     1         (1.D0-2.D0*R*T(I)/ECN1)/(C*ECN1)))
  168 CONTINUE
C
      WRITE(3,200)
  200 FORMAT(4X,'T',8X,'V',8X,'VFIT',6X,'VDD',7X,'VCR',7X,'VCN',
     1       8X,'VD')
      DO 220 I=1,M
      WRITE(3,210) T(I),V(I),VFIT(I),VDD(I),VCR(I),VCN(I),VD(I)
  210 FORMAT(F7.2,6F10.6)
  220 CONTINUE
      WRITE(3,230)
  230 FORMAT(6X,'X',10X,'Y',8X,'YFIT',7X,'YCR',7X,'YCRF',8X,'YCN',
     1      7X,'YCNF')
      DO 250 I=M,1,-1
      WRITE(3,240) X(I),Y(I),YFIT(I),YCR(I),YCRF(I),YCN(I),YCNF(I)
  240 FORMAT(F10.5,6F11.6)
  250 CONTINUE

      WRITE(3,260)
  260 FORMAT(10X,'X',13X,'YDD',11X,'YDDF')
      DO 280 I=ML,1,-1
      WRITE(3,270) XD(I),YDD(I),YDDF(I)
  270 FORMAT(3F15.8)
  280 CONTINUE

      WRITE(3,290)
  290 FORMAT(35X,'A',14X,'E')
```

```
      WRITE(3,300) RA,E
  300 FORMAT('INTEGRAL METHOD',10X,2D15.3)
      WRITE(3,310)  RAD,ED
  310 FORMAT('FRIEDMAN METHOD',10X,2D15.3)
      WRITE(3,320)  RCR,ECR
  320 FORMAT('COATS-REDFERN METHOD',5X,2D15.3)
      WRITE(3,330)  RCN,ECN
  330 FORMAT('CHEN-NUTTALL METHOD',6X,2D15.3)
C
      WRITE(3,340)
  340 FORMAT(//'ANALYSIS WITHOUT THE ABNORMAL END DATA POINTS')
      WRITE(3,200)
      DO 350 I=1,M
      WRITE(3,210) T(I),V(I),VFIT1(I),VDD1(I),VCR1(I),VCN1(I),VD(I)
  350 CONTINUE
      WRITE(3,230)
      DO 360 I=M1,1,-1
      WRITE(3,240) X1(I),Y1(I),YFIT1(I),YCR1(I),YCRF1(I),YCN1(I),
     1             YCNF1(I)
  360 CONTINUE
      WRITE(3,260)
      DO 370 I=ML1,1,-1
      WRITE(3,270) XD1(I),YDD1(I),YDDF1(I)
  370 CONTINUE
      WRITE(3,290)
      WRITE(3,300) RA1,E1
      WRITE(3,310) RAD1,ED1
      WRITE(3,320) RCR1,ECR1
      WRITE(3,330) RCN1,ECN1

      ENDFILE(UNIT = 3)
      CLOSE(UNIT = 3)
      STOP
      END

      SUBROUTINE GAUSS(A,N,NDR,NDC,X,RNORM,IREEOR)
      IMPLICIT REAL*8(A-H,O-Z)
      DIMENSION A(NDR,NDC),X(N),B(50,51)
      NM=N-1
      NP=N+1

      DO 20 I=1,N
         DO 10 J=1,NP
         B(I,J)=A(I,J)
   10    CONTINUE
   20 CONTINUE

      DO 70 K=1,NM
         KP=K+1
         BIG=ABS(B(K,K))
         IPIVOT=K
         DO 30 I=KP,N
            AB=ABS(B(I,K))
            IF(AB.GT.BIG) THEN
              BIG=AB
              IPIVOT=I
            ENDIF
   30    CONTINUE
         IF(IPIVOT.NE.K) THEN
           DO 40 J=K,NP
            TEMP=B(IPIVOT,J)
            B(IPIVOT,J)=B(K,J)
            B(K,J)=TEMP
```

```
40      CONTINUE
      ENDIF
        IF(B(K,K).EQ.0.D0) THEN
          IERROR=2
          RETURN
        ENDIF
       DO 60 I=KP,N
        QUOT=B(I,K)/B(K,K)
        B(I,K)=0.D0
        DO 50 J=KP,NP
          B(I,J)=B(I,J)-QUOT*B(K,J)
50      CONTINUE
60     CONTINUE
70   CONTINUE
     IF(B(N,N).EQ.0.D0) THEN
       IERROR=2
       RETURN
     ENDIF
     X(N)=B(N,NP)/B(N,N)
     DO 90 I=NM,1,-1
       SUM=0.D0
       DO 80 J=I+1,N
          SUM=SUM+B(I,J)*X(J)
 80    CONTINUE
       X(I)=(B(I,NP)-SUM)/B(I,I)
 90  CONTINUE

     RSQ=0.D0
     DO 110 I=1,N
       SUM=0.D0
       DO 100 J=1,N
       SUM=SUM+A(I,J)*X(J)
100    CONTINUE
       RSQ=RSQ+(A(I,NP)-SUM)**2
110  CONTINUE
     RNORM=DSQRT(RSQ)
     IERROR=1
     RETURN
     END

     SUBROUTINE FLSQP(X,Y,M,N,A,VAR)
     IMPLICIT REAL*8(A-H,O-Z)
     DIMENSION X(M),U(51),Y(M),V(51),A(N),B(11),COEFF(10,11),SUMU(18)
     NP=N+1
     NM2=2*(N-1)
     XMIN=X(1)
     XMAX=X(1)
     YMIN=Y(1)
     YMAX=Y(1)
     DO 10 K=2,M
       XMIN=DMIN1(XMIN,X(K))
       XMAX=DMAX1(XMAX,X(K))
       YMIN=DMIN1(YMIN,Y(K))
       YMAX=DMAX1(YMAX,Y(K))
10   CONTINUE
     XP=XMIN+XMAX
     XM=XMAX-XMIN
     YP=YMIN+YMAX
     YM=YMAX-YMIN
     DO 20 K=1,M
       U(K)=(2.D0*X(K)-XP)/XM
       V(K)=(2.D0*Y(K)-YP)/YM
20   CONTINUE
```

```
      DO 30 L=1,NM2
        SUMU(L)=0.D0
30    CONTINUE
      DO 40 I=1,N
        COEFF(I,NP)=0.D0
40    CONTINUE
      DO 70 K=1,M
        TERMU=U(K)
        DO 50 L=1,NM2
          SUMU(L)=SUMU(L)+TERMU
          TERMU=TERMU*U(K)
50      CONTINUE
        TERMV=V(K)
        DO 60 I=1,N
          COEFF(I,NP)=COEFF(I,NP)+TERMV
          TERMV=TERMV*U(K)
60      CONTINUE
70    CONTINUE
      DO 90 I=1,N
        DO 80 J=1,N
          IF(I.EQ.1.AND.J.EQ.1) THEN
            COEFF(I,J)=M
          ELSE
            COEFF(I,J)=SUMU(I+J-2)
          ENDIF
80      CONTINUE
90    CONTINUE
      CALL GAUSS(COEFF,N,10,11,B,RNORM,IERROR)
      DO 110 I=1,N
        IM=I-1
        SUM=B(I)
        IF(I.NE.N) THEN
          DO 100 J=I+1,N
            SUM=SUM+NOMIAL(IM,J-1)*(-XP/XM)**(J-I)*B(J)
100       CONTINUE
        ENDIF
        A(I)=YM*(2.D0/XM)**IM*SUM/2.D0
110   CONTINUE
      A(1)=A(1)+YP/2.D0
      SSUM=0.D0
      DO 130 K=1,M
        SUM=A(1)
        TEMP=1.D0
        DO 120 J=2,N
          TEMP=TEMP*X(K)
          SUM=SUM+A(J)*TEMP
120     CONTINUE
        SSUM=SSUM+(Y(K)-SUM)**2
130   CONTINUE
      VAR=SSUM/(M-N)
      RETURN
      END
C
      FUNCTION NOMIAL(I,J)
      NOMIAL=1
      IF(J.LE.I.OR.I.EQ.0) RETURN
      DO 10 ICOUNT=1,I
        NOMIAL=NOMIAL*(J-ICOUNT+1)/ICOUNT
10    CONTINUE
      RETURN
      END
```

Fitting Results for Run#61 with Single Overall First Order Reaction Models

T	V	VFIT	VDD	VCR	VCN	VD
273.16	0.390000	0.001835	0.002088	0.002148	0.002148	0.000000
323.01	0.390000	0.023641	0.025793	0.023518	0.025587	0.000000
397.66	0.390000	0.345736	0.361193	0.290610	0.344936	0.011796
416.31	0.610000	0.585664	0.606667	0.476451	0.575114	0.035241
449.51	1.780000	1.348438	1.378113	1.042352	1.291552	0.055533
474.36	3.160000	2.335505	2.365809	1.747062	2.201061	0.066265
499.26	4.810000	3.831136	3.849982	2.785390	3.559491	0.083534
524.16	6.890000	5.980990	5.967688	4.245088	5.488858	0.087500
548.16	8.990000	8.805194	8.732291	6.133121	8.000267	0.110782
571.81	11.610000	12.411952	12.245013	8.524594	11.187995	0.118889
598.81	14.820000	17.595572	17.272655	11.962289	15.756300	0.130263
621.61	17.790000	22.839938	22.346199	15.476020	20.384440	0.147681
648.56	21.770000	29.925783	29.196143	20.332535	26.678746	0.175139
675.51	26.490000	37.688713	36.712478	25.870783	33.669396	0.206579
698.31	31.200000	44.476911	43.311675	30.979525	39.903756	0.235341
710.76	34.130000	48.156937	46.905714	33.886906	43.346999	0.326897
725.26	38.870000	52.337141	51.007448	37.339291	47.326756	0.373793
739.76	44.290000	56.333893	54.953606	40.825516	51.215466	0.468269
750.16	49.160000	59.050742	57.653200	43.324175	53.915945	0.522892
758.46	53.500000	61.113169	59.713761	45.305721	56.002775	0.591304
768.81	59.620000	63.538995	62.152120	47.748745	58.505153	0.607229
777.11	64.660000	65.358755	63.993571	49.676613	60.422057	0.563855
785.41	69.340000	67.061108	65.727472	51.569099	62.251570	0.389558
797.86	74.190000	69.387621	68.118229	54.327247	64.819982	0.237903
810.26	77.140000	71.430956	70.242956	56.960587	67.156536	0.129317
822.71	78.750000	73.211498	72.118937	59.473007	69.272460	0.046753
849.66	80.010000	76.196155	75.337198	64.396759	73.063267	0.013253
874.56	80.340000	78.041713	77.401913	68.261742	75.662338	0.004019
949.21	80.640000	80.292291	80.117552	75.953570	79.566076	0.000000
973.16	80.640000	80.485864	80.384632	77.371350	80.041927	0.000000

X	Y	YFIT	YCR	YCRF	YCN	YCNF
0.00103	-9.179704	-9.481708	-9.850486	-10.057252	0.931758	0.694442
0.00105	-9.153117	-9.584969	-9.800649	-10.153178	0.973291	0.594723
0.00114	-9.464879	-9.943113	-10.043230	-10.485878	0.704377	0.248866
0.00118	-9.566304	-10.076571	-10.122604	-10.609854	0.616063	0.119986
0.00122	-9.778232	-10.230119	-10.311201	-10.752494	0.417698	-0.028295
0.00123	-9.936654	-10.304503	-10.459026	-10.821594	0.265328	-0.100127
0.00125	-10.132381	-10.380896	-10.644309	-10.892559	0.075499	-0.173899
0.00127	-10.361963	-10.460023	-10.863514	-10.966065	-0.148292	-0.250311
0.00129	-10.541413	-10.514183	-11.036105	-11.016377	-0.323952	-0.302613
0.00130	-10.712212	-10.569512	-11.200091	-11.067776	-0.491018	-0.356045
0.00132	-10.904251	-10.640204	-11.383700	-11.133445	-0.678478	-0.424311
0.00133	-11.035355	-10.698303	-11.508095	-11.187417	-0.805974	-0.480417
0.00135	-11.181704	-10.772943	-11.646099	-11.256753	-0.947876	-0.552496
0.00138	-11.345282	-10.880580	-11.798158	-11.356744	-1.105396	-0.656441
0.00141	-11.494671	-10.992609	-11.936160	-11.460814	-1.248887	-0.764627
0.00143	-11.586662	-11.092512	-12.018476	-11.553619	-1.335942	-0.861103
0.00148	-11.743532	-11.285013	-12.157867	-11.732445	-1.484068	-1.047000
0.00154	-11.917910	-11.530008	-12.311971	-11.960034	-1.648598	-1.283590
0.00161	-12.085959	-11.796246	-12.460149	-12.207358	-1.807311	-1.540695
0.00167	-12.232599	-12.040200	-12.590281	-12.433980	-1.946443	-1.776279
0.00175	-12.426729	-12.354252	-12.765208	-12.725721	-2.132134	-2.079558
0.00182	-12.632724	-12.654757	-12.954679	-13.004877	-2.331130	-2.369754
0.00191	-12.839908	-12.987432	-13.145370	-13.313918	-2.531581	-2.691016
0.00200	-13.132499	-13.366387	-13.421133	-13.665951	-2.817570	-3.056972
0.00211	-13.477522	-13.785127	-13.749606	-14.054942	-3.156376	-3.461346
0.00222	-13.968892	-14.249277	-14.224727	-14.486117	-3.641916	-3.909573
0.00240	-14.914993	-14.955857	-15.149524	-15.142499	-4.580806	-4.591914
0.00251	-15.283782	-15.404530	-15.506541	-15.559297	-4.945827	-5.025195

X	YDD	YDDF
0.00123417	0.60807557	0.04009520
0.00125335	0.60895559	-0.03490237
0.00127322	0.54271001	-0.11258481
0.00128682	0.56647688	-0.16575592
0.00130071	0.36674818	-0.22007510
0.00131846	0.08485328	-0.28947602
0.00133305	-0.18634571	-0.34651452
0.00135179	-0.44043312	-0.41979110
0.00137882	-0.80468691	-0.52546313
0.00140694	-1.04618577	-0.63544672
0.00143203	-1.43585946	-0.73352542
0.00148036	-1.65717687	-0.92251219
0.00154188	-1.90582279	-1.16303342
0.00160873	-2.14174758	-1.42441033
0.00166998	-2.31340313	-1.66390972
0.00174883	-2.45237380	-1.97222821
0.00182428	-2.56023804	-2.26724630
0.00190781	-2.82504563	-2.59384664
0.00200296	-2.89923461	-2.96588292
0.00210810	-3.15234745	-3.37697689
0.00222464	-3.34667896	-3.83265228
0.00240206	-3.81617456	-4.52633118
0.00251471	-4.91334683	-4.96681167

	A	E
INTEGRAL METHOD	0.151D+03	0.331D+05
FRIEDMAN METHOD	0.130D+03	0.325D+05
COATS-REDFERN METHOD	0.591D+02	0.308D+05
CHEN-NUTTALL METHOD	0.104D+03	0.320D+05

Anthony-Howard Model FORTRAN Program with L-M Nonlinear Regression

```
C
C
      INTEGER NDATA,MA,MFIT,NCA
      PARAMETER(NDATA=30,MA=3,MFIT=3,NCA=3)
      DOUBLE PRECISION X(NDATA),Y(NDATA),A(MA),SIG(NDATA),AF,BF,YF,
     1     COVAR(NCA,NCA),ALPHA(NCA,NCA),CHISQ,ALAMDA,YFIT(NDATA),T,
     2     EO,S,Z
      COMMON /ZDATA/T,EO,S,Z
      EXTERNAL MRQMIN,MRQCOF,GAUSSJ,COVSRT,FUNCS,FUNC0,FUNC1,
     1         FUNC2,FUNC3,QROMB,TRAPZD,POLINT
      INTEGER LISTA(MA)
      DATA LISTA/1,2,3/
      DATA SIG/12*1.D-1,6*1.D-5,12*1.D-1/
      DATA A/115000.D0,15000.D0,500000000.0D0/
C     DATA FOR RUN 61:CAN61.DAT X=T (C) + 273.16 K
      DATA X/273.16D0,323.01D0,397.66D0,416.31D0,449.51D0,474.36D0,
     1       499.26D0,524.16D0,548.16D0,571.81D0,598.81D0,621.61D0,
     2       648.56D0,675.51D0,689.31D0,710.76D0,725.26D0,739.76D0,
     3       750.16D0,758.46D0,768.81D0,777.11D0,785.41D0,797.86D0,
     4       810.26D0,822.71D0,849.66D0,874.56D0,949.21D0,973.16D0/
      DATA Y/ 0.39D0, 0.39D0, 0.39D0, 0.61D0, 1.78D0, 3.16D0, 4.81D0,
     1        6.89D0, 8.99D0,11.61D0,14.82D0,17.79D0,21.77D0,26.49D0,
     2       31.20D0,34.13D0,38.87D0,44.29D0,49.16D0,53.50D0,59.62D0,
     3       64.66D0,69.34D0,74.19D0,77.14D0,78.75D0,80.01D0,80.34D0,
     4       80.64D0,80.64D0/
      OPEN(UNIT=3,FILE='SLM61.DAT',ACCESS='SEQUENTIAL',
     1     STATUS='OLD')
      DO 10 I=1,NDATA
      X(I)=X(I)-273.16D0
   10 CONTINUE
      ALAMDA=-0.001D0
      CALL MRQMIN(X,Y,SIG,NDATA,A,MA,LISTA,MFIT,COVAR,
     1            ALPHA,NCA,CHISQ,FUNCS,ALAMDA)
      WRITE(3,100) A
  100 FORMAT(5X,3F20.6)
      VSTAR=Y(NDATA)
      AF=A(1)-4.D0*A(2)
      BF=A(1)+4.D0*A(2)
      EO=A(1)
      S=A(2)
      Z=A(3)
      DO 200 I=1,NDATA
      T=X(I)+273.16D0
      CALL  QROMB(FUNC0,AF,BF,YF)
      YFIT(I)=VSTAR*(1.D0-YF/(2.506628D0*A(2)))
  200 CONTINUE
      DO 400 I=1,NDATA
      WRITE(3,300) X(I),Y(I),YFIT(I)
  300 FORMAT(5X,3F20.5)
  400 CONTINUE
      ENDFILE(UNIT=3)
      CLOSE(UNIT=3)
      STOP
      END

      SUBROUTINE MRQMIN(X,Y,SIG,NDATA,A,MA,LISTA,MFIT,
     *        COVAR,ALPHA,NCA,CHISQ,FUNCS,ALAMDA)
      INTEGER MMAX,MA,MFIT,NCA,KK,K,J,IHIT
      PARAMETER (MMAX=20)
      INTEGER LISTA(MA)
      DOUBLE PRECISION X(NDATA),Y(NDATA),SIG(NDATA),A(MA),ALAMDA,CHISQ,
     *      COVAR(NCA,NCA),ALPHA(NCA,NCA),ATRY(MMAX),BETA(MMAX),DA(MMAX),
```

```
     *      OCHISQ
      EXTERNAL FUNCS
      IF(ALAMDA.LT.0.D0) THEN
        KK=MFIT+1
        DO 12 J=1,MA
          IHIT=0
          DO 11 K=1,MFIT
            IF(LISTA(K).EQ.J)IHIT=IHIT+1
 11       CONTINUE
          IF (IHIT.EQ.0) THEN
            LISTA(KK)=J
            KK=KK+1
          ELSE IF (IHIT.GT.1) THEN
            PAUSE 'Improper permutation in LISTA'
          ENDIF
 12     CONTINUE
        IF (KK.NE.(MA+1)) PAUSE 'Improper permutation in LISTA'
        ALAMDA=0.001D0
        CALL MRQCOF(X,Y,SIG,NDATA,A,MA,LISTA,MFIT,ALPHA,BETA,NCA,CHISQ,F
     * UNCS)
        OCHISQ=CHISQ
        DO 13 J=1,MA
          ATRY(J)=A(J)
 13     CONTINUE
      ENDIF
 100  DO 15 J=1,MFIT
        DO 14 K=1,MFIT
          COVAR(J,K)=ALPHA(J,K)
 14     CONTINUE
      COVAR(J,J)=ALPHA(J,J)*(1.D0+ALAMDA)
        DA(J)=BETA(J)
 15   CONTINUE
      CALL GAUSSJ(COVAR,MFIT,NCA,DA,1,1)
      IF(ALAMDA.EQ.0.D0)THEN
        CALL COVSRT(COVAR,NCA,MA,LISTA,MFIT)
        RETURN
      ENDIF
      DO 16 J=1,MFIT
C       WRITE(3,*) 'DA(',J,')=',DA(J)
      IF((DABS(DA(1))+DABS(DA(2))+DABS(DA(3))).LT.1.D1) THEN
      ATRY(LISTA(J))=A(LISTA(J))+DA(J)
      ELSE
      ATRY(LISTA(J))=A(LISTA(J))+DA(J)*1.0D-60
      ENDIF
 16   CONTINUE
      IF((DABS(DA(1))+DABS(DA(2))+DABS(DA(3))).LT.1.D-250) RETURN
      CALL MRQCOF(X,Y,SIG,NDATA,ATRY,MA,LISTA,MFIT,COVAR,DA,NCA,CHISQ,
     *          FUNCS)
C     IF((DABS(CHISQ-OCHISQ)/CHISQ).LT.1D-3) RETURN
      IF(CHISQ.LT.OCHISQ) THEN
      ALAMDA=0.1D0*ALAMDA
        OCHISQ=CHISQ
        DO 18 J=1,MFIT
          DO 17 K=1,MFIT
            ALPHA(J,K)=COVAR(J,K)
 17       CONTINUE
          BETA(J)=DA(J)
          A(LISTA(J))=ATRY(LISTA(J))
 18     CONTINUE
      ELSE
        ALAMDA=10.D0*ALAMDA
        CHISQ=OCHISQ
        DO 180 J=1,MFIT
```

```
          DO 170 K=1,MFIT
            ALPHA(J,K)=COVAR(J,K)
  170       CONTINUE
          BETA(J)=DA(J)
          A(LISTA(J))=ATRY(LISTA(J))
  180     CONTINUE
        ENDIF
C       WRITE(*,*) 'CHISQ=',CHISQ,'  OCHISQ=',OCHISQ
C       WRITE(*,*) A
        GOTO 100
        RETURN
        END

        SUBROUTINE MRQCOF(X,Y,SIG,NDATA,A,MA,LISTA,MFIT,ALPHA,BETA,NALP,
       * CHISQ,FUNCS)
        INTEGER NDATA,MA,MFIT,NALP,I,J,K,MMAX
        PARAMETER (MMAX=3)
        INTEGER LISTA(MFIT)
        DOUBLE PRECISION X(NDATA),Y(NDATA),SIG(NDATA),ALPHA(NALP,NALP),
       * BETA(MA),DYDA(3),A(3),XI,DY,SIG2I,WT,CHISQ
        DO 12 J=1,MFIT
          DO 11 K=1,J
          ALPHA(J,K)=0.D0
  11      CONTINUE
        BETA(J)=0.D0
  12    CONTINUE
        CHISQ=0.D0
        DO 15 I=1,NDATA
          XI=X(I)
          CALL FUNCS(XI,A,YMOD,DYDA,3)
        SIG2I=1.D0/(SIG(I)*SIG(I))
        DY=Y(I)-YMOD
          DO 14 J=1,MFIT
            WT=DYDA(LISTA(J))*SIG2I
            DO 13 K=1,J
              ALPHA(J,K)=ALPHA(J,K)+WT*DYDA(LISTA(K))
  13        CONTINUE
            BETA(J)=BETA(J)+DY*WT
  14      CONTINUE
          CHISQ=CHISQ+DY*DY*SIG2I
  15    CONTINUE
        DO 17 J=2,MFIT
          DO 16 K=1,J-1
            ALPHA(K,J)=ALPHA(J,K)
  16      CONTINUE
  17    CONTINUE
        RETURN
        END
C
        SUBROUTINE GAUSSJ(A,N,NP,B,M,MP)
        INTEGER NMAX,N,NP,M,MP,I,J,K,IROW,ICOL,L,LL
        PARAMETER (NMAX=50)
        INTEGER     IPIV(NMAX),INDXR(NMAX),INDXC(NMAX)
        DOUBLE PRECISION A(NP,NP),B(NP,MP),DUM,BIG,PIVINV
        DO 11 J=1,N
          IPIV(J)=0
  11    CONTINUE
        DO 22 I=1,N
        BIG=0.D0
          DO 13 J=1,N
            IF(IPIV(J).NE.1)THEN
              DO 12 K=1,N
                IF (IPIV(K).EQ.0) THEN
```

```
                IF (ABS(A(J,K)).GE.BIG)THEN
                  BIG=ABS(A(J,K))
                  IROW=J
                  ICOL=K
                ENDIF
              ELSE IF (IPIV(K).GT.1) THEN
                PAUSE 'Singular matrix'
              ENDIF
12          CONTINUE
          ENDIF
13      CONTINUE
        IPIV(ICOL)=IPIV(ICOL)+1
        IF (IROW.NE.ICOL) THEN
          DO 14 L=1,N
            DUM=A(IROW,L)
            A(IROW,L)=A(ICOL,L)
            A(ICOL,L)=DUM
14        CONTINUE
          DO 15 L=1,M
            DUM=B(IROW,L)
            B(IROW,L)=B(ICOL,L)
            B(ICOL,L)=DUM
15        CONTINUE
        ENDIF
        INDXR(I)=IROW
        INDXC(I)=ICOL
        IF (A(ICOL,ICOL).EQ.0.D0) PAUSE 'Singular matrix.'
        PIVINV=1./A(ICOL,ICOL)
        A(ICOL,ICOL)=1.
        DO 16 L=1,N
          A(ICOL,L)=A(ICOL,L)*PIVINV
16      CONTINUE
        DO 17 L=1,M
          B(ICOL,L)=B(ICOL,L)*PIVINV
17      CONTINUE
        DO 21 LL=1,N
          IF(LL.NE.ICOL)THEN
            DUM=A(LL,ICOL)
            A(LL,ICOL)=0.D0
            DO 18 L=1,N
              A(LL,L)=A(LL,L)-A(ICOL,L)*DUM
18          CONTINUE
            DO 19 L=1,M
              B(LL,L)=B(LL,L)-B(ICOL,L)*DUM
19          CONTINUE
          ENDIF
21      CONTINUE
22    CONTINUE
      DO 24 L=N,1,-1
        IF(INDXR(L).NE.INDXC(L))THEN
          DO 23 K=1,N
            DUM=A(K,INDXR(L))
            A(K,INDXR(L))=A(K,INDXC(L))
            A(K,INDXC(L))=DUM
23        CONTINUE
        ENDIF
24    CONTINUE
      RETURN
      END
C
      SUBROUTINE COVSRT(COVAR,NCVM,MA,LISTA,MFIT)
      INTEGER NCVM,MA,LISTA,MFIT,I,J
      INTEGER LISTA(MFIT)
```

```
      DOUBLE PRECISION COVAR(NCVM,NCVM),SWAP
      DO 12 J=1,MA-1
        DO 11 I=J+1,MA
        COVAR(I,J)=0.D0
 11     CONTINUE
 12   CONTINUE
      DO 14 I=1,MFIT-1
        DO 13 J=I+1,MFIT
          IF(LISTA(J).GT.LISTA(I)) THEN
            COVAR(LISTA(J),LISTA(I))=COVAR(I,J)
          ELSE
            COVAR(LISTA(I),LISTA(J))=COVAR(I,J)
          ENDIF
 13     CONTINUE
 14   CONTINUE
      SWAP=COVAR(1,1)
      DO 15 J=1,MA
        COVAR(1,J)=COVAR(J,J)
      COVAR(J,J)=0.D0
 15   CONTINUE
      COVAR(LISTA(1),LISTA(1))=SWAP
      DO 16 J=2,MFIT
        COVAR(LISTA(J),LISTA(J))=COVAR(1,J)
 16   CONTINUE
      DO 18 J=2,MA
        DO 17 I=1,J-1
          COVAR(I,J)=COVAR(J,I)
 17     CONTINUE
 18   CONTINUE
      RETURN
      END
C
      SUBROUTINE FUNCS(XX,A,Y,DYDA,NA)
      INTEGER NA,NAA
      DOUBLE PRECISION  A(3),DYDA(3),XX,Y,T,EO,S,Z,VSTAR,YY,AA,BB,
     *                  Y1,Y2,Y3
      EXTERNAL     FUNC0,FUNC1,FUNC2,FUNC3,QROMB,POLINT,TRAPZD
      COMMON  /ZDATA/T,EO,S,Z
      NAA=NA
      VSTAR=80.64D0
      R=8.314D0
      B=50.0D0
      AA=A(1)-4.D0*A(2)
      BB=A(1)+4.D0*A(2)
      EO=A(1)
      S=A(2)
      Z=A(3)
      T=XX+273.13D0
      CALL QROMB(FUNC0,AA,BB,Y)
      YY=Y
      Y=VSTAR*(1.D0-YY/(2.506628D0*S))
      CALL QROMB(FUNC1,AA,BB,Y1)
      DYDA(1)=Y1+DEXP(-Z*R*T**2/(B*(EO+4.D0*S))*DEXP(-(EO+4.D0*S)/(R*T)
     *            )*(1.D0-2.D0*R*T/(EO+4.D0*S)))*DEXP(-8.D0)-DEXP(-Z*R*T**2
     *            /(B*(EO-4.D0*S))*DEXP(-(EO-4.D0*S)/(R*T))*(1.D0-2.D0*R*T/
     *            (EO-4.D0*S)))*DEXP(-8.D0)
      DYDA(1)=-DYDA(1)*VSTAR/(2.506628D0*S)
      CALL QROMB(FUNC2,AA,BB,Y2)
      DYDA(2)=Y2+4.D0*DEXP(-Z*R*T**2/(B*(EO+4.D0*S))*DEXP(-(EO+4.D0*S)/
     *            (R*T))*(1.D0-2.D0*R*T/(EO+4.D0*S)))*DEXP(-8.D0)+4.D0*DEXP
     *            (-Z*R*T**2/(B*(EO-4.D0*S))*DEXP(-(EO-4.D0*S)/(R*T))*(1.D0
     *            -2.D0*R*T/(EO-4.D0*S)))*DEXP(-8.D0)
      DYDA(2)=-VSTAR*(YY/S-DYDA(2))/(2.506628D0*S)
```

```
      CALL QROMB(FUNC3,AA,BB,Y3)
      DYDA(3)=-Y3*VSTAR/(2.506628D0*S)
      RETURN
      END

      SUBROUTINE QROMB(FUNC,A,B,SS)
      INTEGER JMAX,JMAXP,J,K,KM,L
      DOUBLE PRECISION EPS,A,B,SS,DSS
      PARAMETER(EPS=5.D-3,JMAX=500,JMAXP=JMAX+1,K=5,KM=4)
      DOUBLE PRECISION S(JMAXP),H(JMAXP)
      EXTERNAL FUNC
      H(1)=1.
      DO 11 J=1,JMAX
        CALL TRAPZD(FUNC,A,B,S(J),J)
        IF (J.GE.K) THEN
          L=J-KM
        CALL POLINT(H(L),S(L),K,0.D0,SS,DSS)
        IF (DABS(DSS).LT.EPS*DABS(SS)) RETURN
        ENDIF
        S(J+1)=S(J)
      H(J+1)=0.25D0*H(J)
 11   CONTINUE
      PAUSE 'Too many steps.'
      END
C
      SUBROUTINE TRAPZD(FUNC,A,B,S,N)
      INTEGER N,IT,J
      DOUBLE PRECISION A,B,S,DEL,TNM,SUM,X
      IF (N.EQ.1) THEN
        S=0.5D0*(B-A)*(FUNC(A)+FUNC(B))
        IT=1
      ELSE
        TNM=IT
        DEL=(B-A)/TNM
      X=A+0.5D0*DEL
      SUM=0.D0
        DO 11 J=1,IT
          SUM=SUM+FUNC(X)
          X=X+DEL
 11     CONTINUE
      S=0.5D0*(S+(B-A)*SUM/TNM)
        IT=2*IT
      ENDIF
      RETURN
      END
C
      SUBROUTINE POLINT(XA,YA,N,X,Y,DY)
      INTEGER I,M,N,NS,NMAX
      PARAMETER (NMAX=10)
      DOUBLE PRECISION XA(N),YA(N),C(NMAX),D(NMAX),X,Y,DY,DIFT,HO,HP,W,
     *           DEN
      NS=1
      DIF=DABS(X-XA(1))
      DO 11 I=1,N
      DIFT=DABS(X-XA(I))
        IF (DIFT.LT.DIF) THEN
          NS=I
          DIF=DIFT
        ENDIF
        C(I)=YA(I)
        D(I)=YA(I)
 11   CONTINUE
      Y=YA(NS)
```

```
      NS=NS-1
      DO 13 M=1,N-1
        DO 12 I=1,N-M
          HO=XA(I)-X
          HP=XA(I+M)-X
          W=C(I+1)-D(I)
          DEN=HO-HP
          IF(DEN.EQ.0.D0)PAUSE
          DEN=W/DEN
          D(I)=HP*DEN
          C(I)=HO*DEN
   12     CONTINUE
          IF (2*NS.LT.N-M)THEN
            DY=C(NS+1)
          ELSE
            DY=D(NS)
            NS=NS-1
          ENDIF
          Y=Y+DY
   13   CONTINUE
        RETURN
        END
C
        DOUBLE PRECISION FUNCTION      FUNC0(E)
        DOUBLE PRECISION T,EO,S,Z,E
        COMMON/ZDATA/T,EO,S,Z
        R=8.314D0
        B=50.0D0
        FUNC0=DEXP(-Z*R*T**2/(B*E)*DEXP(-E/(R*T))*(1.D0-2.D0*R*T/E))
       1          *DEXP(-0.5D0*((E-EO)/S)**2)
        RETURN
        END
C
        DOUBLE PRECISION FUNCTION FUNC1(E)
        DOUBLE PRECISION T,EO,S,Z,E
        COMMON /ZDATA/T,EO,S,Z
        R=8.314D0
        B=50.0D0
        FUNC1=DEXP(-Z*R*T**2/(B*E)*DEXP(-E/(R*T))*(1.D0-2.D0*R*T/E))
       1           *DEXP(-0.5D0*((E-EO)/S)**2)*(E-EO)/S**2
        RETURN
        END
C
        DOUBLE PRECISION FUNCTION      FUNC2(E)
        DOUBLE PRECISION T,EO,S,Z,E
        COMMON /ZDATA/T,EO,S,Z
        R=8.314D0
        B=50.0D0
        FUNC2=DEXP(-Z*R*T**2/(B*E)*DEXP(-E/(R*T))*(1.D0-2.D0*R*T/E))*
       1           DEXP(-0.5D0*((E-EO)/S)**2)*(E-EO)**2/S**3
        RETURN
        END
C
        DOUBLE PRECISION FUNCTION      FUNC3(E)
        DOUBLE PRECISION T,EO,S,Z,E
        COMMON /ZDATA/T,EO,S,Z
        R=8.314D0
        B=50.0D0
        FUNC3=DEXP(-Z*R*T**2/(B*E)*DEXP(-E/(R*T))*(1.D0-2.D0*R*T/E))*(-R
       *       *T**2/(B*E))*DEXP(-E/(R*T))*(1.D0-2.D0*R*T/E)*DEXP(-0.5D0*((E-
       *       EO)/S)**2)
        RETURN
        END
```

Fitting Result with Anthony-Howard Model for RUN#61

E J/mol	s J/mol	k s^{-1}
114999.999951	14999.998064	500000004.536339

T °C	V_{exp}	V_{mod}
.00000	.39000	-.00868
49.85000	.39000	-.00783
124.50000	.39000	.04946
143.15000	.61000	.10393
176.35000	1.78000	.34987
201.20000	3.16000	.82673
226.10000	4.81000	1.69501
251.00000	6.89000	3.04457
275.00000	8.99000	5.27093
298.65000	11.61000	8.66743
325.65000	14.82000	13.68217
348.45000	17.79000	18.60192
375.40000	21.77000	26.42453
402.35000	26.49000	36.10305
416.15000	31.20000	41.01006
437.60000	34.13000	47.87946
452.10000	38.87000	52.29991
466.60000	44.29000	56.74668
477.00000	49.16000	59.87655
485.30000	53.50000	62.26663
495.65000	59.62000	65.02800
503.95000	64.66000	67.00712
512.25000	69.34000	68.74093
524.70000	74.19000	70.88771
537.10000	77.14000	72.60551
549.55000	78.75000	74.08491
576.50000	80.01000	76.79565
601.40000	80.34000	78.57816
676.05000	80.64000	80.37077
700.00000	80.64000	80.52666

APPENDIX E FORTRAN Program for Two-Stage First Order Reaction Model

```
C     Original experimental data:
C     V(M)     Experimental volatile content %
C     VD(M)    Experimental dV/dT,VD(I)=(V(I+1)-V(I))/(T(I+1)-T(I))
C     T(M)     Experimental temperature
C     X(M)     1/T(M) in K
C     M        No. of experimental data points
C     LN       No. of experimental data points omitted at the beginning for
C              fitting
C
C     VF       Fitting results in the entire temperature range
C
C     First reaction fitting parameters (Section below temperature 450 oC)
C     N        No. of first reaction data points
C     V1(N)    Experimental volatile content %
C     VD1(N)   Experimental dV/dT
C     T1(N)    Experimental temperature
C     X1(N)    1/T1(N)
C     A1(2)    Fitting array used in FLSQP subroutine for first reaction
C     Y1(N)    Fitting parameter derived from V1(N) using relative method
C     Y1F(N)   Fitted value for Y1(N) using relative method
C     V1F(N)   Fitted volatile using relative method
C
C     First reaction fitting parameters (Section below temperature 450 oC)
C     MN       No. of second reaction data points
C     V2(MN)   Experimental volatile content %
C     VD2(MN)  Experimental dV/dT
C     T2(MN)   Experimental temperature
C     X2(MN)   1/T2(MN)
C     A2(2)    Fitting array used in FLSQP subroutine for second reaction
C     Y2(MN)   Fitting parameter derived from V2(MN) using relative method
C     Y2F(MN)  Fitted value for Y2(MN) using relative method
C     V2F(MN)  Fitted volatile using relative method
C
C     Subscript for each method
C
C     NT       Integral method
C     CR       Coats-Redfern method
C     CN       Chen-Nuttall method
C     FM       Friedman method
C
      IMPLICIT REAL*8(A-H,O-Z)
      PARAMETER (M=37,N=14,MN=14,LN=4)
      EXTERNAL NOMIAL
      DIMENSION V(M),T(M),X(M),A1(2),A2(2),VD(M)
      DIMENSION V1(N),T1(N),X1(N),V2(MN),T2(MN),X2(MN),VD1(N),VD2(MN),
     1 Y1NT(N),Y1FNT(N),V1FNT(N),Y2NT(MN),Y2FNT(MN),V2FNT(MN),VFNT(M),
     2 Y1CR(N),Y1FCR(N),V1FCR(N),Y2CR(MN),Y2FCR(MN),V2FCR(MN),VFCR(M),
     3 Y1CN(N),Y1FCN(N),V1FCN(N),Y2CN(MN),Y2FCN(MN),V2FCN(MN),VFCN(M),
     4 Y1FM(N),Y1FFM(N),V1FFM(N),Y2FM(MN),Y2FFM(MN),V2FFM(MN),VFFM(M)
      DIMENSION VDNT(M),VDCR(M),VDCN(M),VDFM(M)
C     canmet pitch 25 oC/min and 800 oC
       DATA   V/99.96D0,99.94D0,99.50D0,98.98D0,97.83D0,96.14D0,94.43D0,
     1  92.41D0,90.17D0,87.92D0,85.52D0,82.67D0,81.30D0,79.35D0,77.45D0,
     2  74.91D0,72.41D0,69.25D0,65.96D0,62.65D0,59.69D0,56.33D0,51.74D0,
     3  46.48D0,41.57D0,36.49D0,32.58D0,28.48D0,25.14D0,22.84D0,21.38D0,
     4  20.30D0,19.97D0,19.71D0,19.48D0,19.28D0,19.16D0/
      DATA     T/ 50.22D0,100.32D0,135.40D0,153.77D0,175.47D0,200.52D0,
     1  225.60D0,250.65D0,275.70D0,300.75D0,325.80D0,350.85D0,362.55D0,
     2  375.90D0,387.60D0,400.95D0,414.32D0,426.00D0,437.70D0,447.72D0,
     3  456.07D0,464.42D0,474.45D0,484.45D0,492.80D0,500.00D0,507.85D0,
     4  516.20D0,526.22D0,537.90D0,551.27D0,576.32D0,601.37D0,649.80D0,
```

```
     5  699.90D0,750.00D0,800.12D0/
      DATA R,VO,C/8.314D0,80.84D0,25.D0/
      OPEN(UNIT = 3, FILE = 'FIT2RN1.DAT',
     1     ACCESS = 'SEQUENTIAL', STATUS = 'OLD')

      E1=250.D3

      DO 10 I=1,M
      V(I)=100.D0-V(I)
      T(I)=T(I)+273.16D0
      X(I)=1.D0/T(I)
   10 CONTINUE

      DO 20 I=1,N
      V1(I)=V(LN+I)
      T1(I)=T(LN+I)
      X1(I)=X(LN+I)
   20 CONTINUE

      DO 30 I=1,MN
      V2(I)=V(LN+N+I)
      T2(I)=T(LN+N+I)
      X2(I)=X(LN+N+I)
   30 CONTINUE
C
C     INTERGRAL METHOD
C
C            First reaction
C
   40 E1OLD=E1
      DO 50 I=1,N
      Y1NT(I)=DLOG(-C*DLOG(1.D0-V1(I)/VO)/(R*T1(I)*T1(I)))
     1     -DLOG(1.D0-2.D0*R*T1(I)/E1)
   50 CONTINUE
      CALL FLSQP(X1,Y1NT,N,2,A1,VAR)
      E1=-A1(2)*R
      IF(DABS(E1-E1OLD).LT.1.0D-8) THEN
      RK1=EXP(A1(1))*E1
      VAR1=VAR
      GOTO 60
      ENDIF
      GOTO 40
   60 CONTINUE
      DO 70 I=1,N
      Y1FNT(I)=A1(1)+A1(2)*X1(I)
      V1FNT(I)=VO*(1.D0-EXP(-RK1*R*T1(I)*T1(I)*EXP(-E1/(R*T1(I)))*(1.D0-
     1       2.D0*R*T1(I)/E1)/(C*E1)))
   70 CONTINUE
C
C            Second reaction
C
      E2=E1
   80 E2OLD=E2
      DO 90 I=1,MN
      Y2NT(I)=DLOG(-C*DLOG(1.D0-V2(I)/VO)/(R*T2(I)*T2(I)))
     1        -DLOG(1.D0-2.D0*R*T2(I)/E2)
   90 CONTINUE
      CALL FLSQP(X2,Y2NT,MN,2,A2,VAR)
      E2=-A2(2)*R
      IF(DABS(E2-E2OLD).GE.1.0D-8) GOTO 80
      RK2=EXP(A2(1))*E2
      DO 100 I=1,MN
      Y2FNT(I)=A2(1)+A2(2)*X2(I)
```

```
      V2FNT(I)=VO*(1.D0-EXP(-RK2*R*T2(I)*T2(I)*EXP(-E2/(R*T2(I)))
     1       *(1.D0-2.D0*R*T2(I)/E2)/(C*E2)))
  100 CONTINUE
      WRITE(*,*) 'INTEGRAL METHOD SUCCESSFUL'
C
C     Coats-Redfern method
C
C             First reaction
C
      DO 110 I=1,N
      Y1CR(I)=DLOG(-C*DLOG(1.D0-V1(I)/VO)/(R*T1(I)*T1(I)))
  110 CONTINUE
      CALL FLSQP(X1,Y1CR,N,2,A1,VAR)
      E1CR=-A1(2)*R
      RK1CR=EXP(A1(1))*E1CR
      DO 120 I=1,N
      Y1FCR(I)=A1(1)+A1(2)*X1(I)
      V1FCR(I)=VO*(1.D0-EXP(-RK1CR*R*T1(I)*T1(I)*EXP(-E1CR/(R*T1(I)))*
     1       (1.D0-2.D0*R*T1(I)/E1CR)/(C*E1CR)))
  120 CONTINUE
C
C             Second reaction
C
      DO 130 I=1,MN
      Y2CR(I)=DLOG(-C*DLOG(1.D0-V2(I)/VO)/(R*T2(I)*T2(I)))
  130 CONTINUE
      CALL FLSQP(X2,Y2CR,MN,2,A2,VAR)
      E2CR=-A2(2)*R
      RK2CR=EXP(A2(1))*E2CR
      DO 140 I=1,MN
      Y2FCR(I)=A2(1)+A2(2)*X2(I)
      V2FCR(I)=VO*(1.D0-EXP(-RK2CR*R*T2(I)*T2(I)*EXP(-E2CR/(R*T2(I)))
     1       *(1.D0-2.D0*R*T2(I)/E2CR)/(C*E2CR)))
  140 CONTINUE
      WRITE(*,*) 'COATS-REDFERN METHOD SUCESSFUL'
C
C
C     Chen-Nuttall method
C
C             First reaction
C
      E1CN=E1CR
  150 EOLD=E1CN
      DO 160 I=1,N
      Y1CN(I)=DLOG(-C*(E1CN+2.D0*R*T1(I))*DLOG(1.D0-V1(I)/VO)/
     1        (T1(I)*T1(I)*R))
  160 CONTINUE
      CALL  FLSQP(X1,Y1CN,N,2,A1,VAR)
      E1CN=-R*A1(2)
      IF(DABS(E1CN-EOLD).GE.1.0D-8) GOTO 150
      RK1CN=EXP(A1(1))
      DO 170 I=1,N
      Y1FCN(I)=A1(1)+A1(2)*X1(I)
      V1FCN(I)=VO*(1.D0-EXP(-RK1CN*R*T1(I)*T1(I)*EXP(-E1CN/(R*T1(I)))*
     1       (1.D0-2.D0*R*T1(I)/E1CN)/(C*E1CN)))
  170 CONTINUE
C
C             Second reaction
C
      E2CN=E1CN
  180 EOLD=E2CN
      DO 190 I=1,MN
      Y2CN(I)=DLOG(-C*(E2CN+2.D0*R*T2(I))*DLOG(1.D0-V2(I)/VO)/(T2(I)*
```

```
     1        T2(I)*R))
  190 CONTINUE
      CALL FLSQP(X2,Y2CN,MN,2,A2,VAR)
      E2CN=-R*A2(2)
      IF(DABS(E2CN-EOLD).GE.1.0D-8)  GOTO 180
      RK2CN=EXP(A2(1))
      DO 200 I=1,MN
      Y2FCN(I)=A2(1)+A2(2)*X2(I)
      V2FCN(I)=VO*(1.D0-EXP(-RK2CN*R*T2(I)*T2(I)*EXP(-E2CN/(R*T2(I)))*
     1        (1.D0-2.D0*R*T2(I)/E2CN)/(C*E2CN)))
  200 CONTINUE
      WRITE(*,*) 'CHEN-NUTTAL METHOD SUCESSFUL'
C
C
C      Friedman Method
C

      DO 210 I=1,M-1
      VD(I)=(V(I+1)-V(I))/(T(I+1)-T(I))
  210 CONTINUE
      VD(M)=VD(M-1)

      DO 220 I=1,N
      VD1(I)=VD(LN+I)
  220 CONTINUE
      DO 230 I=1,MN
      VD2(I)=VD(LN+N+I)
  230 CONTINUE
C
C
C             First reaction
      DO 240 I=1,N
      Y1FM(I)=DLOG(C/VO*VD1(I))-DLOG(1.D0-V1(I)/VO)
  240 CONTINUE
      CALL FLSQP(X1,Y1FM,N,2,A1,VAR)
      E1FM=-A1(2)*R
      RK1FM=EXP(A1(1))
      DO 250 I=1,N
      Y1FFM(I)=A1(1)+A1(2)*X1(I)
      V1FFM(I)=VO*(1.D0-EXP(-RK1FM*R*T1(I)*T1(I)*EXP(-E1FM/(R*T1(I)))*
     1        (1.0D0-2.D0*R*T1(I)/E1FM)/(C*E1FM)))
  250 CONTINUE
C
C           Second reaction
C
      DO 260 I=1,MN
      Y2FM(I)=DLOG(C/VO*VD2(I))-DLOG(1.D0-V2(I)/VO)
  260 CONTINUE
      CALL FLSQP(X2,Y2FM,MN,2,A2,VAR)
      E2FM=-A2(2)*R
      RK2FM=EXP(A2(1))
      DO 270 I=1,MN
      Y2FFM(I)=A2(1)+A2(2)*X2(I)
      V2FFM(I)=VO*(1.D0-EXP(-RK2FM*R*T2(I)*T2(I)*EXP(-E2FM/(R*T2(I)))*
     1        (1.D0-2.D0*R*T2(I)/E2FM)/(C*E2FM)))
  270 CONTINUE
      WRITE(*,*) 'FRIEDMAN METHOD SUCESSFUL'
C
C      Calculate the volatile content in the entire temperature range
C
      DO 280 I=1,M
      IF((T(I)-273.16).LT.450.D0) THEN
      VFNT(I)=VO*(1.D0-EXP(-RK1*R*T(I)*T(I)*EXP(-E1/(R*T(I)))*(1.D0-
```

```
     1       2.D0*R*T(I)/E1)/(C*E1)))
      VFCR(I)=VO*(1.D0-EXP(-RK1CR*R*T(I)*T(I)*EXP(-E1CR/(R*T(I)))*
     1       (1.D0-2.D0*R*T(I)/E1CR)/(C*E1CR)))
      VFCN(I)=VO*(1.D0-EXP(-RK1CN*R*T(I)*T(I)*EXP(-E1CN/(R*T(I)))*
     1       (1.D0-2.D0*R*T(I)/E1CN)/(C*E1CN)))

      VFFM(I)=VO*(1.D0-EXP(-RK1FM*R*T(I)*T(I)*EXP(-E1FM/(R*T(I)))*
     1       (1.0D0-2.D0*R*T(I)/E1FM)/(C*E1FM)))
      ELSE
      VFNT(I)=VO*(1.D0-EXP(-RK2*R*T(I)*T(I)*EXP(-E2/(R*T(I)))
     1      *(1.D0-2.D0*R*T(I)/E2)/(C*E2)))
      VFCR(I)=VO*(1.D0-EXP(-RK2CR*R*T(I)*T(I)*EXP(-E2CR/(R*T(I)))
     1      *(1.D0-2.D0*R*T(I)/E2CR)/(C*E2CR)))
      VFCN(I)=VO*(1.D0-EXP(-RK2CN*R*T(I)*T(I)*EXP(-E2CN/(R*T(I)))*
     1       (1.D0-2.D0*R*T(I)/E2CN)/(C*E2CN)))
      VFFM(I)=VO*(1.D0-EXP(-RK2FM*R*T(I)*T(I)*EXP(-E2FM/(R*T(I)))*
     1       (1.D0-2.D0*R*T(I)/E2FM)/(C*E2FM)))
      ENDIF
  280 CONTINUE


C
C           Calculate the rate at entire temperature range
C
      DO 290 I=1,M
      IF((T(I)-273.16D0).LT.450.D0) THEN
      VDNT(I)=RK1*EXP(-E1/R/T(I))*(VO-V(I))/C
      VDCR(I)=RK1CR*EXP(-E1CR/R/T(I))*(VO-V(I))/C
      VDCN(I)=RK1CN*EXP(-E1CN/R/T(I))*(VO-V(I))/C
      VDFM(I)=RK1FM*EXP(-E1FM/R/T(I))*(VO-V(I))/C
      ELSE
      VDNT(I)=RK2*EXP(-E2/R/T(I))*(VO-V(I))/C
      VDCR(I)=RK2CR*EXP(-E2CR/R/T(I))*(VO-V(I))/C
      VDCN(I)=RK2CN*EXP(-E2CN/R/T(I))*(VO-V(I))/C
      VDFM(I)=RK2FM*EXP(-E2FM/R/T(I))*(VO-V(I))/C
      ENDIF
  290 CONTINUE
C
C     Calculate the absolute average deviation ERROR
C
      SEENT=0.D0
      SEECR=0.D0
      SEECN=0.D0
      SEEFM=0.D0
      DO 450 I=1,M
      SEENT=SEENT+(V(I)-VFNT(I))**2
      SEECR=SEECR+(V(I)-VFCR(I))**2
      SEECN=SEECN+(V(I)-VFCN(I))**2
      SEEFM=SEEFM+(V(I)-VFFM(I))**2
  450 CONTINUE
      SEENT=SQRT((SEENT)/(DBLE(M)-2.D0))
      SEECR=SQRT((SEECR)/(DBLE(M)-2.D0))
      SEECN=SQRT((SEECN)/(DBLE(M)-2.D0))
      SEEFM=SQRT((SEEFM)/(DBLE(M)-2.D0))
      WRITE(*,*) SEENT,SEECR,SEECN,SEEFM
C
C           Printing results of V1, V2, V1F and V2F
C
      DO 500 I=1,M
      T(I)=T(I)-273.16D0
  500 CONTINUE
      WRITE(3,550)
  550 FORMAT(//'Fitting results in the selected temperature range')
```

```
      WRITE(3,600)
  600 FORMAT(4X,'T',8X,'V',8X,'VFNT',5X,'VFCR',6X,'VFCN',6X,'VFFM',
     1       8X,'VD')
      DO 620 I=1,N
      WRITE(3,610) T(LN+I),V(LN+I),V1FNT(I),V1FCR(I),V1FCN(I),V1FFM(I),
     1             VD(LN+I)
  610 FORMAT(F7.2,6F10.6)
  620 CONTINUE

      DO 640 I=1,MN
      WRITE(3,630) T(LN+N+I),V(LN+N+I),V2FNT(I),V2FCR(I),V2FCN(I),
     1             V2FFM(I),VD(LN+N+I)
  630 FORMAT(F7.2,6F10.6)
  640 CONTINUE
      WRITE(3,650)
  650 FORMAT(//'Activation energies and pre-exponential factor for both
     1 reactions')
      WRITE(3,660)
  660 FORMAT(30X,'E1',10X,'K1',10X,'E2',10X,'K2')
      WRITE(3,670) E1,RK1,E2,RK2
  670 FORMAT('Integral method',10X,4F12.3)
      WRITE(3,680) E1CR,RK1CR,E2CR,RK2CR
  680 FORMAT('Coats-Redfern method',5X,4F12.3)
      WRITE(3,690) E1CN,RK1CN,E2CN,RK2CN
  690 FORMAT('Chen-Nuttall method',6X,4F12.3)
      WRITE(3,700) E1FM,RK1FM,E2FM,RK2FM
  700 FORMAT('Friedman method',10X,4F12.3)
C
C     Printing the results of Y1, Y2, Y1F and Y2F
C
      WRITE(3,701)
  701 FORMAT(//'Experimental results Y1,Y2 and fitted results Y1F,Y2F')
      WRITE(3,702)
  702 FORMAT(4X,'T',5X,'YNT',5X,'YFNT',4X,'YCR',5X,'YFCR',4X,'YCN',5X,
     1       'YFCN',4X,'YFM',5X,'YFFM')
      DO 704 I=MN,1,-1
      WRITE(3,703) X2(I),Y2NT(I),Y2FNT(I),Y2CR(I),Y2FCR(I),Y2CN(I),
     1             Y2FCN(I),Y2FM(I),Y2FFM(I)
  703 FORMAT(F8.6,8F8.3)
  704 CONTINUE
      DO 705 I=N,1,-1
      WRITE(3,703) X1(I),Y1NT(I),Y1FNT(I),Y1CR(I),Y1FCR(I),Y1CN(I),
     1             Y1FCN(I),Y1FM(I),Y1FFM(I)
  705 CONTINUE
C
C     Printing the results in the entire temperature range
C
      WRITE(3,710)
  710 FORMAT(//'Fitting results in the entire temperature range')
      WRITE(3,720)
  720 FORMAT(4X,'T',7X,'V',7X,'VFNT',6X,'VFCR',6X,'VFCN',6X,'VFFM')
      DO 740 I=1,M
      WRITE(3,730) T(I),V(I),VFNT(I),VFCR(I),VFCN(I),VFFM(I)
  730 FORMAT(F7.2,5F10.6)
  740 CONTINUE
C
C     Printing the standard deviation
C
      WRITE(3,742)
  742 FORMAT(//'standard deviation for each method above')
      WRITE(3,746) SEENT,SEECR,SEECN,SEEFM
  746 FORMAT(17X,4F10.6)
C
```

```
C     Printing the rates in the entire temperature range
C
      WRITE(3,750)
  750 FORMAT(//'Fitting rate dV/dT in the entire temperature reange')
      WRITE(3,760)
  760 FORMAT(4X,'T',6X,'VD',7X,'VDNT',6X,'VDCR',6X,'VDCN',6X,'VDFM')
      DO 770 I=1,M
      WRITE(3,730) T(I),VD(I),VDNT(I),VDCR(I),VDCN(I),VDFM(I)
  770 CONTINUE

      ENDFILE(UNIT = 3)
      CLOSE(UNIT = 3)
      STOP
      END

      SUBROUTINE GAUSS(A,N,NDR,NDC,X,RNORM,IREEOR)
      IMPLICIT REAL*8(A-H,O-Z)
      DIMENSION A(NDR,NDC),X(N),B(50,51)
      NM=N-1
      NP=N+1
      IREEOR=3
      DO 20 I=1,N
         DO 10 J=1,NP
         B(I,J)=A(I,J)
   10    CONTINUE
   20 CONTINUE

      DO 70 K=1,NM
         KP=K+1

         BIG=ABS(B(K,K))
         IPIVOT=K
         DO 30 I=KP,N
            AB=ABS(B(I,K))
            IF(AB.GT.BIG) THEN
              BIG=AB
              IPIVOT=I
            ENDIF
   30    CONTINUE

         IF(IPIVOT.NE.K) THEN
           DO 40 J=K,NP
            TEMP=B(IPIVOT,J)
            B(IPIVOT,J)=B(K,J)
            B(K,J)=TEMP
   40    CONTINUE
      ENDIF

         IF(B(K,K).EQ.0.D0) THEN
           IERROR=2
           RETURN
         ENDIF
        DO 60 I=KP,N
         QUOT=B(I,K)/B(K,K)
         B(I,K)=0.D0
         DO 50 J=KP,NP
           B(I,J)=B(I,J)-QUOT*B(K,J)
   50    CONTINUE
   60   CONTINUE
   70 CONTINUE
      IF(B(N,N).EQ.0.D0) THEN
        IERROR=2
        RETURN
```

```
      ENDIF
      X(N)=B(N,NP)/B(N,N)
      DO 90 I=NM,1,-1
        SUM=0.D0
        DO 80 J=I+1,N
           SUM=SUM+B(I,J)*X(J)
   80   CONTINUE
        X(I)=(B(I,NP)-SUM)/B(I,I)
   90 CONTINUE


      RSQ=0.D0
      DO 110 I=1,N
        SUM=0.D0
        DO 100 J=1,N
        SUM=SUM+A(I,J)*X(J)
  100   CONTINUE
        RSQ=RSQ+(A(I,NP)-SUM)**2
  110 CONTINUE
      RNORM=DSQRT(RSQ)
      IERROR=1
      RETURN
      END

      SUBROUTINE FLSQP(X,Y,M,N,A,VAR)
      IMPLICIT REAL*8(A-H,O-Z)
      DIMENSION X(M),U(51),Y(M),V(51),A(N),B(11),COEFF(10,11),SUMU(18)
      NP=N+1
      NM2=2*(N-1)
      XMIN=X(1)
      XMAX=X(1)
      YMIN=Y(1)
      YMAX=Y(1)
      DO 10 K=2,M
        XMIN=DMIN1(XMIN,X(K))
        XMAX=DMAX1(XMAX,X(K))
        YMIN=DMIN1(YMIN,Y(K))
        YMAX=DMAX1(YMAX,Y(K))
   10   CONTINUE
      XP=XMIN+XMAX
      XM=XMAX-XMIN
      YP=YMIN+YMAX
      YM=YMAX-YMIN
      DO 20 K=1,M
        U(K)=(2.D0*X(K)-XP)/XM
        V(K)=(2.D0*Y(K)-YP)/YM
   20   CONTINUE
      DO 30 L=1,NM2
        SUMU(L)=0.D0
   30   CONTINUE
      DO 40 I=1,N
        COEFF(I,NP)=0.D0
   40   CONTINUE
      DO 70 K=1,M
        TERMU=U(K)
        DO 50 L=1,NM2
          SUMU(L)=SUMU(L)+TERMU
          TERMU=TERMU*U(K)
   50     CONTINUE
        TERMV=V(K)
        DO 60 I=1,N
          COEFF(I,NP)=COEFF(I,NP)+TERMV
          TERMV=TERMV*U(K)
```

```
 60      CONTINUE
 70    CONTINUE
       DO 90 I=1,N
         DO 80 J=1,N
           IF(I.EQ.1.AND.J.EQ.1) THEN
             COEFF(I,J)=M
           ELSE
             COEFF(I,J)=SUMU(I+J-2)
           ENDIF
 80      CONTINUE
 90    CONTINUE
       CALL GAUSS(COEFF,N,10,11,B,RNORM,IERROR)
       DO 110 I=1,N
         IM=I-1
         SUM=B(I)
         IF(I.NE.N) THEN
           DO 100 J=I+1,N
             SUM=SUM+NOMIAL(IM,J-1)*(-XP/XM)**(J-I)*B(J)
100        CONTINUE
         ENDIF
         A(I)=YM*(2.D0/XM)**IM*SUM/2.D0
110   CONTINUE
      A(1)=A(1)+YP/2.D0
      SSUM=0.D0
      DO 130 K=1,M
        SUM=A(1)
        TEMP=1.D0
        DO 120 J=2,N
          TEMP=TEMP*X(K)
          SUM=SUM+A(J)*TEMP
120     CONTINUE
        SSUM=SSUM+(Y(K)-SUM)**2
130   CONTINUE
      VAR=SSUM/(M-N)
      RETURN
      END
C
      FUNCTION NOMIAL(I,J)
      NOMIAL=1
      IF(J.LE.I.OR.I.EQ.0) RETURN
      DO 10 ICOUNT=1,I
        NOMIAL=NOMIAL*(J-ICOUNT+1)/ICOUNT
 10   CONTINUE
      RETURN
      END
```

2-Stage First Order Reaction Model Fitting Results

CANMET pitch 25 °C/min, 800 °C final temperature RUN# CAN48

Experimental results Y1,Y2 and fitted results Y1F,Y2F

T	YNT	YFNT	YCR	YFCR	YCN	YFCN	YFM	YFFM
.001177	-10.718	-10.575	-10.939	-10.794	.412	.556	-1.242	-.179
.001213	-10.836	-10.882	-11.049	-11.095	.297	.251	-.723	-.349
.001233	-10.958	-11.053	-11.168	-11.263	.176	.081	-.299	-.443
.001251	-11.104	-11.208	-11.310	-11.414	.031	-.073	-.195	-.529
.001267	-11.268	-11.344	-11.471	-11.548	-.132	-.208	-.112	-.604
.001280	-11.434	-11.460	-11.635	-11.662	-.297	-.324	-.089	-.668
.001293	-11.570	-11.572	-11.768	-11.771	-.432	-.435	-.331	-.730
.001306	-11.736	-11.676	-11.932	-11.873	-.598	-.539	-.239	-.788
.001320	-11.884	-11.800	-12.078	-11.994	-.745	-.661	-.620	-.856
.001338	-12.037	-11.951	-12.228	-12.143	-.898	-.812	-.907	-.940
.001356	-12.170	-12.107	-12.358	-12.296	-1.029	-.967	-1.178	-1.026
.001371	-12.267	-12.240	-12.453	-12.426	-1.126	-1.099	-1.393	-1.099
.001387	-12.354	-12.377	-12.538	-12.560	-1.213	-1.235	-1.591	-1.175
.001407	-12.455	-12.545	-12.636	-12.725	-1.313	-1.402	-1.735	-1.267
.001430	-11.979	-12.050	-12.736	-12.779	-2.380	-2.429	-1.964	-2.384
.001455	-12.100	-12.114	-12.839	-12.832	-2.489	-2.487	-2.063	-2.437
.001483	-12.199	-12.190	-12.916	-12.896	-2.573	-2.556	-2.479	-2.501
.001513	-12.307	-12.269	-13.004	-12.962	-2.668	-2.628	-2.506	-2.567
.001541	-12.392	-12.341	-13.071	-13.022	-2.742	-2.693	-2.696	-2.628
.001573	-12.485	-12.426	-13.144	-13.093	-2.822	-2.770	-2.834	-2.699
.001603	-12.551	-12.504	-13.193	-13.158	-2.878	-2.840	-3.077	-2.764
.001670	-12.705	-12.680	-13.312	-13.306	-3.011	-3.000	-3.150	-2.912
.001742	-12.853	-12.872	-13.425	-13.466	-3.138	-3.173	-3.357	-3.073
.001822	-13.018	-13.081	-13.558	-13.642	-3.285	-3.363	-3.454	-3.249
.001909	-13.231	-13.311	-13.738	-13.834	-3.480	-3.571	-3.489	-3.441
.002005	-13.487	-13.563	-13.963	-14.045	-3.719	-3.799	-3.620	-3.653
.002111	-13.792	-13.843	-14.238	-14.279	-4.009	-4.052	-3.810	-3.887
.002229	-14.299	-14.153	-14.716	-14.538	-4.502	-4.333	-3.843	-4.147

Fitting results in the entire temperature range

T	V	VFNT	VFCR	VFCN	VFFM
50.22	.040000	.155567	.143757	.173164	.254039
100.32	.060000	.585928	.446609	.583486	.789804
135.40	.500000	1.231859	.842096	1.151879	1.488240
153.77	1.020000	1.733712	1.126916	1.574572	1.990044
175.47	2.170000	2.504867	1.541807	2.204314	2.719006
200.52	3.860000	3.671561	2.135001	3.126396	3.756867
225.60	5.570000	5.172992	2.858170	4.276503	5.014856
250.65	7.590000	7.032889	3.711836	5.662237	6.489252
275.70	9.830000	9.265615	4.693808	7.285796	8.170753
300.75	12.080000	11.867032	5.795725	9.138123	10.038886
325.80	14.480000	14.815040	7.003953	11.200199	12.064187
350.85	17.330000	18.070076	8.299930	13.443768	14.209525
362.55	18.700000	19.680585	8.928980	14.543901	15.240696
375.90	20.650000	21.577142	9.660695	15.832638	16.431792
387.60	22.550000	23.282974	10.311053	16.986420	17.482892
400.95	25.090000	25.269189	11.059527	18.324429	18.683748
414.32	27.590000	27.289795	11.811514	19.680511	19.880750
426.00	30.750000	29.071447	12.466628	20.872552	20.915811
437.70	34.040000	30.863205	13.117667	22.068282	21.937321
447.72	37.350000	32.397342	13.668495	23.089827	22.796086
456.07	40.310000	41.062072	35.863390	40.231548	52.110546
464.42	43.670000	45.481618	39.961255	44.595503	54.815420
474.45	48.260000	50.810762	45.020628	49.878827	57.945213
484.45	53.520000	55.999556	50.100606	55.050838	60.904851
492.80	58.430000	60.121639	54.273443	59.184363	63.232246

500.00	63.510000	63.449886	57.755135	62.541985	65.122477
507.85	67.420000	66.779021	61.365837	65.923123	67.051542
516.20	71.520000	69.922558	64.928926	69.142386	68.945288
526.22	74.860000	73.101714	68.744113	72.433783	70.996004
537.90	77.160000	75.971799	72.468759	75.450494	73.078863
551.27	78.620000	78.230589	75.729994	77.874822	75.066625
576.32	79.700000	80.249327	79.254115	80.124226	77.755774
601.37	80.030000	80.759516	80.506863	80.733312	79.351849
649.80	80.290000	80.839754	80.836274	80.839570	80.575569
699.90	80.520000	80.840000	80.839998	80.840000	80.812883
750.00	80.720000	80.840000	80.840000	80.840000	80.838394
800.12	80.840000	80.840000	80.840000	80.840000	80.839947

Fitting rate dV/dT in the entire temperature range

T	VD	VDNT	VDCR	VDCN	VDFM
50.22	.000399	.005196	.004289	.005420	.007594
100.32	.012543	.015487	.010694	.014563	.018972
135.40	.028307	.028220	.017650	.025052	.031347
153.77	.052995	.036999	.022115	.031991	.039298
175.47	.067465	.049144	.027976	.041305	.049740
200.52	.068182	.065595	.035494	.053529	.063140
225.60	.080639	.084826	.043850	.067409	.078044
250.65	.089421	.106264	.052710	.082443	.093857
275.70	.089820	.129585	.061912	.098369	.110288
300.75	.095808	.154713	.071431	.115130	.127292
325.80	.113772	.180904	.080943	.132188	.144295
350.85	.117094	.206557	.089793	.148424	.160123
362.55	.146067	.218426	.093755	.155798	.167211
375.90	.162393	.230390	.097522	.163007	.173957
387.60	.190262	.239737	.100294	.168466	.178925
400.95	.186986	.248123	.102472	.173057	.182836
414.32	.270548	.255705	.104300	.177062	.186123
426.00	.281197	.256427	.103506	.176486	.184728
437.70	.330339	.254908	.101856	.174410	.181803
447.72	.354491	.249397	.098818	.169807	.176398
456.07	.402395	.558800	.454728	.539926	.539964
464.42	.457627	.585505	.475201	.565276	.533028
474.45	.526000	.599901	.485379	.578632	.509290
484.45	.588024	.585343	.472178	.564076	.464358
492.80	.705556	.543249	.437149	.523123	.407799
500.00	.498089	.466302	.374454	.448745	.334071
507.85	.491018	.403712	.323475	.388251	.275146
516.20	.333333	.314930	.251757	.302658	.203760
526.22	.196918	.231569	.184618	.222364	.140963
537.90	.109200	.166329	.132199	.159569	.094482
551.27	.043114	.119123	.094357	.114163	.062666
576.32	.013174	.083148	.065462	.079540	.038128
601.37	.005369	.078905	.061765	.075349	.031788
649.80	.004591	.089660	.069471	.085356	.028688
699.90	.003992	.084197	.064620	.079924	.021745
750.00	.002394	.048626	.037002	.046039	.010352
800.12	.002394	.000000	.000000	.000000	.000000

CANMET pitch 50 °C/min, 800 °C final temperature RUN#33

Experimental results Y1,Y2 and fitted results Y1F,Y2F

T	YNT	YFNT	YCR	YFCR	YCN	YFCN	YFM	YFFM
.001169	-10.078	-10.036	-10.328	-10.283	.939	.983	-.645	.522
.001207	-10.197	-10.328	-10.437	-10.568	.824	.693	-.131	.277
.001223	-10.306	-10.455	-10.543	-10.692	.716	.567	.429	.171
.001240	-10.450	-10.587	-10.683	-10.820	.574	.437	.488	.061
.001265	-10.725	-10.776	-10.953	-11.005	.300	.248	.437	-.098

.001290	-11.035	-10.973	-11.258	-11.197	-.008	.053	.280	-.263
.001309	-11.231	-11.119	-11.450	-11.340	-.203	-.092	.014	-.385
.001328	-11.406	-11.269	-11.622	-11.487	-.377	-.241	-.262	-.511
.001344	-11.526	-11.393	-11.739	-11.607	-.496	-.363	-.523	-.614
.001360	-11.642	-11.519	-11.852	-11.730	-.611	-.488	-.688	-.720
.001369	-11.695	-11.583	-11.904	-11.793	-.664	-.552	-.824	-.773
.001386	-11.800	-11.714	-12.006	-11.920	-.768	-.682	-.946	-.883
.001407	-11.916	-11.882	-12.118	-12.085	-.883	-.849	-1.186	-1.024
.001430	-12.030	-12.056	-12.229	-12.254	-.995	-1.021	-1.329	-1.169
.001453	-12.137	-12.235	-12.332	-12.429	-1.101	-1.199	-1.511	-1.320
.001486	-12.249	-12.496	-12.440	-12.684	-1.212	-1.458	-1.868	-1.539
.001542	-11.846	-11.792	-12.571	-12.495	-2.271	-2.843	-2.210	-2.429
.001603	-11.993	-11.945	-12.678	-12.623	-2.393	-3.038	-2.502	-2.517
.001669	-12.123	-12.109	-12.770	-12.761	-2.499	-3.251	-2.748	-2.613
.001746	-12.277	-12.305	-12.885	-12.924	-2.629	-3.509	-2.842	-2.726
.001824	-12.453	-12.501	-13.026	-13.089	-2.784	-3.772	-2.870	-2.840
.001910	-12.645	-12.716	-13.184	-13.269	-2.956	-4.039	-3.016	-2.964
.002003	-12.885	-12.951	-13.391	-13.466	-3.178	-4.397	-3.094	-3.100
.002117	-13.206	-13.237	-13.677	-13.704	-3.481	-4.806	-3.260	-3.265
.002232	-13.656	-13.527	-14.096	-13.948	-3.916	-5.734	-3.344	-3.434

Fitting results in the entire temperature range

T	V	VFNT	VFCR	VFCN	VFFM
50.10	.320000	.159415	.138895	.171486	.591272
99.10	.310000	.556368	.404340	.539215	1.242183
125.80	.400000	.971510	.650541	.898298	1.709785
152.50	1.060000	1.585018	.986978	1.405702	2.241225
174.80	2.010000	2.282442	1.345596	1.961703	2.718060
199.25	3.370000	3.271052	1.826008	2.724890	3.253745
226.00	4.960000	4.650494	2.459542	3.756319	3.823297
250.45	6.640000	6.202251	3.136557	4.883752	4.293595
274.95	8.420000	8.042902	3.904061	6.188210	4.678267
299.45	10.430000	10.164493	4.752172	7.658213	4.934511
326.15	12.620000	12.776137	5.753620	9.429510	5.013092
350.65	14.760000	15.416117	6.726081	11.185607	4.845490
375.15	17.410000	18.248549	7.729867	13.037547	4.388759
399.60	20.810000	21.219655	8.740720	14.948457	3.578859
415.20	23.700000	23.166671	9.379280	16.184024	2.842789
426.35	26.510000	24.573239	9.828113	17.068403	2.197203
437.45	29.700000	25.979937	10.265765	17.945754	1.445455
448.60	33.180000	27.394181	10.693524	18.820292	.570909
457.50	36.470000	39.517420	33.781513	38.494790	35.907049
461.95	38.200000	41.620283	35.681101	40.558965	37.622476
470.85	42.010000	45.875263	39.583898	44.747626	41.113278
479.75	46.100000	50.133976	43.581692	48.958655	44.651810
490.90	52.050000	55.353100	48.633913	54.150658	49.087966
502.05	58.550000	60.295076	53.615079	59.107162	53.445751
517.60	67.700000	66.450372	60.191753	65.355186	59.225680
533.20	74.020000	71.494238	66.051103	70.566098	64.475386
544.35	76.480000	74.320833	69.637644	73.542262	67.790289
555.45	77.950000	76.495891	72.644783	75.875617	70.678095
582.15	79.280000	79.517704	77.569040	79.235903	75.862118
624.45	79.950000	80.709446	80.389877	80.675051	79.724209
689.05	80.150000	80.789924	80.787785	80.789835	80.758907
800.00	80.790000	80.790000	80.790000	80.790000	80.789999

Fitting rate dV/dT in the entire temperature range

T	VD	VDNT	VDCR	VDCN	VDFM
50.10	-.000204	.005149	.004026	.005205	.014815
99.10	.003371	.014337	.009492	.013161	.026812
125.80	.024719	.022507	.013844	.019799	.034799
152.50	.042601	.033148	.019120	.028094	.043396
174.80	.055624	.043952	.024167	.036234	.050842

199.25	.059439	.057756	.030292	.046329	.059121
226.00	.068712	.075246	.037675	.058758	.068311
250.45	.072653	.093094	.044861	.071103	.076549
274.95	.082041	.112617	.052407	.084293	.084603
299.45	.082022	.133237	.060054	.097901	.092158
326.15	.087347	.156988	.068543	.113247	.100004
350.65	.108163	.179303	.076215	.127353	.106566
375.15	.139059	.200430	.083110	.140330	.111726
399.60	.185256	.218394	.088506	.150892	.114728
415.20	.252018	.226248	.090434	.155076	.114691
426.35	.287387	.228010	.090280	.155429	.112787
437.45	.312108	.227007	.089065	.153929	.109668
448.60	.369663	.223431	.086886	.150727	.105486
457.50	.388764	.532799	.421759	.510357	.408986
461.95	.428090	.545977	.431532	.522721	.414753
470.85	.459551	.563999	.444443	.539453	.419756
479.75	.533632	.570667	.448386	.545314	.416309
490.90	.582960	.549467	.430191	.524450	.391181
502.05	.588424	.492026	.383888	.469098	.342084
517.60	.405128	.352553	.273787	.335617	.237411
533.20	.220628	.220429	.170413	.209535	.143936
544.35	.132432	.160001	.123312	.151940	.102276
555.45	.049813	.119715	.091986	.113573	.074962
582.15	.015839	.085249	.065050	.080693	.050908
624.45	.003096	.072702	.054917	.068592	.040506
689.05	.005768	.098935	.073711	.092926	.050168
800.00	.005768	.000000	.000000	.000000	.000000

CANMET pitch 100 °C/min, 800 °C final temperature RUN# CAN41

Experimental results Y1,Y2 and fitted results Y1F,Y2F

T	YNT	YFNT	YCR	YFCR	YCN	YFCN	YFM	YFFM
.001215	-9.982	-10.109	-10.192	-10.319	1.162	1.036	1.132	1.357
.001227	-10.127	-10.209	-10.335	-10.417	1.019	.937	1.252	1.207
.001239	-10.289	-10.311	-10.495	-10.517	.857	.834	1.184	1.052
.001251	-10.449	-10.416	-10.653	-10.620	.697	.730	1.023	.893
.001263	-10.600	-10.523	-10.801	-10.725	.548	.624	.815	.732
.001276	-10.732	-10.632	-10.931	-10.832	.416	.516	.567	.568
.001295	-10.904	-10.800	-11.100	-10.996	.245	.349	.260	.315
.001315	-11.045	-10.973	-11.238	-11.166	.105	.177	-.064	.054
.001342	-11.204	-11.210	-11.392	-11.398	-.053	-.059	-.377	-.304
.001378	-11.375	-11.523	-11.558	-11.705	-.222	-.370	-.695	-.776
.001424	-11.148	-11.131	-11.716	-11.686	-1.195	-1.903	-1.067	-1.216
.001482	-11.340	-11.317	-11.879	-11.853	-1.370	-2.145	-1.370	-1.367
.001544	-11.521	-11.519	-12.032	-12.033	-1.535	-2.371	-1.625	-1.531
.001602	-11.693	-11.706	-12.181	-12.201	-1.695	-2.661	-1.754	-1.684
.001664	-11.888	-11.908	-12.352	-12.381	-1.877	-2.934	-1.879	-1.848
.001743	-12.146	-12.164	-12.583	-12.609	-2.121	-3.288	-2.041	-2.056
.001817	-12.383	-12.404	-12.799	-12.824	-2.348	-3.626	-2.280	-2.251
.001912	-12.691	-12.711	-13.081	-13.099	-2.643	-4.065	-2.521	-2.501
.002001	-13.050	-12.999	-13.419	-13.357	-2.992	-6.243	-2.655	-2.736

Fitting results in the entire temperature range

T	V	VFNT	VFCR	VFCN	VFFM
51.20	.090000	.037815	.037196	.041788	.089455
148.60	.250000	.590487	.449749	.571244	.885730
175.80	.570000	1.038072	.750431	.977237	1.416064
199.20	1.250000	1.603755	1.113857	1.478432	2.031820
226.50	2.410000	2.532160	1.686924	2.283696	2.965834
249.80	3.670000	3.599821	2.323655	3.192784	3.966103
277.10	5.330000	5.226674	3.265426	4.555680	5.392814
300.50	7.100000	6.980181	4.255858	6.004666	6.840918

327.70	9.650000	9.465350	5.632465	8.035294	8.783387
351.10	12.140000	11.997734	7.015564	10.086823	10.667295
374.50	14.860000	14.888488	8.581675	12.415906	12.731221
401.70	18.310000	18.668993	10.623569	15.452627	15.326578
429.00	22.540000	22.858725	12.894257	18.818725	18.101062
452.40	27.110000	24.023730	20.524340	23.460954	12.033339
471.90	32.190000	32.039011	27.552988	31.302714	19.205596
487.40	37.200000	39.156521	33.951636	38.293751	26.792290
499.10	41.820000	44.774625	39.137117	43.836819	33.573404
510.80	47.510000	50.417374	44.497372	49.432639	41.053280
518.60	51.880000	54.098071	48.095553	53.101808	46.260754
526.40	56.710000	57.645267	51.656872	56.655377	51.486260
534.20	61.610000	61.002373	55.130548	60.037606	56.570802
542.00	66.120000	64.118252	58.466153	63.197157	61.348836
549.70	69.670000	66.915944	61.576999	66.054835	65.613673
565.30	74.330000	71.624776	67.164201	70.925638	72.426814
584.80	77.000000	75.640965	72.531486	75.178599	77.215667
612.10	78.280000	78.362692	76.972609	78.178239	79.134416
651.00	78.820000	79.242162	79.033522	79.221177	79.299688
701.60	78.970000	79.299799	79.296617	79.299639	79.300000
752.30	79.150000	79.300000	79.299996	79.300000	79.300000
799.00	79.300000	79.300000	79.300000	79.300000	79.300000

Fitting rate dV/dT in the entire temperature range

T	VD	VDNT	VDCR	VDCN	VDFM
51.20	.001643	.001454	.001318	.001541	.002970
148.60	.011765	.014541	.010325	.013569	.019344
175.80	.029060	.023057	.015584	.020970	.028129
199.20	.042491	.032670	.021262	.029134	.037294
226.50	.054077	.046802	.029274	.040884	.049829
249.80	.060806	.061441	.037273	.052823	.061992
277.10	.075641	.081694	.047974	.069056	.077848
300.50	.093750	.101366	.058032	.084558	.092374
327.70	.106410	.126246	.070346	.103839	.109705
351.10	.116239	.148975	.081254	.121176	.124680
374.50	.126838	.172396	.092180	.138785	.139336
401.70	.154945	.199582	.104463	.158895	.155372
429.00	.195299	.223821	.114859	.176369	.168297
452.40	.260513	.372701	.304524	.360559	.240177
471.90	.323226	.460019	.373598	.444225	.347618
487.40	.394872	.521182	.421329	.502595	.444381
499.10	.486325	.551505	.444351	.531302	.513459
510.80	.560256	.553150	.444231	.532368	.560853
518.60	.619231	.532058	.426392	.511745	.570239
526.40	.628205	.487780	.390098	.468866	.552005
534.20	.578205	.424184	.338550	.407489	.506336
542.00	.461039	.350260	.278993	.336273	.440551
549.70	.298718	.282713	.224756	.271267	.374077
565.30	.136923	.177523	.140595	.170142	.259549
584.80	.046886	.103931	.081937	.099474	.171268
612.10	.013882	.062954	.049333	.060145	.121581
651.00	.002964	.044749	.034788	.042650	.106607
701.60	.003550	.050080	.038566	.047596	.152880
752.30	.003212	.035344	.026987	.033506	.134973
799.00	.003212	.000000	.000000	.000000	.000000

CANMET pitch 150 °C/min, 800 °C final temperature RUN# CAN58

Experimental results Y1,Y2 and fitted results Y1F,Y2F

T	YNT	YFNT	YCR	YFCR	YCN	YFCN	YFM	YFFM
.001129	-9.519	-9.531	-9.685	-9.696	1.934	1.922	1.899	1.852
.001152	-9.801	-9.796	-9.963	-9.958	1.652	1.657	1.496	1.600

.001175	-10.008	-10.073	-10.167	-10.231	1.446	1.382	1.088	1.337
.001192	-10.245	-10.261	-10.401	-10.417	1.210	1.194	1.356	1.158
.001209	-10.483	-10.459	-10.637	-10.613	.973	.997	1.113	.969
.001226	-10.704	-10.658	-10.855	-10.810	.752	.798	.853	.779
.001244	-10.895	-10.866	-11.044	-11.015	.562	.591	.510	.582
.001262	-11.155	-11.079	-11.302	-11.226	.303	.379	.536	.379
.001291	-11.380	-11.411	-11.523	-11.554	.078	.047	-.201	.062
.001321	-11.702	-11.759	-11.841	-11.898	-.243	-.300	-.202	-.269
.001363	-11.895	-12.082	-12.198	-12.383	-1.225	-2.063	-.728	-.731
.001419	-12.285	-12.398	-12.574	-12.688	-1.610	-3.575	-1.284	-1.089
.001480	-13.148	-12.742	-13.424	-13.021	-2.468	-5.479	-1.244	-1.479
.001753	-14.167	-14.274	-14.395	-14.500	-3.470	-10.911	-3.259	-3.216

Fitting results in the entire temperature range

T	V	VFNT	VFCR	VFCN	VFFM
51.80	.060000	.000151	.000154	.000159	.000068
203.75	.000000	.074681	.063126	.073340	.070851
297.20	.780000	.701829	.555184	.672535	.866054
402.35	2.850000	4.237655	3.194776	3.986740	6.378226
431.60	7.050000	6.330544	4.732698	5.934912	9.894506
460.70	10.840000	9.115970	8.027129	8.983551	9.795881
484.10	15.870000	15.080683	13.282723	14.852779	15.812360
501.65	21.770000	21.204772	18.726693	20.883108	21.863492
519.20	27.110000	28.796499	25.568963	28.370146	29.251362
530.90	33.840000	34.576969	30.867080	34.082948	34.821159
542.60	39.520000	40.770361	36.649493	40.218947	40.756949
554.15	46.400000	47.076315	42.676873	46.486832	46.786606
566.00	53.900000	53.464116	48.967499	52.863180	52.903960
577.55	60.980000	59.309409	54.942318	58.729828	58.537902
595.10	66.750000	66.854625	63.119819	66.368983	65.934092
612.65	72.410000	72.240913	69.523827	71.899768	71.411071
624.35	75.110000	74.582095	72.607495	74.342314	73.913015
653.60	75.950000	77.155327	76.597077	77.095814	76.930663
723.65	76.820000	77.589951	77.589461	77.589928	77.589731
799.55	77.590000	77.590000	77.590000	77.590000	77.590000

Fitting rate dV/dT in the entire temperature range

T	VD	VDNT	VDCR	VDCN	VDFM
51.80	-.000395	.000009	.000009	.000009	.000005
203.75	.008347	.002221	.001826	.002159	.002333
297.20	.019686	.015110	.011640	.014342	.020546
402.35	.143590	.067985	.049723	.063308	.113490
431.60	.130241	.090575	.065475	.083982	.158347
460.70	.214957	.206107	.178311	.202428	.213433
484.10	.336182	.310924	.267476	.304952	.314499
501.65	.304274	.398138	.341129	.390105	.396048
519.20	.575214	.501982	.428456	.491390	.491444
530.90	.485470	.538596	.458575	.526912	.521913
542.60	.595671	.576667	.489815	.563825	.553269
554.15	.632911	.576449	.488506	.563295	.547803
566.00	.612987	.533933	.451440	.521455	.502590
577.55	.328775	.451831	.381193	.441036	.421484
595.10	.322507	.388681	.326871	.379098	.357799
612.65	.230769	.242157	.203026	.236009	.220097
624.35	.028718	.137569	.115110	.134011	.124013
653.60	.012420	.136916	.114024	.133220	.121026
723.65	.010145	.155215	.127955	.150649	.131517
799.55	.010145	.000000	.000000	.000000	.000000

Syncrude pitch 25 °C/min, 800 °C final temperature RUN# Syn43

Experimental results Y1,Y2 and fitted results Y1F,Y2F

T	YNT	YFNT	YCR	YFCR	YCN	YFCN	YFM	YFFM
.001206	-10.639	-10.787	-10.867	-11.014	.435	.287	-.368	.449
.001220	-10.774	-10.907	-10.999	-11.132	.301	.168	.155	.269
.001233	-10.937	-11.009	-11.159	-11.232	.139	.067	.321	.116
.001243	-11.111	-11.093	-11.331	-11.313	-.034	-.016	.437	-.009
.001251	-11.227	-11.156	-11.446	-11.375	-.150	-.079	.282	-.104
.001262	-11.350	-11.242	-11.566	-11.459	-.272	-.164	-.057	-.233
.001275	-11.487	-11.351	-11.701	-11.566	-.409	-.273	-.294	-.397
.001294	-11.647	-11.509	-11.857	-11.720	-.567	-.429	-.626	-.633
.001314	-11.773	-11.671	-11.980	-11.878	-.692	-.590	-.951	-.876
.001335	-11.873	-11.837	-12.077	-12.041	-.791	-.755	-1.242	-1.126
.001359	-11.964	-12.035	-12.164	-12.234	-.881	-.951	-1.529	-1.422
.001381	-12.027	-12.213	-12.223	-12.409	-.943	-1.129	-1.783	-1.690
.001430	-11.847	-11.692	-12.320	-12.146	-1.684	-2.380	-2.092	-1.879
.001484	-11.970	-11.889	-12.422	-12.330	-1.796	-2.644	-2.211	-2.023
.001541	-12.111	-12.102	-12.542	-12.530	-1.927	-2.930	-2.278	-2.177
.001603	-12.292	-12.331	-12.703	-12.745	-2.097	-3.245	-2.295	-2.344
.001670	-12.504	-12.580	-12.894	-12.978	-2.299	-3.590	-2.412	-2.525
.001743	-12.765	-12.850	-13.136	-13.232	-2.551	-3.973	-2.525	-2.722
.001822	-13.063	-13.145	-13.414	-13.509	-2.840	-4.398	-2.746	-2.937
.001910	-13.399	-13.469	-13.731	-13.812	-3.168	-4.874	-3.015	-3.172
.002005	-13.761	-13.824	-14.074	-14.146	-3.522	-5.410	-3.361	-3.431
.002112	-14.233	-14.218	-14.528	-14.516	-3.987	-6.017	-3.619	-3.718
.002230	-14.714	-14.655	-14.991	-14.926	-4.461	-6.711	-4.149	-4.036
.002361	-15.242	-15.144	-15.502	-15.385	-4.983	-7.514	-4.653	-4.392

Fitting results in the entire temperature range

T	V	VFNT	VFCR	VFCN	VFFM
50.05	.100000	.045729	.041916	.047220	.183638
75.12	.150000	.119218	.103723	.120245	.379017
100.17	.190000	.274938	.228622	.271701	.712813
125.22	.600000	.573755	.458602	.556947	1.242274
150.30	1.000000	1.102366	.851063	1.053327	2.032195
175.35	1.860000	1.971729	1.476784	1.858037	3.146510
200.40	3.270000	3.317881	2.420624	3.088735	4.648328
225.47	5.630000	5.293673	3.776935	4.876388	6.592209
250.52	8.600000	8.048237	5.638572	7.348210	9.012339
275.57	12.650000	11.715766	8.094285	10.620223	11.926517
300.62	17.690000	16.384554	11.214130	14.773021	15.326583
325.70	23.580000	22.079089	15.044083	19.839594	19.182983
350.75	29.640000	28.709136	19.576469	25.762834	23.426576
375.80	35.840000	36.099426	24.769893	32.422129	27.979782
400.87	41.510000	43.975909	30.533683	39.617613	32.748024
425.92	46.950000	51.972562	36.716279	47.067418	37.615765
450.97	52.400000	46.345424	40.187785	45.322347	22.184007
462.67	55.440000	53.099613	46.439729	51.985524	28.545636
476.05	59.570000	60.768890	53.788245	59.598577	37.089753
487.72	63.810000	67.125449	60.146397	65.959294	45.439528
499.42	68.730000	72.929307	66.244810	71.822067	54.279365
511.12	74.310000	77.960176	71.854825	76.963617	63.075784
519.47	78.470000	81.002113	75.458219	80.110255	68.995159
526.15	81.640000	83.089095	78.061344	82.291746	73.348936
531.17	84.140000	84.454969	79.842218	83.732460	76.333647
537.85	86.990000	86.011279	81.970639	85.390236	79.863493
546.20	88.850000	87.563757	84.241244	87.067081	83.504374
556.22	89.870000	88.918606	86.412761	88.558719	86.728488
574.60	90.460000	90.308221	89.019474	90.140012	89.881430
599.65	90.560000	90.918100	90.551567	90.878470	90.944794
624.72	90.580000	91.020123	90.955365	91.014822	91.028241
651.45	90.750000	91.029652	91.024145	91.029359	91.029996
674.82	90.800000	91.029991	91.029642	91.029980	91.030000
699.90	90.950000	91.030000	91.029991	91.030000	91.030000
724.95	90.900000	91.030000	91.030000	91.030000	91.030000

750.00	90.890000	91.030000	91.030000	91.030000	91.030000
775.05	91.040000	91.030000	91.030000	91.030000	91.030000
800.12	91.030000	91.030000	91.030000	91.030000	91.030000

Fitting rate dV/dT in the entire temperature range

T	VD	VDNT	VDCR	VDCN	VDFM
50.05	.001994	.001964	.001713	.001984	.006238
75.12	.001597	.004483	.003716	.004425	.011371
100.17	.016367	.009153	.007260	.008858	.019116
125.22	.015949	.017014	.012987	.016182	.029980
150.30	.034331	.029395	.021687	.027532	.044581
175.35	.056287	.047477	.033988	.043869	.063032
200.40	.094136	.072355	.050421	.066049	.085283
225.47	.118563	.104373	.070989	.094241	.110524
250.52	.161677	.143776	.095669	.128543	.138203
275.57	.201198	.188875	.123200	.167355	.166266
300.62	.234848	.237368	.152042	.208607	.192835
325.70	.241916	.286149	.180256	.249594	.215958
350.75	.247505	.333937	.207161	.289273	.235538
375.80	.226167	.377615	.230969	.325032	.250227
400.87	.217166	.419042	.252973	.358567	.262075
425.92	.217565	.454277	.270933	.386595	.269273
450.97	.259829	.518990	.417385	.499692	.285043
462.67	.308670	.571709	.457946	.549754	.343355
476.05	.363325	.615731	.491032	.591258	.408191
487.72	.420513	.629331	.500008	.603604	.453461
499.42	.476923	.606242	.479920	.580793	.473687
511.12	.498204	.531899	.419588	.509003	.449582
519.47	.474551	.445717	.350744	.426201	.397909
526.15	.498008	.363080	.285167	.346972	.338350
531.17	.426647	.283894	.222655	.271176	.273100
537.85	.222754	.180931	.141638	.172724	.181460
546.20	.101796	.108144	.084465	.103164	.114152
556.22	.032100	.064882	.050539	.061841	.072722
574.60	.003992	.039440	.030575	.037535	.049169
599.65	.000798	.042837	.033005	.040689	.061295
624.72	.006360	.053212	.040760	.050450	.086728
651.45	.002139	.043029	.032767	.040720	.079952
674.82	.005981	.043910	.033276	.041490	.090944
699.90	-.001996	.019056	.014370	.017978	.044086
724.95	-.000399	.038199	.028670	.035983	.098155
750.00	.005988	.050227	.037529	.047247	.142614
775.05	-.000399	-.004339	-.003228	-.004076	-.013548
800.12	-.000399	.000000	.000000	.000000	.000000

Syncrude pitch 50 °C/min, 800 °C final temperature RUN# Syn29

Experimental results Y1,Y2 and fitted results Y1F,Y2F

T	YNT	YFNT	YCR	YFCR	YCN	YFCN	YFM	YFFM
.001230	-10.282	-10.384	-10.476	-10.578	.929	.826	.683	.962
.001244	-10.463	-10.514	-10.655	-10.705	.748	.697	.855	.775
.001262	-10.700	-10.681	-10.888	-10.869	.512	.531	.651	.533
.001281	-10.930	-10.852	-11.116	-11.038	.282	.361	.440	.285
.001292	-11.047	-10.957	-11.231	-11.141	.167	.256	.210	.133
.001308	-11.179	-11.101	-11.360	-11.283	.035	.113	-.076	-.076
.001328	-11.309	-11.285	-11.488	-11.463	-.095	-.070	-.410	-.342
.001361	-11.455	-11.592	-11.629	-11.765	-.239	-.375	-.870	-.787
.001391	-11.336	-11.124	-11.718	-11.493	-.921	-1.148	-1.216	-1.112
.001442	-11.480	-11.354	-11.846	-11.713	-1.057	-1.384	-1.451	-1.275
.001492	-11.625	-11.578	-11.977	-11.927	-1.196	-1.637	-1.547	-1.434
.001545	-11.795	-11.818	-12.132	-12.157	-1.359	-1.938	-1.630	-1.605
.001602	-11.997	-12.076	-12.321	-12.404	-1.556	-2.266	-1.720	-1.788

.001670	-12.257	-12.382	-12.565	-12.698	-1.809	-2.624	-1.879	-2.006
.001743	-12.570	-12.716	-12.863	-13.018	-2.116	-2.943	-2.063	-2.243
.001824	-12.944	-13.079	-13.222	-13.366	-2.484	-3.409	-2.315	-2.502
.001896	-13.300	-13.404	-13.566	-13.677	-2.836	-3.884	-2.606	-2.732
.002001	-13.861	-13.878	-14.111	-14.131	-3.391	-4.673	-2.980	-3.069
.002107	-14.375	-14.361	-14.611	-14.594	-3.900	-6.428	-3.596	-3.413
.002285	-15.392	-15.162	-15.608	-15.362	-4.911	-8.201	-4.158	-3.983

Fitting results in the entire temperature range

T	V	VFNT	VFCR	VFCN	VFFM
51.65	.140000	.009799	.009251	.010091	.069018
100.00	.190000	.076477	.066885	.076391	.315460
164.50	.480000	.603673	.489475	.585025	1.453963
201.35	1.520000	1.542227	1.209491	1.474579	2.903798
226.70	2.760000	2.716734	2.089952	2.577077	4.403386
254.35	5.230000	4.728916	3.574526	4.452674	6.612174
275.10	7.850000	6.892639	5.154681	6.459578	8.712572
300.40	11.990000	10.464453	7.749320	9.761545	11.826934
325.75	17.060000	15.226500	11.209405	14.156507	15.572819
351.10	22.760000	21.261362	15.629579	19.730895	19.927271
374.15	28.370000	27.825962	20.516929	25.816720	24.368376
397.20	34.000000	35.271960	26.202357	32.765722	29.197021
420.20	39.550000	43.319420	32.574092	40.353804	34.309169
445.55	45.630000	52.465639	40.203254	49.112623	40.152213
461.65	49.930000	45.544597	40.142579	44.732081	25.361219
480.10	56.230000	57.049162	51.010700	56.134667	37.631151
491.60	61.490000	64.046787	57.913998	63.119553	46.535234
500.85	66.500000	69.320859	63.320820	68.418263	54.065860
507.75	70.620000	72.949788	67.174942	72.086372	59.693159
519.25	77.790000	78.265718	73.090112	77.503543	68.630844
530.80	83.510000	82.552398	78.202721	81.925942	76.428641
540.00	86.620000	85.182659	81.583735	84.676348	81.413289
553.80	88.850000	87.920141	85.456989	87.589287	86.580788
574.55	89.660000	89.941164	88.853273	89.808968	89.957255
599.90	89.980000	90.609394	90.362395	90.584542	90.669984
650.55	90.220000	90.699888	90.698331	90.699812	90.700000
698.95	90.400000	90.700000	90.700000	90.700000	90.700000
749.60	90.570000	90.700000	90.700000	90.700000	90.700000
800.30	90.700000	90.700000	90.700000	90.700000	90.700000

Fitting rate dV/dT in the entire temperature range

T	VD	VDNT	VDCR	VDCN	VDFM
51.65	.001034	.000490	.000446	.000497	.002632
100.00	.004496	.002968	.002509	.002925	.009479
164.50	.028223	.017630	.013835	.016868	.033618
201.35	.048915	.038858	.029491	.036688	.058773
226.70	.089331	.062112	.046199	.058174	.081707
254.35	.126265	.096965	.070713	.090106	.111234
275.10	.163636	.129992	.093525	.120147	.135785
300.40	.200000	.177651	.125892	.163208	.167061
325.75	.224852	.232004	.162139	.211965	.198132
351.10	.243384	.290795	.200647	.264330	.227298
374.15	.244252	.345237	.235665	.312477	.250483
397.20	.241304	.399266	.269833	.359941	.270272
420.20	.239842	.450452	.301601	.404580	.285841
445.55	.267081	.499500	.331252	.446924	.296595
461.65	.341463	.577103	.476958	.560143	.371255
480.10	.457391	.663253	.545310	.642807	.489652
491.60	.541622	.675488	.553640	.654083	.541543
500.85	.597101	.646257	.528390	.625343	.552650
507.75	.623478	.595681	.486170	.576110	.533992
519.25	.495238	.454474	.369847	.439180	.439911
530.80	.338043	.299108	.242723	.288809	.312035

540.00	.161594	.193218	.156450	.186448	.213631
553.80	.039036	.105838	.085423	.102036	.127370
574.55	.012623	.078144	.062780	.075238	.106271
599.90	.004738	.074164	.059265	.071297	.116186
650.55	.003719	.088169	.069767	.084523	.179029
698.95	.003356	.090528	.071034	.086578	.229655
749.60	.002564	.062715	.048819	.059842	.196353
800.30	.002564	.000000	.000000	.000000	.000000

Syncrude pitch 100 °C/min, 800 °C final temperature RUN# Syn18

Experimental results Y1,Y2 and fitted results Y1F,Y2F

T	YNT	YFNT	YCR	YFCR	YCN	YFCN	YFM	YFFM
.001127	-9.308	-9.498	-9.564	-9.751	1.722	1.534	.232	1.444
.001158	-9.516	-9.743	-9.764	-9.990	1.517	1.291	.996	1.152
.001176	-9.785	-9.889	-10.028	-10.132	1.250	1.146	1.482	.978
.001191	-10.007	-10.001	-10.247	-10.241	1.029	1.035	1.452	.844
.001205	-10.215	-10.116	-10.452	-10.354	.822	.921	1.225	.707
.001220	-10.398	-10.235	-10.631	-10.469	.641	.803	.947	.566
.001236	-10.552	-10.356	-10.782	-10.587	.487	.683	.653	.422
.001251	-10.677	-10.480	-10.904	-10.708	.364	.560	.336	.273
.001267	-10.772	-10.606	-10.996	-10.831	.270	.435	.016	.123
.001284	-10.850	-10.737	-11.071	-10.958	.192	.305	-.242	-.033
.001301	-10.918	-10.871	-11.135	-11.089	.126	.172	-.435	-.193
.001324	-10.997	-11.056	-11.209	-11.269	.049	-.011	-.639	-.413
.001343	-11.055	-11.199	-11.264	-11.408	-.009	-.152	-.724	-.583
.001368	-11.131	-11.396	-11.337	-11.599	-.084	-.347	-.830	-.818
.001393	-11.100	-10.908	-11.415	-11.214	-.489	-.811	-.882	-.689
.001427	-11.212	-11.087	-11.518	-11.388	-.598	-.973	-.973	-.818
.001455	-11.318	-11.236	-11.617	-11.532	-.700	-1.143	-.977	-.924
.001492	-11.453	-11.432	-11.744	-11.722	-.832	-1.319	-1.114	-1.064
.001523	-11.579	-11.596	-11.863	-11.881	-.956	-1.503	-1.153	-1.182
.001555	-11.720	-11.768	-11.997	-12.047	-1.094	-1.696	-1.228	-1.304
.001589	-11.868	-11.946	-12.139	-12.220	-1.239	-1.950	-1.357	-1.432
.001624	-12.032	-12.133	-12.295	-12.401	-1.400	-2.218	-1.463	-1.565
.001661	-12.210	-12.327	-12.467	-12.589	-1.576	-2.562	-1.593	-1.704
.001709	-12.463	-12.584	-12.712	-12.838	-1.826	-2.998	-1.740	-1.888
.001760	-12.760	-12.855	-13.000	-13.101	-2.120	-3.473	-1.922	-2.082
.001826	-13.145	-13.204	-13.376	-13.438	-2.502	-4.077	-2.241	-2.331
.001909	-13.593	-13.644	-13.813	-13.865	-2.946	-5.319	-2.719	-2.646
.001999	-14.121	-14.124	-14.330	-14.330	-3.471	-6.997	-3.127	-2.989
.002114	-15.006	-14.735	-15.203	-14.922	-4.353	-9.207	-3.556	-3.426

Fitting results in the entire temperature range

T	V	VFNT	VFCR	VFCN	VFFM
50.40	.010000	.001540	.001496	.001588	.016485
101.40	.000000	.018878	.017085	.018978	.105664
152.30	.080000	.129853	.111371	.128043	.442528
199.90	.420000	.550585	.453851	.535174	1.293837
227.10	1.120000	1.116204	.902845	1.077492	2.185278
250.80	2.050000	1.948625	1.553575	1.871033	3.301432
274.60	3.440000	3.247629	2.557005	3.103598	4.816467
295.00	5.330000	4.856552	3.789285	4.624784	6.483361
312.00	7.450000	6.635186	5.144724	6.302401	8.163141
329.00	9.930000	8.884788	6.854845	8.420862	10.127888
342.60	12.160000	11.066733	8.513106	10.473818	11.914502
356.20	14.630000	13.618970	10.455958	12.874559	13.896846
369.80	17.290000	16.562265	12.704596	15.643977	16.076091
383.40	20.210000	19.907563	15.275332	18.794581	18.449990
397.00	23.230000	23.653224	18.177902	22.328055	21.012616
414.00	26.990000	28.871191	22.274075	27.264504	24.466045
427.50	30.220000	33.395664	25.885633	31.561762	27.389481

444.50	34.100000	39.480515	30.848632	37.371937	31.268862
458.10	37.280000	30.294054	25.465104	29.445278	17.320647
471.70	40.440000	36.300444	30.645522	35.289245	21.944588
481.90	42.920000	41.121766	34.873027	39.993312	25.922760
495.50	46.340000	47.837747	40.887724	46.571202	31.885258
505.70	49.260000	52.973813	45.607671	51.626478	36.804164
515.90	52.570000	58.079517	50.426936	56.678531	42.037160
526.00	56.470000	62.995823	55.214767	61.574160	47.440367
536.20	61.340000	67.710001	59.976033	66.304153	53.008302
546.40	67.070000	72.070023	64.570176	70.718213	58.555721
556.60	73.250000	75.990181	68.907305	74.728841	63.938346
566.80	79.270000	79.408748	72.906769	78.269233	69.011118
577.00	84.200000	82.293013	76.502948	81.298659	73.641053
590.60	88.020000	85.308779	80.594647	84.526661	78.944401
614.40	89.670000	88.564528	85.747974	88.135044	85.506564
644.90	90.020000	90.176356	89.132030	90.041295	89.407948
699.30	90.270000	90.574109	90.516899	90.569747	90.561938
801.20	90.580000	90.580000	90.579999	90.580000	90.580000

Fitting rate dV/dT in the entire temperature range

T	VD	VDNT	VDCR	VDCN	VDFM
50.40	-.000196	.000089	.000084	.000091	.000721
101.40	.001572	.000832	.000734	.000829	.003566
152.30	.007143	.004537	.003793	.004433	.011985
199.90	.025735	.015877	.012761	.015295	.029320
227.10	.039241	.029010	.022876	.027756	.045017
250.80	.058403	.046410	.036052	.044166	.062805
274.60	.092647	.070968	.054374	.067202	.084707
295.00	.124706	.098349	.074537	.092766	.106299
312.00	.145882	.125836	.094563	.118330	.125877
329.00	.163971	.157746	.117598	.147911	.146683
342.60	.181618	.186382	.138102	.174379	.163949
356.20	.195588	.217506	.160227	.203072	.181427
369.80	.214706	.250916	.183810	.233795	.198912
383.40	.222059	.285889	.208314	.265870	.215849
397.00	.221176	.322448	.233749	.299315	.232321
414.00	.239259	.370407	.266876	.343077	.252370
427.50	.228235	.408066	.292643	.377325	.266473
444.50	.233824	.456957	.325871	.421681	.283511
458.10	.232353	.392638	.311918	.376596	.235294
471.70	.243137	.449670	.355393	.430556	.279832
481.90	.251471	.493090	.388258	.471541	.315379
495.50	.286275	.550524	.431395	.525615	.364805
505.70	.324510	.588064	.459198	.560798	.399845
515.90	.386139	.616536	.479789	.587278	.429851
526.00	.477451	.627702	.486870	.597254	.448357
536.20	.561765	.609276	.471047	.579092	.445692
546.40	.605882	.552983	.426173	.525030	.414022
556.60	.590196	.458760	.352468	.435121	.351351
566.80	.483333	.335994	.257369	.318359	.263082
577.00	.280882	.212114	.162001	.200783	.169709
590.60	.069328	.098484	.074930	.093104	.081032
614.40	.011475	.044710	.033800	.042177	.038554
644.90	.004596	.036952	.027721	.034769	.033719
699.30	.003042	.033062	.024494	.030979	.033079
801.20	.003042	.000000	.000000	.000000	.000000

Syncrude pitch 150 °C/min, 800 °C final temperature RUN# Syn08

Experimental results Y1,Y2 and fitted results Y1F,Y2F

T	YNT	YFNT	YCR	YFCR	YCN	YFCN	YFM	YFFM
.001129	-8.944	-9.092	-9.181	-9.327	2.158	2.011	.707	1.861

.001153	-9.102	-9.290	-9.333	-9.521	2.002	1.814	1.507	1.643
.001171	-9.317	-9.445	-9.544	-9.672	1.788	1.660	1.795	1.473
.001190	-9.581	-9.605	-9.804	-9.829	1.526	1.501	1.742	1.297
.001203	-9.764	-9.715	-9.984	-9.936	1.344	1.392	1.677	1.176
.001217	-9.942	-9.828	-10.160	-10.046	1.166	1.280	1.494	1.052
.001230	-10.107	-9.941	-10.322	-10.157	1.003	1.168	1.280	.928
.001244	-10.243	-10.058	-10.456	-10.272	.867	1.051	.965	.798
.001258	-10.351	-10.177	-10.560	-10.387	.760	.934	.658	.668
.001273	-10.437	-10.300	-10.644	-10.508	.675	.812	.364	.533
.001288	-10.513	-10.426	-10.717	-10.631	.600	.687	.171	.394
.001311	-10.610	-10.619	-10.810	-10.820	.504	.494	-.063	.182
.001335	-10.695	-10.818	-10.892	-11.014	.420	.297	-.261	-.037
.001368	-10.808	-11.098	-10.999	-11.288	.309	.019	-.415	-.345
.001394	-10.787	-10.634	-11.086	-10.926	-.124	-.269	-.479	-.297
.001421	-10.892	-10.784	-11.184	-11.072	-.227	-.486	-.517	-.409
.001449	-11.001	-10.938	-11.287	-11.222	-.334	-.714	-.605	-.525
.001489	-11.162	-11.158	-11.439	-11.434	-.491	-.954	-.715	-.690
.001530	-11.349	-11.387	-11.617	-11.657	-.674	-1.210	-.800	-.862
.001574	-11.553	-11.630	-11.813	-11.893	-.876	-1.549	-.956	-1.044
.001620	-11.784	-11.888	-12.036	-12.145	-1.104	-1.918	-1.121	-1.238
.001682	-12.125	-12.231	-12.366	-12.477	-1.440	-2.314	-1.309	-1.496
.001749	-12.481	-12.603	-12.711	-12.839	-1.793	-2.748	-1.676	-1.775
.001821	-12.947	-13.004	-13.167	-13.228	-2.255	-3.218	-1.906	-2.076
.001900	-13.438	-13.442	-13.648	-13.654	-2.743	-3.957	-2.406	-2.405
.001986	-13.882	-13.916	-14.083	-14.115	-3.185	-6.081	-3.021	-2.761
.002120	-14.878	-14.663	-15.064	-14.840	-4.176	-9.310	-3.387	-3.321

Fitting results in the entire temperature range

T	V	VFNT	VFCR	VFCN	VFFM
50.00	.020000	.000891	.000867	.000917	.007966
125.75	.070000	.034308	.030388	.034164	.134342
198.50	.320000	.396712	.330372	.386644	.896348
230.45	.970000	.938068	.764888	.907488	1.746136
253.10	1.630000	1.623374	1.306550	1.563176	2.669480
275.90	2.850000	2.694018	2.143508	2.583332	3.949116
298.55	4.820000	4.276303	3.369713	4.085792	5.642770
321.35	7.260000	6.553257	5.123781	6.242050	7.845678
344.00	10.660000	9.663453	7.513555	9.182153	10.591947
362.30	13.840000	12.900822	10.003840	12.240464	13.249213
380.45	17.410000	16.819236	13.031557	15.943453	16.286221
398.60	21.390000	21.474008	16.658307	20.348467	19.723079
416.90	25.520000	26.901856	20.942446	25.498709	23.578196
430.40	28.720000	31.342672	24.502038	29.726985	26.655275
444.05	32.080000	36.156700	28.427027	34.329008	29.947086
457.70	35.380000	28.033573	23.801644	27.333528	18.612215
476.00	39.830000	36.320795	31.011915	35.421705	25.296279
489.50	43.350000	43.062424	37.006635	42.024491	31.104254
503.15	47.390000	50.205200	43.520235	49.050957	37.654348
512.30	50.520000	55.048013	48.054191	53.837831	42.353987
521.45	54.040000	59.830187	52.646333	58.587362	47.227206
530.45	58.280000	64.382933	57.147460	63.134447	52.111450
539.60	63.460000	68.766400	61.629215	67.541374	57.077576
548.60	69.320000	72.755015	65.867186	71.582191	61.864936
557.75	75.110000	76.412080	69.927104	75.320122	66.530691
566.90	80.170000	79.617170	73.668578	78.629972	70.894557
580.55	85.600000	83.505731	78.543562	82.705429	76.659233
594.20	88.350000	86.344521	82.480538	85.744533	81.356480
612.35	89.590000	88.711449	86.251528	88.354415	85.839815
639.65	89.970000	90.211576	89.281375	90.095072	89.313126
689.60	90.300000	90.613468	90.562245	90.609490	90.585096
798.80	90.620000	90.620000	90.620000	90.620000	90.620000

Fitting rate dV/dT in the entire temperature range

T	VD	VDNT	VDCR	VDCN	VDFM
50.00	.000660	.000054	.000051	.000055	.000376
125.75	.003436	.001397	.001208	.001379	.004351
198.50	.020344	.011908	.009689	.011514	.021734
230.45	.029139	.024939	.019867	.023937	.037795
253.10	.053509	.039780	.031266	.038002	.053566
275.90	.086976	.060793	.047191	.057825	.073400
298.55	.107018	.088697	.068073	.084034	.096922
321.35	.150110	.125044	.094960	.118035	.124536
344.00	.173770	.168954	.127063	.158945	.154501
362.30	.196694	.210191	.156917	.197232	.180199
380.45	.219284	.255424	.189377	.239103	.206139
398.60	.225683	.303822	.223798	.283764	.231577
416.90	.237037	.355679	.260370	.331479	.256700
430.40	.246154	.394629	.287620	.367218	.274068
444.05	.241758	.433662	.314724	.402941	.290120
457.70	.243169	.389133	.314606	.375285	.260778
476.00	.260741	.473696	.380539	.455912	.326435
489.50	.295971	.537611	.429941	.516685	.377864
503.15	.342077	.596677	.475083	.572649	.427533
512.30	.384699	.627795	.498431	.601965	.455504
521.45	.471111	.647704	.512801	.620502	.475739
530.45	.566120	.644567	.508947	.616969	.479042
539.60	.651111	.608896	.479497	.582329	.457857
548.60	.632787	.534725	.420008	.510976	.406636
557.75	.553005	.435741	.341385	.416050	.335093
566.90	.397802	.327743	.256132	.312683	.254815
580.55	.201465	.184725	.143840	.176034	.145923
594.20	.068320	.097515	.075665	.092822	.078226
612.35	.013919	.053958	.041679	.051288	.044148
639.65	.006607	.045216	.034702	.042890	.038054
689.60	.002930	.035875	.027236	.033912	.031660
798.80	.002930	.000000	.000000	.000000	.000000

APPENDIX F Summary of Kinetic Parameters of the 2-Stage Model

E_1, E_2	Reaction activation energy	J/mol
k_{o1}, k_{o2}	pre-exponential factors	min^{-1}
s.e.e	Standard deviation for each method, %	

CANMET pitch 25 °C/min., 800 °C

Activation energies and pre-exponential factors for both reactions

	E_1	k_{o1}	E_2	k_{o2}	s.e.e
2-Integral	21895.871	5.534	71347.395	44484.445	1.425598
2-Coats-Redfern	18317.044	1.207	69931.248	28659.014	8.666605
2-Chen-Nuttall	19815.807	2.663	70918.682	40047.550	4.464558
2-Friedman	18356.762	2.169	39422.571	222.056	5.683572

CANMET Pitch 50 °C/min., 800 °C

Activation energies and pre-exponential factor for both reactions

	E_1	k_{o1}	E_2	k_{o2}	s.e.e
2-Integral	20907.935	7.649	64473.015	24448.637	2.128091
2-Coats-Redfern	17507.079	1.688	62943.175	15044.712	8.270525
2-Chen-Nuttall	18939.224	3.717	63977.704	21585.114	4.639823
2-Friedman	12109.801	0.833	54006.641	3350.699	11.413135

CANMET pitch 100 °C/min., 800 °C

Activation energies and pre-exponential factor for both reactions

	E_1	k_{o1}	E_2	k_{o2}	s.e.e.
2-Integral	26914.040	39.637	72117.918	111143.981	1.446535
2-Coats-Redfern	24063.137	12.482	70720.507	72034.563	4.703861
2-Chen-Nuttall	25429.522	24.221	71699.067	100310.634	1.899520
2-Friedman	21904.369	12.635	108819.449	31432193.146	5.279363

CANMET pitch 150 °C/min., 800 °C

Activation energies and pre-exponential factor for both reactions

	E_1	k_{o1}	E_2	k_{o2}	s.e.e
2-Integral	46648.168	552.339	96651.309	3510920.010	0.975426
2-Coats-Redfern	45065.482	304.766	95534.758	2529475.085	2.908742
2-Chen-Nuttall	46065.844	463.684	96377.125	3296730.811	1.027556
2-Friedman	52896.511	2804.999	92011.326	1699475.805	1.499851

Syncrude Pitch 25 °C/min., 800 °C

Activation energies and pre-exponential factor for both reactions

	E_1	k_{o1}	E_2	k_{o2}	s.e.e.
2-Integral	30825.690	51.805	67665.168	25546.591	1.941470
2-Coats-Redfern	28925.970	22.282	66149.761	15973.274	5.238812
2-Chen-Nuttall	29969.525	38.048	67185.904	22714.511	2.066038
2-Friedman	22436.425	7.251	101506.600	3875272.258	9.746673

Syncrude pitch 50 °C/min., 800 °C

Activation energies and pre-exponential factor for both reactions

	E_1	k_{o1}	E_2	k_{o2}	s.e.e
2-Integral	37574.160	298.225	76570.633	196413.926	2.079083
2-Coats-Redfern	36007.909	152.170	75271.326	131230.169	4.555376
2-Chen-Nuttall	36950.208	240.377	76200.343	179430.028	1.827761
2-Friedman	26717.957	28.783	110908.304	34882245.211	8.003341

Syncrude pitch 100 °C/min., 800 °C

Activation energies and pre-exponential factor for both reactions

	E_1	k_{o1}	E_2	k_{o2}	s.e.e
2-Integral	44166.789	1326.666	65511.067	35233.527	2.970666
2-Coats-Redfern	42786.603	750.710	63799.493	21122.231	4.667832
2-Chen-Nuttall	43670.266	1126.495	64938.056	30754.384	2.683058
2-Friedman	31580.121	99.840	78074.842	166743.612	8.111536

Syncrude pitch 150 °C/min., 800 °C

Activation energies and pre-exponential factor for both reactions

	E_1	k_{o1}	E_2	k_{o2}	S.e.e
2-Integral	46141.423	2549.212	69808.233	103113.970	2.859655
2-Coats-Redfern	44831.086	1485.078	68221.838	64209.953	4.405498
2-Chen-Nuttall	45685.309	2194.201	69303.236	91513.836	2.586208
2-Friedman	34645.511	248.057	76752.670	216684.308	6.605246

APPENDIX G Kinetic Reaction Rate Constant lnk - 1/T for CANMET and Syncrude Pitches

CANMET PITCH 2-stage model kinetic reaction rate lnk-1/T

Integral method

1/T K^{-1}	25 °C/min	50 °C/min	100 °C/min	150 °C/min
800 - 450 °C				
0.93183	2.70633	2.87824	3.53565	4.23878
0.97736	2.31555	2.52511	3.14066	3.70941
1.02758	1.88462	2.13570	2.70507	3.12564
1.08324	1.40700	1.70410	2.22230	2.47863
1.14527	0.87469	1.22308	1.68424	1.75753
1.21483	0.27771	0.68362	1.08081	0.94883
1.29339	-0.39649	0.07438	0.39933	0.03553
1.38282	-1.16391	-0.61910	-0.37638	-1.00407
450 - 50 °C				
1.38282	-1.93090	-1.44292	-0.79669	-1.44456
1.48553	-2.20140	-1.70122	-1.12919	-2.02085
1.60472	-2.51531	-2.00096	-1.51504	-2.68962
1.74471	-2.88399	-2.35301	-1.96822	-3.47507
1.91146	-3.32314	-2.77234	-2.50801	-4.41066
2.11345	-3.85510	-3.28030	-3.16189	-5.54398
2.36317	-4.51277	-3.90830	-3.97029	-6.94512
2.67982	-5.34669	-4.70459	-4.99532	-8.72174
3.09444	-6.43866	-5.74729	-6.33755	-11.04810

Chen-Nuttall method

1/T K^{-1}	25 °C/min	50 °C/min	100 °C/min	150 °C/min
800 - 450 °C				
0.93183	2.64931	2.80918	3.48004	4.20656
0.97736	2.26088	2.45877	3.08734	3.67869
1.02758	1.83253	2.07235	2.65428	3.09658
1.08324	1.35779	1.64407	2.17431	2.45141
1.14527	0.82867	1.16674	1.63938	1.73235
1.21483	0.23528	0.63142	1.03945	0.92594
1.29339	-0.43486	0.02687	0.36194	0.01523
1.38282	-1.19767	-0.66128	-0.40927	-1.02141
450 - 50 °C				
1.38282	-2.31640	-1.83714	-1.04233	-1.52266
1.48553	-2.56120	-2.07111	-1.35648	-2.09176
1.60472	-2.84529	-2.34263	-1.72105	-2.75218
1.74471	-3.17894	-2.66153	-2.14923	-3.52783
1.91146	-3.57637	-3.04138	-2.65925	-4.45174
2.11345	-4.05780	-3.50150	-3.27706	-5.57091
2.36317	-4.65299	-4.07037	-4.04087	-6.95456
2.67982	-5.40769	-4.79168	-5.00937	-8.70900
3.09444	-6.39592	-5.73620	-6.27756	-11.00630

CANMET SINGLE OVERALL MODEL lnk-1/T

700 - 50 °C				
1/T K^{-1}	Integral	C-R	C-N	Friedman
1.02758	0.92624	0.27246	0.68931	0.85065
1.08324	0.70466	0.06628	0.47509	0.63309
1.14527	0.45771	-0.16351	0.23635	0.39061
1.21483	0.18075	-0.42122	-0.03141	0.11868
1.29339	-0.13202	-0.71227	-0.33379	-0.18843
1.38282	-0.48805	-1.04356	-0.67799	-0.53800
1.48553	-0.89697	-1.42406	-1.07331	-0.93951
1.60472	-1.37151	-1.86562	-1.53208	-1.40544
1.74471	-1.92884	-2.38423	-2.07089	-1.95267
1.91146	-2.59270	-3.00196	-2.71269	-2.60450
2.11345	-3.39686	-3.75024	-3.49013	-3.39409
2.36317	-4.39107	-4.67536	-4.45129	-4.37027
2.67982	-5.65170	-5.84840	-5.67003	-5.60805
3.09444	-7.30243	-7.38442	-7.26590	-7.22885

Coats-Redfern method

1/T K^{-1}	25 °C/min	50 °C/min	100 °C/min	150 °C/min
800 - 450 °C				
0.93183	2.42538	2.56415	3.25860	4.03605
0.97736	2.04236	2.21941	2.87125	3.51280
1.02758	1.61998	1.83923	2.44410	2.93577
1.08324	1.15184	1.41788	1.97069	2.29624
1.14527	0.63009	0.94827	1.44305	1.58347
1.21483	0.04496	0.42161	0.85132	0.78411
1.29339	-0.61585	-0.17317	0.18305	-0.11864
1.38282	-1.36804	-0.85019	-0.57763	-1.14622
450 - 50 °C				
1.38282	-2.85843	-2.38831	-1.47800	-1.77594
1.48553	-3.08472	-2.60459	-1.77527	-2.33268
1.60472	-3.34732	-2.85558	-2.12025	-2.97876
1.74471	-3.65574	-3.15036	-2.52542	-3.73756
1.91146	-4.02311	-3.50149	-3.00804	-4.64140
2.11345	-4.46812	-3.92682	-3.59265	-5.73627
2.36317	-5.01830	-4.45267	-4.31542	-7.08987
2.67982	-5.71592	-5.11944	-5.23188	-8.80622
3.09444	-6.62940	-5.99253	-6.43193	-11.05370

Friedman method

1/T K^{-1}	25 °C/min	50 °C/min	100 °C/min	150 °C/min
800 - 450 °C				
0.93183	0.98447	2.06390	5.06693	4.03326
0.97736	0.76855	1.76810	4.47092	3.52931
1.02758	0.53044	1.44190	3.81365	2.97356
1.08324	0.26654	1.08037	3.08520	2.35762
1.14527	-0.02759	0.67743	2.27331	1.67114
1.21483	-0.35744	0.22555	1.36279	0.90126
1.29339	-0.72997	-0.28479	0.33451	0.03180
1.38282	-1.15400	-0.86569	-0.83597	-0.95788
450 - 50 °C				
1.38282	-2.27891	-2.19688	-1.10676	-0.85881
1.48553	-2.50569	-2.34648	-1.37736	-1.51230
1.60472	-2.76886	-2.52009	-1.69139	-2.27065
1.74471	-3.07795	-2.72399	-2.06022	-3.16131
1.91146	-3.44611	-2.96687	-2.49953	-4.22221
2.11345	-3.89209	-3.26108	-3.03170	-5.50733
2.36317	-4.44346	-3.62481	-3.68963	-7.09615
2.67982	-5.14259	-4.08602	-4.52387	-9.11074
3.09444	-6.05806	-4.68995	-5.61626	-11.74870

SYNCRUDE PITCH 2-STAGE MODEL KINETIC reaction rate lnk-1/T

Integral method

1/T K^{-1}	25 °C/min	50 °C/min	100 °C/min	150 °C/min
800 - 450 °C				
0.93183	2.56439	3.60600	3.12732	3.71953
0.97736	2.19378	3.18661	2.76851	3.33718
1.02758	1.78509	2.72413	2.37282	2.91555
1.08324	1.33213	2.21155	1.93428	2.44824
1.14527	0.82729	1.64027	1.44551	1.92741
1.21483	0.26112	0.99958	0.89736	1.34330
1.29339	-0.37828	0.27603	0.27832	0.68366
1.38282	-1.10610	-0.54757	-0.42633	-0.06721
450 - 50 °C				
1.38282	-1.17957	-0.55165	-0.15558	0.16910
1.48553	-1.56039	-1.01584	-0.70122	-0.40093
1.60472	-2.00232	-1.55452	-1.33442	-1.06243
1.74471	-2.52136	-2.18718	-2.07809	-1.83935
1.91146	-3.13961	-2.94078	-2.96391	-2.76478
2.11345	-3.88852	-3.85364	-4.03694	-3.88578
2.36317	-4.81441	-4.98224	-5.36355	-5.27170
2.67982	-5.98842	-6.41327	-7.04567	-7.02903
3.09444	-7.52573	-8.28713	-9.24830	-9.33014

Coats-Redfern method

1/T K^{-1}	25 °C/min	50 °C/min	100 °C/min	150 °C/min
800 - 450 °C				
0.93183	2.26465	3.34835	2.80748	3.42366
0.97736	1.90234	2.93608	2.45804	3.05000
1.02758	1.50280	2.48145	2.07270	2.63794
1.08324	1.05998	1.97756	1.64561	2.18125
1.14527	0.56645	1.41598	1.16961	1.67226
1.21483	0.01296	0.78616	0.63578	1.10143
1.29339	-0.61212	0.07489	0.03291	0.45677
1.38282	-1.32364	-0.73474	-0.65332	-0.27703
450 - 50 °C				
1.38282	-1.70731	-0.96399	-0.49543	-0.15327
1.48553	-2.06466	-1.40883	-1.02402	-0.70712
1.60472	-2.47936	-1.92506	-1.63742	-1.34984
1.74471	-2.96641	-2.53135	-2.35786	-2.10469
1.91146	-3.54655	-3.25353	-3.21599	-3.00384
2.11345	-4.24931	-4.12835	-4.25550	-4.09301
2.36317	-5.11814	-5.20989	-5.54065	-5.43957
2.67982	-6.21980	-6.58128	-7.17020	-7.14699
3.09444	-7.66237	-8.37702	-9.30401	-9.38275

Chen-Nuttall method

1/T K^{-1}	25 °C/min	50 °C/min	100 °C/min	150 °C/min
800 - 450 °C				
0.93183	2.50061	3.55706	3.05557	3.65679
0.97736	2.13262	3.13970	2.69990	3.27720
1.02758	1.72683	2.67945	2.30768	2.85862
1.08324	1.27707	2.16935	1.87297	2.39469
1.14527	0.77580	1.60083	1.38848	1.87763
1.21483	0.21364	0.96325	0.84513	1.29775
1.29339	-0.42123	0.24320	0.23150	0.64287
1.38282	-1.14389	-0.57642	-0.46699	-0.10256
450 - 50 °C				
1.38282	-1.34581	-0.66351	-0.23656	0.09500
1.48553	-1.71605	-1.11999	-0.77606	-0.46940
1.60472	-2.14571	-1.64973	-1.40214	-1.12436
1.74471	-2.65033	-2.27188	-2.13745	-1.89360
1.91146	-3.25141	-3.01297	-3.01331	-2.80988
2.11345	-3.97952	-3.91067	-4.07428	-3.91980
2.36317	-4.87969	-5.02052	-5.38598	-5.29202
2.67982	-6.02110	-6.42779	-7.04918	-7.03197
3.09444	-7.51571	-8.27053	-9.22706	-9.31034

Friedman method

1/T K^{-1}	25 °C/min	50 °C/min	100 °C/min	150 °C/min
800 - 450 °C				
0.93183	3.79334	4.93696	3.27364	3.68381
0.97736	3.23737	4.32950	2.84601	3.26343
1.02758	2.62428	3.65962	2.37445	2.79985
1.08324	1.94477	2.91718	1.85180	2.28605
1.14527	1.18745	2.08971	1.26929	1.71341
1.21483	0.33812	1.16171	0.61602	1.07120
1.29339	-0.62106	0.11369	-0.12174	0.34593
1.38282	-1.71288	-1.07925	-0.96153	-0.47963
450 - 50 °C				
1.38282	-1.75058	-1.08406	-0.64897	-0.24873
1.48553	-2.02776	-1.41413	-1.03911	-0.67674
1.60472	-2.34942	-1.79717	-1.49186	-1.17343
1.74471	-2.72720	-2.24704	-2.02360	-1.75679
1.91146	-3.17719	-2.78291	-2.65698	-2.45165
2.11345	-3.72228	-3.43202	-3.42422	-3.29336
2.36317	-4.39619	-4.23453	-4.37277	-4.33399
2.67982	-5.25070	-5.25210	-5.57551	-5.65348
3.09444	-6.36962	-6.58455	-7.15044	-7.38128

Compensation Effect of Kinetic Parameters Derived other 2-Stage Methods

The logarithms of reaction rate constants, calculated with the kinetic parameters derived from the 2-stage Coats-Redfern method, were plotted in Figures G.1 and G.4 for CANMET and Syncrude pitch respectively. The logarithms of reaction rate constants, calculated with the kinetic parameters derived from the 2-stage Chen-Nuttall method, were plotted in Figures G.2 and G.5 for CANMET and Syncrude pitch respectively. The logarithms of reaction rate constants, calculated with the kinetic parameters derived from the 2-stage Friedman method, were plotted in Figures G.3 and G.6 for CANMET and Syncrude pitch respectively. Examination of these graphs reveals that the second criterion of compensation effect is not met.

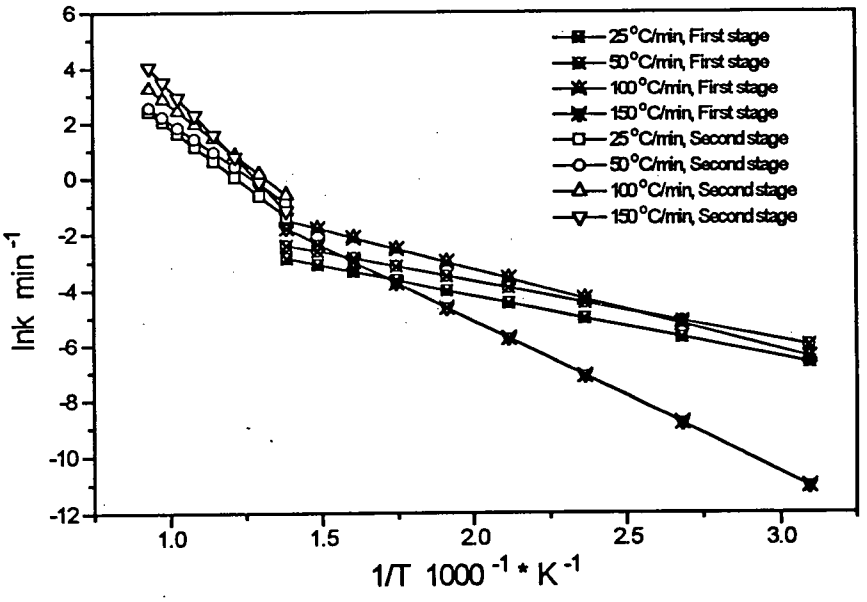

Figure G.1 CANMET pitch pyrolysis kinetic reaction rate as a function of temperature at different heating rates and final temperature 800 °C with 2-stage Coats-Redfern method

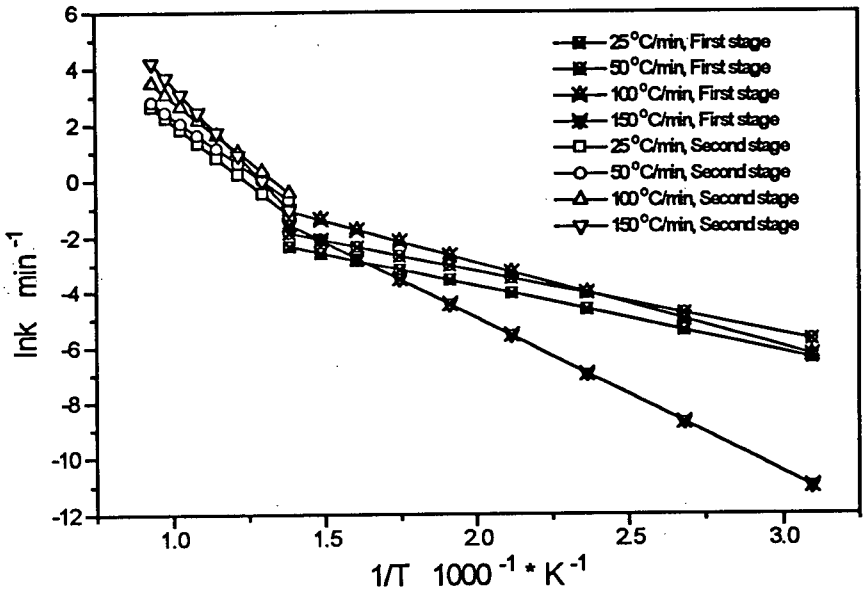

Figure G.2 CANMET pitch pyrolysis kinetic reaction rate as a function of temperature at different heating rates and final temperature 800 °C with 2-stage Chen-Nuttall method

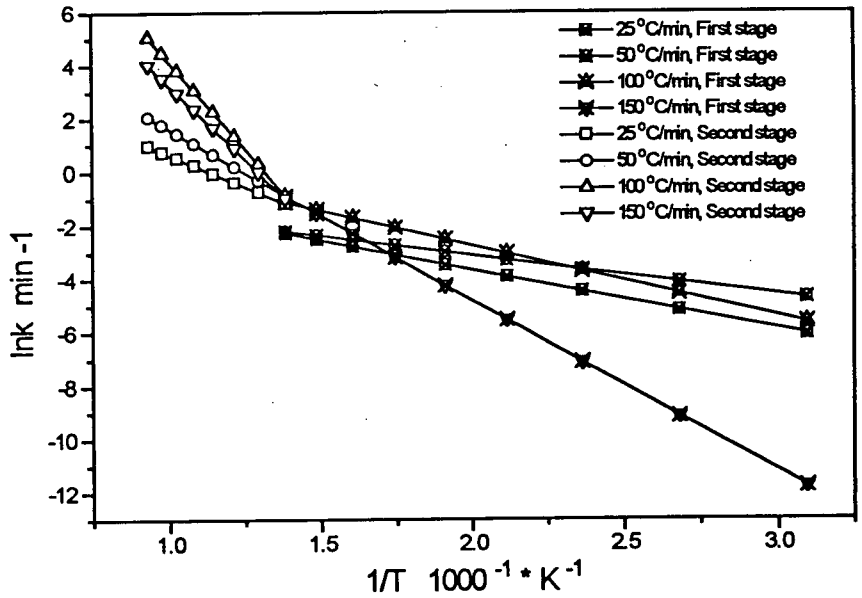

Figure G.3 CANMET pitch pyrolysis kinetic reaction rate as a function of temperature at different heating rates and final temperature 800 °C with 2-stage Friedman method

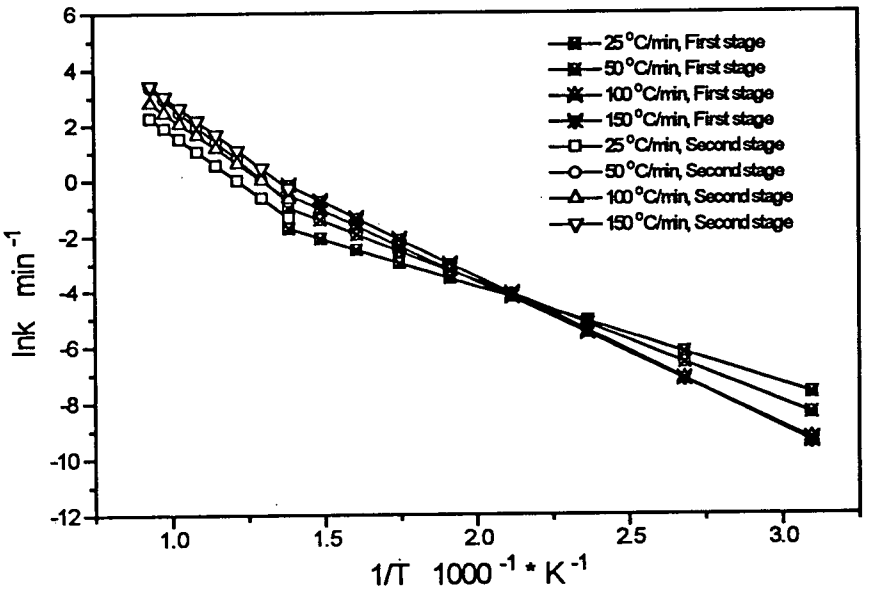

Figure G.4 Syncrude pitch pyrolysis kinetic reaction rate as a function of temperature at different heating rates and final temperature 800 °C with 2-stage Coats-Redfern method

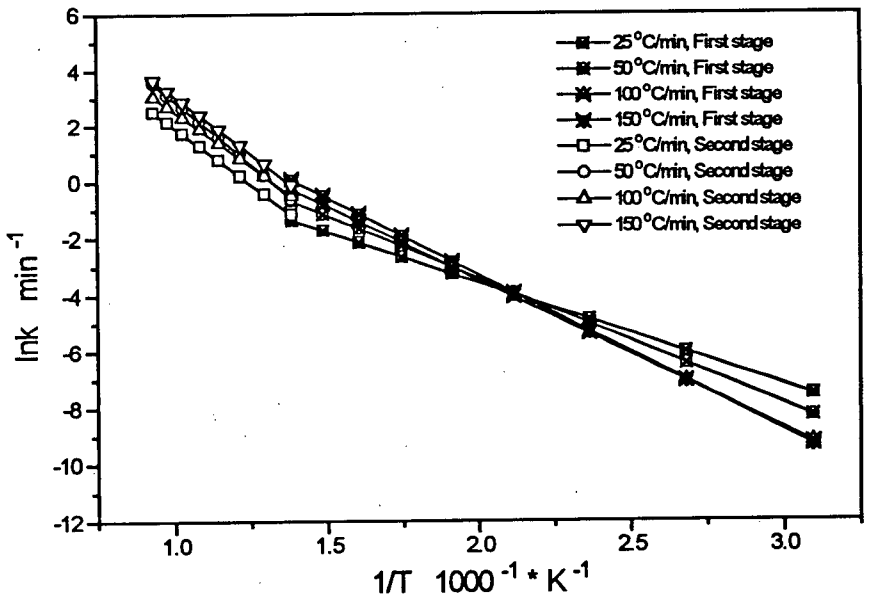

Figure G.5 Syncrude pitch pyrolysis kinetic reaction rate as a function of temperature at different heating rates and final temperature 800 °C with 2-stage Chen-Nuttall method

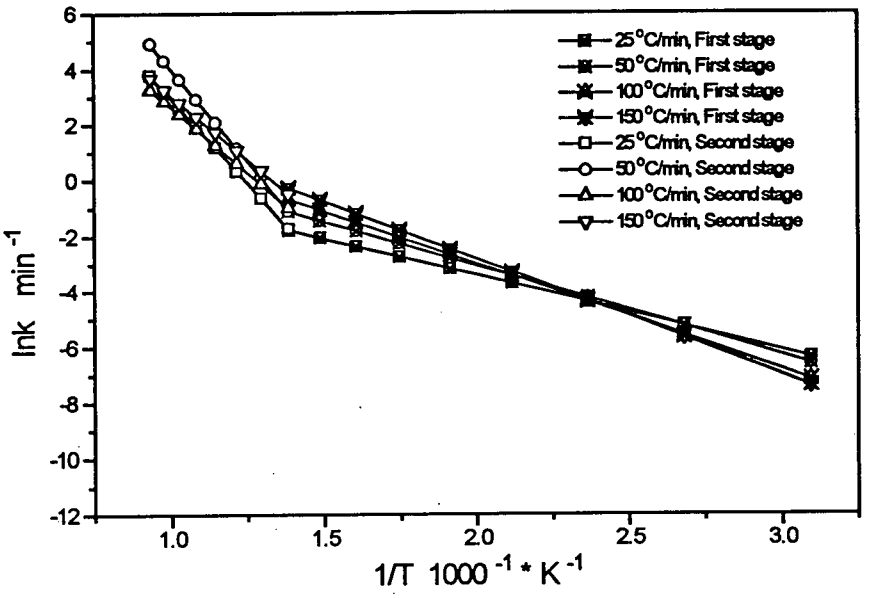

Figure G.6 Syncrude pitch pyrolysis kinetic reaction rate as a function of temperature at different heating rates and final temperature 800 °C with 2-stage Friedman method

APPENDIX H Volatile Yield Predicted via the Single Set Kinetic Parameters for Different Heating Rates

800 °C CANMET pitch

25 °C/min			50 °C/min			100 °C/min			150 °C/min		
t min	Vexp	Vmod	t min	Vexp	Vmod	t min	Vexp	Vmod	t min	Vexp	Vmod
0.01	0.04	0.00	0.00	0.32	0.00	0.01	0.09	0.00	0.01	0.06	0.00
2.01	0.06	0.04	0.98	0.31	0.02	0.99	0.25	0.05	1.03	0.00	0.15
3.42	0.50	0.13	1.52	0.40	0.05	1.26	0.57	0.11	1.65	0.78	1.09
4.15	1.02	0.24	2.05	1.06	0.12	1.49	1.25	0.21	2.35	2.85	5.25
5.02	2.17	0.45	2.50	2.01	0.22	1.77	2.41	0.40	2.54	7.05	7.45
6.02	3.86	0.88	2.99	3.37	0.43	2.00	3.67	0.67	2.74	10.84	10.68
7.02	5.57	1.60	3.52	4.96	0.81	2.27	5.33	1.16	2.89	15.87	16.75
8.03	7.59	2.75	4.01	6.64	1.38	2.51	7.10	1.77	3.01	21.77	22.70
9.03	9.83	4.49	4.50	8.42	2.25	2.78	9.65	2.78	3.13	27.11	29.85
10.03	12.08	7.00	4.99	10.43	3.50	3.01	12.14	3.97	3.21	33.84	35.18
11.03	14.48	10.45	5.52	12.62	5.43	3.25	14.86	5.52	3.28	39.52	40.82
12.03	17.33	14.97	6.01	14.76	7.84	3.52	18.31	7.85	3.36	46.40	46.53
12.50	18.70	17.47	6.50	17.41	10.96	3.79	22.54	10.83	3.44	53.90	52.33
13.04	20.65	20.63	6.99	20.81	14.84	4.02	27.11	13.38	3.52	60.98	57.70
13.50	22.55	23.64	7.30	23.70	17.73	4.22	32.19	19.52	3.63	66.75	64.88
14.04	25.09	27.36	7.53	26.51	19.99	4.37	37.20	25.62	3.75	72.41	70.40
14.57	27.59	31.32	7.75	29.70	22.40	4.49	41.82	30.90	3.83	75.11	73.05
15.04	30.75	34.95	7.97	33.18	24.96	4.61	47.51	36.67	4.02	75.95	76.57
15.51	34.04	38.69	8.15	36.47	27.39	4.69	51.88	40.71	4.49	76.82	77.59
15.91	37.35	41.95	8.24	38.20	29.60	4.76	56.71	44.85	5.00	77.59	77.59
16.24	40.31	44.60	8.42	42.01	34.30	4.84	61.61	49.01			
16.58	43.67	49.98	8.60	46.10	39.31	4.92	66.12	53.12			
16.98	48.26	56.32	8.82	52.05	45.84	5.00	69.67	57.04			
17.38	53.52	62.24	9.04	58.55	52.43	5.15	74.33	64.27			
17.71	58.43	66.67	9.35	67.70	61.14	5.35	77.00	71.35			
18.00	63.51	70.01	9.66	74.02	68.59	5.62	78.28	76.99			
18.31	67.42	73.09	9.89	76.48	72.78	6.01	78.82	79.15			
18.65	71.52	75.69	10.11	77.95	75.92	6.52	78.97	79.30			
19.05	74.86	77.93	10.64	79.28	79.80	7.02	79.15	79.30			
19.52	77.16	79.52	11.49	79.95	80.77	7.49	79.30	79.30			
20.05	78.62	80.40	12.78	80.15	80.79						
21.05	79.70	80.81	15.00	80.79	80.79						
22.05	80.03	80.84									
23.99	80.29	80.84									
26.00	80.52	80.84									
28.00	80.72	80.84									
30.00	80.84	80.84									

Syncrude pitch 800 °C

25 °C/min			50 °C/min			100 °C/min			150 °C/min		
t min	Vexp	Vmod	t min	Vexp	Vmod	t min	Vexp	Vmod	t min	Vexp	Vmod
0.00	0.10	0.00	0.03	0.14	0.00	0.00	0.01	0.00	0.00	0.02	0.00
1.00	0.15	0.02	1.00	0.19	0.03	0.51	0.00	0.02	0.51	0.07	0.03
2.01	0.19	0.06	2.29	0.48	0.37	1.02	0.08	0.12	0.99	0.32	0.35
3.01	0.60	0.18	3.03	1.52	1.12	1.50	0.42	0.54	1.20	0.97	0.81
4.01	1.00	0.46	3.53	2.76	2.20	1.77	1.12	1.12	1.35	1.63	1.40
5.01	1.86	1.04	4.09	5.23	4.26	2.01	2.05	1.98	1.51	2.85	2.32
6.02	3.27	2.18	4.50	7.85	6.67	2.25	3.44	3.36	1.66	4.82	3.67
7.02	5.63	4.23	5.01	11.99	10.94	2.45	5.33	5.08	1.81	7.26	5.61
8.02	8.60	7.67	5.52	17.06	17.02	2.62	7.45	7.00	1.96	10.66	8.27
9.02	12.65	13.01	6.02	22.76	25.09	2.79	9.93	9.45	2.08	13.84	11.04
10.02	17.69	20.71	6.48	28.37	34.08	2.93	12.16	11.84	2.20	17.41	14.41
11.03	23.58	30.93	6.94	34.00	44.25	3.06	14.63	14.64	2.32	21.39	18.45
12.03	29.64	43.21	7.40	39.55	54.88	3.20	17.29	17.88	2.45	25.52	23.21
13.03	35.84	56.42	7.91	45.63	66.08	3.33	20.21	21.57	2.54	28.72	27.14
14.03	41.51	68.85	8.23	49.93	45.92	3.47	23.23	25.69	2.63	32.08	31.45
15.04	46.95	78.83	8.60	56.23	56.23	3.64	26.99	31.42	2.72	35.38	17.86
16.04	52.40	62.72	8.83	61.49	62.52	3.78	30.22	36.37	2.84	39.83	23.56
16.51	55.44	69.40	9.02	66.50	67.33	3.95	34.10	42.97	2.93	43.35	28.44
17.04	59.57	76.10	9.16	70.62	70.70	4.08	37.28	25.56	3.02	47.39	33.91
17.51	63.81	80.89	9.39	77.79	75.77	4.22	40.44	31.05	3.08	50.52	37.85
17.98	68.73	84.61	9.62	83.51	80.08	4.32	42.92	35.55	3.14	54.04	41.96
18.44	74.31	87.27	9.80	86.62	82.90	4.46	46.34	41.98	3.20	58.28	46.13
18.78	78.47	88.59	10.08	88.85	86.12	4.56	49.26	47.01	3.26	63.46	50.44
19.05	81.64	89.37	10.49	89.66	88.98	4.66	52.57	52.14	3.32	69.32	54.69

19.25	84.14	89.81	11.00	89.98	90.34	4.76	56.47	57.21	3.39	75.11	58.97
19.51	86.99	90.25	12.01	90.22	90.70	4.86	61.34	62.21	3.45	80.17	63.13
19.85	88.85	90.60	12.98	90.40	90.70	4.96	67.07	66.98	3.54	85.60	68.98
20.25	89.87	90.84	13.99	90.57	90.70	5.07	73.25	71.41	3.63	88.35	74.24
20.98	90.46	91.00	15.01	90.70	90.70	5.17	79.27	75.41	3.75	89.59	80.05
21.99	90.56	91.03				5.27	84.20	78.91	3.93	89.97	86.01
22.99	90.58	91.03				5.41	88.02	82.76	4.26	90.30	90.11
24.06	90.75	91.03				5.64	89.67	87.26	4.99	90.62	90.62
24.99	90.80	91.03				5.95	90.02	89.80			
26.00	90.95	91.03				6.49	90.27	90.56			
27.00	90.90	91.03				7.51	90.58	90.58			
28.00	90.89	91.03									
29.00	91.04	91.03									
30.00	91.03	91.03									

Volatile Yield Predicted via the Single Set Kinetic Parameters for Different Final Temperature

100 °C/min CANMET pitch

750 °C	V_{exp} %	V_{mod} %	850 °C	V_{exp} %	V_{mod} %	950 °C	V_{exp} %	V_{mod} %
50.6	0.16	0.00	49.3	0.00	0.00	51.1	0.29	0.00
151.8	0.34	0.06	150.6	0.00	0.05	152.2	0.53	0.06
202.4	1.04	0.23	197.4	0.50	0.20	175.6	1.45	0.11
225.8	1.90	0.40	232.5	1.35	0.46	202.8	2.55	0.24
249.2	2.85	0.67	252.0	2.26	0.70	222.2	3.79	0.38
276.4	4.37	1.15	291.0	4.26	1.49	249.5	5.43	0.68
299.8	6.02	1.75	322.1	6.55	2.53	276.7	7.28	1.18
327.0	8.47	2.76	349.4	9.00	3.86	300.1	9.17	1.80
350.4	10.95	3.95	376.7	11.98	5.67	327.3	11.47	2.83
377.6	14.05	5.78	400.1	14.61	7.67	350.6	13.82	4.04
401.0	17.09	7.81	423.5	17.82	10.14	377.9	16.81	5.92
424.3	20.48	10.30	446.9	21.57	13.10	401.2	19.67	7.99
451.6	25.64	13.22	466.3	25.85	17.52	424.6	23.09	10.55
474.9	31.58	20.70	481.9	29.96	23.25	447.9	27.46	13.61
490.5	36.67	27.07	497.5	34.59	30.04	467.4	32.51	18.39
502.2	41.70	32.51	509.2	39.07	35.73	482.9	37.44	24.32
510.0	45.81	36.40	520.9	44.43	41.77	494.6	41.67	29.51
521.7	53.18	42.51	532.6	50.68	47.98	506.3	46.50	35.24
525.6	55.86	44.59	540.4	55.22	52.09	517.9	52.13	41.33
533.3	61.28	48.72	548.2	59.87	56.08	525.7	56.46	45.56
541.1	66.20	52.85	556.0	64.33	59.87	533.5	60.85	49.82
552.8	71.47	58.78	563.8	68.12	63.40	541.3	65.12	54.04
568.4	75.54	65.81	571.6	71.21	66.58	545.2	67.09	56.10
583.9	77.50	71.34	591.0	75.40	72.79	552.9	70.59	60.04
607.3	78.67	76.62	610.6	77.19	76.52	564.6	74.52	65.53
626.8	78.88	78.64	649.5	78.02	78.84	580.2	77.73	71.61
650.1	79.06	79.44	700.2	78.38	79.01	595.7	79.05	75.98
700.7	79.40	79.60	750.8	78.58	79.01	623.0	80.06	79.98
750.0	79.60	79.60	801.5	78.74	79.01	650.2	80.33	81.07
			850.8	79.01	79.01	751.4	80.77	81.23
						852.5	81.07	81.23
						949.8	81.23	81.23

50 °C/min Syncrude pitch

750 °C	V_{exp} %	V_{mod} %	850 °C	V_{exp} %	V_{mod} %	950 °C	V_{exp} %	V_{mod} %
50.4	0.03	0.00	51.6	0.06	0.00	51.1	0.21	0.00
99.9	0.10	0.03	102.2	0.02	0.03	99.7	0.29	0.03
158.1	0.56	0.30	164.4	0.48	0.37	148.3	0.56	0.21
190.4	1.46	0.82	201.3	1.36	1.12	182.4	1.52	0.65
224.9	3.35	2.11	228.9	2.80	2.32	206.7	2.71	1.31
250.8	5.88	3.94	252.0	4.80	4.03	233.5	5.31	2.61
276.6	9.79	6.90	277.3	7.88	6.97	257.8	8.42	4.61
300.3	14.02	10.95	300.4	11.70	10.92	277.2	11.62	6.99
326.2	19.16	17.19	325.7	16.76	16.99	301.5	16.41	11.20
349.9	24.83	24.73	348.7	21.89	24.21	325.8	22.06	17.09
375.8	30.94	34.85	374.1	28.07	34.00	350.2	28.00	24.83
399.5	36.59	45.41	399.4	34.44	45.21	376.9	34.79	35.36
425.3	42.40	57.38	424.8	40.76	56.91	401.2	40.74	46.24
449.0	47.91	67.69	447.8	46.75	66.92	425.5	46.39	57.50
462.0	51.12	46.22	466.2	52.50	48.40	447.4	52.04	67.07
474.9	54.96	53.45	482.3	59.46	57.39	464.5	57.61	47.64
483.5	58.00	58.28	493.8	65.60	63.63	476.6	62.93	54.46
492.0	61.50	62.92	503.1	71.20	68.36	486.3	67.86	59.86

498.6	64.42	66.35	514.6	78.24	73.71	496.1	73.42	65.09
507.2	69.23	70.64	526.1	83.85	78.33	505.8	78.51	69.98
515.8	74.30	74.54	537.6	87.32	82.14	513.1	82.10	73.38
526.6	80.25	78.82	549.1	88.80	85.07	520.4	85.05	76.48
535.2	84.12	81.72	567.6	89.49	88.16	530.1	87.68	80.10
546.0	87.41	84.68	599.8	89.78	90.24	542.3	88.98	83.79
561.1	89.45	87.61	650.5	90.03	90.61	556.8	89.49	86.97
574.0	89.93	89.19	701.2	90.23	90.61	600.6	90.17	90.66
599.8	90.38	90.59	749.5	90.39	90.61	651.7	90.27	91.01
651.6	90.53	90.96	800.2	90.50	90.61	700.3	90.65	91.01
750.7	90.96	90.96	850.9	90.61	90.61	751.4	90.88	91.01
						800.0	90.75	91.01
						851.1	90.97	91.01
						897.3	90.89	91.01
						952.9	91.01	91.01

APPENDIX I The Effect of the Number of Significant Digits and Sample Weight Analysis

The effect of number of significant digits and change of reaction rate constant k ±1% and ±2% was checked. The following temperature T is in oC and the volatile content V is in % of the original sample weight. Each symbol is defined in the FORTRAN program. Run Can48 is fitted in the following results.

The results show that a change of the number of significant digits from 5 to 2 caused 0.0052%, 0.005239%,0.5548%,1.742%,26.66% of s.e.e. but made no noticeable effect on the fitting of the volatile content vs temperature curve, as shown in Figure I.1.

The results also show that a change of k from the best fitting values caused 3.629%, 1.053%, 0.5186%, 2.496% for -2%, -1%, +1, +2% change of k, but the made no noticeable effect on the fitting of the volatiles vs temperature curve, as shown in Figure I.1.

Fitting results in the entire temperature range with the change of significant digits

T	V	V5	V4	V3	V2
50.22	.040000	.155612	.155925	.155187	.148259
100.32	.060000	.586071	.587093	.584630	.561560
135.40	.500000	1.232127	1.234082	1.229293	1.184507
153.77	1.020000	1.734067	1.736689	1.730211	1.669683
175.47	2.170000	2.505345	2.508926	2.499990	2.416585
200.52	3.860000	3.672206	3.677123	3.664705	3.548955
225.60	5.570000	5.173826	5.180311	5.163737	5.009436
250.65	7.590000	7.033928	7.042167	7.020847	6.822622
275.70	9.830000	9.266864	9.276985	9.250461	9.004178
300.75	12.080000	11.868485	11.880535	11.848537	11.551843
325.80	14.480000	14.816680	14.830612	14.793103	14.445798
350.85	17.330000	18.071870	18.087541	18.044737	17.648988
362.55	18.700000	19.682439	19.698846	19.653715	19.236753
375.90	20.650000	21.579050	21.596222	21.548593	21.108932
387.60	22.550000	23.284918	23.302686	23.253032	22.795035
400.95	25.090000	25.271160	25.289514	25.237764	24.760882
414.32	27.590000	27.291778	27.310609	27.257016	26.763636
426.00	30.750000	29.073425	29.092580	29.037604	28.531953
437.70	34.040000	30.865168	30.884554	30.828418	30.312592
447.72	37.350000	32.399281	32.418790	32.361847	31.839053
456.07	40.310000	41.063754	41.020945	40.747694	42.488916
464.42	43.670000	45.483339	45.439130	45.158472	46.936603
474.45	48.260000	50.812486	50.767717	50.485304	52.261405
484.45	53.520000	56.001230	55.957289	55.681786	57.400808
492.80	58.430000	60.123230	60.081089	59.818183	61.447106
500.00	63.510000	63.451378	63.411572	63.164263	64.686734
507.85	67.420000	66.780378	66.743855	66.517930	67.898483
516.20	71.520000	69.923750	69.891393	69.692140	70.899546
526.22	74.860000	73.102690	73.075913	72.911869	73.895247
537.90	77.160000	75.972522	75.952435	75.830062	76.553672
551.27	78.620000	78.231054	78.217958	78.138651	78.599589
576.32	79.700000	80.249473	80.245260	80.219989	80.361467
601.37	80.030000	80.759543	80.758742	80.753972	80.779498
649.80	80.290000	80.839754	80.839749	80.839723	80.839849
699.90	80.520000	80.840000	80.840000	80.840000	80.840000
750.00	80.720000	80.840000	80.840000	80.840000	80.840000
800.12	80.840000	80.840000	80.840000	80.840000	80.840000

standard deviation for each method above

1.425523 1.417689 1.400758 1.805715

the s.e.e. relative change in % with 5, 4, 3, 2 digits

.005239 .554801 1.742416 26.663709

Fitting results in the entire temperature range with the change of k

T	V	VM2	VM1	VFT	VP1	VP2
50.22	.040000	.152449	.154003	.155557	.157111	.158665
100.32	.060000	.574217	.580055	.585893	.591731	.597568
135.40	.500000	1.207336	1.219562	1.231787	1.244009	1.256230
153.77	1.020000	1.699306	1.716460	1.733611	1.750758	1.767901
175.47	2.170000	2.455396	2.480063	2.504722	2.529373	2.554017
200.52	3.860000	3.599583	3.635475	3.671350	3.707208	3.743050
225.60	5.570000	5.072560	5.122645	5.172698	5.222717	5.272703
250.65	7.590000	6.898025	6.965290	7.032493	7.099636	7.166718
275.70	9.830000	9.090637	9.177923	9.265102	9.352175	9.439143
300.75	12.080000	11.647051	11.756806	11.866387	11.975795	12.085028
325.80	14.480000	14.546404	14.680464	14.814254	14.947773	15.081021
350.85	17.330000	17.750740	17.910142	18.069141	18.227739	18.385936
362.55	18.700000	19.337387	19.508723	19.679582	19.849964	20.019872
375.90	20.650000	21.206920	21.391776	21.576059	21.759771	21.942914
387.60	22.550000	22.889470	23.085980	23.281823	23.477003	23.671520
400.95	25.090000	24.849839	25.059293	25.267963	25.475853	25.682965
414.32	27.590000	26.845596	27.067503	27.288498	27.508585	27.727767
426.00	30.750000	28.606588	28.838855	29.070089	29.300295	29.529477
437.70	34.040000	30.378797	30.620875	30.861791	31.101552	31.340163
447.72	37.350000	31.897207	32.147183	32.395883	32.643312	32.889478
456.07	40.310000	40.493876	40.778982	41.062074	41.343165	41.622269
464.42	43.670000	44.891975	45.188016	45.481620	45.772805	46.061593
474.45	48.260000	50.210075	50.511906	50.810763	51.106675	51.399671
484.45	53.520000	55.406352	55.704705	55.999558	56.290952	56.578928
492.80	58.430000	59.549749	59.837641	60.121640	60.401799	60.678169
500.00	63.510000	62.907169	63.180613	63.449888	63.715057	63.976182
507.85	67.420000	66.278446	66.530923	66.779023	67.022820	67.262391
516.20	71.520000	69.476530	69.701777	69.922559	70.138965	70.351080
526.22	74.860000	72.729934	72.918005	73.101715	73.281164	73.456452
537.90	77.160000	75.690399	75.833076	75.971800	76.106680	76.237823
551.27	78.620000	78.045114	78.139443	78.230589	78.318659	78.403756
576.32	79.700000	80.188263	80.219546	80.249327	80.277679	80.304670
601.37	80.030000	80.747584	80.753756	80.759516	80.764891	80.769907
649.80	80.290000	80.839682	80.839720	80.839754	80.839783	80.839809
699.90	80.520000	80.840000	80.840000	80.840000	80.840000	80.840000
750.00	80.720000	80.840000	80.840000	80.840000	80.840000	80.840000
800.12	80.840000	80.840000	80.840000	80.840000	80.840000	80.840000

standard deviation for each method above

1.477343 1.440612 1.425819 1.432991 1.461189

the s.e.e. relative change in % with k: -/+1% and -/+2%

3.629687 1.053194 .015486 .518604 2.496592

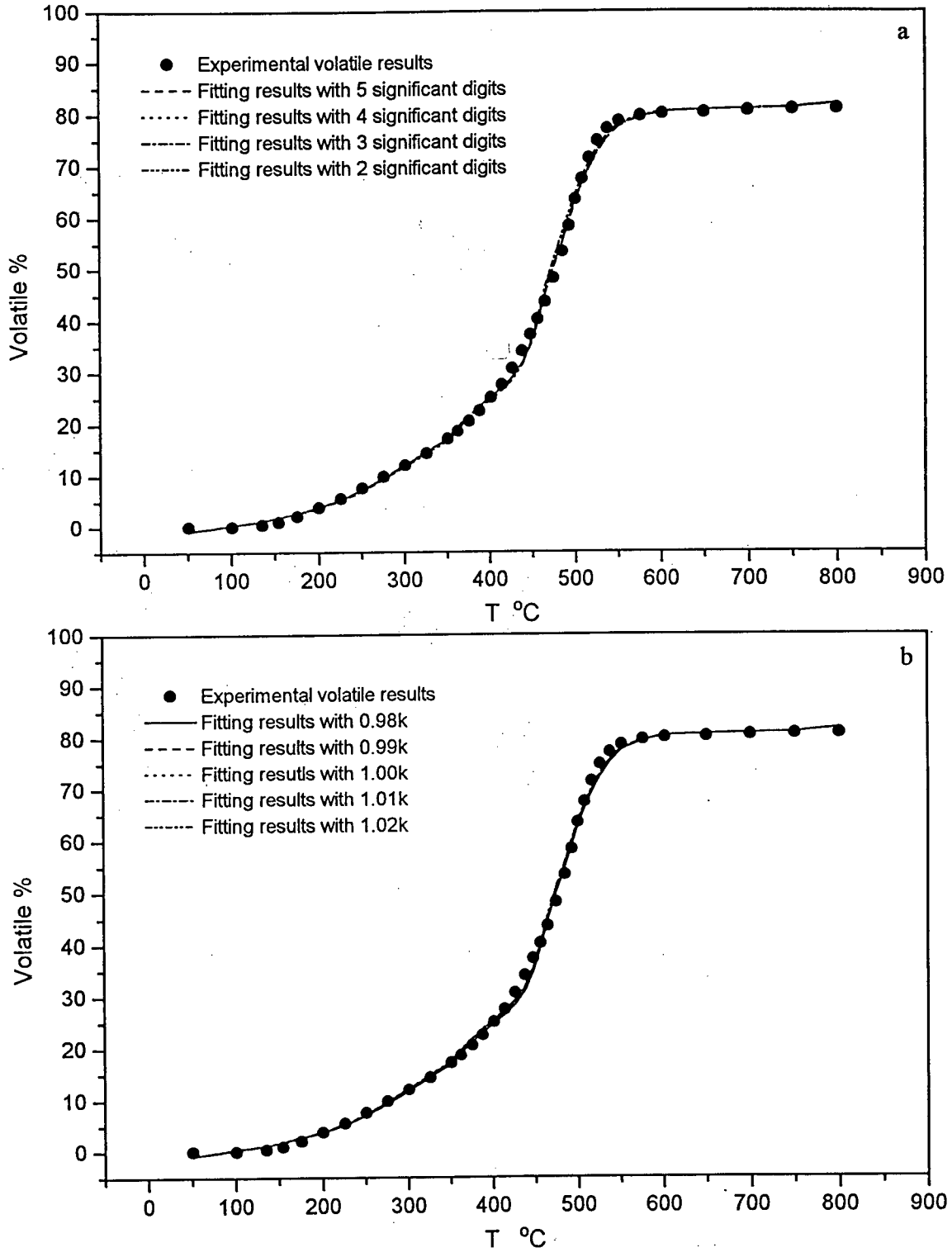

Figure I.1 Effect of the number of significant digits (a) and the change of k in the range of ±1% and ±2% from the best fit values (b)

The Statistical Analysis of Sample Size Effect

The statistical analysis of sample size effect is examined with results in Tables 4.1.1 and 4.1.2 and the analysis results are listed in the following Table I.1. The results show that the volatile yield is roughly constant and the deviation is small in the sample size range for both heating rates. It is therefore believed that results reflect the intrinsic kinetics and are not significantly affected by mass transfer in these sample size ranges.

Table I.1 Statistical Analysis of Sample Size Effect

	7.774~12.034 mg at heating rate 100 °C/min		8.011~13.157 mg at heating rate 50 °C/min	
	$V_{t=0}$ %	$V_{t=10}$ %	$V_{t=0}$ %	$V_{t=10}$ %
Average V yield	80.12	80.43	80.57	81.01
Standard Deviation	0.8	0.7	0.3	0.5
No. of Data Points	5	5	8	8